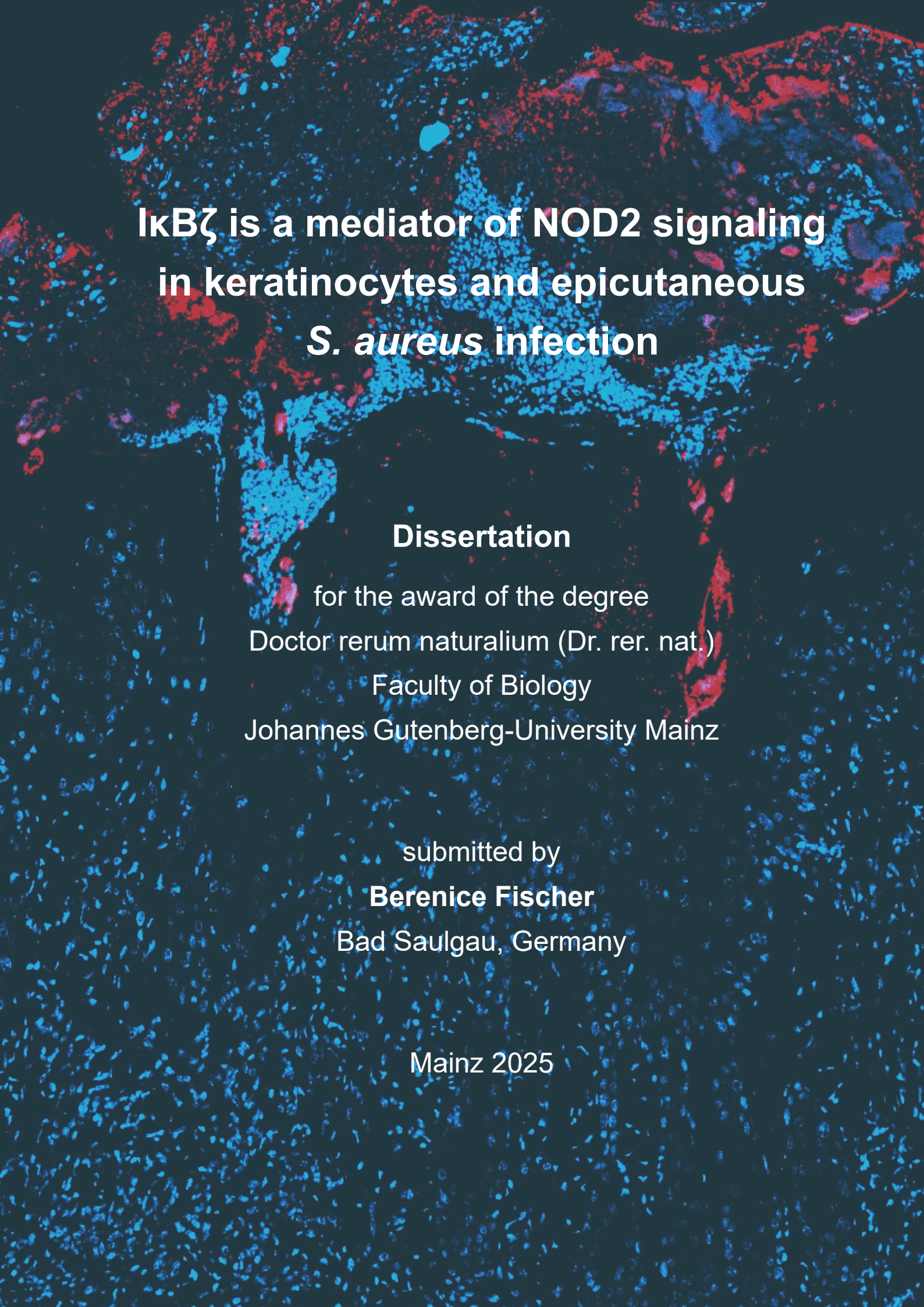

IκBζ is a mediator of NOD2 signaling in keratinocytes and epicutaneous *S. aureus* infection

Dissertation

for the award of the degree
Doctor rerum naturalium (Dr. rer. nat.)
Faculty of Biology
Johannes Gutenberg-University Mainz

submitted by
Berenice Fischer
Bad Saulgau, Germany

Mainz 2025

Printed with official permission by the Johannes Gutenberg-University Mainz, Faculty of Biology

Dean of the faculty: Prof. Dr. Eckhard Thines

1st Referee: [redacted]

2nd Referee: [redacted]

Primary Supervision: [redacted]

Supervisor (Second): [redacted]

Day of oral examination: 16.12.2025

Affidavit

Hereby I declare that my dissertation entitled “IκBζ is a mediator of NOD2 signaling in keratinocytes and epicutaneous *S. aureus* infection” is the result of my own work. No other sources, aids or materials than quoted were used.

Furthermore, I confirm that this thesis has not been submitted yet in another or identical form in the context of any previous graduation procedure.

Eidesstattliche Versicherung

Hiermit versichere ich eidesstattlich, dass ich meine Dissertation mit dem Titel “IκBζ is a mediator of NOD2 signaling in keratinocytes and epicutaneous *S. aureus* infection” (zu Deutsch: “IκBζ als Mediator unter dem NOD2 Signalweg in Keratinozyten und bei epikutaner *S. aureus* Infektion) selbständig angefertigt habe. Es wurden keine anderen Quellen, Hilfsmittel oder Materialien verwendet, als von mir angegeben.

Ich erkläre außerdem, dass diese Dissertation noch in keiner Form, weder ähnlich noch identisch, in einem anderen Gradierungsverfahren zuvor vorgelegt wurde.

Mainz, September 2025

Preface

Parts of this dissertation have been published in the following article:

Fischer B, Kolb A, Focaccia E, Kübelbeck T, Klein M, Löck D, et al. *NOD2-Induced IκBζ Mediates a Protective Host Response against Epicutaneous Staphylococcus aureus Infection*. J Invest Dermatol. **2025.**

As first-author, I was the primary contributor to experimental work, raw data acquisition and data analysis. Besides, I co-drafted both the initial version and the revised manuscript.
The contents presented in the published article were adapted, revised and further expanded by me for the purpose of this dissertation. Editing of images, as well as the design of the final graphs presented in this work were exclusively completed by me.
Research was conducted between 2019 and 2024 in the working groups of Prof. Dr. Klaus Schulze-Osthoff (Department of Molecular Medicine at the Interfaculty Institute of Biochemistry of the Eberhard Karls University Tübingen) and Prof. Dr. Daniela Kramer (Department of Dermatology of the University Medical Center Mainz). No competing interests were declared among involved cooperation partners, neither in the performance of individual experimental steps, nor in putting the raw data together for both the published manuscript and this dissertation. In case of experimental support, contributors and Core Facility members of the University Medical Center Mainz are declared as such in the individual chapters of this dissertation (*chapters 3.Methods and 4.Results*).

Abstract

The atypical IκB protein IκBζ, encoded by *NFKBIZ*, constitutes a transcriptional co-factor of NF-κB, which is stimulus-dependently expressed in a variety of cell types. In this study, we investigated the role of IκBζ in epicutaneous *Staphylococcus aureus* (*S. aureus*) infection. By analyzing *NFKBIZ*-depleted, *S. aureus*-infected primary human keratinocytes and keratinocyte-specific IκBζ knockout mice, we uncovered that IκBζ expression in keratinocytes is critical to mediate a protective host response against *S. aureus*. This was due to the fact that IκBζ controlled the expression of a subset of *S. aureus*-responsive genes, being responsible for IL-17/IL-36 responses and the maintenance of the skin barrier.

Although keratinocytes also sense *S. aureus* with external TLR2 receptors, we further identified *S. aureus* internalization and subsequent NOD2 activation as being mandatory for a Regnase-1-dependent expression of IκBζ and its pro-inflammatory target genes. Loss of IκBζ *in vivo* led to an impaired host defense, such as reduced secretion of antimicrobial peptides and less recruitment of innate and adaptive immune cells (neutrophils, monocytes, effector $CD4^+$ T-cells, and γδ T-cells) to the side of infection, besides damage of skin tissue and stronger dissemination of bacteria. Therefore, this study discovered IκBζ as key player in the newly identified course of NOD2-IκBζ signaling, providing substantial support in the protection against pathogenic *S. aureus* skin infections.

Keywords: *IκBζ, NFKBIZ, keratinocytes, NOD2, TLR2, MDP, Staphylococcus aureus, MRSA, antimicrobial peptides*

Zusammenfassung

Das atypische IκB Protein IκBζ, welches durch das Gen *NFKBIZ* codiert wird, stellt einen transkriptionellen Cofaktor von NF-κB dar und wird Stimulus-abhängig in einer Vielzahl von Zelltypen exprimiert. In dieser Studie wurde die Rolle von IκBζ während der epikutanen Infektion mit *Staphylococcus aureus* (*S. aureus*) genauer evaluiert. Die Analyse von *S. aureus*-infizierten, *NFKBIZ*-deletierten primären humanen Keratinozyten und von Mäusen mit einem Keratinozyten-spezifischen *Nfkbiz* Knockout ergab, dass die Expression von IκBζ in diesen Zellen eine entscheidende Rolle in der Vermittlung der Immunabwehr des Wirts gegen *S. aureus* darstellt. Dies beruht darauf, dass IκBζ in der Lage ist, die Expression eines Teils an *S. aureus*-responsiven Genen zu kontrollieren, die sowohl für eine IL-17/IL-36 vermittelte Immunantwort wichtig sind, als auch für die Aufrechterhaltung und Verstärkung einer funktionalen Hautbarriere.
Obwohl Keratinozyten *S. aureus* auch über ihren externen TLR2 Rezeptor wahrnehmen, konnten wir feststellen, dass die Internalisierung von *S. aureus* und die darauffolgende Aktivierung des NOD2 Rezeptors entscheidend ist, um eine Regnase-1-abhängige Expression von IκBζ und seinen pro-inflammatorischen Zielgenen zu erreichen. Der Verlust von IκBζ im epidermalen Kompartiment *in vivo* führte zu einer beeinträchtigten Wirtsreaktion, wie zum Beispiel einer verminderten Sekretion von antimikrobiellen Peptiden oder der Rekrutierung von Immunzellen des angeborenen und adaptiven Immunsystems am Infektionsherd (Neutrophile, Monozyten, $CD4^+$ T-Effektorzellen und γδ T-Lymphozyten), sowie zu einem Gewebeschaden der Haut und einer verstärkten Ausbreitung der Bakterien.
Zusammengefasst wurde durch diese Studie bewiesen, dass IκBζ eine Schlüsselfigur in dem neu identifizierten Signalweg zwischen NOD2 und IκBζ darstellt, der eine wesentliche, unterstützende Rolle im Schutz gegen eine pathogene *S. aureus* Hautinfektion einnimmt.

Schlagwörter: *IκBζ, NFKBIZ, Keratinozyten, NOD2, TLR2, MDP, Staphylococcus aureus, MRSA, antimikrobielle Peptide*

Table of Contents

Abbreviations

% (v/v)	percent volume per volume (concentration of solution)
(Z)-4-Hydroxy-Tam	OH-Tamoxifen
°C	degree Celsius
3' UTR	3’-untranslated region
5' UTR	5’-untranslated region
AMPs	antimicrobial peptides
AP-1	activator protein-1
approx.	approximately
APS	ammonium peroxodisulfate
ATP	adenosine triphosphate
BCL	B-cell lymphoma protein
bp	base pairs
BPE	bovine pituitary extract
BSA	bovine serum albumin Fraction V
CARD	caspase activation and recruitment domain-containing protein
Cat.	catalog number
CCL	CC-chemokine ligand
CCL20	CC-chemokine ligand 20
CD25	cluster of differentiation 25
CD4	cluster of differentiation 4
CFU	colony forming units
ChIP	chromatin immunoprecipitation
Ct	cycle threshold
ctrl	control
CXCL	C-X-C motif chemokine
CXCL10	C-X-C motif chemokine 10
CytoD	cytochalasin D
DAPI	4',6-Diamidino-2-Phenylindole, Dilactate
diff.	differentiated primary human keratinocytes
DMSO	dimethylsulfoxid
DNA	desoxyribonucleic acid
E. coli	*Escherichia coli*
e.g.	for example
ECL	enhanced chemiluminesce
EDTA	ethylenediamintetraacetic acid
EGF	epidermal growth factor
EGTA	ethylenegylcol-bis (β-aminoethyl ether)-N, N, N', N'-tetraacetic acid
ER	endoplasmic reticulum
EtOH	ethanol
FACS	fluorescence-activated cell sorting
FCS	fetal calf serum
FFPE	formalin-fixed paraffin-embedded
g	gram
gDNA	genomic DNA
Gent/Amph B	gentamicin/ amphotericin B antibiotic solution
GEO	Gene Expression Omnibus
GSEA	gene set enrichment analysis
h	hours
H&E	hematoxylin and eosin
H3	histone H3
HBS	HEPES buffered saline
HCl	hydrochloric acid
HE	hematoxylin and eosin (staining)
hg	human genome (primer sequence)
HiSa	heat-inactivated *S. aureus* cultures
hKC	primary human keratinocytes
HRP	horseradish peroxidase

HSC70	heat shock cognate protein 70
IBD	inflammatory bowel disease
ICAM	intercellular adhesion molecule
IFNγ	interferon gamma
IgG	immunoglobulin G
IKK	inhibitor of NF-κB kinase
IKKβ	inhibitor of NF-κB kinase beta
IL-	interleukin-
IL-17A	interleukine-17A
IL1R	interleukin-1 receptor
IL-1β	interleukine-1 beta
IL-36α	interleukine-36 alpha
IMQ	Imiquimod
IRAKs	IL-1 receptor-associated kinases
IκB	inhibitor of κB
K14, KRT14	keratin-14
kDa	kilo Dalton
KO	knockout
L18-MDP	enhanced MDP-LD
LAC	Los Angeles County jail
LB-Amp	Luria Broth medium supplemented with ampicillin
LCE	late cornified envelope protein
LCN2	lipocalin-2
LPS	lipopolysaccharides
MALT1	mucosa-associated lymphoid tissue lymphoma translocation protein 1
MAPK	mitogen-activated protein kinase
MAPK3	mitogen-activated protein kinase 3
MAVS	mitochondrial antiviral signaling
MB	human myoglobin locus
MDP	muramyl dipeptide
mg	milligram
mg	murine genome (primer sequence)
min	minutes
mKC	primary murine keratinocytes
mL	milliliter
mM	millimolar
MOI	multiplicity of infection
mRNA	messenger ribonucleic acid
MRSA	methicillin-resistant S. aureus
MW	molecular weight
MyD88	myeloid differentiation primary response protein 88
N°	number
Na_2EDTA	ethylenediamine tetraacetic acid disodium salt dihydrate
NaAc	sodium acetate
NaOH	sodium hydroxide
NBD	nucleotide-binding domain
NET	neutrophil extracellular traps
NF-κB	nuclear factor of kappa light polypeptide gene enhancer in B-cells
NGS	normal goat serum
NHS	normal horse serum
NIK	NF-κB inducing kinase
NLR	NOD-like receptors
NLS	nuclear localisation sequence
nM	nanomolar
NOD	nucleotide-binding oligomerization domain-containing protein, also NOD receptor
NOD1	NOD receptor 1, also CARD4, NLRC1
NOD2	NOD receptor 2, also CARD15, NLRC2
nt	nucleotides
OD_{600}	optical density at 600 nm
OE	overexpression
p	phospho
P/S	penicillin/streptomycin antibiotic solution

Pam_3CSK_4	Pam3Cys-Ser-(Lys)4, TLR1/2 ligand
PAMP	pathogen-associated molecular patterns
PBS	phosphate buffered saline
PBST	0.01% PBS-Tween
PCR	polymerase chain reaction
PETP	peptide transporter proteins
PGN	peptidoglycan
PGN-Sandi	ultrapure peptidoglycan of *S. aureus*
PIC	proteinase inhibitor cocktail
ProteoJuice	ProteoJuice protein transfection reagent
qPCR	quantitative real-time polymerase chain reaction
rec.	recombinant
RIG-I	retinoic acid-inducible gene-I
RIPK2	receptor-interacting serine/threonine-protein kinase 2
RNA	ribonucleic acid
ROS	reactive oxygen species
rpm	rounds per minute
RT	room temperature
S. aureus	*Staphylococcus aureus*
S. epidermidis	*Staphylococcus epidermidis*
S1, S2	biosafety level S1, S2
SD	standard deviation
SDS	sodium dodecyl sulfate
SDS-PAGE	sodium dodecyl sulfate-polyacrylamide gel electrophoresis
sec	seconds
SEM	standard error of the mean
seq	sequencing
sh RNA	small hairpin RNA
ssRNA	single-stranded RNA
SSTI	skin and soft tissue infections
STAT	signal transducer and activator of transcription
T7SS	*S. aureus* specific type VII secretion system
TAB2/3	TAK1 binding proteins 2 and 3
TAD	transactivation domain
TAE	Tris-acetate-EDTA
TAK1	TGFβ-associated kinase 1
TARC	Translational Animal Research Center Mainz
TBST	Tris Buffered Saline with Tween 20
TCR	T-cell receptor
TEMED	tetramethylethylendiamine
Th1, Th2, Th17	T helper cells 1, 2, 17
TIRAP	TIR domain-containing adaptor protein
TLR	Toll-like receptor
TNFα	tumor necrosis factor alpha
TRAF6	tumor necrosis factor receptor-associated factor 6
Tri-DAP	Tri-diaminopimelic acid
TSB	tryptic soy broth
undif.	undifferentiated, basal primary human keratinocytes
untr	untreated
UTR	untranslated region
V	volt
VCAM	vascular cell adhesion molecule
w/o	without
WT	wild-type
ZC3H12A	Zinc finger CCCH domain-containing protein 12A, also Regnase-1
µg	microgram
µL	microliter
µM	micromolar

1. Introduction

1.1 The skin – the largest organ of the human body

1.1.1 Function and structure of the epidermis

The human skin constitutes a physical barrier between our body and the surrounding environment, wherefore it is designated as our largest organ [1]. Not only does it maintain our body temperature and prevents water loss, but together with its resident immune cells, it provides an essential protection against any physically or chemically induced exterior injuries and comprises several first-line defense mechanisms counteracting the exposure to pathogenic microorganisms [1].

The mammalian skin is structured into three different layers, each serving another purpose. In the innermost, organ-shielding subcutis fat gets stored as a source of energy besides its function to regulate the body temperature of the organism [2].

The largest and intermediate layer comprises the dermis, containing elastic tissue and collagen, which is held responsible for the skin's flexibility aside from the presence of hair follicles, sweat glands, or nerve endings. While fibroblasts represent the main cell type, the dermal layer harbors several immune cell populations such as macrophages, mast cells, or lymphocytes, which are highly sensitive to any stimulus [2]. Being crossed by both lymphatics and blood vessels, the dermis provides a substantial supply of nutrients for the overlying, outermost epidermis. Here, mainly keratinocytes reside among a few other cell populations [2].

In the last decades, research revealed a rising importance of keratinocytes besides immune cells, contributing to both the immunosurveillance, as well as the establishment of an immune homeostasis in the skin. To investigate their potential to sense pathogens, danger signals, or stress, understanding of their development within the epidermis is fundamental (see ***Figure 1.1.1***)

At first, the basal skin cells are produced in the lowest epidermal layer flanking the dermis (*Stratum basale*), where they remain only for a short time in an undifferentiated state. Due to recurrently formed cells, the previous generations start aging, lose contact with the basement membrane, and move forward to the upper skin layers (*Stratum spinosum, Stratum granulosum*), all the while undergoing stronger cell differentiation with steeply rising calcium concentrations [3]. During this process, also called keratinization or cornification of keratinocytes, well-structured proteins and lipids are synthesized, which are later required to form the cornified envelope. Terminally differentiated keratinocytes then migrate to the outermost layer (*Stratum corneum*), comprising the so-called skin barrier that provides structural stability, hydration of the skin, and a robust shield against various environmental threats, until they finally become apoptotic due to the lack of nutrient supply [1, 4].

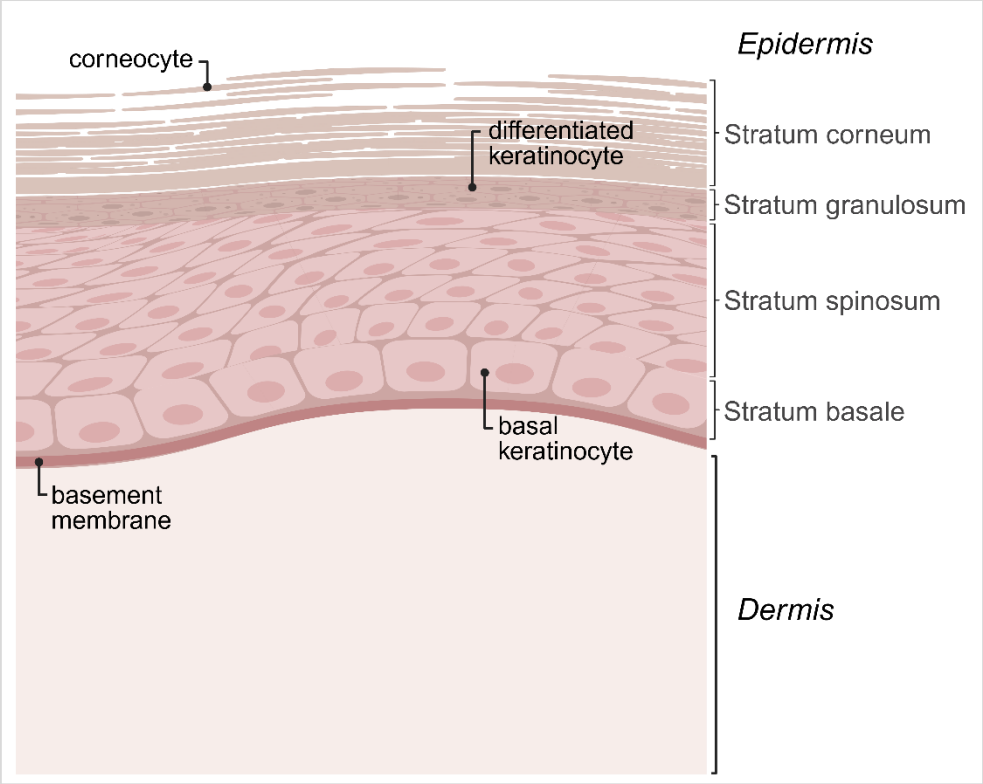

Figure 1.1.1: Structure of the mammalian skin, composed of the dermis and several epidermal layers.
Adapted from [1], created with BioRender (for reference see chapter 6.1)

Since our outer skin layer is primarily composed of terminally differentiated skin cells aside from corneocytes, which are constantly challenged by stress factors like mechanical injury or inflammation, they are more prone to encounter pathogens. Hence, these keratinocytes require higher sensitivity for bacteria recognition per se.
Having a closer look on the composition of the cornified envelope reveals a highly complex network of proteins and lipids, comprising many structural proteins, such as filaggrin, loricrin, involucrin, keratins or elafin, required for proper keratinization [5, 6], but also “late” cornified envelope proteins, which are incorporated in later time points into the envelope. Interestingly, these have recently been reported to possess antibacterial activity in addition to their function in maintaining a functional skin barrier [7, 8].

1.1.2 Immunological function of keratinocytes

Beyond their function to maintain the integrity of the skin barrier, keratinocytes serve as sentinels of the immune system, regulating the homeostasis of skin tissue in general [2]. Of all cell types, the epidermis mostly comprises keratinocytes, which strongly regulate inflammatory responses upon secretion of antimicrobial peptides, growth factors, cytokines, and chemokines, so-called chemotactic cytokines [2, 9]. The latter are held responsible for the activation and recruitment of leukocytes, such as neutrophils, to the side of inflammation or infection, respectively [10]. Additionally, keratinocytes possess different receptors to sense e.g., pathogen-associated molecular patterns, but also cytokines, and can thereby re-stimulate adjacent, yet uninvolved skin cells to further amplify inflammatory responses [11].

Interestingly, the sensitivity of keratinocytes towards all kinds of internal or environmental stimulating agents and physical stress manifests in the induction of variable signaling pathways, which also highly depend on their cell differentiation status and maturation level. For example, the barrier of the skin is not composed of basal keratinocytes, because less differentiated cells are more likely to get infected by pathogens [12]. Regarding the latter, epithelial cells indeed play an active role in the immunosurveillance of the skin by balancing immune responses addressed to harmless skin commensals or potential pathogenic microorganisms [2, 11, 13].

1.1.3 Dysregulation of immune homeostasis in skin diseases

The surveillance of triggered immune responses must occur under highly sensitive and controlled terms, since sloppy to absent reactions might lead to severe tissue damage, infections, or tumor formation, while on the other hand, exorbitant reactions promote the development of autoimmune diseases or chronic skin inflammation [11, 13]. This further means that a well-balanced host immune response is required to maintain the integrity and proper function of the skin [2].

Beyond that, a malfunctioning skin barrier represents the hallmark of many auto-inflammatory skin disease pathologies, which are often associated with defects in the formation of the epidermal layers. For example, the hyperproliferation of keratinocytes constitutes a classical effect in the disease pathology of psoriasis, while in both psoriasis and atopic dermatitis the dehydration of the epidermis due to trans epidermal water loss is common [5]. The latter, for example, is often caused by loss-of-function mutations or decreased expression of the epidermal differentiation marker filaggrin, predisposing such patients to develop atopic dermatitis with a high risk [4, 5, 14].

Above that, a noteworthy accompanying effect of skin diseases, which negatively affect the barrier integrity, is their elevated risk of developing recurring bacterial infections. This is especially the case in atopic dermatitis patients, being highly susceptible to recurrent cutaneous infections with staphylococci due to their massive colonization of e.g., *S. aureus*, on both lesional and non-lesional areas of the skin [15].

1.2 IκBζ: an atypical IκB protein mediates pro-inflammatory responses

1.2.1 The atypical IκB protein IκBζ in the NF-κB pathway

A key feature of both innate and adaptive immune cell populations, as well as keratinocytes, is their rapid response to a broad variety of stimuli, which is implemented upon transcriptional modifications. These can be modulated with the aid of transcription factors, such as the pleiotropic nuclear factor of kappa light polypeptide gene enhancer in B-cells (NF-κB) [16, 17]. The latter consists of hetero- or homodimers of the Rel protein family, which can bind to the κB binding motif in promoter regions of respective target genes to a variable extent in order to repress or activate gene expression, using their N-terminal Rel homology domain [16, 18]. However, to prevent a stimulus-dependent NF-κB-driven activation of pro-inflammatory responses in resting cells, NF-κB is held back in the cytoplasm. In case of the rapid activation of the canonical NF-κB pathway, NF-κB gets sequestered and regulated by inhibitor of κB (IκB) proteins [19]. Under stimulation conditions, the classical cytoplasmic IκB proteins (IκBα, IκBβ, IκBε, p100, and p105), which are constitutively expressed, become phosphorylated and dissociate from NF-κB, thereby enabling its translocation into the nucleus.

Other than that, atypical IκBs, such as IκBζ, $IκB_{NS,}$ and BCL-3, localize directly to the nucleus and regulate the transcriptional activity of NF-κB by acting as its transcriptional co-factors, further promoting and fine-tuning either the induction or repression of NF-κB-dependent gene expression [20, 21].

IκBζ, which is encoded by *NFKBIZ,* becomes expressed in an inducible manner in a variety of innate and adaptive immune cells under highly stimulus- and time-dependent conditions. However, in resting cells its expression is rather marginal [20, 22, 23].

After reaching the nucleus due its nuclear localization signal (NLS), being exclusively present in IκBζ, IκBζ can directly bind to the chromatin or interact with other regulatory proteins and transcription factors. Some of these interactions are established due to its transactivation domain (TAD), which displays binding sites for several proteins. For example, it was reported that the IκBζ expression gets increased upon DNA binding of activator protein 1 (AP-1) family members [24] or the signal transducer and activator of transcription (STAT) factors [25], which are known to be integrated with NF-κB on the chromatin [20].

Apart from that, IκBζ exhibits C-terminal ankyrin repeat domains, a common feature present in both typical and atypical IκB proteins, enabling the interaction with NF-κB [20, 26]. Being a primary response gene of the latter, IκBζ further exerts a transcription-regulating function on secondary response genes through nucleosome remodeling. Hereby, IκBζ might influence the accessibility for transcription factors to promoter regions of genomic DNA in order to initiate transcription by RNA polymerases [21].

Hence, the hitherto poorly understood influence of IκBζ on nucleosome remodeling might display a critical factor during stimulation, bearing the potential of being highly cell type-specific and time-dependent, since the manifestation of remarkable effects on target gene expression takes time [26, 27]. On the contrary to canonical NF-κB gene regulation, activation of the non-canonical NF-κB pathway happens rather slowly and persistent, and involves the NF-κB inducing kinase (NIK), selectively triggering the translocation of RelB-p52 heterodimers to the nucleus [28]. However, a coherence between NIK and IκBζ have not been investigated so far.

All in all, the precise mechanism of cell-type specific IκBζ-dependent differential gene regulation under distinct stimulating conditions is incompletely understood and still requires more research in the future [19].

1.2.2 Inflammatory signaling pathways inducing IκBζ expression in skin

The induction of IκBζ can be achieved by multiple signaling pathways in the skin, following inflammation-induced activation of a variety of membrane-bound cytokine or bacteria sensing receptors, such as the interleukin-1 family receptors stimulated with IL-33, IL-36, and IL-1β or IL-17, respectively, or Toll-like receptors 2, 4, or 5 (TLR) activated by the bacterial components flagellin, peptidoglycan (PGN), or lipopolysaccharides (LPS). *Feng et al.* [20] categorized these pathways further according to their subsequent downstream regulation, finally leading to the activation of certain transcription factors, such as NF-κB, STAT3, or AP-1 family members. Consequently, the function of IκBζ does not only correlate with the respective upstream signaling pathway leading to its induction, but also with the absence or presence of regulatory proteins forming complexes with IκBζ on promoter regions of IκBζ target genes [20]. An example for the latter are POU transcription factors, which were recently reported to engage in a complex with IκBζ together on certain IκBζ target genes exhibiting the respective peptide binding site [17].

Moreover, the induction of IκBζ and its elicited pro-inflammatory gene expression can be enzymatically modulated post transcription upon stabilization of cytosolic *NFKBIZ* mRNA via the degradation of regulatory RNases, such as Regnase-1 (encoded by *ZC3H12A*) [29-31] and Regnase-3 (encoded by *ZC3H12C*) [32, 33] (see ***Figure 1.2.2***).

For instance, in a bacterial infection scenario host cell-derived pattern recognition receptors are stimulated and subsequently trigger the activation of the caspase recruitment domain-containing protein 14 (CARD14), which is mainly expressed in keratinocytes [30]. CARD14 further oligomerizes with B-cell lymphoma (BCL-10) and the protease MALT1 (mucosa- associated lymphoid tissue lymphoma translocation protein 1) to form a CARD14-BCL-10-MALT1 complex, which takes part in the downstream activation of NF-κB. Classically, Regnase-1 is cleaved and thereby inactivated post-translationally by the protease MALT1, leading to the removal of the RNase-introduced hairpins on the 3'-untranslated region (UTR) of the respective *NFKBIZ* mRNA and thus, stabilization of the mRNA transcript [29].

Besides its protease activity, the CARD14-BCL-10-MALT1 complex also serves as a scaffold for the recruited IκB kinase (IKK) complex, promoting phosphorylation and thus, degradation of Regnase-1, as well.
In the end, the dual functions of this complex result in the stabilization and translation of *NFKBIZ* mRNA into IκBζ protein, which immediately translocates into the nucleus. Here it acts as a co-factor for previously recruited transcription factors such as NF-κB, shaping the induction of pro-inflammatory responses, such as IκBζ-dependent gene expressions [30, 34-36].

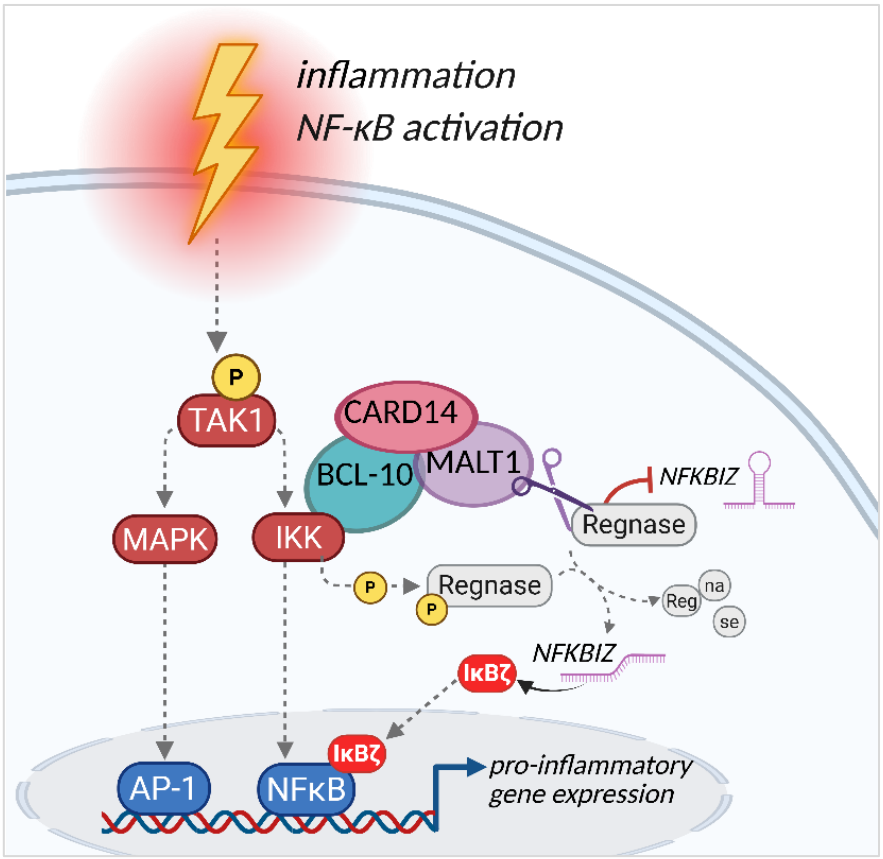

Figure 1.2.2: Schematic overview of NF-κB-dependent pro-inflammatory gene induction with Regnase-1-dependent stabilization of cytoplasmic NFKBIZ mRNA upon TAK1 activation in keratinocytes.
Auto-phosphorylation of TAK1 (TGFβ-associated kinase 1) is evoked upon NF-κB-activation under inflammatory conditions in keratinocytes and leads to the activation of MAPK (mitogen-activated protein kinase) and IκB kinase (IKK) signaling cascades. Consequently, these result in the induction of NF-κB-dependent pro-inflammatory gene expression. In parallel, the caspase recruitment domain-containing protein 14 (CARD14) is activated and further oligomerizes with B-cell lymphoma (BCL-10) and the protease MALT1 (mucosa-associated lymphoid tissue lymphoma translocation protein 1). The CARD14-BCL-10-MALT1 complex triggers several signaling cascades and serves as a scaffold for the recruited IκB kinase (IKK) complex. Cytoplasmic regulatory RNases, in short Regnases, destabilize NFKBIZ mRNA due to the introduction of short hairpins but can be post-translationally inactivated by either MALT1 cleavage or upon IKK-complex induced phosphorylation. NFKBIZ mRNA is then stabilized in the cytosol and translated. IκBζ protein translocates into the nucleus and acts as a transcriptional co-factor for previously recruited transcription factors, e.g. NF-κB and activator protein-1 (AP-1) family members, leading to the induction of pro-inflammatory gene expression. Adapted from [30, 34-36], created with BioRender (for reference see chapter 6.1)

1.2.3 Downstream regulation and function of IκBζ in skin diseases

In the last decade, several studies have addressed the immunomodulatory function of IκBζ in the context of the development of autoinflammatory skin diseases or during lymphoma, thereby assigning it as a crucial transcriptional regulator contributing to a functional immune homeostasis [20, 22, 37-39]. Since IκBζ itself lacks any enzymatic activity and cannot be directly targeted for inhibition, targeting a dysfunctional IκBζ signaling constitutes a new therapeutic approach [40, 41].

In general, IκBζ can both inhibit or activate NF-κB target genes [20], as well as it mediates the induction of several pro-inflammatory cytokines (e.g. *IL36G, IL1B*), chemokines (e.g. *CXCL2, CXCL5*) and antimicrobial peptides (*DEFB4*) upon the induction of IL-36- and IL-17A- signaling [42]. Especially the latter signaling pathway can result in chronic inflammation when being overexpressed in the skin [22, 43].

In terms of cutaneous inflammation, it is known from the literature that an overexpression of IκBζ, and thus its target genes as well, can under certain circumstances, such as environmental influences, genetic predisposition or other hitherto unknown factors, positively contribute to the development of psoriatic lesions both in mouse models and human skin [22, 37]. On the other hand, a specific *Nfkbiz* knockout in the KRT14-positive cell compartment, referred to as *Nfkbiz*$^{\Delta K14\text{-}cre}$ mice, showed a protective effect on the skin when being treated with imiquimod, a TLR7/8 agonist commonly used to artificially induce a psoriatic, lesional skin phenotype [37, 39]. However, it remains rather unknown whether IκBζ plays a physiological role in the skin, such as in the formation of the skin barrier, or not.

Regarding bacterial infections, the full potential of IκBζ to regulate pathogen-induced inflammatory signaling in the skin so far remains largely unexplored. Nevertheless, its absence can be associated with an imbalance of skin microbiota and provides a substantially increased risk for the expansion of a variety of *Staphylococcus* species [38, 44].

1.3 *Staphylococcus aureus – an opportunistic human pathogen*

1.3.1 Staphylococcus aureus – friend or foe?

The opportunistic human pathogen *Staphylococcus aureus* (*S. aureus*) is a gram-positive commensal that can colonize the skin and nasal cavity, among other microbes. Within longitudinal studies, about 30% of healthy individuals were identified as carriers of this specimen, tolerating it unconditionally [45] while others combat its persistent colonization or even succumb to infection [45-47].

Albeit its constant exposure to lots of different species of bacteria that are potentially pathogenic, human skin usually does not get infected. This can be explained by the fact that keratinocytes per se secrete a variety of antimicrobial peptides, such as β-defensins and RNase7. The latter, for instance, is held responsible for diminishing the risk and susceptibility to *S. aureus* skin colonization or infections [48, 49].

Moreover, the epidermis is primarily colonized by commensal bacteria, such as *Staphylococcus epidermidis* (*S. epidermidis*), which also has been reported to protect against the colonization or overabundance of cutaneous *S. aureus* due to its specific secretome [50]. However, dysbiosis in the skin microbiota might cause an imbalance between different *Staphylococcus* strains and contributes to an impaired host defense, which in turn increases the risk of developing skin infections.

Being the causative agent for a broad range of diseases, ranging from mild to strong skin and soft tissue infections (SSTI) with non-healing lesions and abscess formation, infections with *S. aureus* represent a huge health risk. For instance, especially patients being susceptible to skin diseases such as atopic dermatitis are at risk, since they often exhibit a disrupted epithelial barrier and polymorphisms in structural proteins like filaggrin [50-52]. Moreover, further penetration into the organism over the blood stream bears the life-threatening risk of progressive bacteremia or pneumonia and, in severe cases, endocarditis or multi-organ failure due to septic shock [51]. The exact molecular mechanism behind the switch from being a tolerated skin commensal to a dangerous pathogen is not fully understood but is rather multifactorial, depending on the current composition of the skin microbiota, the activity and effectiveness of host responses, and the virulence per se of the specific *S. aureus* specimen.

1.3.2 The emergence of pathogenic MRSA strains

Over the last decades, humanity has been facing severe problems in the treatment of various bacterial infections due to the lack of novel treatment options or antibiotic agents, while bacteria strains with rising antibiotic resistance have emerged. This even led to the designation of a special term for staphylococci with strong β-lactam resistance, which are referred to as methicillin-resistant *S. aureus* (MRSA) strains [53]. For example, the latter is held responsible for more than 100,000 deaths in records from 2019 distributed over 204 countries [54], due to its treatment resistance, which emphasizes the degree of infection.

MRSA represents a prominent candidate elevating hospitalization rates with high mortality, especially in patients with an impaired immune system. Therefore, intensive investigations regarding the characterization of strains have been conducted since the early 2000's. Upon different epidemic outbreaks in the US and Europe the identification of differences in virulence factors, pathogenicity islands acquired via horizontal gene transfer, and plasmid compositions became a major aim [55].
The model strain of this study USA300 wild-type LAC, referred to as *S. aureus* USA300 WT, is a particularly virulent strain that originates from a community-associated isolate of a prisoner in the Los Angeles County jail (LAC) between 2002 to 2003 and was characterized within the USA300 lineage [55-57]. Not only does this strain produce several toxins and induce biofilm formation, but it is capable of causing persistent, chronic skin infections due to higher internalization rates, survival, and further proliferation in infected host cells, such as keratinocytes [55-57].

1.3.3 Bacterial signaling and escape strategies during *S. aureus* infection

Representing a gram-positive microorganism, *S. aureus* possesses a selectively permeable inner plasma membrane which is connected to the cell wall via the periplasmic space [58, 59]. The staphylococcal cell wall itself is composed of so-called pathogen-associated molecular patterns (PAMP), namely a thick layer of PGN and other unique structural molecules, such as lipoteichoic acids and lipopeptides. Apart from the potential antibiotic resistance in certain strains, *S. aureus* possesses a variety of virulence factors contributing to the development of severe and persistent skin infections. These result from an enhanced ability to colonize the epidermis or invade and survive intracellularly within keratinocytes to escape our immune system [60-62].
Interestingly, a small percentage of *S. aureus* manages to survive within professional phagocytes, e.g. neutrophils and monocytes, despite being engulfed in phagosomes [63]. According to the literature, these factors can be categorized into three groups, allowing bacterial adhesion, tissue damage via toxins, and interference with the immune system of infected host cells [58, 62].
For instance, staphylococcal cell wall-anchored surface proteins fundamentally add to the pathogenicity of a particular strain, as they are required in the first place, enabling the adhesion of bacteria to the epithelial host cells. Hence, this process bears the potential to start a biofilm formation, based on recurring colonization, proliferation, and detachment of bacteria to maintain an infection of the skin [62]. It has been discovered that the staphylococcal adhesion procedure can take place both dependently and independently of host cell-derived fibronectin. The latter, for instance, can be used to bridge host-derived α5β1 integrins and *S. aureus*-derived superficial fibronectin binding proteins, leading to host cell binding [64]. In the end, adhesion aims at the endocytosis of *S. aureus* on behalf of the host cell and subsequently, the invasion of keratinocytes without being recognized by the immune system [64].

A prominent example is the staphylococcal cell wall anchored protein A, which prevents the redirection of innate immune responses via blocking of the Fc region of immunoglobulin G (IgG) antibodies and thus, phagocytosis and subsequent clearance [58, 65], as well as it can additionally induce a targeted cell death in a variety of immune cells [66].

Besides, *S. aureus* secretes several types of virulence factors, such as superantigens and pore-forming toxins, leading to both disruption and lysis of infected host cells. This might result in a massive release of cytokines and, as a direct consequence of subsequently dysregulated T-cell proliferation, a progressing development of skin autoimmune diseases or toxic shock syndrome in infected patients [62, 67].

Additionally, *S. aureus* secrets extracellular enzymes, such as coagulases and nucleases, to induce apoptosis in infected host cells and to segregate respective molecules for its own nutrient supply. Not only do the latter highly support the survival of bacteria escaping from host-derived neutrophil extracellular traps (NET) and trigger the apoptosis of macrophages, but they also promote *S. aureus* proliferation and further dissemination within the infected tissue [62, 68]. However, the exact molecular mechanisms to circumvent, manipulate, and escape host immune responses to establish a persistent epicutaneous *S. aureus* infection with the aid of bacterial internalization remains only partly discovered and requires further investigation [69].

1.4 Host responses against epicutaneous *S. aureus* infections

1.4.1 First-line defense mechanisms and innate immune responses

As emphasized above, host defense mechanisms need to cover a broad range of staphylococcal strategies to avoid their manipulation and circumvention of the human immune system. To the detriment of *S. aureus* and as a first-line defense mechanism, pathogen-associated structures of the cell wall get rapidly recognized by specific host cell receptors of keratinocytes and professional phagocytes of the innate immune system, such as monocyte-derived macrophages and neutrophils, leading ideally to the phagocytosis of bacteria, the subsequent induction of pro-inflammatory signaling cascades to fight the infection and lastly, bacterial clearance [62, 70, 71].

As a result of an epicutaneous infection, epithelial cells initiate a massive secretion of antimicrobial peptides (AMPs) with a broad action spectrum, which further draws innate immune cell populations to the side of infection, especially neutrophils and macrophages, to promote bacterial clearance [42, 52]. Since AMPs are already constitutively expressed, their upregulation upon the encounter with pathogenic bacteria happens quite fast and provides a reliable defense mechanism [52].

Besides, during a pathogen-induced inflammation of the skin, keratinocytes immediately start to prime neutrophils via the secretion of neutrophil-attracting chemokines. Subsequently, epicutaneously sensed *S. aureus* gets engulfed by the recruited neutrophils into phagosomes, where they promote oxidative stress due to the generation of reactive oxygen species (ROS) in the presence of phagosomal enzymes and AMPs, such as lysozyme and defensins. Hence, this combination ultimately leads to the enzymatic killing of bacteria [53, 72, 73].

Above that, the formation of so-called neutrophil extracellular traps (NETs) was discovered in the early 20th century [74], and represents another crucial host defense mechanism combating epicutaneous *S. aureus* infections, since its web-like structure aims to trap and facilitate the degradation of virulence factors of the invading bacteria.

However, pathogenic *S. aureus* strains have adapted to ROS to a certain extent, for example via the production of antioxidants, such as its prominent golden pigment, and continue to escape neutrophil-driven immune responses from time to time [53, 72].

1.4.2 Adaptive immune responses as a second line of host defense

During the later course of an infection, the activation of adaptive immune responses and thus, second-line host defense mechanisms are elicited. These amplify the innate immune responses by further recruitment of other innate immune cell populations to the side of infection and by fostering the functionality of neutrophils, rather than counteracting bacterial survival directly [53, 71, 75]. For instance, CD4-positive thymic effector lymphocytes, such as the T helper cell subsets Th1, Th2, and Th17, as well as γδ T-cells, have been reported to secrete specific cytokines, promoting either cell- or antibody-mediated immune responses against *S. aureus* [53].

While Th1 cells represent notable producers of interferon gamma (IFNγ) among other innate immune cells, being responsible for the activation of professional phagocytes to kill intracellular pathogens and to elongate their life span, their dysregulation is associated with a higher bacterial burden in patients with topical skin infections [53, 71, 75]. Aside from that, the expression of Th17-related cytokines, such as IL-17A or IL-17F, does not only contribute to a functional epithelial barrier but further promotes antimicrobial characteristics due to the induction of pro-inflammatory gene expression, as well as the induction of neutrophilic responses [53].

Likewise, increasing numbers of γδ T-cells, being additionally responsible for the expression of IL-17, have been reported to infiltrate into *S. aureus*-infected skin tissue and strongly increase local inflammation, favoring autoinflammation, albeit diminishing the overall bacterial burden [75].

On the contrary, an increased expression of Th2-related cytokines, such as IL-4 and IL-13, has been strongly implicated in the disease pathology of atopic dermatitis patients, leading to an impaired secretion of AMPs accompanied by the disruption of the epithelial barrier. Hence, patients with an overshooting Th2 cell response are reported to be highly susceptible to cutaneous infections with *S. aureus* [53].

In general, dysregulated proliferation and cytokine release mediated by T-cell subsets are associated with an increased risk for the development of autoinflammatory skin diseases, such as atopic dermatitis or psoriasis, bearing the potential to promote a dysbiosis between skin microbiota, resulting in the colonization or inadvertently in the persistent infection with pathogenic bacteria, such as *S. aureus.*

1.4.3 Dermal pathogen recognition receptors and their ligands

Keratinocytes and innate immune cells can sense infectious pathogens colonizing or invading the skin with the aid of selective dermal pattern recognition receptors, such as RIG-I-like or NOD-like receptors (NLR), Toll-like receptors (TLR), or DNA and RNA sensors, among others [76]. Since these receptors comprise a crucial element in the mammalian immune system, they are highly responsive to their particular ligands and can induce a variety of downstream signaling cascades, e.g. inflammasome-, interferon- or NF-κB-dependent pro-inflammatory gene regulation, to prevent a progressing infection [42, 76]. For this study, two groups of receptors were of major interest, both playing a crucial role in the recognition of *S. aureus* [77].

The membrane-bound Toll-like receptor 2 (TLR2) is expressed on both epithelia and innate immune cells and senses extracellular bacteria upon recognition of bacterial cell wall components, e.g. lipopeptides, PGN, and lipoteichoic acids. Depending on its ligand, TLR2 forms activated heterodimers with either TLR6 (with di-acylated lipopeptide) or TLR1 (with tri-acylated lipopeptide) [77].

However, the ability of *S. aureus* to internalize and proliferate within keratinocytes in the epidermal compartment further allocates importance to an internal pathogen receptor of the NLR family: the nucleotide-binding oligomerization domain containing 2 (NOD2) receptor, also known as caspase recruitment domain 15 (CARD15), contains a central nucleotide-binding domain and resides in the cytoplasm of keratinocytes and phagocytic cells [78] in its auto-inhibited form. As soon as muramyl-dipeptide (MDP), a component of the bacterial PGN, gets internalized and drives the NOD2 self-oligomerization upon binding to the C-terminal leucine-rich repeats, activation of the NOD2 receptor is established [77-79].

Not only does the induced signaling of both extracellular and intracellular pathogen receptors contribute to an effective antimicrobial host defense, but it ideally leads to the bacterial clearance of the infected cells. For instance, the latter has been studied in the past in the context of polymorphisms in the sequence of NOD2 and TLR2 receptors, promoting chronic skin diseases and a high susceptibility for recurring cutaneous *S. aureus* infections [77, 80-82].

1.5 Involvement of NOD2 signaling in inflammatory responses

1.5.1 Signaling cascades of the NOD2 and TLR2 pathogen recognition receptors

For a better understanding of the potential regulation of pro-inflammatory responses mediated by both mentioned receptors, their hitherto known signaling cascades will be explained in greater detail in the following.

Upon activation with MDP [77], the intracellular NOD2 receptor establishes a homotypic interaction between its own caspase activation and recruitment domain (CARD) and the CARD of the receptor-interacting serine/threonine-protein kinase 2 (RIPK2; see ***Figure 1.5.1***, left side). The latter subsequently stabilizes itself upon auto-phosphorylation, before an E3 ligase attaches to it, and consecutively polyubiquitinates RIPK2 [78].

On the other hand, the ligand-mediated activation of the extracellular TLR1/2 heterodimer, which is experimentally established using a TLR1/2 agonist such as Pam_3CSK_4 [76, 83], recruits the cytosolic TIR domain-containing adaptor protein TIRAP (see ***Figure 1.5.1***, right side). The latter then leads to the recruitment of the myeloid differentiation primary response protein 88 (MyD88), which is, apart from TLR3, commonly used by all Toll-like receptors. Next, a complex with different IL-1 receptor-associated kinases (IRAKs) binds to the activated MyD88, enabling an interaction with the tumor necrosis factor receptor-associated factor 6 (TRAF6). The latter represents another E3 ligase, which then catalyzes its activation post-translationally via polyubiquitination and recruits TAK1 binding proteins (TAB2/3) [76].

In both TLR2 and NOD2 receptor signaling cascades, polyubiquitination ultimately results in the recruitment of the TGFβ-associated kinase 1 (TAK1) [78], a mitogen-activated protein kinase 3 (MAPK3), which gets activated upon auto-phosphorylation. TAK1, in turn, can either lead to an induction of the MAPK signaling cascade or to the activation of canonical IKK complexes [78].

While the receptor activation explicitly depends on the cellular localization of bacterial components, the downstream mediators inducing pro-inflammatory gene expression due to the binding of important transcription factors, e.g. NF-κB or AP-1 family members, appear to overlap [76, 78, 84, 85]. However, whether an IκBζ-dependent pro-inflammatory gene expression can be elicited to an equal extent by both receptors has not been investigated so far.

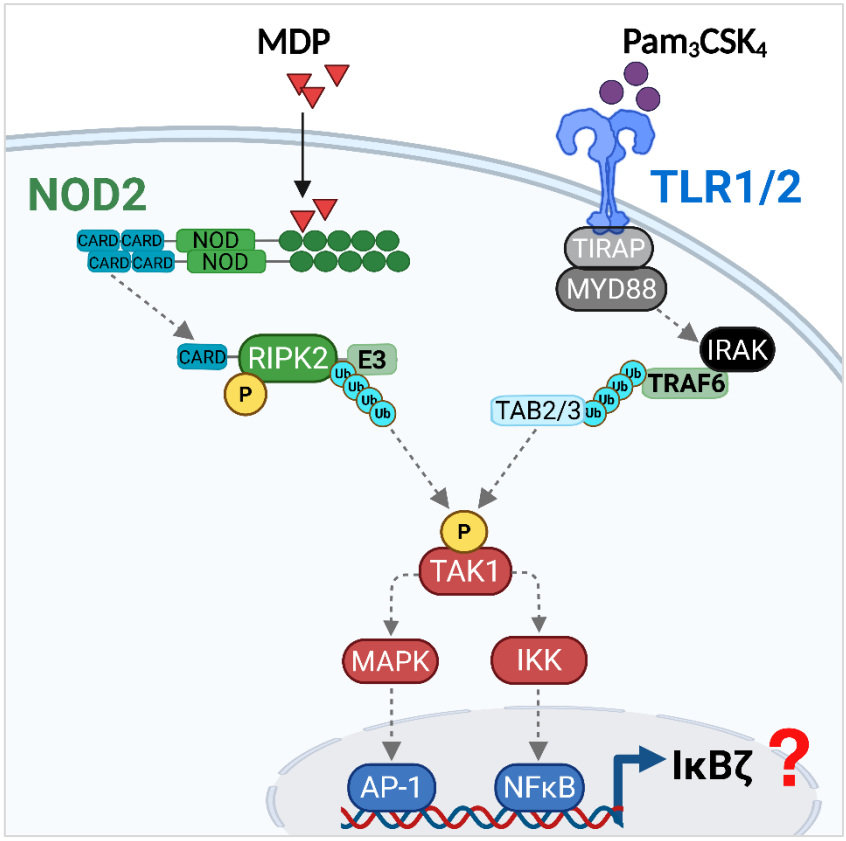

Figure 1.5.1: Scheme of TLR2 and NOD2 receptor signaling pathways in keratinocytes leading to pro-inflammatory gene expression.
NOD2 receptor activation is induced upon uptake of bacterial cell wall component MDP, leading to the dimerization of auto-inhibited NOD2 in the cytoplasm. Subsequent signaling involved the CARD-mediated activation of the receptor-interacting protein kinase 2 (RIPK2), which is stabilized upon auto-phosphorylation mediated by an E3 ubiquitin ligase. Likewise, heterodimeric TLR1/2 receptor can be activated with a TLR1/2 ligand, such as Pam_3CSK_4, in a MyD88-dependent manner, leading to the recruitment of several IRAK complexes. These establish an interaction with the E3 ligase TRAF6 (tumor necrosis factor receptor-associated factor 6), which catalyzes its activation upon polyubiquitination post translation, recruiting the TAK1 binding proteins TAB2/3. Ultimately, both receptors initiate a polyubiquitin-mediated activation and further auto-phosphorylation of the TGFβ-associated kinase 1 (TAK1) and, consequently, activation of mitogen-activated protein kinase (MAPK) and IκB kinase (IKK) signaling cascades. These results in NF-κB- or activator-protein-1 (AP-1) family member-dependent immune responses. Whether both pathogen receptors equally induce IκBζ-dependent pro-inflammatory gene expression remains unknown. Scheme was adapted from [76-78, 84] and created with BioRender (for reference see chapter 6.1).

1.5.2 Importance of NOD2 receptor activation for bacterial clearance in skin tissue

Regarding the discussed first-line defense mechanisms in the skin, the host cell requires a fast and accurate pathogen recognition procedure. Especially since *S. aureus* tries to evade these responses by manipulating the antimicrobial responses with its virulence factors or by hiding within infected host cells, it is obvious that an insufficient intracellular sensing mechanism is accompanied by an impaired neutrophil activity, which further results in an augmented susceptibility to epicutaneous infections [53]. Also, a recent collaboration study gave proof of the ability of keratinocyte-derived, RIPK2-mediated NOD2 signaling to drive the formation of NETs *in vitro* during *S. aureus* infections, while keratinocytes responded to NET-associated RNA via the induction of psoriasis-related gene expressions [86].

Even though TLR2 was reported to mediate direct immune responses against *S. aureus* and thus contributes to bacterial clearance [53], some *in vivo* data of infected *Tlr2*$^{-/-}$ knockout mice allocated less importance of this receptor signaling pathway. At steady-state, these mice were already strongly susceptible to superficial *S. aureus* infections [87], even though the loss of *Tlr2* further elevated strong host defense mechanisms under experimental infection conditions. However, when compared to infected control wild-type mice, only marginal effects were detected in infected *Tlr2*$^{-/-}$ animals [88, 89].

On the contrary, subcutaneous infection models of *Nod2*$^{-/-}$ deficient mice, for example, showed a more severe phenotype compared to wild-type animals, with larger skin abscess formation and an impaired bacterial clearance [88, 90]. Conversely, non-infected knockout mice remained healthy at steady-state without the development of spontaneous skin infections [91].

Hence, it needs to be emphasized that differing experimental setups, such as colonization or infection models with living *S. aureus* cultures, can only be compared to a limited extent. Apart from the pathogenicity of the used strain or the timing and duration of an experiment, the counteracting host responses and triggered signaling pathways highly differ between epicutaneously, subcutaneously, intradermally or intravenously administered bacteria. Thus, the pathogen recognition receptors NOD2 and TLR2 seem to elicit a differential expression of target genes, meaning their signaling pathways are not redundant but differ in their effectiveness to induce innate and adaptive immune responses to fight epicutaneous *S. aureus* infections [88, 90].

1.5.3 Reported function of NOD2 receptor signaling in other diseases

Apart from its function to recognize cell wall components of gram-positive pathogens in skin tissue, mutations and polymorphisms of internal NOD2 receptors have also been observed in the context of different inflammatory diseases [79], since they are not only expressed by keratinocytes but epithelial and mucosal cells in general, as well as phagocytic neutrophils and monocytes [78].

For example, several loss- and gain-of-function point mutations occurring in the peptidoglycan-recognizing region of the C-terminal leucine-rich repeats in the NOD2 receptor bear the strongest genetic risk for the development of inflammatory bowel diseases, such as Crohn's disease [78, 92-94], early-onset sarcoidosis [95], or Blau syndrome [79, 96]. However, genetic alterations in the internal receptor might also occur in the central nucleotide-binding domain (NBD) composed of the NOD-like protein, leading to an overshooting NF-κB activity, which is completely independent of the presence of PGN fragments [79, 93, 97].

Moreover, the perturbation of the actin cytoskeleton of the infected host cell caused upon bacterial invasion into the cell might give another hint to dysfunctional receptor activation. This is due to the fact, that the interaction between the structural host membrane protein vimentin and intracellular NOD2 possesses the regulating function to induce autophagy in the infected host cell, as well as NF-κB activation [79, 98].

With regard to viral infections, NOD2 can further sense single-stranded RNA (ssRNA), such as that of the influenza virus, in a mitochondrial antiviral signaling (MAVS)-dependent fashion [76, 79, 99], albeit in the absence of PGN.

Furthermore, linking the cellular stress of the host-derived endoplasmic reticulum (ER), caused by its functional disruption through viruses, parasites or bacteria exploiting the ER for their growth and synthesis, to diabetes and cardiovascular damages gives rise to the unresolved question, whether all the mentioned signaling cascades do have a certain key modulator in common [76, 79, 100, 101]. Hence, investigating the potential of IκBζ to specifically shape the NOD2-mediated responses, represents an interesting topic in the field of both inflammatory skin and bowel diseases.

1.6 Aim of this study

Although IκBζ was recently identified in several studies to play a crucial role in maintaining a healthy skin microbiome or regulating pro-inflammatory gene transcription during IL-36- or IL-17-induced psoriasis, its capacity to support host defense mechanisms during skin infections remains rather unexplored.

We hypothesized that specific pathogen recognition pathways can potentially induce IκBζ in keratinocytes. Therefore, we investigated the pro-inflammatory responses downstream of the bacteria-sensing receptors NOD2 and TLR2 using the pathogenic wild-type MRSA strain LAC of the USA300 lineage. Besides, we further aimed to explore these potential immunomodulatory functions of IκBζ during an experimental *S. aureus* infection in both human and murine primary keratinocytes, as well as IκBζ-dependent effects on the ability of bacteria to invade and internalize the keratinocytes, to avoid further bacterial clearance.

Above that, we were interested in the function of keratinocyte-derived IκBζ in the context of an epicutaneous *S. aureus* infection *in vivo*, to evaluate its potential to drive local immune responses and to fight the propagation and dissemination of *S. aureus* in skin tissues with mild barrier defects.

As our group extensively studied IL-36-dependent immune responses in the context of psoriasis in the past [22, 37, 42], further intention of this project was to unveil potential similarities between NOD2 receptor-mediated, *S. aureus*-driven, and IL-36-related pro-inflammatory gene expression depending significantly on IκBζ. Such a crosstalk of IκBζ-dependent regulation might be of great relevance for future studies, addressing the treatment of skin diseases in patients prone to superficial infections with bacteria due to an impaired skin barrier and host defense.

2. Materials

2.1 Animals

All mice used for *S. aureus* infections *in vivo* in this study were bred in the animal facilities of the Translational Animal Research Center (TARC) Mainz in Rhineland-Palatinate, Germany (AG Kramer). Skin tissue of these mouse strains was used for *in vitro* stimulations and infections, as well as from Tamoxifen-inducible *Zc3h12a* knockout and control tissue, which Prof. Dr. Vigo Heissmeyer kindly provided from the Helmholtz Centre Munich, Germany. For animal ethics and experimental permissions, see *chapter 3.5.1*.

Table 1: Mouse lines

Mouse strain Origin/ Reference	**Abbreviation**	**Genetic variation/ mutation**
B6.Cg.Nfkbiz<tm1.1Muta> AG Kramer [102]	*Nfkbiz*$^{fl/fl}$ *mKC: WT*	Control animals, *Nfkbiz* gene is flanked with loxP sites between exon 5 and 7 (RIKEN, Stock RBRC06410)
B6.N.Cg-Tg(KRT14-cre)1Amc/J AG Kramer [37, 103]	*KRT14-cre*	Transgenic mouse strain expressing a Cre recombinase under the control of the human keratin 14 (K14) promoter (Jackson Laboratories, Stock 018964)
B6.Cg.Nfkbiz<tm1.1Muta> Tg(KRT14-cre)/Tarc AG Kramer [37]	*Nfkbiz*$^{\Delta K14\text{-}cre}$ *mKC: Nfkbiz*$^{-/-}$	Cell-specific *Nfkbiz* knockout in KRT14-positive cells due to gene deletion based on Cre-mediated gene recombination
Zc3h12a$^{fl/fl}$ AG Heissmeyer [104, 105]	*Zc3h12a*$^{fl/fl}$ mKC: WT	Control animals, Zc3h12a gene is flanked with loxP sites at both sides of exon 3
Zc3h12a$^{Rosa26\text{-}creERt2}$ AG Heissmeyer [104]	*mKC: Zc3h12a*$^{-/-}$	Tamoxifen-inducible Regnase-1 knockout (encoded by the gene *Zc3h12a*), based on temporal Cre-mediated gene recombination. This mouse line was generated by crossing floxed *Zc3h12a* animals with transgenic Rosa26-CreERt2 mice, which express a tamoxifen-inducible Cre recombinase under the control of the ubiquitously expressed Rosa26 promoter

2.2 Eukaryotic cell culture

Table 2: Eukaryotic cell lines

Cell line	Origin	Cultivation medium	Supplements
HEK293T	Immortalized human embryonic kidney cells with enhanced transfection efficiency and viral packaging through expression of the SV40 large T antigen. Cells were purchased from DSMZ Leibniz Institute Braunschweig, Germany (Stock ACC 635)	DMEM, low glucose (Thermo Fisher Sc.)	• 10% FCS • 1% P/S
HaCaT	Immortalized keratinocyte cell line with partial to full differentiation phenotype, initially extracted from back skin of a male patient. Cells were donated by Petra Boukamp from the German Cancer Research Center in Heidelberg, Germany [106]	DMEM, low glucose (Thermo Fisher Sc.)	• 10% FCS • 1% P/S
undif. hKC	Undifferentiated primary human keratinocytes isolated from the epidermis of foreskin tissue	CnT-07 Epithelial Proliferation Medium (CELLnTEC)	• CnT-07 supplements: A, B, C • 0.2% Gent/Amph B
diff. hKC	Differentiated primary human keratinocytes isolated from the epidermis of foreskin tissue, with $CaCl_2$ differentiation 72 h prior to the experiment	CnT-07 Epithelial Proliferation Medium (CELLnTEC)	• CnT-07 supplements: A, B, C • 0.2% Gent/Amph B • 2 mM $CaCl_2$
mKC	Primary murine keratinocytes isolated from the skin of the mouse tail tissue	K-SFM (Keratinocyte-SFM, Thermo Fisher Sc.)	• K-SFM supplements: EGF1-53, BPE • 1% P/S • 0.05 mM $CaCl_2$

Table 3: Media and reagents used for human and murine cell culture

Reagent	Company	Cat. N°
Acetic acid, 100%	VWR International	20.104.298
Calcium chloride ($CaCl_2$)	Sigma-Aldrich	C1016
CnT-07 Epithelial Proliferation Medium+ supplements	CELLnTEC	CnT-07
Collagen I, bovine, 5 mg/mL	Thermo Fisher Scientific	A10644-01
Dimethyl sulfoxide (DMSO)	Carl Roth	A994
Doxycycline hyclate BioChemica	PanReac AppliChem	A2951,0025
Dulbecco's Modified Eagle Medium (DMEM), low glucose, pyruvate	Thermo Fisher Scientific	31885-023
Dulbecco's Phosphate Buffered Saline (DPBS) w/o $CaCl_2$ and $MgCl_2$,1X	Sigma-Aldrich	D8537
Fetal Calf Serum (FCS)	Sigma-Aldrich	F7524
Gentamicin/Amphotericin solution (Gent/Amph B) (5 mg/mL Gent, 125 µg/mL Amph B), 500X	Thermo Fisher Scientific	R01510
HEPES solution, 1 M	Sigma-Aldrich	H0887-100ML
Keratinocyte-SFM, with L-glutamine	Thermo Fisher Scientific	17005034
Keratinocyte-SFM supplements: rh epidermal growth factor (EGF 1-53), bovine pituitary extract (BPE)	Thermo Fisher Scientific	37000015
Opti-MEM I (1X) + GlutaMAX-I	Thermo Fisher Scientific	51985-026
Penicillin/Streptomycin solution (P/S) (10,000 U/mL Pen, 10 mg/mL Strep), 100X	Sigma-Aldrich	P0781
Puromycin, 10 mg/mL	InvivoGen	ant-pr-1
RPMI-1640 medium, with L-Glutamine and $NaHCO_3$	Sigma-Aldrich	R8758
Trypsin-EDTA, 0.05%, phenol red	Thermo Fisher Scientific	25300054

2.3 Bacteria

Table 4: Bacteria strains

Strain	Abbreviation	Cultivation medium/ agar	Origin/ Reference
NEB 5-alpha *Escherichia coli* (transformation efficient)	competent *E. coli*	Luria/Miller (LB) medium/ agar ± 100 µg/mL ampicillin	NewEngland Biolabs, Cat. C2987H
Staphylococcus aureus USA300 wild-type LAC (MRSA strain)	*S. aureus USA300 WT LAC*	Tryptic Soy Broth (TSB) medium/ agar	Bernhard Krismer (Eberhard Karls University Tübingen)
Heat-inactivated S. *aureus* USA300 wild-type LAC	*HiSa*	Tryptic Soy Broth (TSB) medium/ agar	Self-made
Staphylococcus epidermidis wild-type 1457	*S. epidermidis*	Tryptic Soy Broth (TSB) medium/ agar	Birgit Schittek (Eberhard Karls University Tübingen)

Table 5: Media and reagents used for bacteria cultivation

Reagent	Company	Cat. N°
Ampicillin	Carl Roth	K029
LB-Agar (Luria/Miller)	Carl Roth	X969
LB-Medium (Luria/Miller)	Carl Roth	X968
Tryptic Soy Agar	Sigma-Aldrich	22091
Tryptic Soy Broth (TSB) NutriSelect Basic	Sigma-Aldrich	T8907

2.4 Consumables

Table 6: Consumables

General consumables	**Company**	**Cat. N°**
Centrifugation tubes, 15 mL	Greiner	188271-N
Centrifugation tubes, 50 mL	Greiner	227261
PCR Single Cap 8x SoftStrips, 0.2 mL	Biozym	710980
PCR single tube, 0.2 ml, PCR performance tested, transparent, PP, flat cap	Sarstedt	72.737.002
Pipette tips, gel loading standard 0.5 µL to 200 µL	Thermo Fisher Scientific	LC1001
Pipette tips, 10 µL	Sarstedt	70.3010
Pipette tips, 1000 µL	Sarstedt	70.3050.020
Pipette tips, 200 µL	Sarstedt	70.3030.020
Reaction tubes, safe-seal 1.5 mL	Sarstedt	72.706
Reaction tubes, safe-seal 2 mL	Sarstedt	72.695.500
Consumables for bacteria	**Company**	**Cat. N°**
Bacteria culture tubes polypropylene graduated,14 mL	Carl Roth	EC03.1
Cuvettes, 1,5mL, semi-micro, PS	Brand	759015
Parafilm M Lab. Sealing Film	Santa Cruz	sc-200311
Petri dishes with lid, polystyrene 100x15 mm, sterile	Sigma-Aldrich	P5731-500EA
Consumables for cell culture	**Company**	**Cat. N°**
Cell culture plate with lid, sterile White Opaque 96-well (Perkin Elmer X50 CulturePlate, LLC 6005680)	Fisher Scientific	50-905-1585
Cell strainer EASYstrainer, 100 µm	Carl Roth	CNA1.1
CELLSTAR sterile cell culture dish w lid, 100x 20 mm	Greiner	664160
CELLSTAR sterile cell culture dish w lid, 145x 20 mm	Greiner	639160
CELLSTAR sterile cell culture multiwell w lid, 6-well	Greiner	657960
CELLSTAR sterile cell culture multiwell w lid, 12-well	Greiner	665970
Consumables for cell culture	**Company**	**Cat. N°**
Cryo tube CRYO.S, 2 ML, PP, round bottom, sterile	Greiner	121280
Millipore Millex-GP sterile filters, 22 µm	Sigma-Aldrich	SLGP033RS
Millipore Millex-HA sterile filters, 45 µm	Sigma-Aldrich	SLHA033SS
Serological pipettes, plugged, sterile, 5 mL	Sarstedt	86.1687.010
Serological pipettes, plugged, sterile, 10 mL	Sarstedt	86.1254.025
Serological pipettes, plugged, sterile, 25 mL	Sarstedt	86.1685.020
Syringe BD Discardit II, luer lock, sterile, 10 mL	BD Becton Dickinson	03626823
Syringe BD Discardit II, luer lock, sterile, 20 mL	BD Becton Dickinson	07358756
Syringe BD Plastipak, luer lock, sterile, 50/60 mL	BD Becton Dickinson	359-060
Venting filters Midisart 2000, sterile 0.2 µm	VWR	SARP17805-E
Consumables for flow cytometry	**Company**	**Cat. N°**
GentleMACS C Tubes, purple	Miltenyi Biotech	130-096-334
Round Bottom polystyrene test tube with cell strainer, Snap Cap, Falcon, 5 mL	Corning	352235
Round Bottom polystyrene test tube, Falcon, 5 mL	Fisher Scientific	10579511
Consumables for immunohistochemistry	**Company**	**Cat. N°**
Accessories glass inserts for staining trough	Carl Roth	H552.1
Accessories wire hanger for glass staining rack	Carl Roth	H553.1
Coverslips, glass thickness N°1, 24 x 60 mm	Carl Roth	1P73.1

Consumables for immunohistochemistry	**Company**	**Cat. N°**
Embedding cassettes: accessories sponges	Carl Roth	TT56.1
Embedding cassettes for biopsies, with lid	Kabe Labortechnik	053786
Histology Epredia Adhesion slides Superfrost Plus	Carl Roth	H867.1
ImmEdge hydrophobic barrier (PAP) pen	Biozol	VEC-H-4000
Staining trough, glass	Carl Roth	H554.1
Staining trough acc. to Schiefferdecker, PMP	Carl Roth	XC73.1
Consumables for *in vivo* experiments	**Company**	**Cat. N°**
Dissecting tools, set for anatomy	Carl Roth	0829.1
Injekt F solo syringe, 1 mL	Braun	9166017V
Leukoplast Fixomull Stretch, 10 cm x 2 m	Sanicare Apotheke	14219995
Paper filter discs for finn chambers, 12 mm	Smart Practise	AL7210
Surgical tape Leukoplast, 12.5 mm x 5 m	Carl Roth	N532.1
Waterproof plaster, 30mm x 40mm	dm-drogerie markt	Mivolis
Consumables for RNA and protein extraction	**Company**	**Cat. N°**
Cell scraper, 2-position blade, size: M	Sarstedt	83.3951
GentleMACS M Tubes, orange	Miltenyi Biotech	130-093-236
Nitrocellulose blotting membrane (Amersham Protran), pore size 0,2 µm, 300mm x 4m	Sigma-Aldrich	GE10600001
PCR plates hard-shell 384-well, thin wall skirted, white	BioRad	HSP3805
PCR Plate Sealing Film Microseal 'B', adhesive	BioRad	MSB1001
QubitTM Flex Assay Tube Strips	Thermo Fisher Scientific	Q33252
Whatman blotting paper ROTILABO,1.5 mm,60x58cm	Carl Roth	CL75.1

2.5 Chemicals and reagents

Table 7: General chemicals and reagents

Reagent	**Company**	**Cat. N°**
1,4-Dithiothreit (DTT)	Carl Roth	6908
2-Propanol Ph. Eur. (Isopropanol), ≥ 99.9%	Hedinger	GH 05001
Agarose LE Standard	Genaxxon	M3044.500
Ammonium chloride (NH_4Cl)	Carl Roth	P726.1
Ammonium peroxydisulfate (APS)	Carl Roth	9592
Ampicillin sodium salt, 97%	Carl Roth	K029.1
Bovine Serum Albumin (BSA), Fraction V	Carl Roth	8076
Bromphenol blue sodium salt	Carl Roth	A512.2
Calcium chloride ($CaCl_2$)	Sigma-Aldrich	C1016
Chloroform	Sigma-Aldrich	1024451000
Citric acid	Carl Roth	X863.1
Collagen I, Bovine, 5 mg/mL	Thermo Fisher Scientific	A1064401
Complete Mini Protease Inhibitor Cocktail (PIC)	Roche	4693124001
Desoxyadenosine triphosphate (dATP)	Thermo Fisher Scientific	R0141
Desoxycytidine triphosphate (dCTP)	Thermo Fisher Scientific	R0151
Desoxyguanosine triphosphate (dGTP)	Thermo Fisher Scientific	R0161
Desoxythymidine triphosphate (dTTP)	Thermo Fisher Scientific	R0171
Diethylpyrocarbonat (DEPC)	Carl Roth	K028.1
Dimethyl sulfoxide (DMSO)	Carl Roth	A994

Reagent	Company	Cat. N°
Di-sodium hydrogen phosphate dihydrate (Na_2HPO_4 x 2 H_2O)	Sigma-Aldrich	106580
Distilled water	Carl Roth	1CX3.2
DNA/RNA-dye peqGREEN	VWR International	732-3196
Dr. Schumacher OPTISAL plus disinfectant solution	hygi.de	105258
D-sucrose	Carl Roth	4661.1
Dulbecco's Phosphate Buffered Saline powder (PBS), 10X w/o: Ca und Mg	PAN Biotech	P04-53010P
Dulbecco's Phosphate Buffered Saline (PBS), 1X	Sigma-Aldrich	D8537
Dynabeads Protein G	Invitrogen	10003D
Ethanol, 100%	Carl Roth	K928.4
Ethanol, 96% denatured	Carl Roth	T171.7
Ethylenediamine tetraacetic acid disodium salt dihydrate (Na_2EDTA x 2 H_2O)	Carl Roth	8043
Ethylene gylcol tetraacetic acid (EGTA)	PanReac AppliChem	A0878
Fixation buffer	BioLegend	420801
GeneRuler 100 bp DNA ladder	Thermo Fisher Scientific	SM0243
Glacial Acetic Acid, ≥ 99%	Sigma-Aldrich	A6283-500mL
Glucose	Carl Roth	HN06
Glycerol, waterfree, 99.5%	Carl Roth	3783.1
Glycine, blotting grade	Carl Roth	0079.4
Glycoblue coprecipitant,15 mg/mL	Invitrogen	AM9515
Hanks′ Balanced Salt solution (HBSS), with Mg^+, Ca^{2+}	Sigma-Aldrich	55037C-1000ML
Hydrochloric acid (HCl), 37% fuming	Carl Roth	4625
Hydrogen peroxide (H_2O_2), 30%	Carl Roth	8070.4
Isoflurane CP	CP Pharma	1214
Lithium chloride (LiCl)	Sigma-Aldrich	L9650-100G
Magnesium chloride ($MgCl_2$)	Carl Roth	KK36.1
Mayer's Hematoxylin Solution, 1g/L	Sigma-Aldrich	MHS32-1L
Nonfat dried milk powder	PanReac AppliChem	A0830
Normal Chicken Serum blocking solution	Biozol/Vectorlabs	VEC-S-3000-20
Normal Goat Serum (NGS)	Cell Signaling	5425S
Normal Horse Serum (NHS)	Biozol	LIN-ENH9010
NP-40 alternative detergent solution, sterile, 10%	Sigma-Aldrich	492018
Nuclease-Free Water (not DEPC-treated, Ambion)	Thermo Fisher Scientific	AM9937
Oligo(dT)18 Primer	Thermo Fisher Scientific	SO132
PageRuler prestained protein ladder	Thermo Fisher Scientific	26617
PMA (Phorbol 12-myristate 13-acetate)	Sigma-Aldrich	P1585-5MG
Potassium chloride (KCl)	Carl Roth	HN02
ProLong™ Diamond Antifade Mountant	Thermo Fisher Scientific	P36961
QIAzol® Lysis Reagent	QIAGEN	79306
Random hexamer primer	Thermo Fisher Scientific	SO142
ROTI Histol	Carl Roth	6640.5
ROTI Aqua-Phenol, ready-to-use RNA extraction	Carl Roth	A980.3
ROTI Histofix, 4.5% formaldehyde (buffered, pH 7)	Carl Roth	2213.5
ROTI Histokitt	Carl Roth	6638.2
Rotiphorese Gel 40 (37.5:1)	Carl Roth	T802.1
Saponin	AppliChem	A4518.0100

Reagent	Company	Cat. N°
Schülke Terralin liquid disinfectant	intermedical24	0013641
SDS pellets, ≥ 99 %	Carl Roth	CN30.2
Sodium acetate (NaAc)	Carl Roth	6773
Sodium chloride (NaCl)	VWR International	27810
Sodium deoxycholate (NaDoc)	AppliChem	A1531,0100
Sodium dodecyl sulfate (SDS)	Carl Roth	CN80
Sodium hydrogen carbonate ($NaHCO_3$)	Sigma-Aldrich	1063290500
Sodium hydroxide (NaOH), pellets	Carl Roth	6771.1
TEMED (Tetramet hylethylenediamine)	Carl Roth	2367.3
Tris Buffered Saline with Tween 20 (TBST), 10X	Cell Signaling	9997S
TRIS, buffer grade 99.3%	Carl Roth	AE15.6
Tri-sodium citrate dihydrate ($C_6H_5Na_3O_7$ x 2 H_2O)	Carl Roth	3580.3
Triton X-100	Carl Roth	6683
Tween 20	Serva Feinbiochemica	37470
Urea	Carl Roth	3941.3
Xylene (isomers), ≥ 97 %	Carl Roth	9713.3
β-Glycerophosphate disodium salt hydrate	Sigma-Aldrich	G9422

Table 8: Transfection reagents

Reagent	Company	Cat. N°
Calcium chloride ($CaCl_2$)	Sigma-Aldrich	C1016
Lipofectamine2000 Reagent	InvitroGen	11668-030
Polybrene transfection reagent	Sigma-Aldrich	TR-1003-G
ProteoJuiceTM Protein Transfection Reagent	Novagen	71281-3

2.6 Enzymes and purchased buffers

Table 9: Enzymes

Reagent	Company	Cat. N°
Dispase, 5 U/mL	StemCell	07913
DNase I, from bovine pancreas, 100 mg	Sigma	11284932001
DNase I, RNase-free HC, 50 U/µL	Thermo Fisher Scientific	EN0523
Liberase TM Research Grade Roche, 100 mg	Sigma-Aldrich	5401127001
RevertAid Reverse Transcriptase, 200 U/µL	Thermo Fisher Scientific	EP0442

Table 10: Purchased buffers

Reagent	Company	Cat. N°
DNA Loading Dye, 6X	Thermo Fisher Scientific	R0611
DreamTaq Hot Start PCR Mastermix	Thermo Fisher Scientific	K9012
GreenMasterMix w/o ROX, 2X	Genaxxon	M3023
Maxima SYBR Green/ROX qPCR Master Mix, 2X	Thermo Fisher Scientific	K0222
Reaction buffer for Reverse Transcriptase, 5X	Thermo Fisher Scientific	EP0441
Reaction Buffer with $MgCl_2$ for DNase I, 10X	Thermo Fisher Scientific	B43
Ribolock RNase Inhibitor, 40 U/µL	Thermo Fisher Scientific	EO0382

2.7 Kits

Table 11: Purchased kits

Kit	Company	Cat. N°
Dual-Glo Luciferase Assay System	Promega	E2980
ECL Western Blotting Substrate	Promega	W1001
GeneJET Plasmid Miniprep Kit	Thermo Fisher Scientific	K0503
NucleoBond Xtra Maxi Kit	Macherey-Nagel	740414
Proteome Profiler Mouse Cytokine Array Kit Panel A	R&D systems	ARY006
PureYield Plasmid Midiprep System	Promega	A2495
QIAGEN MinElute PCR Purification Kit	QIAGEN	28004
Qubit Protein Assay Kit	Thermo Fisher Scientific	Q33212
SignalStain DAB Substrate Kit	Cell Signaling	8059S
WesternBright Chemilumineszenz Substrat Sirius	Advansta	K-12043-D20

2.8 Antibodies

Table 12: Primary and secondary antibodies for Western blot

Primary antibody	Dilution factor	Diluted in	Host	Company	Cat. N°
GAPDH	1:2000	5% milk/PBS	Rabbit	Cell Signaling	2118
Histone H3	1:1000	5% milk/PBS	Rabbit	abcam	ab1791
HSC70 (mouse)	1:1000	5% milk/PBS	Mouse	Santa Cruz Biotechnology	sc-7298
IκBζ (human)	1:1000	5% milk/PBS	Rabbit	Cell Signaling	9244
NOD2	1:500	5% BSA/PBS	Rabbit	MyBioSource	MBS9603353
Phospho-IκBα (Ser32)	1:500	5% BSA/PBS	Rabbit	Cell Signaling	2859
Phospho-p38 MAPK (Thr180/Tyr182)	1:500	5% BSA/PBS	Rabbit	Cell Signaling	4511
Phospho-STAT1 (Tyr701)	1:500	5% BSA/PBS	Rabbit	Cell Signaling	9167
Phospho-STAT3 (Tyr705)	1:500	5% BSA/PBS	Rabbit	Cell Signaling	9131
Staphylococcus aureus protein	1:1000	5% milk/PBS	Rabbit	abcam	ab20920
β-Actin	1:5000	5% milk/PBS	Mouse	Cell Signaling	3700
Secondary antibody	**Dilution factor**	**Diluted in**	**Host**	**Company**	**Cat. N°**
anti-mouse IgG, HRP-linked	1:5000	5% milk/PBS	Goat	Jackson Immuno Research	115-035-003
anti-rabbit IgG, HRP-linked	1:5000	5% milk/PBS	Goat	Jackson Immuno Research	111-035-003

Table 13: Antibodies for ChIP

Antibody	Amount	Host	Company	Cat. N°
IgG isotype control (ChIP Grade), polyclonal	2 µg	Rabbit	abcam	ab46540
IκBζ (raised against the peptide CRKGADPSTRNLENEQ)	2 µg	Rabbit	Eurogentec	home-made

Table 14: Conjugated antibodies, isotype controls and cell dyes for FACS analysis

Antibody	Dilution factor	Clone	Company	Cat. N°
Anti-mouse CD16/32 (TruStain FcX)	1:100	93	BioLegend	101320
APC anti-mouse CD25	1:50	3C7	BioLegend	101910
APC anti-mouse γδ TCR	1:50	GL3	BioLegend	118116
APC anti-mouse Ly6C	1:50	HK1.4	BioLegend	128016
PE anti-mouse CD4	1:50	GK1.5	BioLegend	100408
PE anti-mouse Ly6G	1:50	1A8	BioLegend	127608
Isotype APC Mouse IgG2a, κ	1:50	RTK4530	BioLegend	400612
Isotype PE Mouse IgG2a, κ	1:50	RTK4530	BioLegend	400636
Isotype PE Hamster IgG2, κ	1:50	B81-3	BD Becton Dickinson	550085
CellROX Green	1:5000	/	Thermo Fisher	C10492
DAPI (4',6-Diamidino-2-Phenylindole, dilactate)	1:2000	/	BioLegend	422801
SYTOX Red	1:1000	/	Thermo Fisher	C10492

Table 15: Primary and secondary antibodies for immunohistochemistry

Primary antibody	Dilution factor	Company	Cat. N°
Anti-mouse CD3	1:200	Novus Biologicals	NB600-1441
Anti-mouse Cleaved Caspase-3 (Asp175)	1:500	Cell Signaling	9664
Anti-mouse MPO	1:200	R&D Systems	AF3667
Anti-mouse NOD2	1:100	MyBiosource	MBS9603353
Secondary antibody	**Dilution factor**	**Company**	**Cat. N°**
Anti-rabbit HRP SignalStain Boost IHC Detection Reagent	/	Cell Signaling	8114S
Anti-goat HRP	1:500	Thermo Fisher	A15999

Table 16: Primary and secondary antibodies for immunofluorescence microscopy

Antibody	Dilution factor	Company	Cat. N°
Protein A	1:500	Sigma-Aldrich	P3775
Anti-rabbit AF594	1:500	Thermo Fisher	A-21442
Hoechst33342 (nucleus stain)	1: 10,000	Thermo Fisher	H21492

2.9 Plasmids and luciferase reporter constructs

Table 17: List of plasmids for in vitro transfections

Plasmid	Description	Source	Resistance
pMD2.G	VSV-G envelope expressing vector	Addgene, Cat. 12259	Ampicillin
psPAX2	Second-generation packaging plasmid	Addgene, Cat. 12260	Ampicillin
pLKO.1-puro	Empty lentiviral control plasmid (*sh ctrl*)	Addgene, Cat. 8453	Ampicillin, Puromycin
sh NFKBIZ	sh RNA against human *NFKBIZ* (*sh NFKBIZ*)	pLKO.1-TRCN0000147551	Ampicillin, Puromycin
pRDI292	Empty lentiviral mammalian over-expression control plasmid (ctrl OE)	Provided by Stephan Hailfinger (University Medical Center Münster)	Ampicillin, Puromycin
IκBζ OE	IκBζ overexpression construct, cloned into lenti pRDI292; tagged with FLAG (IκBζ OE)	Provided by Stephan Hailfinger (University Medical Center Münster)	Ampicillin, Puromycin
pCR3.1	Empty control plasmid	Invitrogen, Cat. V79020	Ampicillin
pCR3.1-FLAG-NFKBIZ	IκBζ overexpression construct, cloned into pCR3.1 cut with EcoRI+NotI, tagged with FLAG	Provided by Stephan Hailfinger (University Medical Center Münster), generated with GeneArt, [22]	Ampicillin
pcDNA5-NOD2-EGFP	NOD2 overexpression construct, EGFP tagged	Addgene, Cat. 131207	Ampicillin
GFP	Lentiviral vector with coding sequence for GFP under the control of a CMV promoter	Provided by AG Dietrich, GSH Frankfurt, Germany	Ampicillin

Table 18: List of luciferase reporter constructs

Plasmid	Description	Source	Resistance
pRL-TK Renilla	Reporter gene luciferase construct as a normalizing transfection control	Provided by Margot Thome (University of Lausanne, Dep. of Biochemistry, Switzerland); Promega, Cat. E2241	Ampicillin
pGL3-DEFB4	DEFB4 firefly luciferase promoter construct	Provided by Jan Wehkamp [107] (University of California School of Medicine, Dep. of Medical Microbiology and Immunology, United States)	Ampicillin

2.10 Oligonucleotides

Table 19: Genotyping primer

Primer	Sequence 5' – 3'	Genotyping protocol
Flox F1	GCAAATATTCCCCAGGACCAG	*Nfkbiz flox*
Flox R	GTCTTCACAGCAGGTTATTCACG	*Nfkbiz flox*
Flox F3	TCAGTGCCAGGTGCGTCTGAG	*Nfkbiz flox*
HumanKRT14promF	GCTTAGCCAGGGTGACAGAG	*K14-cre*
HumanKRT14promR	GCTGCCTGGATTTCTCTTTG	*K14-cre*

Table 20: Human oligonucleotide sequences for gene expression analysis

Human primer	Sequence 5' – 3'	Gene
hgCCL20_F	TGTCAGTGCTGCTACTCCAC	*CCL20*
hgCCL20_R	GATTTGCGCACACAGACAAC	
hgCXCL8_F	AAACTGGGTGCAGAGGGTTG	*CXCL8*
hgCXCL8_R	GCTTGAAGTTTCACTGGCATC	
hgCXCL10_F	TGCAAGCCAATTTTGTCCACG	*CXCL10*
hgCXCL10_R	CTGCATCGATTTTGCTCCCC	
hgDEFB1_F	CTCTGTCAGCTCAGCCTC	*DEFB1*
hgDEFB1_R	CTTGCAGCACTTGGCCTTCCC	
hgDEFB4A_F	CCAGCCATCAGCCATGAGGGT	*DEFB4A*
hgDEFB4A_R	GGAGCCCTTTCTGAATCCGCA	
hgFLG_F	TTCGGCAAATCCTGAAGAATCC	*FLG*
hgFLG_R	TGTGCTTTCTGTGCTTGTGTC	
hgICAM1_F	GGGCAGTCAACAGCTAAAACC	*ICAM1*
hgICAM1_R	GGTAAGGTTCTTGCCCACTG	
hgIL17C_F	TGTATCGATGCACGGACGG	*IL17C*
hgIL17C_R	CGTGGATGAACTCGGTGTGG	
hgIL36B_F	CAGCATTAAGCCTGTCACTC	*IL36B*
hgIL36B_R	GCACAGAAGAGACAGAGATC	
hgIL36G_F	CTGGAGCCACGATTCAGTCC	*IL36G*
hgIL36G_R	AGGGTCCACACTTGCTGATTC	
hgIVL_F	AGTGGAGGTCCCATCAAAGC	*IVL*
hgIVL_R	TCAGGCAGTCCCTTTACAGC	
hgNFKBIA_F	AAGTGATCCGCCAGGTGAAG	*NFKBIA*
hgNFKBIA_R	CTCACAGGCAAGGTGTAGGG	
hgNFKBIZ_F	ACACCCACAAACCAACTCTGG	*NFKBIZ*
hgNFKBIZ_R	TGCTGAACACTGGAGGAAGTC	
hgNOD2_F	GCATTGAGGCTGGGGAATAAC	*NOD2*
hgNOD2_R	ACTCTGTTGCCCCAGAATCC	
hgPGLYRP4	CTGGAGTGTCACGACCAGAC	*PGLYRP4*
hgPGLYRP4	CCCAACCAGGAAGTTGTAGGC	
hgPI3_F	AGCCAGTCAAAGGTCCAGTC	*PI3*
hgPI3_R	CTTTCAAGCAGCGGTTAGGG	
hgRPL37A_F	AGATGAAGAGACGAGCTGTGG	*RPL37A*
hgRPL37A_R	CTTTACCGTGACAGCGGAAG	
hgS100A8_F	TGTCTCTGATGGCCTGAAGC	*S100A8*
hgS100A8_R	ACAGCTGACAAGAGACATGC	
hgU6RNA_F	CTCGCTTCGGCAGCACA	*U6snRNA*
hgU6RNA_R	AACGCTTCACGAATTTGC	

Table 21: Murine oligonucleotide sequences for gene expression analysis

Murine primer	Sequence 5' – 3'	Gene
mgActb_F	AGGAGTACGATGAGTCCGGC	*Actb*
mgActB_R	GGTGTAAAACGCAGCTCAGTA	
mgCxcl1_F	ACGTGTTGACGCTTCCCTTG	*Cxcl1*
mgCxcl1_R	TCCTTTGAACGTCTCTGTCCC	
mgCcl20_F	ACTACGACTGTTGCCTCTCG	*Ccl20*
mgCcl20_R	CTTGACTCTTAGGCTGAGGAGG	
mgDefb1_F	TTCAAGCCTCATCTGTCAGCC	*Defb1*
mgDefb1_R	GAGAATGCCAACACCTGGCTC	
mgDefb4_F	GGTGCTGCTGTCTCCACTTG	*Defb4*
mgDefb4_R	TATTCATCTTGCTGGTTCTTCGTC	
mgIl1b_F	AGCTGAAAGCTCTCCACCTC	*Il1b*
mgIl1b_R	GCTTGGGATCCACACTCTCC	
mgIl17a_F	GCCCTCAGACTACCTCAACC	*Il17a*
mgIl17a_R	TTCCCTCCGCATTGACACAG	
mgIl17c_F	GGAGACAGCATGAAGGACCTC	*Il17c*
mgIl17c_R	GCTTCTGTGGGTAGCGGTTC	
mgIl23a_F	CAGCTCTCTCGGAATCTCTGC	*Il23a*
mgIl23a_R	TGTCCTTGAGTCCTTGTGGG	
mgIl36a_F	GCCTGTTCTGCACAAAGGATG	*Il36a*
mgIl36a_R	ACAGCGATGAACCAACCAGG	
mgIl36g_F	GTCAGCGTGACTATCCTCCC	*Il36g*
mgIl36g_R	TGGCTTCATTGGCTCAGGG	
mgNfkbiz_F	GAGGAGAAATCGGAGGAGTCG	*Nfkbiz*
mgNfkbiz_R	GCTCAACCTGGCTTACTTCTAC	
mgNod2_F	AACTTCTTGTCCCTGAGGGTG	*Nod2*
mgNod2_R	TCCAGAATGGCACTGTTCCTG	
mgRpl37a_F	CCAAGGCCTACCACCTTCAG	*Rpl37a*
mgRpl37a_R	CTTGGGTTTCGGCGTTGTTC	
mgS100a8_F	TCGAGGAGTTCCTTGCGATG	*S100a8*
mgS100a8_R	TGCTACTCCTTGTGGCTGTC	
mgZc3h12a_F	ACAGACCAGCACATCCTTCG	*Zhc3h12a*
mgZc3h12a_R	ACGTGTCATTGGAGACCACC	

Table 22: Human ChIP primer for qPCR

ChIP primer	Sequence 5' – 3'	Gene
MB forward	CTCATGATGCCCCTTCTTCT	*MB (human myoglobin locus)*
MB reverse	GAAGGCGTCTGAGGACTTAAA	
IL17C forward	TGTGTAGGTGCTCAGGTTGG	*IL17C*
IL17C reverse	GCATCAGGACACAGACATGC	
IL36G forward	TGAAGAACAGCATCCAGCAG	*IL36G*
IL36G reverse	CAGGGATAGGGAGCAAACAG	
PI3 forward	GAGCCAGCACTTCTACTCTG	*PI3*
PI3 reverse	GGCGGGTCTGTGGTATTTAC	

2.11 Prepared buffers and Solutions

Table 23: Composition of buffers and stock solutions in general

Stock solutions	Components	MW or % (v/v)	Amount/ volume	ad total volume
1 mg/mL OH-Tamoxifen (=2.58 mM)	(Z)-4-Hydroxy-Tamoxifen	387.51 g/mol	1 mg	/
	EtOH	100%	/	ad 1 mL
20 mM acetic acid → sterile filtration (0.22 µm)	Acetic acid, 100%	60.05.g/mol	114.4 µL	/
	Purified water	/	/	ad 100 mL
100 mg/mL ampicillin	Ampicillin sodium salt	371.39 g/mol	1 g	/
	Purified water	/	/	ad 10 mL
100 mM β-glycerophosphate disodium salt	β-glycerophosphate disodium salt	216.04 g/mol	2.16 g	/
	Purified water	/	/	ad 100 mL
5% BSA → sterile filtration (0.22 µm)	BSA	100%	5 g	/
	Purified water	/	/	ad 100 mL
Digest solution (foreskin)	Dispase solution (5 U/mL)	50%	1.5 mL	/
	Basal CnT-07 medium	50%	1.5 mL	ad 3 mL
Digest solution (mouse tail)	Dispase solution (5 U/mL)	50%	1.5 mL	/
	Basal K-SFM medium	50%	1.5 mL	ad 3 mL
10 mg/mL DNase I (diluted in HBSS), 20 U/µL	DNase I (bovine pancreas)	/	100 mg	/
	HBSS w/ Mg+, Ca2+	/	/	ad 10 mL
250 mM EGTA	EGTA	380.35 g/mol	9.51 g	/
	Purified water	/	/	ad 100 mL
Freezing medium for *E. coli* glycerol stocks	Glycerol, sterile	40%	4 mL	/
	LB-medium, sterile	60%	/	ad 10 mL
Freezing medium for keratinocytes and cell lines	DMSO	10%	1 mL	/
	FCS	90%	9 mL	ad 10 mL
Freezing medium for *S. aureus* glycerol stocks	Glycerol, sterile	40%	4 mL	/
	TSB-medium, sterile	60%	/	ad 10 mL
5 M LiCl	LiCl	42.39 g/mol	2.12 g	/
	Purified water	/	/	ad 10 mL
1 M $MgCl_2$	$MgCl_2$	95.22 g/mol	0.95 g	/
	Purified water	/	/	ad 10 mL
3M NaAc	NaAc	82.03 g/mol	24.6 g	/
	Purified water	/	/	ad 100 mL
5 M NaCl	NaCl	58.44 g/mol	29.22 g	/
	Purified water	/	/	ad 100 mL
10% NaDoc	NaDoc	414.56 g/mol	1 g	/
	Purified water	/	/	ad 10 mL
500 mM Na_2EDTA	Na_2EDTA x 2 H_2O	372.24 g/mol	18.61 g	/
	Purified water	/	/	ad 100 mL
1 M $NaHCO_3$	$NaHCO_3$	84.01 g/mol	0.84 g	/
	Purified water	/	/	ad 10 mL
5 M NaOH	NaOH	40.01 g/mol	20.01 g	/
	Purified water	/	/	ad 100 mL
25X PIC	Protease Inhibitor Cocktail	/	1x pill	/
	RNase-free water	/	/	2 mL
50X PIC	Protease Inhibitor Cocktail	/	1x pill	/
	RNase-free water	/	/	1 mL
100 µg/mL PMA	PMA	616.83 g/mol	0.1 mg	/
	DMSO	100%	/	ad 1 mL
1 M Tris-HCl, pH 7.5 → adjusted with HCl (37%)	TRIS	121.14 g/mol	12.1 g	/
	Purified water	/		ad 100 mL
20% Triton X-100	Triton X-100	100%	20 mL	/
	Purified water	/	/	ad 100 mL
8 M Urea	Urea	60.06 g/mol	48.48 g	/
	Purified water	/	/	ad 100 mL

Table 24: Composition of working solutions in general

Working solutions	Components	Stock conc. or % (v/v)	Final conc.	ad total volume
0.1% BSA	5% BSA, sterile	5%	0.1%	0.2 mL
	1X PBS	/	/	ad 10 mL
Collagen coating solution	Collagen I, bovine protein	5 mg/mL	50 µg/mL	0.5 mL
	Acetic acid	100%	20 mM	49.5 mL
50 mM $CaCl_2$	$CaCl_2$	2 M	50 mM	250 µL
	Purified water	/	/	ad 10 mL
50 mM K-SFM-$CaCl_2$	$CaCl_2$	2 M	50 mM	25 µL
	K-SFM w/o supplements	/	/	ad 1 mL
0.5 µg/mL PMA (working stock)	PMA	100 µg/mL	0.5 µg/mL	5 µL
	PBS	1X	/	ad 1 mL
20 mM Tris-HCl, pH 8	Tris-HCl, pH 7.5 to 8	1 M	20 mM	200 µL
	Purified water	/	/	ad 10 mL
0.1% Triton X-100	Triton X-100	20%	0.1%	50 µL
	Purified water	/	/	ad 10 mL
0.5% Triton X-100	Triton X-100	20%	0.5%	250 µL
	Purified water	/	/	ad 10 mL

Table 25: Composition of transfection buffers

Buffer	Components	Stock conc. or % (v/v)	Final conc.	ad total volume
2 M $CaCl_2$ → sterile filtration (0.22µm)	$CaCl_2$	110.98 g/mol	22.19 g	/
	Purified water	/	/	ad 100 mL
2X HBS transfection buffer, pH 6.8 to 7 (optimized [108]) → adjusted with HCl (37%) → sterile filtration (0.22 µm)	NaCl	58.44 g/mol	270 mM	8 g
	KCl	74.55 g/mol	9.9 mM	0.37 g
	Glucose	180.16 g/mol	11.1 mM	1 g
	HEPES	230.30 g/mol	43.3 mM	5 g
	Na_2HPO_4 x 2 H_2O	177.99 g/mol	1.5 mM	0.13 g
	Purified water	/	/	ad 500 mL

Table 26: Composition of buffers used for protein harvesting

Buffer	Components	Stock conc. or % (v/v)	Final conc.	ad total volume
1X lysis buffer stock	Tris-HCl (pH 7.5)	1 M	20 mM	4 mL
	NaCl	5 M	150 mM	6 mL
	Na_2EDTA	500 mM	1 mM	0.8 mL
	EGTA	250 mM	1 mM	0.4 mL
	Triton X-100	20%	1%	10 mL
	β-glycerophosphate	100 mM	1 mM	2 mL
	Purified water	/	/	ad 200 mL
6X Laemmli buffer	Tris-HCl (pH 6.8)	1 M	350 mM	17.5 mL
	Glycerol	100%	30%	15 mL
	SDS pellets	100%	5 g	/
	DTT	100%	4.65 g	/
	Bromophenol blue	100%	somewhat	/
	Purified water	/	/	ad 50 mL

Table 27: Composition of buffers used for SDS-PAGE and immunoblotting

Buffer	Components	Stock conc., MW or % (v/v)	Final amount	ad total volume
10% APS	APS	228.20 g/mol	10 g	/
	Purified water	/	/	ad 100 mL
5% membrane blocking buffer (5% blocking milk)	Nonfat dry milk powder	100%	5 g	/
	PBS	1X	/	ad 100 mL
0.01% PBS-Tween (PBST)	Tween 20	100%	0.01%	1 mL
	PBS	1X	/	ad 1 L
10X protein buffer	Glycine	75.07 g/mol	185 g	/
	TRIS	121.14 g/mol	30 g	/
	Purified water	/	/	ad 1 L
Running gel buffer: 1.5 M Tris-HCl, pH 8.8 → adjusted with HCl (37%)	TRIS	121.14 g/mol	181.71 g	/
	Purified water	/		ad 1 L
Stacking gel buffer: 0.5 M Tris-HCl, pH 6.8 → adjusted with HCl (37%)	TRIS	121.14 g/mol	30.29 g	/
	Purified water	/		ad 500 mL
10% SDS	SDS pellets	288.38 g/mol	10 g	/
	Purified water	/	/	ad 100 mL
1X SDS-PAGE running buffer	10X protein buffer	10X	1X	100 mL
	10% SDS	10%	1%	10 mL
	Purified water	/	/	ad 1 L
Transfer buffer	10X protein buffer	10X	1X	100 mL
	EtOH	96%	19%	200 mL
	Purified water	/	/	ad 1 L

Table 28: Composition of buffers used for chromatin fractionation

Buffer	Components	Stock conc., MW or % (v/v)	Final conc.	ad total volume
Fractionation buffer A →pH adjusted to 6.8 to 7 →sterile filtration (0.22 µm)	HEPES	1 M	10 mM	1 mL
	KCl	1 M	10 mM	1 mL
	$MgCl_2$	1 M	1.5 mM	150 µL
	D-sucrose	342.30 g/mol	340 mM	11.56 g
	Glycerol	100%	10%	10 mL
	Purified water	/	/	ad 100 mL
	Add fresh per 1 mL:			
	DTT	1 M	1 mM	1 µL
	Protease Inhibitor Cocktail	25X	1X	8 µL
Fractionation buffer B →pH adjusted to 8	Na_2EDTA	500 mM	3 mM	600 µL
	EGTA	250 mM	0.2 mM	8 µL
	DTT	1 M	1 mM	10 µL
	Protease Inhibitor Cocktail	25X	1X	400 µL
	Nuclease-free water	/	/	ad 10 mL

Table 29: Composition of buffers used for chromatin immunoprecipitation (ChIP)

Buffer	Components	Stock conc. or % (v/v)	Final conc.	ad total volume
Bead Wash buffer (at RT)	BSA	5%	0.2%	40 µL
	Incubation buffer w/o SDS	5X	1X	1 mL
ChIP buffer A (at RT) → sterile filtration (0.22 µm)	NaCl	5 M	100 mM	1 mL
	Na_2EDTA (pH 8.0)	500 mM	1 mM	100 µL
	EGTA (pH 8.0)	250 mM	0.5 mM	100 µL
	HEPES	1 M	50 mM	2.5 mL
	Purified water	/	/	ad 50 mL
ChIP buffer B (at 4°C) → sterile filtration (0.22 µm)	Triton X-100	20%	0.25%	625 µL
	Na_2EDTA (pH 8.0)	500 mM	10 mM	1 mL
	EGTA (pH 8.0)	250 mM	0.5 mM	100 µL
	HEPES	1 M	20 mM	1 mL
	Purified water	/	/	ad 50 mL
ChIP buffer C (at 4°C) → sterile filtration (0.22µm)	NaCl	5 M	150 mM	2 mL
	Na_2EDTA (pH 8.0)	500 mM	1 mM	100 µL
	EGTA (pH 8.0)	250 mM	0.5 mM	100 µL
	HEPES	1 M	50 mM	2.5 mL
	Purified water	/	/	ad 50 mL
Elution buffer (at RT) → sterile filtration (0.22 µm)	SDS	10%	1%	5 mL
	NaHCO3	1 M	100 mM	5 mL
	Purified water	/	/	ad 50 mL
1.25 M glycine → sterile filtration (0.22 µm)	Glycine	75.07 g/mol	11.26 g	/
	Purified water	/	/	ad 100 mL
5X incubation buffer w/o SDS (at RT) → sterile filtration (0.22 µm)	Triton X-100	20%	5%	12.5 mL
	NaCl	5 M	0.75 M	7.5 mL
	Na_2EDTA (pH 8.0)	500 mM	5 mM	500 µL
	EGTA (pH 8.0)	250 mM	2.5 mM	500 µL
	HEPES	1 M	100 mM	5 mL
	Purified water	/	/	ad 50 mL
5X incubation buffer with SDS (at RT) → sterile filtration (0.22 µm)	SDS	10%	0.75%	3.75 mL
	Triton X-100	20%	5%	12.5 mL
	NaCl	5 M	0.75 M	7.5 mL
	Na_2EDTA (pH 8.0)	500 mM	5 mM	500 µL
	EGTA (pH 8.0)	250 mM	2.5 mM	500 µL
	HEPES	1 M	100 mM	5 mL
	Purified water	/	/	ad 50 mL
1X incubation buffer (at 4°C)	PIC	25X	1X	40 µL
	SDS	10%	1% (total)	22.5 µL
	Incubation buffer with SDS	5X	1X	1 mL
Protein-DNA crosslinking buffer (1% PFA)	Formaldehyde (PFA)	16%	1%	625 µL
	ChIP buffer A	/	/	787 µL
	PBS	1X	/	ad 10 mL
Protein-Protein crosslinking buffer	DSG in DMSO	0.25 M	2 mM	80 µL
	$MgCl_2$	1 M	1 mM	10 µL
	PBS	1X	/	ad 10 mL
Wash buffer 1 (at 4°C) → sterile filtration (0.22 µm)	SDS	10%	0.1%	500 µL
	NaDOC	10%	0.1%	500 µL
	Triton X-100	20%	1%	2.5 mL
	NaCl	5 M	150 mM	1.5 mL
	Na_2EDTA (pH 8.0)	500 mM	1 mM	100 µL
	EGTA (pH 8.0)	250 mM	0.5 mM	100 µL
	HEPES	1 M	20 mM	1 mL
	Purified water	/	/	ad 50 mL

Buffer	Components	Stock conc. or % (v/v)	Final conc.	ad total volume
Wash buffer 2 (at 4°C) → sterile filtration (0.22 µm)	SDS	10%	0.1%	500 µL
	NaDoc	10%	0.1%	500 µL
	Triton X-100	20%	1%	2.5 mL
	NaCl	5 M	150 mM	5 mL
	Na_2EDTA (pH 8.0)	500 mM	1 mM	100 µL
	EGTA (pH 8.0)	250 mM	0.5 mM	100 µL
	HEPES	1 M	20 mM	1 mL
	Purified water	/	/	ad 50 mL
Wash buffer 3 (at 4°C) → sterile filtration (0.22 µm)	LiCl	5 M	250 mM	2.5 mL
	NaDoc	10%	0.5%	2.5 mL
	NP-40	10%	0.5%	2.5 mL
	Na_2EDTA (pH 8.0)	500 mM	1 mM	100 µL
	EGTA (pH 8.0)	250 mM	0.5 mM	100 µL
	HEPES	1 M	20 mM	1 mL
	Purified water	/	/	ad 50 mL
Wash buffer 4 (at 4°C) → sterile filtration (0.22 µm)	Na_2EDTA (pH 8.0)	500 mM	10 mM	100 µL
	EGTA (pH 8.0)	250 mM	5 mM	100 µL
	HEPES	1 M	200 mM	1 mL
	Purified water	/	/	ad 50 mL

Table 30: Composition of buffers used for genotyping

Buffer	Components	Stock conc. or % (v/v)	Final conc.	ad total volume
6X genotyping loading dye → pH adjusted to 8	Glycerol	100%	60%	6 mL
	Tris-HCl, pH 7.6	1 M	10 mM	100 µL
	Na_2EDTA	500 mM	60 mM	1.2 mL
	Nuclease-free water	/	/	2.7 mL
Genotyping buffer (50 µL per sample)	NaOH	1 M	20 mM	200 µL
	Na_2EDTA	500 mM	0.1 mM	2 µL
	Purified water	/	/	ad 10 mL

Table 31: Composition of tris-acetate-EDTA (TAE) buffer for agarose gels

Buffer	Components	Stock conc. or % (v/v)	Final conc.	ad total volume
50X TAE → pH adjusted to 8	Tris	121.14 g/mol	2 M	242.2 g
	Na_2EDTA	500 mM	50 mM	100 mL
	Glacial acetic acid	60.05 g/mol	5.7%	57.1 mL
	Purified water	/	/	ad 1 L
1X TAE	50X TAE	50X	1X	20 mL
	Purified water	/	/	ad 1L

Table 32: Composition of buffers used for FACS analysis

Buffer	Components	Stock conc. or % (v/v)	Final conc.	Volume
skin FACS digest solution (1 mL per sample)	Liberase TM	2 mg/mL	250 µg/mL	125 µL
	DNase I (diluted in HBSS)	10 mg/mL	100 µg/mL	10 µL
	$CaCl_2$	50 mM	0.5 mM	10 µL
	Basal RPMI medium w/o supplements	/	/	855 µL
FACS buffer (50 mL preparation)	FCS	100%	5%	2.5 mL
	Na_2EDTA	500 mM	1 mM	100 µL
	PBS	/	/	47.4 mL

Table 33: Composition of stock and working solutions for antigen retrieval

Buffer	Components	Stock conc. or MW	Final conc.	ad total volume
Citrate stock buffer, pH 6	Tri-Sodium citrate dihydrate	294.1 g/mol	100 mM	29.41 g
→ adjusted with HCl (37%)	Purified water	/		ad 1 L
10 mM Citrate buffer, pH 6	Citrate buffer, pH 6	100 mM	10 mM	100 mL
→ adjusted with HCl (37%)	Purified water	/		ad 1 L
EDTA stock buffer, pH 8	$Na_2EDTA \times 2\ H_2O$	372.24 g/mol	10 mM	3.72 g
→ adjusted with 5 M NaOH	Purified water	/		ad 1 L
1 mM EDTA buffer, pH 8	EDTA buffer, pH8	10 mM	1 mM	100 mL
→ adjusted with 5 M NaOH	Purified water	/		ad 1 L

Table 34: Composition of blocking buffer for immunofluorescence

Buffer	Components	MW or % (v/v)	Final conc.	ad total volume
IF blocking buffer	DEPC (heat inactivated)	162.14 g/mol	0.1%	10 µL
	Saponin	100%	0.1%	10 µL
	Ribolock RNase Inhibitor	40 U/µL	10 U/µL	4 µL
	Normal Chicken Serum	100%	10%	1 mL
	PBS	/	1X	ad 10 mL

2.12 Technical devices

Table 35: Equipment and technical devices

Technical devices	Company
Agarose gel chamber Perfect Blue	VWR International GmbH, Germany
Bioruptor (sonicator, cooling pump)	Diagenode, United States
Cell Casting Module Mini-PROTEAN Tetra	Biozym, Germany
Cell counting chamber Neubauer improved	Brand, Germany
Centrifuge 5427 R with cooling function	Eppendorf, Germany
Centrifuge Biofuge fresco	Heraeus, Thermo Scientific Germany
Centrifuge Multifuge 3L-R or X3R	Heraeus, Thermo Scientific Germany
Centrifuge Oico	Heraeus, Thermo Scientific Germany
ChemiDoc MP Imaging system	BioRad, Germany
CO_2 incubator for cell culture, HeraCell 150 or 240	Heraeus, Thermo Scientific Germany
CO_2 incubator for cell culture, Typ CB 150	Binder GmbH, Germany
Cycler CFX384 C100 Touch for qPCR	BioRad, Germany
EVOS fl inverted digital fluorescence microscope	Advanced Microscopy Group, United States
Freezer -20°C	Liebherr, Germany; Bosch, Germany
Fusion FX imager camera system	Vilber Lourmat, Germany
GentleMACS Octo tissue dissociator	Miltenyi Biotec B.V. & Co. KG, Germany
HERAfreeze -80°C	Heraeus Thermo Scientific, Germany
Hidex Sense micro plate reader	Hidex, Germany
Ice maschine	Scotsman Ice Systems, Italy
Incubating orbital shaker Professional 3500	VWR International GmbH, Germany
Incubator orbital shaker MaxQ	Thermo Scientific, Germany
Incubator standard, Typ BD23 or 240 (Microbiology)	Binder GmbH, Germany
Inverted microscope Eclipse TS100	Nikon Europe B.V., Netherlands
Isofluran Vaporizer (mobile station)	Rothacher Medical GmbH, Switzerland
Laminar flow cabinet BSK/4 N°6796	Antair BSK-4
Laminar flow cabinet Hera Safe	Heraeus Thermo Scientific, Germany
Light Cycler 480 II	Roche Diagnostics AG, Switzerland
Liquid nitrogen tank ARPEGE 110	CRYOPAL, France
LSR II flow cytometer	BD Becton Dickson, United States
Magnet DynaMag-2	Thermo Fisher Scientific, Germany
Magnetic stirrer	IKA, Germany
Membrane vacuum pump LABOPORT	KNF group, Germany
Microwave Severin 800	SEVERIN Elektrogeräte GmbH, Germany
Minifuge MiniStar	VWR International GmbH, Germany
Mr. Frosty Cell freezer container	Thermo Scientific, Germany
NanoDrop ND-2000 spectrophotometer	PeqLab, Germany
Nano Zoomer 2.0HT	Hamamatsu Photonics K.K., Japan
PCR thermocycler Doppio	VWR International GmbH, Germany
pH-meter WTW-720	SI Analytics, Xylem Analytics Germany
Pipets Eppendorf Research Series 2100 (0.1-2.5 µL; 2-20 µL; 20-200 µL; 100-1000 µL)	Eppendorf, Germany
PowerSupply Perfect Blue	VWR International GmbH, Germany
PowerSupply PowerPac 1000	BioRad, Germany
Printer HL-5380DN	Brother International GmbH, Germany

Technical devices	Company
Qubit Flex Fluorometer	Qubit Thermo Scientific, Germany
Refrigerator 4°C	Liebherr, Germany
Rice steamer 19750-56 (Histology)	RusselHobbs GmbH, Germany
Rotating sample mixer	Dynal Inc., United States
Safety suction system EcoVac	schuett-biotec GmbH, Germany
Scale	Sartorius, Germany
Scantainer Uniprotect NG M	ZOONLAB GmbH, Germany
Shaker Polymax 2040	Heidolph Scientific Products, Germany
Thermo shaker	CellMedia, Germany
Thermomixer comfort	Eppendorf, Germany
Tube roller	VWR International GmbH, Germany
Tube Roller, iRoll Digital	Biozym, Germany
Vac-Man laboratory vacuum manifold #A7231	Promega GmbH, Germany
Vertical autoclave VX	Systec GmbH & Co. KG, Germany
Vertical Electrophoresis Cell Mini Trans-Blot Module, Mini-PROTEAN Tetra	Biozym, Germany
Vis-spectral photometer V-1200	VWR International GmbH, Germany
Vortexer Reax 2000	Heidolph Scientific Products, Germany
Vortex-Genie 1 or 2	Scientific Industries Inc., United States
Water bath TW 20	Julabo Labortechnik, Germany
Zeiss LSM 800 confocal microscope	Carl Zeiss, Germany

2.13 Software

Table 36: Computer software and web-based programs

Software	Company
AxioVision 3.0	Carl Zeiss, Germany
BioRender	Science Suite Inc., Canada (licenced via Research Center for Immunotherapy FZI, Johannes Gutenberg University Mainz) For Publication licences see *chapter 6.1*.
CFX Manager Software	qPCR cycler software; BioRad, Germany
CLC Genomics workbench (v24.0)	QIAGEN Digital Insight, the Netherlands
EnrichR-KG	Gene set enrichment analysis (GSEA), web-server search engine [109] (https://maayanlab.cloud/enrichr-kg)
FlowJo	Tree Star Inc., United States
GraphPad Prism	GraphPad Software Inc., United States
Hidex plate reader software	Hidex, Germany
ImageJ, Win64	NIH (National Institutes of Health), United States
ImageJ Dot blot analyzer, Win64	NIH (National Institutes of Health), United States
Microsoft Office	Microsoft, United States
Morpheus software	Borad Institute, United States (https://software.broadinstitute.org/morpheus)
NanoDrop Software	PeqLab, Germany
Primer3web (v4.1.0)	Whitehead Institute for Biomedical Research, United States; web-interface to Primer3 [110-112] (https://primer3.ut.ee/)
Primer-BLAST	National Center for Biotechnology Information (NCBI), United States [113] (https://www.ncbi.nlm.nih.gov/tools/primer-blast/)
QuPath (v-0.4.3)	Open-source software for digital pathology image analysis [114]
UCSC genome browser using human genome (GRCh38/hg38)	Genomics Institute University of California Santa Cruz, United States [115, 116] (https://genome.ucsc.edu/)
Zen Blue, Version 3	Carl Zeiss, Germany

3. Methods

Consumables and reagents used in this study are listed in greater detail in *chapters 2.2* to *2.7*, while prepared solutions and buffer compositions are further explained in *chapter 2.11* (see ***Table 23*** to ***Table 34***).

3.1 Microbiology

3.1.1 Preparation of media and agar plates for bacteria strains

For competent *Escherichia coli* (*E. coli*) LB-medium or LB-agar, for *Staphylococcus* strains Tryptic Soy Broth (TSB-) medium or TSB-agar (reagents listed in ***Table 5***) were completely dissolved in purified water according to manufacturer's protocols, immediately sterilized in the autoclave and subsequently kept at 4°C until usage. For antibiotic selection, fresh LB-Amp medium was prepared via addition of 100 µg/mL ampicillin to LB-medium when needed. Solidified agar medium was heated in the microwave and completely dissolved before it was poured into sterile petri dishes below the laminar flow cabinet. If antibiotics were required, the melted agar was cooled down to approx. 50°C before adding 100 µg/mL ampicillin.

3.1.2 Transformation of *E. coli*

The plasmids used for luciferase assays, overexpression or knockdown experiments were all amplified in purchased competent NEB 5-alpha *E. coli* with high transformation efficiency (Cat. C2987H, New England Biolabs), which were stored in aliquots of 50 µL in 1.5 mL reaction tubes at -80°C until usage. For transformation, an aliquot was slowly thawed on ice, mixed with 1 µg plasmid DNA (purchased or provided by Stephan Hailfinger) and further incubated for 30 min on ice. Subsequently, competent *E. coli* bacteria were heat-shocked for 45 sec at 42°C in a thermo shaker and cooled down for 2 min on ice. The volume was filled up to 1 mL using 950 µL of pre-warmed LB-medium without antibiotics and the transformed *E. coli* were incubated for 1 h at 37°C, 600 rpm on a thermo shaker. LB-agar plates were supplemented with 100 µg/mL ampicillin were pre-warmed at 37°C in the incubator. After incubation, 100 µL of the transformed *E. coli* cultures were plated on LB-Amp agar for antibiotic selection and incubated overnight at 37°C. The next day, a single colony was picked using a pipette tip and inoculated in 5 mL (Mini-prep; Cat. EC03.1, Carl Roth) or 50 mL (Midi-prep, Erlenmeyer glass beaker) LB-Amp medium, which was cultivated approx. 17 h in a shaking incubator at 37°C, 200 rpm.

3.1.3 Glycerol stocks of transformed *E. coli*

500 µL of the bacteria culture were mixed quickly with 500 µL *E. coli* freezing medium (see ***Table 23***), in a cryo tube and stored at -80°C. Using a sterile inoculation loop, 50 to 100 mL of LB-Amp medium were inoculated with the prepared glycerol stock. The culture was incubated overnight at 37°C, shaking at 200 rpm.

3.1.4 Preparation of plasmid DNA

Extraction of plasmid DNA from 5 mL overnight culture was performed using the GeneJET Plasmid Miniprep Kit (Cat. K0503, Thermo Fisher) according to the manual. Prepared DNA was eluted in 50 µL elution buffer provided in the kit. For higher amounts, 50 to 100 mL of overnight culture were centrifuged (45 min, 4,500 rpm at 4°C). The supernatant was discarded, and plasmid DNA was further extracted from the bacteria pellets using either NucleoBond Xtra Maxi Kit (centrifugation-based; Cat. 740414, Macherey-Nagel) or PureYield Plasmid Midiprep system (Cat. A2495; Promega) according to the manufacturer's instructions. For the latter, column binding and washing were performed under vacuum using the vacuum manifold Vac-Man (Cat. A7231, Promega). Plasmids were eluted via centrifugation using 200 µL nuclease-free water.
After extraction, each plasmid concentration was determined using NanoDrop ND-2000 (PeqLab, Germany) and adjusted to a final concentration of 1 µg/mL using nuclease-free water. The plasmid DNA was stored at -20°C until further usage to avoid frequent thawing, bigger volumes of plasmid DNA were aliquoted.

3.1.5 Cultivation and propagation of *Staphylococcus* strains

The pathogenic, methicillin-resistant *S. aureus* USA300 wild-type LAC strain (assigned *S. aureus* USA300), as well as cultures of the *Staphylococcus epidermidis* wild-type 1457 strain (assigned *S. epidermidis*), were kindly provided by Bernhard Krismer and Birgit Schittek from the Eberhard Karls University, Tübingen.
Bacterial stocks were frozen at -80°C for long term storage in *S. aureus* freezing medium (see ***Table 23***). To generate living *S. aureus or S. epidermidis* cultures, small amounts of the bacterial stocks were plated on TSB agar plates without antibiotics, using a sterile inoculation loop, then the plates were incubated overnight at 37°C. The next day, agar plates with a fully grown bacterial lawn were sealed with parafilm and stored in the fridge at 4°C for a maximum of 2.5 weeks for repetitive *in vitro* experiments.
For *in vivo* studies, cultures were exclusively inoculated from freshly grown *S. aureus* agar plates 2 days before start of the experiment. In general, both *Staphylococcus* strains were cultivated and maintained without any antibiotic selection and all experimental procedures, explained in the following for *S. aureus,* were equally applied to *S. epidermidis* infections *in vitro*.

3.1.6 *S. aureus* preparation for infection experiments

For infection experiments, an overnight culture of 40 mL sterile TSB medium was inoculated with a sterile pipette tip using living *S. aureus* colonies from the plated agar stock. The culture was kept in a sterilized Erlenmeyer flask for 14 to 17 h at 37°C in an orbital shaking incubator (200 rpm). The next day, fresh 40 mL TSB-medium was inoculated with 400 µL overnight culture (1:100 dilution) and incubated under equal shaking conditions for approx. 2 h until the bacteria reached an optical density at 600 nm (OD_{600}) of 0.45 to 0.55, corresponding to their log-growth phase. OD_{600} was measured using the Vis-spectral photometer V-1200 (VWR), TSB medium served as blank solution. When reaching the log-growth phase and thus, optimal infection efficiency, the bacteria culture was transferred to a 50 mL centrifugation tube. The day culture was centrifuged in a pre-cooled centrifuge (5 min, 4,000 rpm at 4°C) and the supernatant was carefully sucked off from the pellet under a sterile laminar flow bench. The pellet was washed once in approx. 20 mL PBS, centrifuged (5 min, 4,000 rpm at 4°C), resuspended in a certain volume of medium or PBS depending on its following utilization (see ***Table 37***) and finally transferred to a new reaction tube. Resuspended bacteria were kept on ice all the time to decelerate bacterial growth and to keep the concentration preferably stable for the subsequent infection experiments.

Table 37: Volumes and media for S. aureus infection experiments

Target cells (ca. cell numbers)	**Blank/ target cell medium**	***S. aureus* resuspension**	**Bacteria for OD_{600}**	**Infection**	**Applied bacteria**
hKC $3.5*10^5$ /6-well	CnT-07 basal medium, w/o supplements	5 mL	undiluted	MOI30	$1.05*10^7$ per 6-well
hKC $3.4*10^6$ /10 cm dish	CnT-07 basal medium, w/o supplements	5 mL	undiluted	MOI30	$1.02*10^8$ per 20 cm plate
hKC $6.6*10^6$ /20 cm dish	CnT-07 basal medium, w/o supplements	5 mL	undiluted	MOI30	$1.98*10^8$ per 20 cm plate
mKC $3.5*10^5$ /6-well	K-SFM medium, w/o supplement	5 mL	undiluted	MOI30	$1.05*10^8$ per 6-well
in vivo	PBS	1 mL	1:50 dilution	$1*10^8$ CFU	100 µL per animal

3.1.7 Calculation of the required amount of *S. aureus*

OD_{600} was measured (undiluted or 1:50 diluted) to determine the final bacteria concentration, which is calculated as follows:

$$OD_{600}\ \text{value} * 10^8\ \frac{\text{bacteria}}{\text{mL}} = \text{X} * 10^8\ \text{bacteria/mL (in respective medium/ PBS)}$$

For all *in vitro* experiments, comprising the infection of both human and murine keratinocytes with living bacteria, target cells were infected using a multiplicity of infection of 30 (MOI 30). Proceeding from a total cell number of approx. $3.5*10^5$ keratinocytes per 6-well at the time of infection, a total of $1.05*10^8$ bacteria were applied. Cell numbers and the amount of bacteria required for 10 cm or 20 cm dishes are presented in ***Table 37***, respectively. After calculating the exact volume of live *S. aureus* (MOI30) to infect the target cells, bacteria were directly added to the seeded cells, considering the volume of medium being 1 mL in case of 6-wells, 13 mL medium per 20 cm plate.
For *in vivo* experiments, $1*10^8$ colony forming units (CFUs) of live *S. aureus* were applied to the back skin of each animal within a volume of 100 µL PBS, therefore a bacteria stock of $1*10^9$ CFU/mL was prepared.

3.1.8 Generation of heat-inactivated *S. aureus* (*HiSa*) cultures

To obtain heat-inactivated *S. aureus* (*HiSa*) cultures the bacteria were cultivated, and concentration was determined as explained above. Likewise, the number of bacteria was calculated, however the volume per 6-well was multiplied by 2. Therefore, an aliquot of live *S. aureus* with the determined bacteria concentration was transferred to a 1.5 mL reaction tube and boiled for 1 h at 90°C with mild shaking (100 rpm) in a thermo shaker, before the *HiSa* was frozen for at least 4 h at -20°C before usage. Infection was carried out as explained before, namely a certain volume of 2x *HiSa* cultures was directly added to the seeded target cells.

3.2 Cell culture

To assure sterility during *in vitro* experiments, the individual steps of this chapter were conducted exclusively below the laminar flow bench.

3.2.1 Collagen coating of plasticware for primary keratinocyte cultivation

For the cultivation or maintenance of both human and murine primary keratinocytes cell culture dishes and plates were freshly coated in advance to enable proper cell adherence. The surface of required cell culture plasticware (6-well, 10 cm or 20 cm) was sufficiently covered with sterile collagen coating solution (see ***Table 24***) and incubated for approx. 30 min at 37°C. Afterwards, the light-sensitive collagen solution was removed and kept in the fridge at 4°C, being re-usable for max. 10 times. The plastic ware was washed once with PBS to remove acid residues potentially harming primary cells.

3.2.2 Isolation of primary human keratinocytes from foreskin

For the preparation of human foreskin, fat tissue was first removed from the biopsies using shears and forceps, and the tissue was washed once with PBS. Tissue of one foreskin was carefully placed into a 10 cm petri dish filled with approx. 3 mL digest solution (see ***Table 23***), composed of equal volumes of basal CnT-07 medium (Cat. CnT-07, CELLnT) without supplements, and Dispase solution (5 U/mL, Cat. 07913, StemCell). It was ensured that only the dermal side was facing the digestion solution while the epidermal part remained uncovered. The digest was incubated overnight at 4°C.
The next day, the epidermis was carefully separated from the digested dermis and placed onto approx. 2 mL Trypsin-EDTA solution (0.05%, Cat. 25300054, Thermo Fisher Scientific), in a fresh petri dish. After 15 min incubation at room temperature (RT), DMEM medium supplemented with 10% fetal calf serum (FCS, Cat. F7524, Sigma-Aldrich) and 1% penicillin/streptomycin solution (P/S, Cat. P0781, Sigma-Aldrich) was added to stop the digestion. Basal keratinocytes were carefully washed out from tissue until the epidermis appeared transparent and the solution was turbid.
Afterwards, the solution was transferred to a 50 mL centrifugation tube using a 100 µm cell strainer and centrifuged (5 min, 1,000 rpm at RT). Supernatant was sucked off from the cell pellet, and the freshly isolated human keratinocytes (hKC) were resuspended in supplemented hKC medium for cultivation. Tissue material was provided by the Department of Urology and Pediatric Urology of the University Medical Center Mainz.

3.2.3 Isolation of primary murine keratinocytes from mouse tails

Mouse tails were swiped in 70% isopropanol before they were cut open lengthways. The entire skin was peeled off from the tail bone, transferred into a 15 mL reaction tube and completely covered with approx. 0.75 mL per tail digestion solution (see ***Table 23***), containing equal volumes of basal Keratinocyte-SFM medium without supplements (K-SFM, Cat. 17005034, Thermo Fisher Scientific) with purchased Dispase solution. Digestion was carried out overnight at 4°C. The next day, the epidermal layer was removed from the tail tissue. Isolation of murine keratinocytes (mKC) was conducted similarly as previously described for human keratinocytes. Since the number of keratinocytes per one tail is sufficient to seed a maximum of five 6-wells, 2 to 4 tails per genotype, e.g. control and knockout animals, were pooled in advance. In the end, cell pellets were resuspended in the required volume of mKC medium supplemented with 0.05 mM $CaCl_2$ and seeded on pre-coated cell culture dishes. In case of mKC isolated from *Zc3h12a*$^{Rosa26\text{-}creERT2}$ mice, knockout induction was achieved via pre-treatment of the seeded cells for 4 days with 1 µM (Z)-4-Hydroxy-Tamoxifen (OH-Tamoxifen, Cat. H7904, Sigma), which was diluted in medium from a stock solution (see ***Table 23***). Detailed information of respective mouse lines is further listed in ***Table 1***.

3.2.4 Cultivation, maintenance and seeding of adherent cells

Freshly isolated mKC were seeded and maintained in supplemented K-SFM medium (Cat. 17005034 and 37000015, Thermo Fisher Scientific) with 1% P/S and 0.05 mM $CaCl_2$. The cells were cultivated until reaching approx. 80% confluency before experiments were conducted, with medium exchanges every 4 days.

Human primary keratinocytes were maintained, cultivated, and seeded in CnT-07 epithelial proliferation medium in the presence of supplements and 0.2% antibiotics comprising final concentrations of 10 µg/mL gentamicin and 0.25 µg/mL amphotericin B (Gent/Amph B, Cat. R01510, Thermo Fisher Scientific). For antibiotic selection of lentiviral knockdown or overexpression cells, the medium was additionally supplemented with 1 µg/mL puromycin (Cat. ant-pr-1, InvivoGen).

Both HEK293T cells and HaCaT cells were maintained and seeded in low glucose DMEM medium (Cat. 31885-023, Thermo Fisher Scientific) supplemented with 10% FCS and 1% P/S. The exact composition of the respective cell culture medium and the required materials used in this study are further provided in ***Table 2*** and ***Table 3***.

In general, all adherent primary keratinocytes or cell lines were cultivated, maintained, and seeded at 37°C and 5% CO_2 under humidified conditions. When reaching a confluent growth of approx. 80 to 90%, cells were split 1:10 twice a week. Therefore, the old medium of adherent keratinocytes (primary cells, HaCaT) was removed, and the cells were washed once with pre-warmed PBS. Trypsinization was carried out by applying approx. 2 mL Trypsin-EDTA solution per 20 cm dish for approx. 10 min, before the reaction was stopped by adding 20 mL of fresh pre-warmed supplemented DMEM medium.

HEK293T cells were carefully split via direct resuspension within their medium and thus, detachment of the cells was carried out without Trypsin-EDTA. Detached and carefully resuspended HaCaT cells and HEK293T cells were counted using a counting chamber (Neubauer improved, Brand) and seeded or simply propagated in 20 mL of fresh supplemented DMEM medium per 20 cm dish.
In case of primary human keratinocytes, the trypsinization medium had to be replaced. The cell suspension was centrifuged (5 min, 1,000 rpm at RT), the medium was sucked off and the cell pellet was carefully resuspended in fresh pre-warmed supplemented hKC medium. Using a maximal passaging number of 4, hKCs were further propagated in 20 mL supplemented hKC medium per pre-coated 20 cm cell culture dish or counted and seeded, respectively. For the differentiation of hKC, the cells were seeded and cultivated 72 h in advance within supplemented hKC medium with antibiotics in the presence of 2 mM $CaCl_2$. A list of seeded cell numbers for each cell line is provided in ***Table 38***.

Table 38: Seeded cell numbers of each cell line and primary keratinocytes

Cell line	Number of seeded cells	Seeding volume	Approx. cell number at treatment start
HEK293T	$4*10^4$ /12-well	1 mL	$4*10^4$ /12-well
	$8*10^4$ /6-well	2 mL	$8*10^4$ /6-well
HaCaT	$4*10^5$ /6-well	2 mL	$4*10^5$ /6-well
Undif. hKC	$3.5*10^5$ /6-well	2 mL	$3.5*10^5$ /6-well
Diff. hKC	$1.2*10^5$ /6-well	2 mL	$3.5*10^5$ /6-well
	$4*10^5$ /10 cm dish	10 mL	$3.4*10^6$ /10 cm dish
	$1.1*10^6$ /20 cm dish	20 mL	$6.6*10^6$ /20 cm dish
mKC	5x 6-wells per tail	2 mL	$3.0 - 3.5*10^5$ /6-well

3.2.5 Freezing and thawing of adherent cells

Cell stocks of primary human keratinocytes and cell lines were stored in liquid nitrogen to ensure the usage of low cultivation passaging numbers. For freezing, all cells were washed once with PBS, trypsinized and stopped with medium supplemented with FCS as explained above. The cell suspension was centrifuged (5 min, 1,000 rpm at RT) and the remaining cell pellet dissolved in freezing medium containing 10% sterile DMSO and 90% FCS, yielding 4 aliquots á 1 mL from one fully grown 20 cm dish. The cryotubes were immediately stored at -80°C in a cell freezing container overnight before they were transferred to liquid nitrogen for long term storage. To defrost cells, cryotubes were quickly thawed, and cells were mixed with 4 mL pre-warmed DMEM medium. After centrifugation (5 min, 1,000 rpm at RT) and thus, removal of toxic DMSO, the remaining cell pellet was carefully resuspended in 18 mL of the respective cell culture medium and seeded on a 20 cm dish. Further cultivation and maintenance were carried out as explained above. Of note, primary murine keratinocytes were used immediately after cell isolation and could not be stored.

3.2.6 Generation of lentiviral NFKBIZ knockdown or IκBζ overexpression

Lipofectamine 2000 transfection method (Cat. 11668-030, InvitroGen) was conducted according to the manufacturer's instructions to generate lentiviral particles in HEK293T cells. For each condition, approx. $5*10^6$ cells were seeded per 20 cm dish in supplemented DMEM medium. The next day, prior to transfection, the total volume of medium was reduced to 8 mL before preparation of the following transfection mixtures (A) and (B). In (A), 10.5 µL Lipofectamine 2000 were pre-mixed with 2.25 mL Opti-MEM I without supplements (Cat. 51985-026, Thermo Fisher Scientific).

In (B), the same volume of medium was mixed with the following plasmids: For *NFKBIZ* knockout experiments, 4.8 µg of the second-generation packaging plasmid psPAX2 and 3 µg of VSV-G envelope-expressing vector pMD2.G were mixed in combination with either 7.5 µg empty pLKO.1-puro plasmid as control (*sh ctrl*) or 7.5 µg of pLKO.1-TRCN0000147551 plasmid encoding shRNA against *NFKBIZ* (*sh NFKBIZ)*.

For the generation of hKC with IκBζ overexpression (OE), equal amounts of packaging plasmids were used in combination with 7.5 µg of the empty mammalian expression vector pRDI292, designated as Control OE, or 7.5 µg of the Flag-tagged *NFKBIZ* overexpression construct (IκBζ OE), which had been cloned into pRDI292 empty vector. Both latter plasmids were kindly provided by Stephan Hailfinger (University Medical Center, Münster); a general list is provided in ***Table 17***.

Next, tubes (A) and (B) were mixed under constant vortexing. After 20 min incubation at RT, the individual transfection mixes were inverted and applied dropwise to the HEK293T cells seeded onto individual 20 cm dishes. Thus, each dish contained a total volume of approx. 13 mL. After 6 h, the medium of the transfected HEK293T cells was carefully replaced with supplemented hKC medium. From here onwards, all experimental procedures were carried out under S2 biosafety level conditions. The same day, hKC with low passaging numbers were seeded onto 10 cm dishes, allowing confluency of max. 50%. After 48 h and 72 h post-transfection, lentivirus-containing supernatant was collected from the transfected HEK293T cells using syringes and filtered through a 45 µm sterile filter into fresh 15 mL centrifugation tubes. To enable optimal transduction of target cells, 10 µg/mL polybrene (Cat. TR-1003-G, Sigma-Aldrich) was added to the lentivirus filtrate in a 1:1000 dilution, before replacing the medium of seeded hKC with the latter.

To control transduction efficiency in both overexpression and knockdown experiments, GFP-expressing lentivirus was generated in parallel. Expression of GFP in target cells was checked approx. 48 h post-transduction under an inverted fluorescence microscope (EVOS fl from AMG, United States). On day 3, transduced hKC were provided with freshly supplemented CnT-07 medium, and the cells were given some days to recover until proliferation was re-established. Upon successful GFP expression in the control-transduced hKC, antibiotic selection was initiated by adding 1 µg/mL puromycin solution (Cat. ant-pr, InvivoGen) into the medium. Selection was maintained all the time for four passages or until start of *in vitro* treatments.

3.2.7 Stimulation and inhibitor treatment of primary keratinocytes

All keratinocytes were pre-starved overnight in their respective cell culture media without supplements or antibiotics. For lentiviral overexpression or knockdown, the cells were additionally washed with PBS to remove remaining puromycin and avoid unspecific pre-activation. Overexpression was directly checked through Western blot via IκBζ protein levels in ctrl OE and IκBζ OE samples, *NFKBIZ* knockdown validation required treatment of *sh ctrl* and *sh NFKBIZ* samples for 1 h with 100 ng/mL IL-36α to induce IκBζ in control hKC. Besides, other human recombinant cytokines, such as IL-17A, TNFα, or IL-1β, were used to stimulate hKC. Detailed information on the used stimuli, receptor agonists, or cytokine concentrations is provided in ***Table 39*** below, information on purchased inhibitors used in this study is depicted in ***Table 40***.

To activate the intracellular NOD2 receptor, 20 µg/mL of MDP (active L-D isomer, Cat. tlrl-mdp, InvivoGen) was mixed with 2.5 µL ProteoJuice Protein transfection reagent (Cat. 71281-3, Novagen) in 100 µL non-supplemented medium per 6-well for 20 min at RT. After incubation, the volume was filled to 1 mL with medium, and MDP simulation was conducted between 1 to 24 h. Besides, hKC were transfected and treated with 1 µg/mL of NOD1 and/or NOD2 agonists (Cat. tlrl-nodkit2, InvivoGen): NOD1 agonist Tri-DAP (Tri-diaminopimelic acid), NOD1/NOD2 agonist PGN-SAndi (ultrapure peptidoglycan of *S. aureus*), or enhanced NOD2 agonist L18-MDP.

For TLR2 receptor activation, cells were treated with 10 µg/mL of TLR1/2 ligand Pam_3CSK_4 (Cat. tlrl-pms, InvivoGen) for 1, 4, or 24 h.

Table 39: Stock and working concentration of stimulating agents and cytokines

Reagent	Agonist	Stock conc.	Final conc.	Solvent
(Z)-4-Hydroxy-Tamoxifen (OH-Tamoxifen)	/	2.58 mM (≈ 1 mg/mL)	1 µM (≈ 0.4 µg/mL)	EtOH/ medium
L18-MDP (enhanced MDP-Lysin18)	NOD2	1 mg/mL	1 µg/mL	Purified water
MDP (Muramyl di-peptide active L-D isomer)	NOD2	5 mg/mL	20 µg/mL 1 µg/mL	Purified water
Pam_3CSK_4	TLR1/2	1 mg/mL	10 µg/mL	Purified water
PGN-Sandi	NOD1/NOD2	200 µg/mL	1 µg/mL	Purified water
rh IL-36α ΔN	/	100 µg/mL	100 ng/mL 20 ng/mL	20 mM Tris-HCl, pH 8
rh IL-17A	/	200 µg/mL	200 ng/mL 100 ng/mL	0.1% BSA in PBS
rh TNFα	/	100 µg/mL	10 ng/mL	0.1% BSA in PBS
rh IL-1β	/	100 µg/mL	100 ng/mL 20 ng/mL	0.1% BSA in PBS
Tri-DAP (Tri-diaminopimelic acid)	NOD1	1 mg/mL	1 µg/mL	Purified water

Primary keratinocytes were further pre-treated in the presence or absence of small molecule inhibitors and their respective solvent (see ***Table 40***): IKKβ inhibitor IMD 0354 (Cat. S2864, Selleckchem), STAT1/STAT3 inhibitor Stattic (Cat. S7024, Selleckchem), indirect inhibition of NOD2 receptor signaling via RIPK2 inhibitor GSK583 (Cat. S8261, Selleckchem), TLR2 receptor inhibitor (Cat. TL2-C29, InvivoGen), and inhibition of bacterial internalization using cytochalasin D (CytoD, Cat. 11330-1, Cayman).

Table 40: Stock and working concentration of inhibitors

Inhibitor	Target	Pre-treatment	Stock conc.	Final conc.	Solvent
Cytochalasin D (CytoD)	Bacteria internalization	/	50 mM 1 mM (working stock)	0.5 µM	DMSO
GSK583	RIPK2	overnight	10 mM	5 µM, 1 µM	DMSO
IMD 0354	IKKβ	2 h	10 mM	10 µM	DMSO
Stattic	STAT3	2 h	10 mM	10 µM	DMSO
TL2-C29	TLR2	2 h	50 mM	50 µM	DMSO

3.2.8 *S. aureus* infection of human and murine keratinocytes

The day before infection, murine and differentiated human keratinocytes were washed once with PBS to remove any antibiotics or $CaCl_2$. The cells were starved overnight in their respective non-supplemented cell culture media. In case of inhibitor treatment, starvation, infection, and further incubation were carried out in the presence of RIPK2 and TLR2 inhibitors or their vehicle controls, respectively (see ***Table 40***).

In vitro infection was carried out using a MOI 30 of either live *S. aureus* USA300 WT cultures or *HiSa* suspensions, as explained before. Keratinocytes were incubated for 1 h at 37°C. Afterwards, the cells were washed twice with PBS to remove excessive bacteria in the culture dishes. Samples were harvested directly for immunoblot analysis or further incubated for 1 to 23 h at 37°C and 5% CO_2 in a humidified atmosphere using basal cell culture media with 1% P/S for mKC or 0.2% Gent/Amph B antibiotics for hKC to kill external bacteria. Keratinocytes were washed twice again with sterile PBS and samples were harvested for immunoblot, RNA, chromatin fractionation, or chromatin immunoprecipitation (ChIP) analysis.

3.2.9 *S. aureus* internalization assay

To assess the capacity of *S. aureus* to internalize into primary keratinocytes, hKC and mKC were seeded in duplicates or triplicates in 6-well plates, which were infected for 1 h with further incubation for 23 h with antibiotics, as explained above.

24 h post-infection, the adherent cells were washed twice with PBS before being trypsinized at 37°C for approx. 15 min using 0.5 mL Trypsin-EDTA per 6-well. Detachment reaction was stopped for each sample individually using 4.5 mL DMEM medium supplemented with 10% FCS. The cells were scraped and carefully resuspended before the cell suspensions were transferred to individual 15 mL centrifugation tubes. After centrifugation (5 min, 1,000 rpm at 4°C) the supernatant was carefully sucked off.

Cell pellets were washed once with PBS under equal centrifugation conditions, then each sample was resuspended in 1 mL 0.1% Triton X-100 in PBS to start mild cell lysis at RT for 1 h.

Lysed cell suspension was thoroughly resuspended and strongly vortexed. 20 µL of each sample (undiluted or 1:10 diluted in PBS) was plated on pre-warmed TSB agar plates in duplicates. After incubation overnight for approx. 15 h at 37°C in a standard incubator, colony-forming units (CFUs) were counted manually to calculate the relative internalized *S. aureus* CFUs per mL of each sample.

3.3 Molecular biology

3.3.1 Design of gene expression or ChIP primers

All gene expression or ChIP primers used for quantitative real-time polymerase chain reaction (qPCR) in this study were self-designed by our working group.

Design of human and murine gene expression primers was conducted using the Nucleotide database and the open-source Primer-BLAST program from NCBI [113] (https://www.ncbi.nlm.nih.gov/tools/primer-blast/), which is based on the Primer3web software [110-112] (https://primer3.ut.ee/) used for ChIP primer design. Design criteria are listed in ***Table 41***.

Table 41: Design criteria for gene expression and ChIP primers

Parameters	Gene expression primers	ChIP primers
Template size	50 to 150 bp	50 to 150 bp
Primer size	18 to 24 nt	18 to 24 nt
GC content	40 to 60 %	40 to 60 %
GC clamp	1	1
Melting temperature	58.0 to 62.0°C	58.0 to 62.0°C
Max Poly-X	3	5
Max 3' stability	5	5
Max Self Complementarity	4	3
Intron inclusion	yes	no

Human and murine mRNA sequences obtained from the Nucleotide database of NCBI (https://www.ncbi.nlm.nih.gov/) served as the basis for the design of gene expression primers. For ChIP primers, genomic DNA sequences of interest were retrieved from the UCSC genome browser [115, 116] (https://genome.ucsc.edu/) using the human genome GRCh38/hg38.

For IκBζ ChIP, corresponding genomic sequences of promoter regions of selected *NFKBIZ* target genes were used as input sequences for the Primer3web software, the design criteria are also listed in ***Table 41***. For the ChIP primers, an intron-spanning primer pair over two adjacent exons was designed to avoid amplification of unspecific or non-coding genomic DNA sequences. Lyophilized primers (metabion international AG, Germany) were reconstituted in RNase-free water at 100 µM and stored at -20°C. For qPCR analysis, working primer solutions were prepared by mixing 10 µM of respective forward and reverse primer in RNase-free water and kept at -20°C.

3.3.2 Quality control and validation of primers

Before new primer pairs were used for standard analysis, their specificity and efficiency were validated. Therefore, a previously analyzed cDNA sample was further diluted in RNase-free water (1:20, 1:40 and 1:80), and measured via qPCR, as explained later in *chapter 3.3.7*. Primer efficiency was judged by the resulting Ct values. A difference of 1.00 Ct value was expected between the 2-fold lower and 2-fold higher diluted cDNA samples, when plotting the log2 of the cDNA dilution against its Ct value.
Hence, a highly efficient primer pair shows a linear regression line with a regression >0.95 and a slope of 1.00, meaning a mathematical difference of 1.00 Ct value between each dilution. Besides, the respective melting curve of each primer pair was analyzed in each template dilution. Sharp melting curves indicate high specificity of the amplified PCR product. However, the emergence of melting curve shoulders or multiple peaks is considered as unspecific primer binding. Neither unspecific nor less efficient primer pairs were kept. Instead, they were discarded and newly designed.

3.3.3 Homogenization of tissue samples for total RNA extraction

Frozen skin tissue (see *chapter 3.5.7*) was transferred to a gentleMACS C Tube (Cat. 130-096-334, Miltenyi), covered in 2 mL QIAzol Lysis Reagent (Cat. 79306, QIAGEN) and harshly homogenized using the gentleMACS dissociator. Lysis was conducted for 10 min on ice before the sample was equally divided into two and transferred to separate reaction tubes.

3.3.4 Isolation of total RNA using phenol-chloroform extraction

For total RNA extraction from cell culture samples, the used medium was discarded, and the adherent cells were covered with 1 mL QIAzol Lysis Reagent (Cat. 79306, QIAGEN). Cells were lysed for 10 min at RT, gently resuspended, and transferred to reaction tubes. The following extraction protocol applies to a lysis volume of 1 mL QIAzol, independent of tissue or cell culture samples. Samples were kept on ice all the time until DNase I digest. 200 µL chloroform (Cat. 1024451000, Sigma-Aldrich) was added for nucleic acid extraction, the suspension was strongly vortexed and incubated for 3 min at RT. Samples were centrifuged in a pre-cooled table-top centrifuge for 5 min (13,000 rpm at 4°C), and the upper phase was carefully transferred to a fresh reaction tube containing 500 µL 100% isopropanol with 2 µL GlycoBlue coprecipitant reagent (Cat. AM9515, Invitrogen) for precipitation. The tubes were vortexed and incubated on ice for 10 min before centrifugation (25 min, 13,000 rpm at 4°C). The supernatant was removed, and the blue precipitate was washed once by adding 150 µL cold 70% EtOH. The remaining pellet was centrifuged (1 min, 13,000 rpm at 4°C) and the liquid was sucked off. The RNA pellet was briefly dried for 30 sec on a heating block at 37°C, before it was resuspended in 100 µL RNase-free water.

3.3.5 DNase I digest of RNA samples

To avoid contamination of RNA with genomic DNA, DNase I digestion was conducted. The RNA sample with 20 µL of DNase I mix was incubated for 30 min at 37°C under constant shaking (600 rpm) on a thermo shaker. Composition of the latter is explained in ***Table 42*** below.

Table 42: Composition of DNase I mix

Component	Volume (1x reaction)
10X Reaction buffer for DNase I	12 µL
DNase I, 50 U/µL	0.25 µL
RiboLock RNase inhibitor, 40 U/µL	1 µL
Nuclease free water	6.8 µL
final Vol.	*20 µL*

Samples were purified by adding 150 µL/sample of a specific phenol-chloroform mixture for RNA extraction (pH 4.5- 5, Cat. A980.3, Carl Roth). The reaction tubes were strongly vortexed and shortly centrifuged (1 min, 13,000 rpm at RT). Fresh 1.5 mL reaction tubes, containing 375 µL 100% EtOH and 17 µL 3 M NaAc, for precipitation were prepared.
After centrifugation, the upper aqueous, RNA-containing phase was transferred to the precipitation mix, the samples were thoroughly vortexed and finally precipitated for at least 1 h at -80°C. RNA extraction was continued with centrifugation (30 min, 13,000 rpm at 4°C), removal of the supernatant, and washing of the RNA pellet with EtOH, as previously described. After briefly drying the sample, RNA was finally resuspended in 10 µL RNase-free water and either kept on ice for subsequent cDNA synthesis or stored at -80°C.

3.3.6 cDNA synthesis

RNA concentration was determined using 1 µL for the NanoDrop ND-2000 (PeqLab, Germany) measurement. Absorption was measured at a wavelength of 260 nm to calculate RNA concentration, while the ratio of 260/280 nm constitutes the ratio of RNA to DNA present in the sample. Yielding a value of >1.9 in the latter represents a sample of high RNA purity. Sample concentrations were adjusted to 1.5 µg RNA/µL with RNase-free water. Next, 1 µg total RNA extracted from cell culture material was mixed with 1 µL random hexamer primers (Cat. SO142, Thermo Fisher Scientific) and filled up to a total volume of 5 µL with RNase-free water. In case of skin tissue obtained from *in vivo* experiments, 4 µg total RNA and 1 µL oligo(dT)18 primers (Cat. SO132, Thermo Fisher Scientific) were mixed, respectively. The RNA-primer-water mixture was incubated for 5 min at 70°C in a thermocycler before 4 µL cDNA master mix (see ***Table 43***) was added. Reverse transcription was carried out for 1 h at 42°C (cell culture) or 37°C (*in vivo* samples). In the end, enzymes were deactivated for 10 min at 70°C, and the samples were cooled down to 4°C. The cDNA samples were diluted 1:10 in RNase-free water and stored at -20°C until further usage.

Table 43: Composition of cDNA master mix

Component	Volume (1x reaction)
Reaction buffer for RT, 5X	2 µL
RevertAid Reverse Transcriptase, 200 U/µL	0.5 µL
RiboLock RNase inhibitor, 40 U/µL	0.5 µL
10 mM dNTPs	1 µL
final Vol.	*4 µL*

3.3.7 Quantification of relative gene expression via qPCR

Real-time PCR was conducted using the CFX384 C100 Touch cycler (BioRad, Germany). Working solutions of validated primer pairs were prepared as described above. All required reagents and cDNA samples were brought to RT and thoroughly vortexed before pipetting. In total, 2.5 µL cDNA was mixed with 10 µL of the respective master mixes of each primer pair (see ***Table 44***) within a 384-well hard-shell plate (Cat. HSP3805, BioRad), which was properly sealed with foil (Cat. MSB1001, BioRad), vortexed and shortly centrifuged (1 min, 1,000 rpm at RT) before being placed into the cycler. The conditions used for the thermocycler protocol are depicted in ***Table 45*** below.

Table 44: Composition of real-time PCR reaction mix

Component	Volume (1x reaction)
Primer working solution, 10 µM	0.5 µL
GreenMasterMix, 2X	6.25 µL
Nuclease-free water	3.25 µL
final Vol.	*10 µL*

Table 45: Real-time PCR thermocycler protocol

Temperature	Time	Cycles
95°C	15 min	-
95°C	15 sec	45x
60°C	45 sec	
95°C	1 min	-
Melting curve 65 to 95°C	0.5°C/ 10 sec	∞

Relative mRNA levels were calculated by normalizing the measured Ct values to the respective human (*RPL37A, U6ssRNA*) or murine (*Rpl37a, Actb*) housekeeping gene using the $2^{-\Delta Ct}$ method. All primer sequences used in this study are listed in ***Table 20*** and ***Table 21***.

3.3.8 RNA sequencing and transcriptome analysis

To sequence selected RNA samples, total RNA was forwarded to Novogene (Munich, Germany) for library construction and next-generation-sequencing. Using 200 ng of total RNA, barcoded mRNA seq libraries were prepared using polyA-tailed mRNA enrichment. Quality control of the final libraries was conducted using Qubit 2.0 and real-time PCR for quantification and the bioanalyzer Agilent 2100 to detect the obtained fragment sizes. After quantification, sequencing of the libraries was conducted on Illumina Novaseq 6000 platform using paired-end 150 cycles (PE150), depending on library concentration.
Raw reads were further processed and mapped against the human reference genome hg38 (GRCh38.109) by Matthias Klein from the NGS core facility (Research Center for Immunotherapy, Mainz) using CLC Genomics workbench (v24.0; QIAGEN) software.

The following default settings were applied:

- count paired reads as two = No
- deletion cost = 3
- global alignment = No
- ignore broken pairs = Yes
- insertion cost = 3
- length fraction = 0,8
- library type = bulk
- maximum number of hits for a read = 10
- mismatch cost = 2
- similarity fraction = 0,8
- strand-specific = both

To evaluate transcriptome data, genes being differentially expressed between untreated and treated cells were filtered for a minimum absolute fold change of > 2 and a difference cut-off of absolute >3. Besides, significantly regulated genes were selected using an adjusted p-value of ≤ 0.05.
To generate heatmaps of transcriptome data Morpheus software (Morpheus, https://software.broadinstitute.org/morpheus) was used, while information about affected signaling pathways was retrieved via gene set enrichment analysis (GSEA) using EnrichR-KG [109] (https://maayanlab.cloud/enrichr-kg). In the latter, significantly enriched pathways are shown, sorted by pathway and p-value, which were obtained from the following libraries: Reactome_2022, GO_Biological_Process_2021 (GO_2021), MGI_Mammalian_Phenotype_Level_4_2021 (MGI_2021) and KEGG_2021_Human (KEGG_2021). Accessibility to transcriptome raw data presented in this study is provided in *chapter 3.9*.

3.4 Protein biochemistry

3.4.1 Protein harvest from cell culture samples

Protein harvest buffer containing 2 M urea was prepared freshly and always kept on ice. The buffer composition is depicted in ***Table 46***, and the ingredients of the individual stocks are explained in ***Table 26***. Reagents are kept at RT. Protease inhibitor cocktail solution (PIC, Cat.4693124001, Sigma) was generated by dissolving one pill in 2 mL purified water to generate 25X stock or in 1 mL to generate 50X stock, respectively. The higher PIC concentration was used for *S. aureus*-treated keratinocytes, since protein degradation was accelerated due to lysed bacteria components. Until usage, PIC stocks were stored at -20°C.

To harvest proteins from cell culture samples, the medium was removed, and the cells were washed once with PBS. 100 µL protein harvest buffer per 6-well was added and distributed thoroughly before the cells were incubated for 10 min on ice. Samples were quickly scraped to avoid protein degradation and transferred to 1.5 mL reaction tubes for brief sonification (Bioruptor from Diagenode, United States) at high power (10 min with 30 sec on/off) under constant cooling to disrupt DNA-protein complexes. Afterwards, the samples were centrifuged (5 min, 3,000 rpm at 4°C) and the protein-containing supernatants were transferred to fresh reaction tubes and kept on ice.

Table 46: Composition of protein harvest buffer for standard and S. aureus-treated samples

Component	Standard (cell culture, skin lysates)	*S. aureus-treated* cell culture
Lysis buffer stock	710 µL	710 µL
8 M Urea	250 µL	250 µL
25X PIC	40 µL	-
50X PIC	-	40 µL
final Vol.	*1 mL*	*1 mL*

3.4.2 Generation of protein lysates from tissue samples

Homogenization of approx. 0.5x 0.5 cm skin tissue was conducted in 300 to 500 µL protein harvest buffer (standard composition, see ***Table 46***) using gentleMACS M homogenization tubes (Cat. 130-093-236, Miltenyi). The samples were processed with the appropriate protein sample settings for M tubes in the gentleMACS dissociator. Homogenized samples were transferred to reaction tubes and centrifuged (5 min, 1,000 rpm at 4°C) to collect larger debris. The protein-containing supernatants were transferred to fresh reaction tubes before the samples were equally sonicated and further processed as explained above for cell culture samples.

3.4.3 Determination of the protein concentration

After sonification, protein concentration was determined in both cell culture samples and homogenized skin protein lysates using Qubit Protein Assay kit (Cat. Q33212, Thermo Fisher Scientific) according to the manual. First, a standard curve was generated with standard solutions included in the kit by mixing 10 µL of each standard with 190 µL of pre-mixed Qubit protein buffer plus Qubit protein reagent. Next, each protein sample was diluted 1:10 in RNase-free water before 1 µL diluted sample was added to 199 µL of pre-mixed Qubit protein buffer plus Qubit protein reagent. After a short incubation of 5 min at RT, individual protein concentrations were determined using the Qubit Flex fluorometer (Thermo Fisher Scientific, Germany). Skin lysates were further stored in aliquots at -80°C, while immunoblot samples were further processed as follows.

3.4.4 Denaturing SDS-PAGE

Protein samples were mixed with ¼ volume 6X Laemmli buffer (see Table 26) and boiled for 10 min at 95°C. Next, the samples were either stored at -20°C and shortly pre-heated for 5 min at 95°C before loading or directly loaded on a two-layered 12% acrylamide/ bis-acrylamide gels for subsequent sodium dodecyl sulphate-polyacrylamide gel electrophoresis (SDS-PAGE). The recipe for 4 gels, each comprising a running gel layer of 12% acrylamide while the upper stacking gel layer consists of 4%, is presented in ***Table 47***.

In theory, SDS is required to separate proteins present in the samples according to their molecular weight, as it masks all protein charges in general. As soon as protein samples are loaded onto the stacking gel, their protein bands become sharpened, while the real separation, depending on their sizes, is visualized in the running gel layer, allowing the detection of protein sizes in the range of 15 to 110 kDa. Acrylamide gels were cast below the fume hood. Next, the gels were then placed into a vertical Mini-PROTEAN Tetra electrophoresis module (Biozym, Germany) with 1X SDS-PAGE running buffer, which was prepared from a 10X concentrated protein buffer stock solution mixed with 1% SDS in purified water (see ***Table 27***).

Gel combs were removed and 20 to 60 µL of pre-heated protein samples were loaded according to their protein concentration (approx. 150 µg) into the respective pockets. 4 µL PageRuler Prestained Protein ladder (Cat. 26617, Thermo Fisher Scientific) was applied to one pocket per gel. An initial voltage of 90 V for the first 15 min, later 140 V were applied to the electrophoresis module until the 10 kDa band of the ladder was visually discontinued.

Table 47: Composition of 12% acrylamide gels for SDS-PAGE (volumes for 4 gels)

Component	Running gel (12%)	Stacking gel (4%)
Purified water	15 mL	14.24 mL
Running gel buffer (1.5 M Tris-HCl, pH 8.8)	12 mL	-
Stacking gel buffer (0.5 M Tris-HCl, pH 6.8)	-	2.4 mL
10% SDS	480 µL	300 µL
Glycerol	4.8 mL	-
Acrylamide-bisacrylamide Rotiphorese Gel 40 (37.5:1)	15 mL	1.9 mL
10% APS	225 µL	200 µL
TEMED	20 µL	20 µL
final Vol. approx. per 1 gel	*4x 12 mL*	*4x 9 mL*

3.4.5 Immunoblotting and membrane development

After SDS-PAGE, protein transfer was conducted by wet immunoblotting technique. The protein-loaded acrylamide gels were placed onto a nitrocellulose membrane (Cat. GE10600001, Sigma-Aldrich) and mounted into a cassette in between two outer layers of sponges and Whatman paper (Cat. CL75.1, Carl Roth). Throughout mounting, the cassette was covered with cold transfer buffer (see ***Table 27***) to keep both the gel and blot membrane wet. The assembled cassettes were placed into vertical Mini-PROTEAN Tetra Trans-Blot modules (Biozym, Germany) together with a cooling pack and covered sufficiently with cold transfer buffer. Additionally, the modules were kept in a basket filled with ice during transfer to prevent overheating of the buffer and thus damage to the acrylamide gel. Protein transfer was achieved by applying a voltage of 100 V for 2 h.

Next, the blot membranes were placed into 50 mL centrifugation tubes filled with blocking buffer, containing 5% nonfat dried milk powder dissolved in PBS. The blots were incubated at RT for 1 h under constant rotation on a tube roller (VWR or Biozym, Germany) to prevent unspecific background staining. The blots were incubated in selected primary antibody dilutions (see ***Table 12***) at 4°C overnight.

The next day, blots were excessively washed with 0.01% PBS-Tween (PBST; 3x 10 min at RT) before 5 mL secondary horse radish peroxidase (HRP)-conjugated antibody mixed in blocking milk (1:5,000 diluted) was applied for 1 h at RT while rotating.

Afterwards, PBST washing was repeated. To develop the blot membranes, the secondary antibody was subsequently visualized upon HRP substrate application using approx. 250 µL/blot developer solution Sirius (Cat. K-12043-D20, Advansta) for weakly expressed proteins, or ECL Western Blotting Substrate (Cat. W1001, Promega) for strongly expressed proteins, respectively. Chemiluminescence was analyzed using Fusion FX imager (Vilber Lourmat, Germany).

3.4.6 Proteome Profiler Array

Analysis of secreted cytokines in PBS- and *S. aureus*-treated mouse skin samples was carried out with the Proteome Profiler Mouse Cytokine Array Kit Panel A (Cat.ARY006, R&D systems), according to the manufacturer′s instructions. For preparation of skin lysates, see *chapters 3.4.2* and *3.4.3*. Before analysis, a fraction of skin lysate was processed for immunoblot analysis, as explained in *chapters 3.4.4* and *3.4.5*, to normalize the cytokine array input samples to equal β-Actin levels (Cat. 3700, Cell signaling). Finally, the cytokine array was carried out by exposing the individual membranes to equal amounts of pooled samples derived from n = 3 animals per treatment group. Development of the membranes was conducted in parallel using Fusion FX imager (Vilber Lourmat, Germany) with equal exposure time. The relative cytokine expression levels were then calculated as relative pixel values using the dot blot analyzer (ImageJ) and normalized to reference spots provided on the membranes.

3.4.7 Transient overexpression of HEK293T cells and luciferase assay

HEK293T cells were transiently overexpressed using the calcium-phosphate transfection method for subsequent luciferase assay. Therefore, cells were seeded in triplicates á 1 mL into 12-well plates in DMEM supplemented with 10% FCS and 1% P/S with a concentration of $4*10^4$ cells/mL. Besides, one Western Blot sample per overexpression was generated alongside the luciferase samples to validate the success of transfection, respectively.

The next day, volumes for the transfection master mix for five 12-wells in total were calculated (see ***Table 48***), containing the following amount of plasmid DNA per one well:

100 ng TK-Renilla plasmid and 400 ng DEFB4 firefly luciferase promoter construct with either 800 ng NOD2-GFP plasmid (Cat. 131207, Addgene) and/or 200 ng of IκBζ plasmid (provided by Stephan Hailfinger) and/or empty pcR3.1 control plasmid (ctrl, Cat. V79020, Invitrogen). Overexpression of HEK293T cells with 1 µg GFP plasmid DNA served as a transfection control. Each master mix, composed of plasmid DNA, purified water, and $CaCl_2$ was immediately mixed, then an equal volume of 2x HBS buffer (see ***Table 25***) was added dropwise during constant vortexing to the mixture. Reactions were incubated for 10 min at RT to allow the formation of DNA-calcium phosphate precipitates.

After incubation, a volume of 140 µL per 12-well was applied dropwise to the seeded HEK293T cells throughout the well. Uptake of DNA was established during the following 24 h under standard cultivation conditions at 37°C. In the last 2 h before sample harvest, the transfected cells were additionally transfected with or without MDP, as explained in *chapter 3.2.7*.

Transfection efficiency was checked in GFP-transfected HEK293T cells under UV light 24 h post-transfection using an inverted fluorescence microscope (EVOS fl from AMG, United States). Overexpression control samples for immunoblot were harvested and analyzed as explained in *chapters 3.4.1* and *3.4.3* to *3.4.5*.

Table 48: Master mixes for transient transfection of HEK293T cells

Components	Amount / Volume (per one 12-well)	Amount / Volume Master Mix (5x reactions)
TK-Renilla plasmid	100 ng	500 ng
DEFB4 firefly luciferase promoter	400 ng	2 µg
Individual samples:		
GFP	1 µg	5 µg
Ctrl • empty pcR3.1 control plasmid	 1 µg	 5 µg
NOD2 OE • NOD2-GFP plasmid • empty pcR3.1 control plasmid	 800 ng Ad 1 µg	 4 µg 1 µg
IκBζ OE • IκBζ plasmid • empty pcR3.1 control plasmid	 200 ng Ad 1 µg	 1 µg 4µg
Combination NOD2 + IκBζ OE • NOD2-GFP plasmid • IκBζ plasmid	 800 ng 200 ng	 4 µg 1 µg
Purified water	62.2 µL	Ad 311 µL
2 M $CaCl_2$	7.8 µL	39 µL
mix thoroughly by vortexing		
2x HBS buffer (pH 6.8 to 7)	70 µL	350 µL
final Vol.	*140 µL*	*700 µL*
vortexing; incubation for 10 min @ RT; dropwise addition to seeded cells		

Quantification of firefly and Renilla luciferase luminescence signals was conducted 24 h post-transfection using a dual luciferase reporter assay kit (Dual-Glo Luciferase assay system, Cat. E2920, Promega) according to the manufacturer's protocol. Therefore, transfected cells were carefully washed with PBS, sucked dry and lysed with 125 µL passive lysis buffer (diluted 1:5 in purified water) per 12-well for 15 min at RT while shaking (Shaker Polymax, Heidolph Scientific). The cells were scraped, the lysis solution was transferred to 1.5 mL reaction tubes, and spun down for 1 min (13,000 rpm, 4°C) in a pre-cooled table-top centrifuge. Supernatants were transferred to fresh reaction tubes and stored at -20°C for later use or kept on ice for immediate use. Next, 50 µL Dual-Glo Luciferase Assay substrate was mixed with 5 µL supernatant within a white 96-well plate (Perkin Elmer X50 CulturePlate White Opaque, Cat. 50-905-1585, Fisher Scientific). Firefly luminescence was immediately measured for 1 sec at 405 nm using a plate reader (Hidex Sense micro from Hidex, Germany). Next, 1X Stop & Glo Reagent was prepared according to the manual. 50 µL of reagent was added to each well of the 96-well plate, the plate was mixed for 3 sec and Renilla luminescence was measured immediately with equal settings. Purified water, instead of supernatant, served as a blank control in both measurements. Expression of the *DEFB4* promoter activity in MDP-stimulated HEK293T cells after 24 h with or without IκBζ and NOD2 overexpression or in combination was calculated as the fold luciferase induction over unstimulated transfected cells, normalized to co-transfected TK-Renilla. Triplicates were used to calculate individual standard deviations (SD) of each treatment. An overview of the plasmids and constructs used for this study is listed in ***Table 17*** and ***Table 18***.

3.4.8 Chromatin fractionation

Chromatin fractionation was performed based on the established protocol of Mendez and Stillman (2000) [117]. 4*10^5 cells of *sh ctrl* and *sh NFKBIZ* knockdown hKC were seeded on two separate 10 cm dishes each and differentiated for 72 h using 2 mM $CaCl_2$. By the time starvation and *S. aureus* infection (1 h, MOI30) were conducted, as described in *chapter 3.2.8*, the seeded keratinocytes had reached a confluency of 80% (approx. 3.4* 10^6 cells). After two washing steps with PBS post infection, sample harvest from both untreated and infected *sh ctrl* and *sh NFKBIZ* cells was conducted. Therefore, cells were scraped and transferred into 1.5 mL reaction tubes. After centrifugation (2 min, 1,000 rpm at 4°C), supernatants were discarded, and the cell pellets were washed once again with PBS. The next steps were conducted exclusively on ice. Cell pellets were resuspended in 200 µL fractionation buffer A (see ***Table 28***) and lysed in 0.5% Triton X-100 for 1.5 h, since differentiated keratinocytes required harsher lysis conditions.

Afterwards, the samples were centrifuged (5 min, 2,000 rpm at 4°C) and the supernatants (S-1) were separated into fresh reaction tubes; the pellet (P-1) was kept on ice in the meantime. Supernatants (S-1) were further clarified by centrifugation (5 min, 13,000 rpm at 4°C) and the resulting supernatant (S-2) was collected as the unbound chromatin fraction. Next, the impure nuclei-containing pellet (P-1) was washed once with 200 µL fractionation buffer A and centrifuged (5 min, 2,000 rpm at 4°C) before the buffer was completely removed. Nuclei were lysed for 30 min on ice using 100 µL fractionation buffer B (see ***Table 28***) per sample. The supernatants generated after subsequent centrifugation (5 min, 3,000 rpm at 4°C) were further added to the unbound chromatin fraction samples (S-2), yielding a total volume of 300 µL. Then, samples were boiled for 5 min at 95°C together with 100 µL 6X Laemmli buffer. The remaining pellets (P-1) were finally resuspended in 100 µL fractionation buffer B, enclosing the chromatin-bound fraction, which was mixed with 100 µL 6X Laemmli before incubation for 20 min at 70°C.

In subsequent immunoblot analysis approx. 40 µL of chromatin-unbound (S-2) versus chromatin-bound (P-1) samples were loaded, and IκBζ protein localization was determined. Hence, GAPDH staining (Cat. 2118, Cell Signaling) was used as non-chromatin control, while histone H3 staining (Cat. ab1791, abcam) marked a pure chromatin-bound fraction in the respective control and knockdown keratinocytes.

3.4.9 Chromatin harvest and preparation for ChIP

For ChIP assay, one 20 cm dish with approx. 1.1*10^6 keratinocytes were seeded to obtain four ChIP reactions. Thus, ctrl and *NFKBIZ* knockdown cells were differentiated for 72 h using 2 mM $CaCl_2$, before *S. aureus* infection (MOI30) was conducted under starvation for 2 h in total with a final confluency of 70% (approx. 6.6* 10^6 cells) upon harvest. Indicated volumes of used ChIP buffers (see ***Table 29***) are representative of one 20 cm dish.

After two PBS washing steps post infection, both untreated and infected *sh ctrl* and *sh NFKBIZ* keratinocytes were crosslinked for 45 min at RT with 5 mL protein-protein crosslinking buffer, containing DSG (Cat. 20593, Thermo Fisher).
Cells were washed twice with PBS and sucked dry, 5 mL master mix was applied for 10 min at RT to perform an additional protein-DNA crosslinking step with paraformaldehyde (PFA, Cat. 28906, Thermo Fisher). Compositions of the crosslinking buffers can be found in ***Table 29***. Crosslinking was stopped by adding 0.5 mL of 1.25 M glycine for 5 min directly to the samples at RT. Crosslinked cells were then washed once with PBS, and the liquid was aspirated. Upon addition of 1.5 mL ChIP buffer B, cell culture dishes were placed on ice for 10 min before the cells were scraped and transferred to individual 2 mL reaction tubes. Chromatin extraction was conducted as follows.
After centrifugation (3 min, 2,000 rpm at 4°C), the chromatin pellets were washed once with PBS, each resuspended in 2 mL cold ChIP buffer C, and incubated for another 5 min on ice. The samples were centrifuged (5 min, 2,000 rpm at 4°C), supernatant was discarded, and the remaining chromatin pellets were carefully resuspended in 440 µL 1X incubation buffer, before the lysates were sonicated for 25 cycles á 1 min (Bioruptor, Diagenode) at high power (30 sec on/off) under constant cooling. After another centrifugation step (5 min, 13,000 rpm at 4°C), the supernatants were transferred to a new reaction tube, and the chromatin was subjected to pre-clearing for the removal of *S. aureus*-derived protein A. This was achieved by incubation of chromatin with 2 µg IgG antibody and 25 µL magnetic beads (Dynabeads protein G, Cat. 10004, Thermo Fisher) for 1 h at 4°C on a rotating mixer. For proper preparation and washing of magnetic beads before usage, see next *chapter 3.4.10*.
The chromatin-bead mixture was put into a magnet rack to separate the beads bound with *S. aureus* protein A from the chromatin-containing supernatant. Thus, the latter was transferred to a new reaction tube and split into several aliquots for subsequent ChIP reactions, which could be stored at -80°C for later usage. Additionally, an input control of 12 µL of each condition was kept overnight at 4°C for later analysis.

3.4.10 Chromatin-immunoprecipitation (ChIP)

Before immunoprecipitation, magnetic Protein G Dynabeads (Cat. 10003D, Invitrogen) were carefully inverted and mixed. For one ChIP reaction, 25 µL beads were required for each treatment condition and cell line. The required amount of beads was transferred to a 1.5 mL reaction tube and was washed in bead wash buffer with twice the volume of beads, to block the beads in advance and to prevent unspecific binding to it. Next, the reaction tube was placed into a magnetic rack (DynaMag-2, Thermo Fisher Scientific, Germany) to remove the supernatant via pipetting. Washing was repeated, and the beads were resuspended again in 25 µL bead wash buffer per reaction and transferred to fresh 1.5 mL reaction tubes. Immunoprecipitation was initiated by mixing the prepared magnetic beads with 146 µL ChIP master mix, 120 µL of the respective chromatin sample, and 2 µg IgG or 5 µL self-made IκBζ antibody, respectively.

ChIP samples were incubated overnight at 4°C on a rotating mixer. A detailed list of one ChIP reaction is provided below in ***Table 49***.

Table 49: Composition of one ChIP reaction

Component	Volume (1x reaction)
Antibody (self-made IκBζ / IgG)	5µL / 2µg
5% BSA	6 µL
Chromatin sample	120 µL
Dynabeads Protein G	25 µL
5X incubation buffer w/o SDS	36 µL
25X PIC solution	12 µL
Nuclease-free water	92 µL
final Vol.	*291 + 5µL IκBζ or IgG*

Information regarding the used ChIP antibodies is included in ***Table 13***, while the composition of the mentioned ChIP buffers is listed in greater detail in ***Table 29***. On the next day, all ChIP samples were washed via magnetic separation using 400 µL buffer per reaction. Before the removal of supernatant, ChIP samples were inverted 4 times, and a series of washing steps were applied:

- 2x wash buffer 1
- 1x wash buffer 2
- 1x wash buffer 3
- 2x wash buffer 4

After washing, the beads were eluted using 200 µL elution buffer and incubated for 20 min at RT while rotating. At the same time, 12 µL input samples (stored overnight at 4°C) were incubated together with 188 µL elution buffer. Subsequently, ChIP samples were placed into the magnetic rack, and the eluate was transferred to a new reaction tube while the beads were discarded.

Next, de-crosslinking was conducted to remove the remaining proteins bound to the DNA. This was achieved by adding 8 µL of 5 M NaCl directly to both the ChIP samples and respective input controls. In total, de-crosslinking was carried out for 4 to 5 h at 65°C while shaking constantly in a thermo shaker (650 rpm).

In the final step, DNA purification was conducted at RT using the QIAGEN MinElute PCR Purification kit (Cat. 28004, QIAGEN) according to the manufacturer's instructions. Hence, 1 mL 5X PB buffer was added to each ChIP and input sample, then 650 µL were loaded onto columns, which were subsequently centrifuged (1 min, 13,000 rpm at RT). The flow-through was discarded, and the remaining sample volume was loaded. Column loading was conducted next with 750 µL PE wash buffer and afterwards with RT buffer, to remove any EtOH residues. Next, the columns were placed into new 1.5 mL reaction tubes to elute DNA with 50 µL of 1:10 diluted EB buffer, which was applied to the center of the column. Samples were incubated for 2 min at RT before final centrifugation and thus, collection of eluates. All ChIP and input samples were stored at 4°C from now on until analysis.

3.4.11 Analysis of ChIP samples using qPCR

ChIP samples were analyzed with real-time PCR using the CFX384 C100 Touch cycler (BioRad, Germany). Before measurement, ChIP samples (stored at 4°C) were warmed up for 10 min at 50°C, while a 1:10 dilution of input samples was prepared with nuclease-free water (e.g. 10 µL input + 90 µL water). Real-time PCR of ChIP samples together with diluted inputs was conducted similarly to gene expression analysis described in *chapter 3.3.7*, also using 2.5 µL sample volume and 10 µL master mix. However, self-designed specific ChIP primers (see ***Table 22***) annealing to genomic DNA and another qPCR Maxima SYBR Green Master Mix (Cat. K0221, Thermo Fisher) were used instead. Thus, the composition of the qPCR reaction mix and the adapted cycler program are enclosed in ***Table 50*** and ***Table 51***.

Table 50: Composition of real-time PCR reaction mix for ChIP samples

Component	Volume (1x reaction)
ChIP primer working solution, 10 µM	0.5 µL
Maxima SYBR Green/ROX, 2X	6.25 µL
Nuclease-free water	3.25 µL
final Vol.	*10 µL*

Table 51: ChIP real-time PCR thermocycler protocol

Temperature	Time	Cycles
95°C	10 min	-
95°C	15 sec	45x
60°C	45 sec	
95°C	1 min	-
Melting curve 65 to 95°C	0.5°C/ 10 sec	∞

For the evaluation of biological IκBζ ChIP triplicates, the percentage of input was calculated by the logarithm to the base 2, of which the measured ChIP Ct values were subtracted from input Ct values. Besides, the input dilution factor of 1:10 (2^{10}=100) was taken into account. Hence, the following formula was used:

$$\%\ of\ input = 2^{(Ct\ input - Ct\ ChIP\ sample)/100 * 100}$$

Measurement of human myoglobin (*MB*) locus was included in the evaluation, serving as an internal negative control.

3.5 Animal work

3.5.1 Animal ethics and permissions

All animal experiments were carried out according to the guidelines for animal care and German law, which were approved by the local animal ethics committee of Rhineland-Palatinate (Landesuntersuchungsamt Rheinland-Pfalz). The *in vivo* experiments were conducted with male and female mice, at the age of 8 to 12 weeks and with a minimum weight of 18 g (permission No. G22-1-049). For *in vitro* experiments, murine keratinocytes were isolated from control and knockout tissue of animals of an equal age and gender (in-house-bred animals: permission No.T 23-01-008, other animals: tissue provided by cooperation partners).

3.5.2 Breeding strategy of *Nfkbiz*$^{\Delta K14\text{-}cre}$ mice

For this study mice with a keratinocyte-specific deletion of *Nfkbiz,* assigned B6.Cg.Nfkbiz<tm1.1Muta> Tg(KRT14-cre)/Tarc (in short: *Nfkbiz*$^{\Delta K14\text{-}cre}$) were generated, while making use of the Cre/loxP recombination system [118].

First, homozygous control mice B6.Cg-Nfkbiz<tm1.1Muta> (in short: *Nfkbiz*$^{fl/fl}$), which carry LoxP sequences between exon 5 and 7 of the gene *Nfkbiz*, were crossed with the homozygous transgenic strain B6.N.Cg-Tg(KRT14-cre)1Amc/J (in short: *KRT14-cre*) bearing a human keratin 14 (K14) promoter, that directs the expression of Cre recombinase (obtained from Jackson Laboratories, Stock 018964).

Genetically, the resulting offspring exhibited a heterogeneous expression of both the *Nfkbiz* flox cassette and the Cre for human *KRT14.* Further consecutive breeding with *KRT14*-positive mice finally resulted in the required *Nfkbiz*$^{\Delta K14\text{-}cre}$ knockout animals expressing a homozygous *Nfkbiz* flox cassette [37]. Successful breeding was ensured via genotyping, using the protocols mentioned in the following chapters. Of note, none of the aforementioned mouse lines represent a genetically burdened breeding.

3.5.3 Extraction of genomic DNA (gDNA) from ear biopsies

Ear skin biopsies of all animals were taken by the animal caretakers and kept at -20°C in reaction tubes until further analysis. To extract genomic DNA (gDNA), one skin punch was transferred to a fresh reaction tube, sufficiently covered with 50 µL genotyping buffer (see ***Table 30***) and boiled for 15 min at 95°C on a heating block. Afterwards, the gDNA samples were put at RT for immediate usage and/or further stored at -20°C.

3.5.4 Generation of mouse genotyping samples

The gDNA samples were mixed in 0.2 mL PCR reaction tubes with their respective DreamTaq Hot Start PCR master mixes (Thermo Fisher, Cat. K9011) using the following volumes and components (see ***Table 52*** and ***Table 53***).

Table 52: Nfkbiz flox PCR reaction mixture

Component	Volume (1x reaction)
gDNA	1 µL
Nuclease-free water	8.7 µL
2X DreamTaq Hot Start PCR Master mix	10 µL
Primer Flox F1	0.1 µL
Primer Flox R	0.1 µL
Primer Flox F3	0.1 µL
final Vol.	*20 µL*

Table 53: KRT14-cre PCR reaction mixture

Component	Volume (1x reaction)
gDNA	2 µL
Nuclease-free water	7.6 µL
2X DreamTaq Hot Start PCR Master mix	10 µL
Primer HumanKRT14promF	0.2 µL
Primer HumanKRT14promR	0.2 µL
final Vol.	*20 µL*

PCR of all samples was conducted using the following thermocycler program (see ***Table 54***). Subsequently, genotyping samples were either analyzed or stored at -20°C in case of later analysis.

Table 54: Genotyping PCR thermocycler protocol

Temperature	Time	Cycles
95°C	3 min	-
95°C	30 sec	34x
60°C	1 min	
72°C	1 min	
72°C	10 min	-
4°C	stored	∞

3.5.5 Agarose gel and evaluation of genotyping results

To prepare a 1.5% agarose gel, 3 g of agarose LE (Cat. M3044.500, Genaxxon) were completely dissolved in 200 mL 1x TAE buffer (see ***Table 31***), while being heated in the microwave. As soon as the solution cooled down to approx. 55°C, 6 µL peqGREEN DNA/RNA-dye (Cat. 732-3196, VWR) was added. The solution was carefully mixed and immediately poured into the agarose gel chamber (Perfect Blue, VWR) with its respective comb and kept untouched for approx. 30 min. After PCR reaction, each genotyping sample was mixed with 4 µL 6X DNA loading dye (Cat. R0611, Thermo Fisher), spun down, and the entire volume was loaded on the solidified agarose gel. Additionally, 4 µL of the GeneRuler 100 bp DNA ladder (Cat. SM0243, ThermoFisher) was added. The gel was run for 1 h with an applied voltage of 140 V, then it is imaged under UV light using the ChemiDoc MP Imaging system (Biorad, Germany). Evaluation of the genotyping results of the respective PCR samples was performed as follows:

Nfkbiz flox PCR:
The *Nfkbiz* flox cassette was present in homozygous samples with a single DNA band at the size of 405 bp, while wild-type samples exhibited a single band at 227 bp. Heterozygous expression of the *Nfkbiz flox* allele was represented by two bands (405 bp and 227 bp), meaning the absence of any gel bands required repetition of the PCR of the respective genotyping sample.

K14-cre PCR:
The expected DNA band size of the Cre of human KRT14 is 350 bp, without discriminating between homozygous and heterozygous gene expression. In this case, the lack of bands represented KRT14-cre negative animals, which were exclusively used as control animals.

3.5.6 Epicutaneous *S. aureus* infection *in vivo*

Based on the precedent genotyping, animals were allocated to different treatment groups (PBS- or *S. aureus*-treated *Nfkbiz*$^{fl/fl}$ and *Nfkbiz*$^{\Delta K14\text{-}cre}$ mice) with respect to their gender, age, and potential weight differences before starting the artificially induced *in vivo* infection. It was experimentally excluded that the skin of control and knockout animals was burdened with *S. aureus* before the topical application of living MRSA (see *chapter 4.16*). The mice were transferred from the animal facility to the cabinets (Scantainer Uniprotect NG, ZOONLAB GmbH), where they were monitored within their assigned groups (2 mice per cage) for several days before treatment started.
The following steps were always carried out under a sufficient oxygen supply (flow rate 5 to 6 L/min) and constant isoflurane anesthesia (Cat. 1214, CP Pharma), which was shortly introduced with 2.5% and then sustained at 1.5% isoflurane, as long as necessary for the treatment.

At day zero (D0), an area of approx. 5x3 cm of the back of all animals was shaved, using a razor, and depilated with shaving cream approx. 24 h before infection. The skin was cleaned with water-wetted paper towel to remove any remaining cream residues and to prevent skin irritation. Then the mice were put into fresh cages. The next day, the weight of the mice was noted before and after packaging. To create a mild barrier effect in the area where the fur had been removed, the back skin was tape-stripped 8 times and cleaned with 70% isopropanol. As soon as the skin was completely dry, two sterile filter discs (Cat. AL7210, Smart Practise) were applied to the middle of the back of each animal, which were either soaked with PBS solution or $1*10^8$ CFUs living *S. aureus* (see preparation of bacteria solution in *chapters 3.1.5* to *3.1.7*). Throughout the infection, the stock solution of bacteria was kept on ice and inverted before each application to avoid major deviations between consecutively infected animals. Filters were immediately covered with a square-shaped, waterproof plaster (30x40 mm, Mivolis), followed by the wrapping up of the animal using a piece of surgical tape (Cat. N532.1, Carl Roth), to secure the plaster, and finally, Fixomull (Cat. 14219995, Sanicare Apotheke) to avoid bacterial contamination in the cages.
To evaluate the reproducibility among several *in vivo* infection experiments and the infectivity of the topically applied living bacteria, a $1:10^6$ dilution of the bacteria stock was prepared in PBS and plated overnight on TSB agar at 37°C to finally count the colony-forming units (CFUs). The following days, the mice were monitored daily for their weight, and eventually, Fixomull bandages were renewed. Weight loss of ≥ 10% was counteracted by supplementing the drinking water with 5% glucose (sterile-filtrated), which was exchanged daily to avert contamination.
On day 2 or day 7, respectively, the mice were sacrificed with an overdose of isoflurane, and their final weight was determined. All coverings were removed, and each mouse was visually scored to determine the severity of the skin inflammation (score points: 0 = healthy appearing skin, 0.5 = scaling, 1 = scaling with mild local infection, 2 = moderate epicutaneous infection affecting <50% of the back skin 3 = strong epicutaneous infection with pus and abscess formation, affecting the whole area).

3.5.7 Sampling of mouse skin post-mortem

The back skin of the affected area was cut into several pieces: Samples for immunoblot and RNA were collected in reaction tubes, snap-frozen with liquid N_2, and stored at -80°C until usage. For immunohistochemistry, a piece of skin (ca 5 x 10 mm) was placed flatly into embedding cassettes and fixed overnight in 4.5% formaldehyde solution (Cat. 2213, Carl Roth) before it was further processed by the Histology Core Facility (Claudia Braun, University Medical Center Mainz) (see also *chapters 3.7.1* and *3.7.2*). For FACS analysis, skin sections of approx. 1 x 1 cm (*S. aureus*-infected mice) or 1.5 x 1.5 cm (PBS-treated mice) were taken, which will be explained in the following chapter.

3.6 Flow cytometry

3.6.1 Back skin digest for fluorescence-activated cell sorting (FACS)

FACS skin digest solution was prepared in advance (see ***Table 32***), keeping 1 mL aliquots in gentleMACS C homogenization tubes (Cat. 130-096-334, Miltenyi Biotech) on ice until usage. The sampled skin sections were then added to the C-tubes and precisely chopped with scissors before being incubated for 1.5 h in a shaking incubator at 37°C. Next, the digested skin samples were gently homogenized for 45 sec using the gentleMACS dissociator (program H, Miltenyi), and digestion was stopped with the addition of 20 mL DMEM medium (10% FCS supplemented). Each single-cell suspension was filtered through a 100 µm cell strainer into a 50 mL tube and centrifuged for 10 min (450 x g at 4°C). Supernatants were carefully sucked off before the pellets were resuspended in 1 mL pre-cooled FACS buffer (see ***Table 32***) and transferred to a 1.5 mL reaction tube. The amount of the single-cell suspension extracted was sufficient to generate at least four different FACS staining samples per animal.

3.6.2 FACS analysis

The following steps were conducted on ice. Homogenized back skin suspensions were centrifuged in a table-top centrifuge (4 min, 3,000 rpm at 4°C), their supernatants were discarded, and the pellets were each resuspended and treated for 10 min on ice with 100 µL Fc-block solution composed of 1 µL anti-mouse TruStain FcX (Cat.101320, BioLegend) in 99 µL FACS buffer. Next, 1 mL FACS buffer was added, and the entire volume was aliquoted into fresh reaction tubes.

The tubes were centrifuged (4 min, 3,000 rpm at 4°C), the supernatants discarded and the individual pellets were surface stained in the dark on ice for the next 30 min using the following antibodies (purchased from BioLegend): anti-Ly6G-PE (Cat.127607, clone 1A8), anti-Ly6C-APC (Cat.128016, clone HK1.4), anti-CD4-PE (Cat.100408, clone GK1.5), anti-CD25-APC (Cat. 101910, clone 3C7) and anti-γδ-APC (Cat.118115, clone GL3). For this, antibody master mixes were prepared containing 1 µL antibody or isotype control in a total volume of 50 µL per sample (e.g. 10 µL antibody A + 10 µL antibody B + 480 µL FACS buffer). After the individual surface staining of samples derived from each animal, each reaction tube was washed with FACS buffer, centrifuged (4 min, 3,000 rpm at 4°C), and the supernatant was finally discarded. To allow live/dead staining, each pellet was co-stained with DAPI (Cat. 422801, BioLegend) using 300 µL of DAPI buffer (DAPI 1:2,000 diluted in FACS buffer). A list of all FACS antibodies is provided in ***Table 14***.

For flow cytometry analysis, samples were transferred to round bottom tubes with cell strainers (Cat. 352235, Corning) and kept on ice in the dark until all data were acquired using the LSR II flow cytometer (Becton Dickson, United States). Gates of the individual immune cell populations were set based on their respective isotype control (Cat.400612, APC Rat IgG2b, κ, BioLegend; Cat.400636, PE Rat IgG2b, κ, BioLegend; Cat.550085, PE Hamster IgG2, κ, BD).

To assess the relative infiltration of immune cells upon epicutaneous *S. aureus* infection or PBS treatment, populations were gated on single, living cells using the software FlowJo (Tree Star Inc.). The gating strategy is further enclosed in ***Supplementary Figure VIII***.

3.6.3 Detection of reactive oxygen species in skin using FACS

To measure reactive oxygen species (ROS) in the skin, an aliquot of the prepared single-cell suspension was taken from each mouse and centrifuged within a 1.5 mL reaction tube (3 min, 2,500 rpm at 4°C). The pellet was resuspended in ca. 300 µL PBS, then cells were counted with a Neubauer cell counting chamber (Brand, Germany), and the concentration was adjusted to approx. $5*10^5$ cells/mL with PBS. Each aliquot was divided into three separate samples á 100 µL using fresh reaction tubes: blank (negative control), rested cells, and PMA re-stimulated (positive control). For PMA stimulation (Cat. P1585-5MG, Sigma-Aldrich), 20 µL of a working stock solution of 0.5 µg/mL PMA in DMSO/PBS was added to the cells (final amount: 10 ng PMA/ sample). Blank and rested samples received 20 µL of PBS instead.
All samples were incubated together at 37°C for 30 min in total, before the volume was filled up to 1 mL total volume with 880 µL PBS. In the meantime, an intermediate working solution of the light-sensitive CellRox Green reagent (Cat. C10492, Thermo Fisher) was prepared by mixing 10 µL of the solution with 90 µL DMSO (1:10 dilution, 250 µM), according to the manufacturer's instructions. Next, 2 µL of this solution was added to the sample groups "rested cells" and "PMA-restimulated", yielding a final concentration of 500 nM CellRox Green in the samples. Blank samples received 2 µL of DMSO as a vehicle instead. After sample incubation under light-protection at 37°C for 20 min, 1 µL of live/dead stain SYTOX Red (5 µM in DMSO, included in the kit) was added, then the samples were further incubated for another 15 min. Within the next 2 h, all samples were transferred to round bottom tubes with cell strainers (Cat. 352235, Corning) and directly measured with the LSR II flow cytometer (Becton Dickson, United States) using the FITC channel for CellRox Green detection and the APC channel for live/dead staining with SYTOX Red. Until all data was acquired, round bottom tubes were kept on ice in the dark. To identify the number of ROS-producing cells, live cells were gated by comparing the "rested cells" (with CellRox) with their respective blank samples (without CellRox) of each animal. Of note, the PMA re-stimulated samples were just measured to ensure proper CellRox staining procedure; their results are not included in this study. Using FlowJo (Tree Star Inc.) software, the percentage of ROS-producing cells per gated live cells was calculated. For the detailed gating strategy, see ***Supplementary Figure IX***.

3.7 Immunohistochemistry

3.7.1 Embedding of formalin-fixed mouse skin into paraffin blocks

After at least 24 h tissue fixation, the 4.5% formaldehyde solution was collected in a specific waste container, and the cassettes containing the back skin samples were washed in PBS. The following steps were carried out by the Histology Core Facility (Claudia Braun, University Medical Center Mainz), being partly automated:

- Dehydration using a series of increasing EtOH concentrations over 2 days at RT
- Clearing using a series of increasing xylene/ decreasing isopropanol concentrations for 1.5 days at RT
- Paraffin infiltration for 3 days at 60°C
- Embedding of the formalin-fixed tissue samples into paraffin blocks (FFPE)

After being hardened all through, the FFPE mouse skin samples were cut into 5 µm thick sections using a microtome, mounted on Superfrost adhesion glass slides (Cat. H867.1, Carl Roth) and dried overnight at RT.

3.7.2 Immunohistochemical staining of murine FFPE skin sections

To make the tissue of FFPE skin sections accessible for subsequent immunohistochemical staining, deparaffinization was carried out. Therefore, the slides were mounted into a glass staining rack (Cat. H553.1, Carl Roth) and put into a pre-heated oven for 1 h at 60°C to melt the paraffin. Afterwards, the rack was transferred quickly into the first staining through glass container (Cat. H554.1, Carl Roth) of a descending EtOH series below the fume hood, the exact protocol is depicted in ***Table 55***.

Table 55: Deparaffinization steps using a descending EtOH series

Solution	Volume percent (v/v)	Duration	Repetition
Xylene (container I)	100%	10 min	1x
Xylene (container II)	100%	10 min	1x
EtOH	100%	10 min	1x
EtOH	96%	10 min	1x
EtOH	70%	10 min	1x
Purified water	/	5 min	3x

To stain tissue and cell sections in general, hematoxylin and eosin staining (HE) was conducted, resulting in pink eosin stains of proteins (cytoplasm, extracellular matrix) and deep blue to purple coloring of nuclei due to hematoxylin [119]. HE staining was exclusively conducted by the Histology Core Facility (Claudia Braun, University Medical Center Mainz). In case of specific antibody staining, the protocol was continued as follows: The glass slides were transferred to a plastic stain through container (Cat. XC73.1, Carl Roth) and an antibody-specific antigen retrieval was conducted, according to ***Table 56***.

The container was sufficiently filled with buffer solution (see buffer compositions in ***Table 33***) to cover the glass slides completely and closed with a lid before being cooked for the indicated period using a rice steamer (RusselHobbs, Germany).

Table 56: Antigen retrieval

Specific staining	Antigen retrieval buffer	Duration
CD3	Citrate buffer, 10 mM, pH 6	40 min
Cleaved Caspase-3 (Asp175)	Citrate buffer, 10 mM, pH 6	40 min
MPO	EDTA buffer, 1 mM, pH 8	20 min
NOD2	Citrate buffer, 10 mM, pH 6	40 min

Next, the container was taken out of the steamer, and the slides were cooled down for 20 min at RT. The slides were then transferred back to the glass staining rack and washed three times with purified water for 5 min. To reduce high background staining of endogenous proteins of different cell compartments and thus, false positive staining [120], the tissue sections were quenched for 10 min in 5% H_2O_2 solution, which was freshly prepared by mixing 30 mL of purchased 30% hydrogen peroxide (Cat. 8070.4, Carl Roth) with 150 mL purified water. The slides were washed again (3 x 5 min in purified water) before the tissue borders were marked using a hydrophobic barrier marker (Cat. VEC-H-4000, Biozol) to enable a continuous application and distribution of all subsequent solutions.

For the following immunohistochemical staining, different antibodies (see ***Table 15***) were used. Their respective buffer compositions are enclosed in ***Table 57***. The glass slides were put into a humid chamber in a horizontal position. The tissue sections were blocked for 1 h at RT by applying a sufficient volume (approx. 100 µL/ section) of 5% normal horse or goat serum diluted in 1x TBST solution (1:10 diluted in purified water; Cat. 9997S, Cell Signaling), covering the previously marked area. The solution was removed and exchanged with the respective primary antibody (diluted in blocking serum) and incubated overnight at 4°C in a humid chamber.

The next day, the primary antibody was removed, and the slides were washed four times for 1 min with 1x TBST buffer via pipetting approx. 350µL/ slide. For secondary antibody staining, ready-to-use anti-rabbit HRP-coupled signal stain boost reagent (Cat. 8114S, Cell Signaling) was applied (approx. 100 µL/ section) according to the manufacturer's protocol (1 to 3 drops/ section), covering the tissue sections sufficiently.

However, in the case of primary staining with polyclonal goat MPO antibody, secondary staining was conducted using 1:500 diluted anti-goat HRP (in 5% horse blocking serum/TBST; Cat. A15999, Thermo Fisher). The slides were incubated for 1 h at 4°C in a humid chamber, and the liquid was removed before washing (4 x 1 min with TBST).

Table 57: Primary and secondary antibody dilutions for immunohistochemistry

Primary Ab	**Host**	**Dilution**	**Dilution buffer**
CD3	Rabbit mAb	1:200	5% normal goat serum in 1x TBST
Cleaved Caspase-3 (Asp175)	Rabbit mAb	1:500	5% normal goat serum in 1x TBST
MPO	Goat pAb	1:200	5% normal horse serum in 1x TBST
NOD2	Rabbit mAb	1:100	5% normal goat serum in 1x TBST
Secondary Ab	**Host**	**Dilution**	**Diluted in**
anti-rabbit HRP SignalStain® Boost IHC Detection Reagent	goat	/	ready-to-use
anti-goat HRP	Donkey	1:500	5% normal horse serum in 1x TBST

Subsequently, SignalStain DAB Substrate (Cat. 8059, Cell Signaling) was applied according to the manufacturer's protocol (1000 µL diluent + 30 µL DAB), covering the tissue sections sufficiently (approx. 100 µL/ section) until the staining started to develop. Development was stopped in time to prevent overstaining by quickly transferring the slides into fresh purified water (CD3 after 10-20 min, CC3 and MPO after 5 to 10 min, and NOD2 after 1 to 5 min). When the slides were transferred back to the glass staining rack, they were covered with purified water for 5 min, which was repeated twice, including water exchanges in between.

To counterstain the tissue sections and visualize nuclei, the glass staining rack was placed for 30 sec in a mixture of 90 mL Mayer's Hematoxylin solution (Cat. MHS32-1L, Sigma) diluted in 350 mL distilled water, while slightly moving the rack up and down under constant coverage with liquid. Immediately after, the staining rack was transferred to a glass container, being supplied constantly with running tap water for 15 min until the tissue started getting blue. The staining was checked under the microscope before starting the dehydration process with an ascending EtOH series below the fume hood (see exact protocol in ***Table 58*** below).

Table 58: Dehydration steps using an ascending EtOH series

Solution	**Volume percent (v/v)**	**Duration**	**Repetition**
EtOH	70%	1 min	1x
EtOH	96%	1 min	1x
EtOH	100%	1 min	1x
Xylene (container II)	100%	5 min	1x
Xylene (container I)	100%	5 min	1x

After tissue dehydration, coverslips were mounted on the slides using Roti Histokitt (Cat. XC73.1, Carl Roth) and remained under the fume hood for approx. 24 h to dry and harden. Histology slides were analyzed under the microscope and finally high-resolution scans were digitalized by the Institute of Pathology (Bonny Adami, University Medical Center Mainz) using the Nano Zoomer 2.0HT (Hamamatsu, Japan).

3.7.3 Confocal immunofluorescence microscopy

Tissue sections of formalin-fixed paraffin-embedded (FFPE) back skin material from PBS-treated and *S. aureus*-infected mice were sent to the collaborating working group of Prof. Dr. Alexander Weber of the Institute of Immunology (Eberhard Karls University Tübingen). Confocal immunofluorescence staining, microscopy and image acquisition was conducted by Dr. Francesca Bork: The experimental procedure started with deparaffinization of the glass slides (1 h at 60°C in the oven), the paraffin was removed from the tissue using RotiHistol (Cat. 6640.5, Carl Roth) and series of ethanol washes (see ***Table 59***).

Table 59: Deparaffinization for immunofluorescence staining using descending EtOH series

Solution	Volume percent (v/v)	Duration	Repetition
RotiHistol (container I)	100%	10 min	1x
RotiHistol (container II)	200%	11 min	1x
EtOH	100%	5 min	1x
EtOH	100%	5 min	1x
EtOH	95%	5 min	1x
EtOH	80%	5 min	1x
EtOH	70%	5 min	1x
Double distilled water	/	30 sec	1x
PBS	/	∞	stored at RT

Next, the slides were boiled for 25 min in 10 mM citrate buffer (pH 6) to reverse formaldehyde crosslinks and perform antigen retrieval, followed by PBS washing steps (3 x 5 min). Borders of the tissue sections were marked using a hydrophobic barrier marker, then the tissue was blocked overnight (approx. 100 µL/ section) within a humid chamber at 4°C in a horizontal position using immunofluorescence blocking buffer (see ***Table 34***) to reduce non-specific background staining signal. Primary and secondary antibodies used for immunofluorescence staining are listed in ***Table 16***, their respective dilutions are enclosed in ***Table 60*** below.

The next day, the solution was replaced with primary antibodies diluted in blocking buffer (approx. 100 µL/ section) and the tissue was incubated for 2 h at RT. The glass slides were washed with PBS (3 x 5 min) using a pipette, before secondary antibodies diluted in blocking buffer (approx. 100 µL/ section) were applied and incubated for 1 h at RT in the dark. From now onwards, the samples were protected from light all the time. Again, excessive antibodies were removed from the tissue sections via PBS washing (3 x 5 min).

Table 60: Antibody dilutions for immunofluorescence

Staining	Target	Host	Dilution in blocking buffer
Primary Ab	Protein A	Rabbit	1:500
Secondary Ab	Anti-rabbit AF594	Chicken	1:500
Hoechst33342	nuclei	/	1: 10,000 (=1 ug/mL)

To stain nuclear DNA, the slides were incubated with 1 µg/mL Hoechst33342 in PBS (Cat. H21492, Thermo Fisher) for 10 min at RT in the dark. Before the slides were mounted with uncoated coverslips, they were washed again (PBS, 3x 5 min), and 8 µL of ProLong Diamond Antifade/ sample (Cat. P36961, Thermo Fisher) was added to the skin sections. Application of the latter preserves fluorescence signal strength during prolonged imaging sessions and achieves a low background signal. The slides were dried at RT overnight in the dark, then microscopy was performed with a Zeiss LSM 800 Confocal microscope (Carl Zeiss, Germany) using Airyscan acquisition to image 3x3 tiles in a 40x objective (2d infection samples, scale: 50 µm) or 6x6 tiles in 20x objective (7d infection samples; scale: 100 µm). Subsequently, the acquired data was processed using ImageJ-Win64 software (NIH).

3.8 Statistical data analysis and illustration

All results obtained in this study are represented as mean values ± standard deviation (SD) in case of *in vitro* stimulations or as mean values ± standard error of the mean (SEM) in case of *in vivo* studies, including information regarding the used animal numbers (n = x mice). Statistical significance was calculated in Microsoft Excel using a 2-tailed Student's t-test, and the p-values are depicted with asterisks (*) or daggers (†) as follows:

* or †	$p < 0.05$
** or ††	$p < 0.01$
*** or †††	$p < 0.001$
ns = not significant	

The data is presented in bar diagrams, while showing individual sample points in addition. Graphs were generated using GraphPad Prism. Images showing the graphical abstract or summaries of the topics investigated, as well as schematic overviews, were created with BioRender.com and are denoted as such (for reference see *chapter 6.1*).

3.9 Data Availability

The recently published RNA-seq data set of *S. aureus*-infected hKC acquired in this study can be retrieved from the database Gene Expression Omnibus (GEO) with the accession number GSE267665. Open-source access is bound to the final publication of our data within the frame of our manuscript entitled *"NOD2-induced IκBζ mediates a protective host response against epicutaneous Staphylococcus aureus infection, Fischer et al. 2025*". All raw data of other RNA-seq data sets, such as the stimulation of hKC with MDP (unpublished) or recombinant human IL-36α (published in *Müller et al. 2018* [22]), or selected genes of the above-mentioned *S. aureus* infection *in vitro* are provided in ***Supplementary Table I*** to ***Supplementary Table IV***, in case the results were used to generate the depicted heatmaps.

4. Results

Within the last decade, several studies have implicated the involvement of the intracellular bacteria recognition receptor NOD2 in the pathogenesis of autoinflammatory skin diseases, such as psoriasis [121] and atopic dermatitis [122], assigning this receptor a novel function apart from its well-studied immunomodulatory role in Crohn's disease, one particular type of inflammatory bowel disease (IBD) [123].
Hence, we wanted to investigate whether the signaling pathways resulting in the activation of intracellular NOD2 receptors and the induction of the co-transcriptional activator IκBζ are intertwined, leading to the promotion of NF-κB-driven responses and subsequently, providing substantial host defense mechanisms in keratinocytes.

4.1 NOD2 activation induces IκBζ expression in keratinocytes

As a starting point of this project, we were interested whether stimulation with muramyl-dipeptide (MDP), a NOD2 agonist, can induce any IκBζ expression in keratinocytes. Since the translocation of MDP is a pre-requisite to induce NOD2 oligomerization and thus, the activation of the intracellular receptor, MDP transfection was conducted.
First, we failed to induce IκBζ protein expression at all in MDP-stimulated HaCaT cells, an immortalized keratinocyte cell line isolated from differentiated human skin (see ***Supplementary Figure I***), suggesting that these cells either lost their responsiveness to NOD2 activation in general or, that the applied stimulus and/ or transfection was not sufficient. Since treatment with recombinant human IL-36α, a common psoriasis-associated stimulus, elicited a strong IκBζ expression in this cell line, following experiments were solely carried out with primary human and murine keratinocytes. Next, it was experimentally excluded that the used transfection reagent ProteoJuice itself leads to the induction of IκBζ protein, when treating undifferentiated human keratinocytes with either ProteoJuice, MDP alone or in combination. Hereby we confirmed that MDP indeed requires translocation into the cytoplasm, accomplished by transfection (see ***Supplementary Figure II***), to elicit IκBζ expression.
To investigate the IκBζ induction levels *in vitro* over time, MDP transfection and stimulation of starved primary human keratinocytes (hKC) was conducted during a time course of 24 h. As signaling pathways and the sensitivity towards stimuli are known to differ between cells with varying differentiation levels [12], experiments were conducted in parallel using both undifferentiated and differentiated keratinocytes (see ***Figure 4.1***), while the latter were additionally exposed to 2 mM $CaCl_2$ for 72 h prior starvation.
Immunoblot analysis (***Figure 4.1***A) revealed, that IκBζ protein induction takes place around 2 h after NOD2 stimulation. This was further verified with the consecutive activation of the MAPK signaling pathway downstream of NOD2, resulting in phosphorylated p38-MAPK (p-p38 T180/182) protein levels. [124, 125].

Equal results were obtained from the analysis of relative *NFKBIZ* gene expression levels upon stimulation with MDP, which peaked around 1 to 2 h post-stimulation (***Figure 4.1***B).
All in all, we proofed that the activation of NOD2 mostly triggers the expression of IκBζ on protein level, while *NFKBIZ* mRNA levels were only mildly upregulated at the same time point, making translation of newly synthesized mRNA unrealistic.
Based on the slightly less sensitive mRNA levels elicited by the MDP stimulus in undifferentiated cells and the fact that the outer skin layer is mostly composed of differentiated skin cells, which can individually act as pathogen sensors, we decided to conduct all following studies exclusively with differentiated keratinocytes.
Bringing a broad experience from the field of psoriasis research into this project, we were aware of strongly differing sensitivities towards *in vitro* stimulations of cells derived from individual donors, such as varying expression levels of IκBζ. Thus, to minimize cell-derived bias throughout the study, we made sure to use primary cell suspensions from mixed donors.

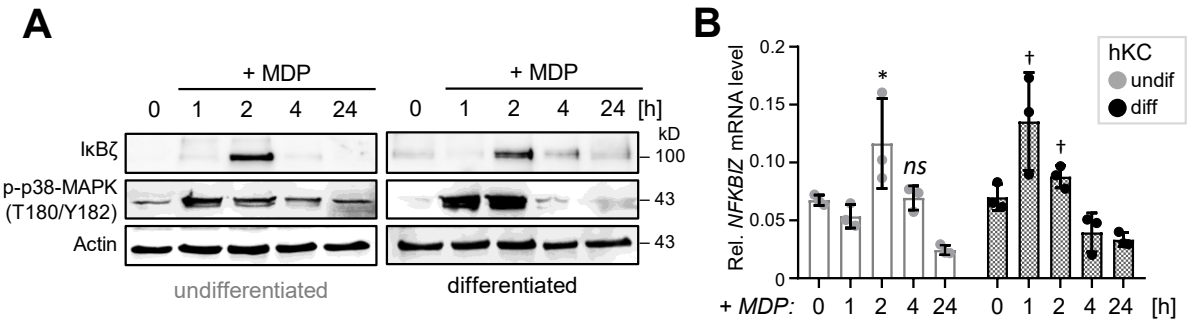

Figure 4.1: NOD2 agonist MDP induces IκBζ expression in both undifferentiated and differentiated primary human keratinocytes.
A. *Differentiated hKC were seeded in parallel to undifferentiated cells but were additionally treated for 72 h with 2 mM CaCl2 prior to stimulation. All cells were treated with 20 µg/mL MDP in the presence of transfection reagent ProteoJuice. Immunoblot analysis shows IκBζ protein expression in a time course of MDP stimulation, which was verified with phosphorylated p38-MAPK (T180/182) protein levels. ß-Actin served as a loading control.*
B. *Relative NFKBIZ mRNA expression in undifferentiated and differentiated hKC; the cells were treated as in (A). For its calculation, values were normalized to the reference gene RPL37A. Shown is the mean of 3 biological replicates ± standard deviation (SD). Significance, compared to untreated control, was calculated using a 2-tailed Student's t-test (undifferentiated: *p < 0.05, ns = not significant; differentiated: p < 0.05).*

4.2 IκBζ expression is elicited downstream of both NOD1 and NOD2 receptors

The pattern recognition receptors of the NOD-like receptor (NLR) family are selectively activated in keratinocytes upon cytoplasmic encounter with bacterial cell wall components, such as peptidoglycan (PGN), depending on the gram status of the respective infiltrating bacteria among other things [126]. Therefore, we wanted to know whether the induction of IκBζ expression might be conserved among the almost structurally identical NOD2 and NOD1 receptors, of which the latter only lacks a second CARD domain.

For this purpose, we treated differentiated hKC in parallel with different NOD1 and/or NOD2 agonists for 2 h (see ***Figure 4.2***). Phosphorylation levels of IκBα (p-IκBα (S32)), being elicited upon NF-κB activation downstream of NOD2 [124], confirmed activation of both receptors. As expected, all applied agonists were able to induce IκBζ protein expression, which correlated with the intensity of p-IκBα detection, implying that both receptors are per se capable of regulating keratinocyte-derived IκBζ expression.

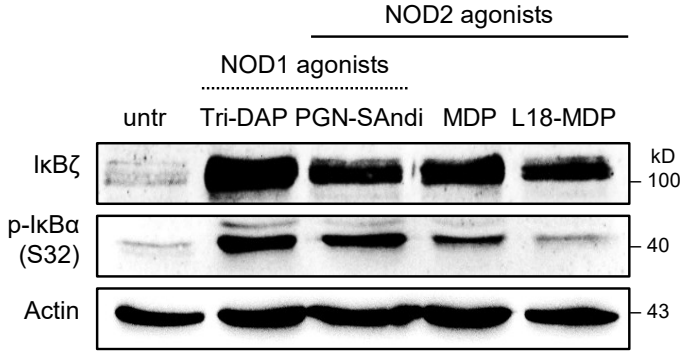

Figure 4.2: IκBζ protein expression can be induced with both NOD1 and NOD2 agonists. *Immunoblot analysis of differentiated hKC after transfection with ProteoJuice and stimulation with 1 µg/mL NOD1 and/or NOD2 agonists for 2 h. The following agonists were applied: selective NOD1 agonist Tri-DAP (Tri-diaminopimelic acid), NOD1/NOD2 agonist PGN-SAndi (ultrapure peptidoglycan of S. aureus), or selective NOD2 agonists MDP and L18-MDP (enhanced MDP-Lysin18). Phosphorylated levels of IκBα (p-IκBα (S32)) indicate successful treatment and activation of the cells, β-actin served as a loading control. The experiment was performed by Franziska Engelmann.*

4.3 NOD2 stimulation does not synergize with other pro-inflammatory stimuli in the induction of IκBζ in keratinocytes

Next, we wanted to investigate whether equal stimulating factors downstream of NOD2 and in general upstream of IκBζ are involved in the induction of IκBζ protein in keratinocytes. Being a transcriptional co-activator of specific NF-κB target genes, IκBζ regulates psoriatic gene expression in a disease-promoting manner. Hence, we transfected hKC with or without MDP for 2 h and further stimulated the cells for the last hour in presence or absence of pro-inflammatory cytokines, such as IL-36α, IL-1β or IL-17A and TNFα, being known to trigger IκBζ expression in keratinocytes [22].
Although immunoblot analysis showed slightly different intensities of IκBζ protein among single treated samples (***Figure 4.3***, left), assumingly correlating with the applied IL-36α and IL-1β concentration, no substantial changes in the IκBζ expression were detected in MDP-transfected samples co-stimulated with IL-36α, IL-1β and IL-17A/ TNFα (***Figure 4.3***, left and right).
Hence, we concluded that the signaling pathways leading either to the NOD2 receptor activation or to the cytokine-dependent pro-inflammatory responses do not act synergistically upon IκBζ protein induction *in vitro*. Also, these data imply the involvement of differing and stimulus-dependent regulators upstream of IκBζ.

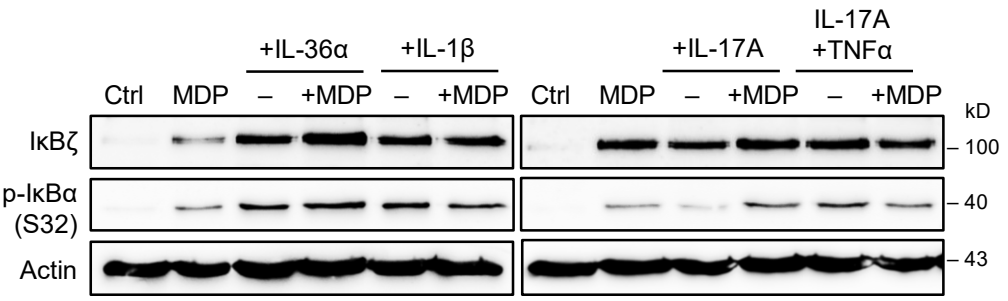

Figure 4.3: MDP-induced IκBζ expression in keratinocytes does not overwrite stimulating effects of psoriasis-related pro-inflammatory cytokines.
Immunoblot analysis of differentiated hKC treated for 2 h with or without 20 µg/mL MDP. For the last hour, cells were either co-stimulated or only treated with 20 ng/mL IL-36α and IL-1ß, 100 ng/mL IL-17A, and 10 ng/mL TNFα. Phosphorylated levels of IκBα (p-IκBα (S32)) indicate successful treatment and activation of the cells, ß-actin served as loading control. The experiment was performed by Franziska Engelmann.

4.4 NOD2-mediated IκBζ expression supports the maintenance of the skin barrier and elicits pro-inflammatory and antimicrobial responses

To study *NFKBIZ*-dependent transcriptional changes upon NOD2 activation, we lentivirally depleted IκBζ from human primary keratinocytes using a *NFKBIZ*-specific shRNA construct (***Figure 4.4***A). Transcriptome analysis of MDP-treated, differentiated control versus *NFKBIZ* knockdown hKC was performed after 24 h and revealed 379 genes being significantly regulated by stimulation with MDP (cut-off: p-values ≤ 0.05, fold change absolute >2, difference absolute >3). Among these genes, around 38% became deregulated in *NFKBIZ* knockdown cells, while most of these genes were not induced anymore upon loss of IκBζ (***Figure 4.4***B – D), proofing the important function of IκBζ as a transcriptional co-activator of NOD2 target gene expression.

This is also reflected in the EnrichR-based gene set enrichment analysis (GSEA) of genes being significantly MDP-regulated and *NFKBIZ*-dependently repressed (see ***Figure 4.4***C). Interestingly, the pathway analysis revealed three distinct groups of genes, which have previously been described in the context of auto-inflammatory skin diseases and bacterial skin infections. For instance, MDP-induced IκBζ is accountable for the proper expression of genes encoding proteins, which are involved in the maintenance of the skin barrier and the differentiation status of keratinocytes, such as late cornified envelope (LCE) proteins. Secondly, the loss of IκBζ revealed an impaired expression of pro-inflammatory genes involved in IL-17/ IL-36-driven responses, including chemotactic cytokines responsible for the recruitment of innate immune cells, such as neutrophils [10]. Lastly, a massive repression of several antimicrobial peptides was observed in *NFKBIZ*-depleted cells, presenting first-line defense mechanisms during an encounter of keratinocytes with bacterial components, comprising defensins (*DEFB1, DEFB4A*), S100 proteins or peptidoglycan recognition proteins (*PGLYRP*) among others. Representative genes of each group are further shown in the heatmap of ***Figure 4.4***D, emphasizing the importance of IκBζ to fight bacterial infections.

Of note, only a few MDP-regulated genes were significantly upregulated in *NFKBIZ*-depleted hKC (see ***Supplementary Figure III***), being responsible for elevated intracellular protein transport and post-translational modifications, aside from a dysregulated assembly of blood vessels or extracellular matrix.

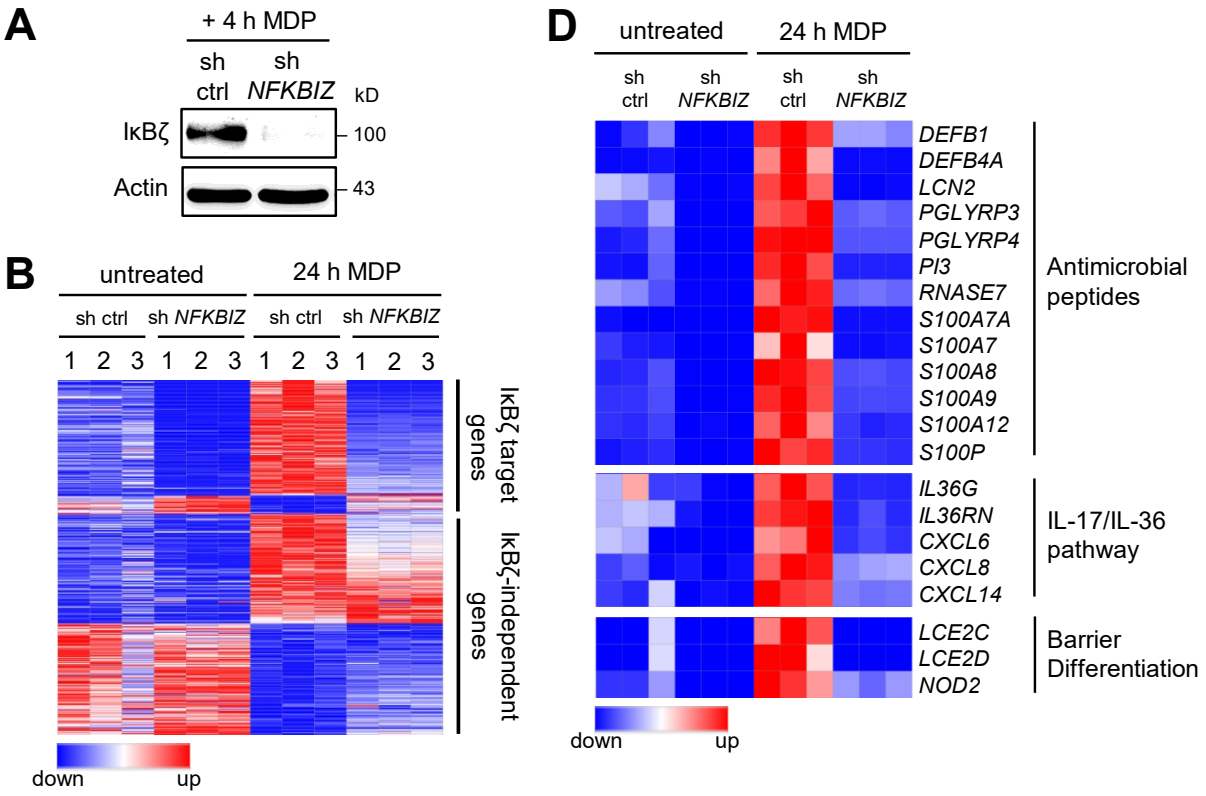

C

Downregulated pathways (*NFKBIZ* dependent)	**p-value**	**Library**
Epidermis development	$3.11*10^{-15}$	GO_2021
Formation of cornified envelope	$3.34*10^{-19}$	Reactome_2022
Impaired skin barrier function	$3.07*10^{-11}$	MGI_2021
Keratinocyte differentiation	$4.68*10^{-14}$	GO_2021
IL-1 family signaling	0.00241	Reactome_2022
IL-17 signaling pathway	$2.88*10^{-10}$	KEGG_2021
IL-36 pathway	0.00076	Reactome_2022
Innate immune response	$4.70*10^{-9}$	GO_2021
Neutrophil migration	0.00011	GO_2021
Antimicrobial peptides	$2.44*10^{-13}$	Reactome_2022
Detection of bacterium	$7.67*10^{-5}$	GO_2021
Increased susceptibility to bacterial infection	0.00663	MGI_2021
Increased susceptibility to induced colitis	0.00284	MGI_2021
NOD-like receptor signaling pathway	0.00508	KEGG_2021
Staphylococcus aureus infection	$2.54*10^{-5}$	KEGG_2021
TAK1-dependent IKK and NF-κB activation	0.00261	Reactome_2022
Toll-like receptor cascades	0.00317	Reactome_2022

Figure 4.4: Transcriptome analysis of MDP-stimulated keratinocytes reveals NFKBIZ-dependent deregulation of skin barrier or antimicrobial and IL-17/ IL-36 responses.
A. *Knockdown validation of differentiated control (sh ctrl) and knockdown (sh NFKBIZ) hKC, transfected and treated with 20 µg/mL MDP for 4 h. ß-Actin served as a loading control.* ***B.*** *Heatmap of all MDP-dependent genes after treating control and NFKBIZ-depleted differentiated hKC for 24 h (same concentrations as in (A); cut-off: p-values ≤ 0.05, fold change absolute >2, difference absolute >3). Red indicates upregulation, blue indicates downregulation.* ***C.*** *Gene set enrichment analysis (GSEA) of downregulated, IκBζ-dependent target genes after 24 h MDP stimulation (from (B)). GSEA was performed with EnrichR. Significantly enriched pathways are shown, sorted by pathway and p-value.* ***D.*** *Heatmap of selected IκBζ target genes from (B), encoding antimicrobial peptides or genes involved in IL-17 and IL-36 signaling and skin barrier function.*

4.5 IκBζ target genes being identified in the beforementioned signaling pathways are induced by MDP in both human and murine keratinocytes

Next, we successfully validated these findings with qPCR analyses of selected target genes (see ***Figure 4.5***A) based on the aforementioned pathways (***Figure 4.4***C and D).

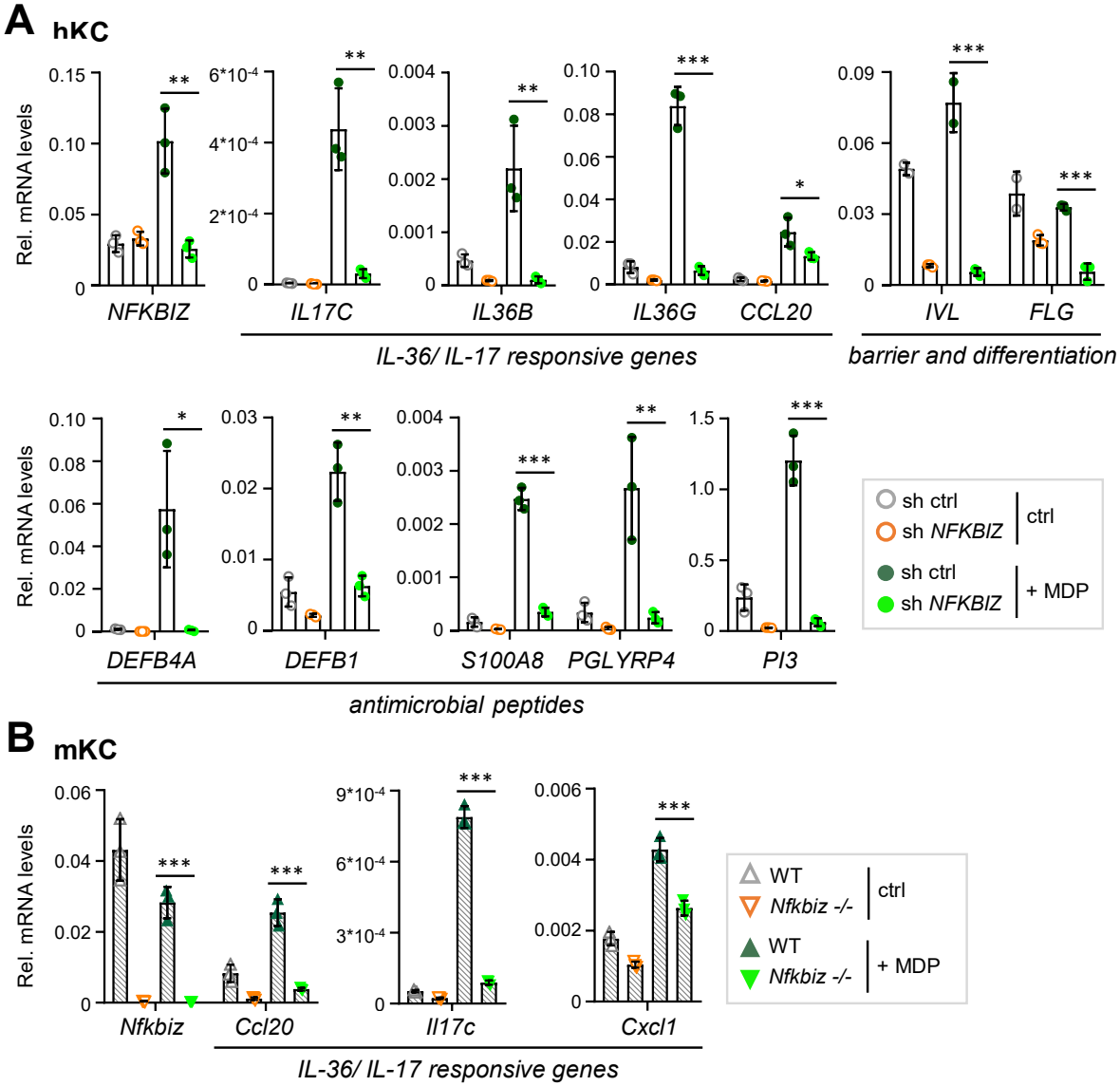

Figure 4.5: Validation of RNAseq shows MDP-dependent gene induction of IκBζ and its target genes in human and murine keratinocytes.

A. *Relative mRNA expression levels of NFKBIZ and IκBζ target genes from differentiated control (sh ctrl) and NFKBIZ-depleted (sh NFKBIZ) primary hKC. Cells were transfected and stimulated for 24 h with 20 µg/mL MDP. For calculation of the relative mRNA levels, values were normalized to the reference gene RPL37A.* ***B.*** *Relative mRNA expression levels of Nfkbiz, validating the knockout, and IκBζ target genes of murine keratinocytes derived from WT or Nfkbiz-depleted (Nfkbiz$^{-/-}$) mice, transfected and stimulated for 1 h with 20 µg/mL MDP. For mKC generation, cells derived from 2 -3 animals per group were pooled before treatment. Relative mRNA levels were normalized over Actb. Experiment was performed by Tanja Kübelbeck. (A) and (B) show the mean of 3 biological replicates ± standard deviation (SD). Significance was calculated using a 2-tailed Student's t-test (*p < 0.05, **p < 0.01, and ***p < 0.001).*

MDP stimulation of control hKC mainly triggered the secretion of antimicrobial peptides, such as defensins (*DEFB4*, *DEFB1),* S100 proteins *(S100A8)* or peptidoglycan recognition proteins *(PGLYRP4)*, which were significantly downregulated in the absence of *NFKBIZ.* Besides, *NFKBIZ*-depleted hKC possessed a diminished expression of genes encoding proteins responsible for the maintenance and formation of the epidermal layer, e.g. seen in filaggrin (*FLG)* and involucrin *(IVL*) expression, and exhibited significantly less IL-17/IL-36-induced responses (e.g. *IL17C, IL36B, IL36G*) and chemokines (*CCL20*), as well.
Likewise, MDP stimulation induced similar target genes in murine control keratinocytes, which were also strongly diminished in their expression levels in murine *Nfkbiz* knockout keratinocytes, isolated from the tails of *Nfkbiz*$^{\Delta K14\text{-cre}}$ KO mice. All in all, these results confirm that IκBζ is a key transcriptional co-activator of pro-inflammatory gene expression, antimicrobial peptides and genes encoding barrier proteins.

4.6 IκBζ and NOD2 synergistically induce *DEFB4* promoter activity

Since the transcriptome analysis revealed strong IκBζ-dependent effects on antimicrobial peptide expression upon NOD2 activation, we were wondering whether IκBζ directly influences the promoter activity of defensins, e.g. *DEFB4*. Representing a first-line defense mechanism against bacterial infections in epithelial cells, the underlying mechanisms leading to the expression and secretion of antimicrobial peptides have been investigated for decades. For example, in the early 20th century *Voss et al.* already discovered the NOD2-mediated activation of the *DEFB4* promoter in an NF-κB-dependent manner [107]. However, at that time no connection to IκBζ was created.
Based on their findings [107], we performed a dual luciferase assay where we transiently transfected HEK293T cells overnight using their *DEFB4* promoter construct, containing firefly luciferase, and a TK-Renilla reporter construct. Besides, plasmid DNA of either control, IκBζ and/ or NOD2 overexpression constructs were transfected, respectively. To mimic NOD2 activation, the cells were additionally treated with the NOD2 agonist MDP in the last 2 h before sample harvest.
Successful IκBζ or NOD2 overexpression was confirmed by immunoblot detection (see ***Figure 4.6***A), albeit showing diminished NOD2 protein levels in the IκBζ-NOD2 co-overexpression sample. When examining the *DEFB4* promoter activity 24 h post transfection (see ***Figure 4.6***B), MDP stimulation did not lead to an increase of luciferase activity in control and NOD2-only transfected cells in our experimental set-up.
Other than that, untreated HEK293T cells bearing an IκBζ overexpression recorded low *DEFB4* promoter activities, which significantly increased upon MDP treatment. Surprisingly, this effect was strongly amplified in HEK293T cells bearing the combined overexpression of NOD2 and IκBζ, where we recorded the strongest *DEFB4* promoter activation visualized in higher folds of luciferase activity.

Hereby we provide evidence that both proteins synergistically induce the *DEFB4* promoter and thus, promote the antibacterial responses via upregulation of antimicrobial peptide-related gene expressions. Hence, we hypothesize that the induction of NOD2-target genes might rely on an additional transcriptional co-factor, such as IκBζ.

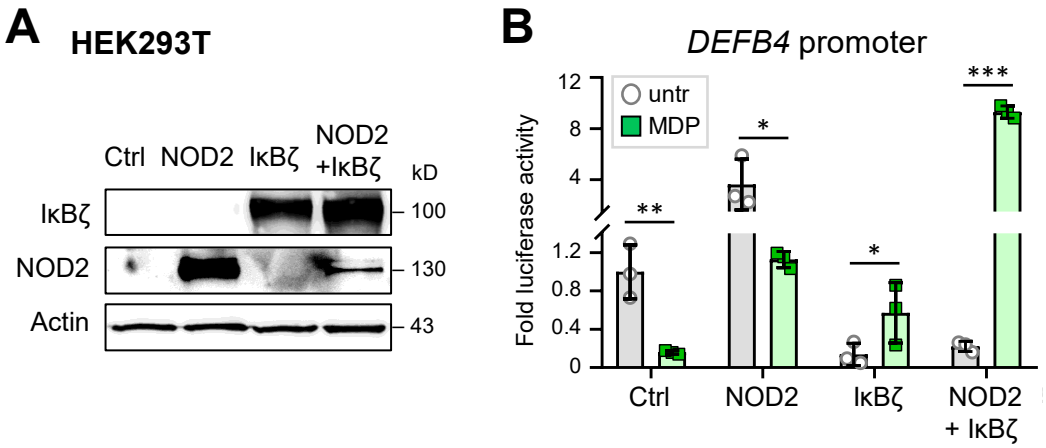

Figure 4.6: Co-expression of IκBζ and NOD2 synergistically activates the DEFB4 promoter in HEK293T cells upon MDP stimulation.

A. *Immunoblot of HEK293T cells validates IκBζ and NOD2 overexpression. Cells were transiently overexpressed for 24 h with the following constructs using the Calcium-Phosphate transfection method: TK-Renilla plasmid, HBD2 promoter construct, NOD2 and/ or IκBζ overexpression plasmids. β-Actin served as a loading control.* ***B.*** *Dual luciferase assay to analyze the DEFB4 promoter activity in control- and MDP-stimulated HEK293T cells after 24 h using luciferase reporter constructs with IκBζ and/or NOD2 overexpression. Cells were transfected with overexpression plasmids as described in (A) and incubated for 24 h. The last 2 h before sample harvest, cells were additionally treated with 20 µg/mL MDP. Relative luciferase activity was calculated as fold induction over unstimulated control cells and normalized to co-transfected TK-Renilla. Significance was calculated using a 2-tailed Student's t-test (*p < 0.05, **p < 0.01, and ***p < 0.001). Raw data were generated by Franziska Engelmann.*

4.7 The transcription factor NF-κB rather than STAT3 induces the IκBζ expression downstream of NOD2 receptor activation

Next, we wanted to investigate potential upstream regulatory mechanisms leading to the induction of IκBζ upon NOD2 activation. Previously, it was published by our group [22], that *NFKBIZ* mRNA expression can be transcriptionally upregulated upon binding of selective transcription factors to the *NFKBIZ* locus, such as the signal transducer and activator of transcription 3 (STAT3) or NF-κB, leading to the induction of pro-inflammatory responses in the context of an IL-36-driven skin inflammation.

Therefore, we treated differentiated hKC with the NOD2 agonist MDP for 2 h in the presence or absence of small molecule inhibitors, blocking either the STAT1/ STAT3 signaling by using 10 µM Stattic, or blocking NF-κB by using 10 µM of the selective IKKβ inhibitor (IKKβi) IMD 0354. Immunoblot analysis revealed that exclusively the abrogation of IKK signaling quenched the MDP-induced IκBζ protein expression, while inhibition of STAT1/3 only slightly diminished this effect (see ***Figure 4.7***). Of note, efficient inhibitor activation was checked by staining for phosphorylated levels of STAT1 (p-STAT1 (Tyr701)) and STAT3 (p-STAT3 (Tyr705)) proteins (for Stattic), or via detection of phosphorylated IκBα (p-IκBα (Ser32)) levels being blocked by the selective IKKβ inhibitor. In conclusion, NF-κB is likely to mediate the induction of IκBζ and its target gene expression upon activation of NOD2, while the contribution of STAT1 or STAT3 to the induction of IκBζ downstream of NOD2 seems unlikely.

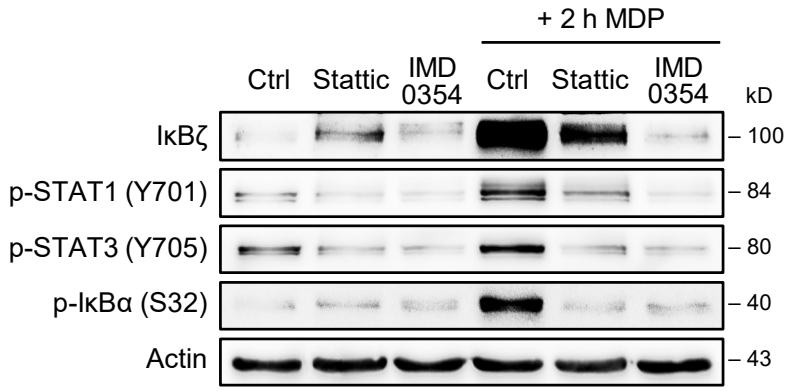

Figure 4.7: NF-κB but not STAT3 is responsible for the MDP-induced IκBζ expression in human keratinocytes.

Immunoblot of IκBζ protein levels of differentiated hKC being treated with STAT1/STAT3 inhibitor Stattic (10µM) or selective IKKβ inhibitor IMD 0354 (10 µM) in presence or absence of NOD2 stimulation. Cells were transfected and treated for 2 h with 20 µ/mL MDP after 45 min pre-incubation with solely inhibitors or DMSO vehicle control. Phosphorylated STAT1 and STAT3 levels (p-STAT1 (Y701), p-STAT3(Y705)) served as Stattic inhibitor controls. Phosphorylated IκBα (p-IκBα(S32)) measures IMD 0354 inhibitor activity besides validating NOD2 activation upon MDP stimulation. β-actin served as a loading control. The experiment was performed by Franziska Engelmann.

4.8 *S. aureus* infection triggers IκBζ expression in human and murine primary keratinocytes

After we revealed that IκBζ is induced upon NOD2 receptor activation and thereby mediates the induction of a subset of NOD2 target genes in both human and murine specimen under optimal stimulation conditions *in vitro*, we wanted to investigate the potential of IκBζ to shape the host defense in keratinocytes in a more physiological setting, such as a bacterial infection.

Therefore, we infected differentiated keratinocytes with living, gram-positive methicillin-resistant *S. aureus* (MRSA) cultures with the wild-type MRSA strain USA300 LAC, which will be continuously abridged in the following under the term "*S. aureus"*, and compared it to the coagulase-negative commensal *Staphylococcus epidermidis (S. epidermidis).* In order to investigate their strain-dependent potential to elicit IκBζ protein expression *in vitro,* hKC were equally infected for 1 h using a multiplicity of 30 (MOI30) of each strain and IκBζ levels were assessed during a time course.

As depicted in ***Figure 4.8***A, unstimulated control cells did not express IκBζ protein at all. However, IκBζ became strongly induced after 1 h (time point +0 h) of infection with pathogenic *S. aureus*, whereas its protein level declined after removal of the bacteria and during longer incubation times in the presence of antibiotics to kill remaining external bacteria (time points +5 h, +23h, ***Figure 4.8***A left). On the contrary, only marginal IκBζ levels were observed immediately after *S. epidermidis* infection (***Figure 4.8***A right).

Besides, *S. aureus* also elicited increased mRNA expressions in both human (*NFKBIZ*) and murine (*Nfkbiz*) keratinocytes (***Figure 4.8***B and ***Figure 4.8***C) on transcriptional level after1 h infection. This might be a hint for post-translational or -transcriptional regulation mechanisms influencing the overall IκBζ expression during infection.

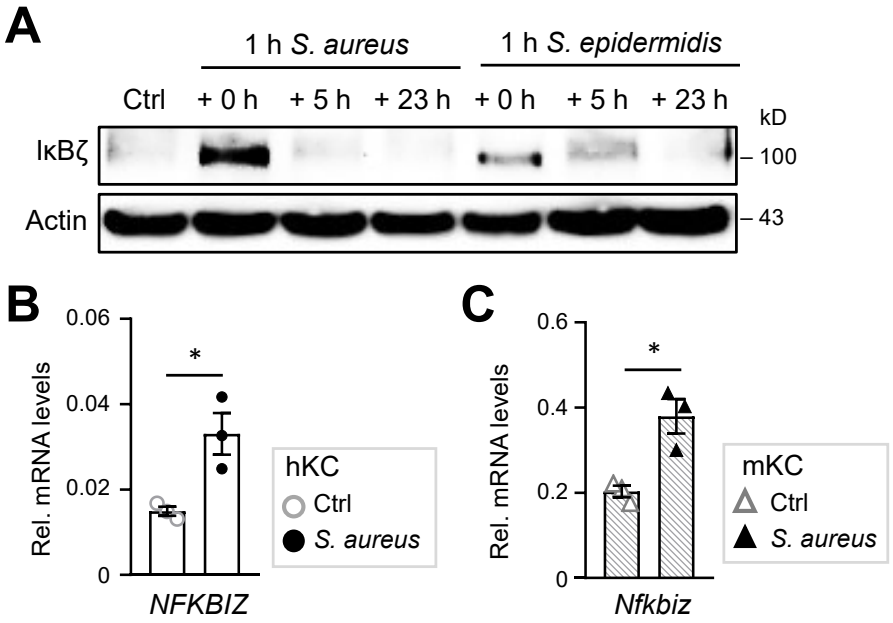

Figure 4.8: IκBζ expression is triggered by infection with pathogenic S. aureus in hKC at an early time point.

A. *Immunoblot analysis of IκBζ in differentiated hKC after infection with S. aureus USA300 WT or S. epidermidis WT 1457 (1 h, MOI 30). After bacterial removal, cells were further incubated as indicated (0 h, 5 h, 23 h). β-Actin served as a loading control.* ***B.*** *NFKBIZ mRNA levels of untreated (Ctrl) versus 1 h S. aureus-infected, differentiated human primary keratinocytes, normalized to RPL37A.* ***C.*** *Nfkbiz mRNA levels in untreated versus 1 h S. aureus-infected murine keratinocytes, normalized to Actb. For mKC generation, cells deriving from 2 - 3 wild-type animals per group were pooled before treatment. (B) and (C) show the mean values of 3 biological replicates ± standard deviation (SD). Significance was calculated using a 2-tailed Student's t-test (*p < 0.05).*

4.9 Inhibition of NOD2 but not TLR2 abrogates *S. aureus*-induced expression of IκBζ and its target genes in human keratinocytes

Keratinocytes have established different sensing mechanisms to identify living bacteria or bacterial components, which rely on the activation of so-called pathogen recognition receptors. During cutaneous infection with pathogenic, gram-positive bacteria, sensing in epidermal keratinocytes is established by the extracellular Toll-like receptor 2 (TLR2), as well as by the intracellular NOD2 receptor upon bacterial invasion or phagocytosis. Since both NOD2 and TLR2 receptors can similarly activate NF-κB and MAPK signaling pathways in a TAK1-dependent manner, albeit their different localization (as described in *chapter 1.5.1*), we expected them to elicit equal levels of IκBζ protein in the presence of their respective agonists MDP (NOD2) and Pam_3CSK_4 (TLR2), which was verified via immunoblot upon 1 h treatment (see ***Supplementary Figure IV***).

Hence, we investigated how far the inhibition of the individual receptor signaling pathways interferes with the *S. aureus*-induced pro-inflammatory gene responses in keratinocytes. To abrogate NOD2 signaling, which cascades in the downstream activation of the adaptor kinase RIPK2, the specific RIPK2 inhibitor GSK583 was used. For the inhibition of the TLR2 receptor, we used the small-molecule inhibitor TL2-C29. Differentiated hKC were infected for 1 h with living *S. aureus* cultures while being treated in the presence or absence of the aforementioned RIPK2 or TLR2 inhibitors (see ***Figure 4.9***A). The results of the immunoblot analysis revealed that *S. aureus*-induced IκBζ protein levels could be quenched exclusively under NOD2-inhibiting conditions, but not when TLR2 signaling was blocked. To exclude any differences in the bacterial infection efficiency, phosphorylated levels of IκBα turned out to be equally strong among the *S. aureus*-treated samples.

At a later time point of infection, we also analyzed the inhibitory effects of both inhibitors on *NFKBIZ* and its target gene expression after 24 h on transcriptional level. Unexpectedly, TLR2-inhibited cells did not quench the *S. aureus*-induced IκBζ-dependent gene expression but instead further increased it, except for the antimicrobial peptides (***Figure 4.9***B). However, pro-inflammatory gene responses were consistently and significantly downregulated upon NOD2 inhibition, albeit we failed to detect a significant decrease of *NFKBIZ* mRNA levels (***Figure 4.9***C), which might be caused by post-transcriptional events such as mRNA stabilization.

In conclusion, we proved that NOD2 receptor signaling, rather than TLR2 activation, mediates the antimicrobial and pro-inflammatory responses upon *S. aureus*-induced IκBζ expression in keratinocytes. Hence, we postulate NOD2 being an important downstream regulator during *S. aureus* infections *in vitro*.

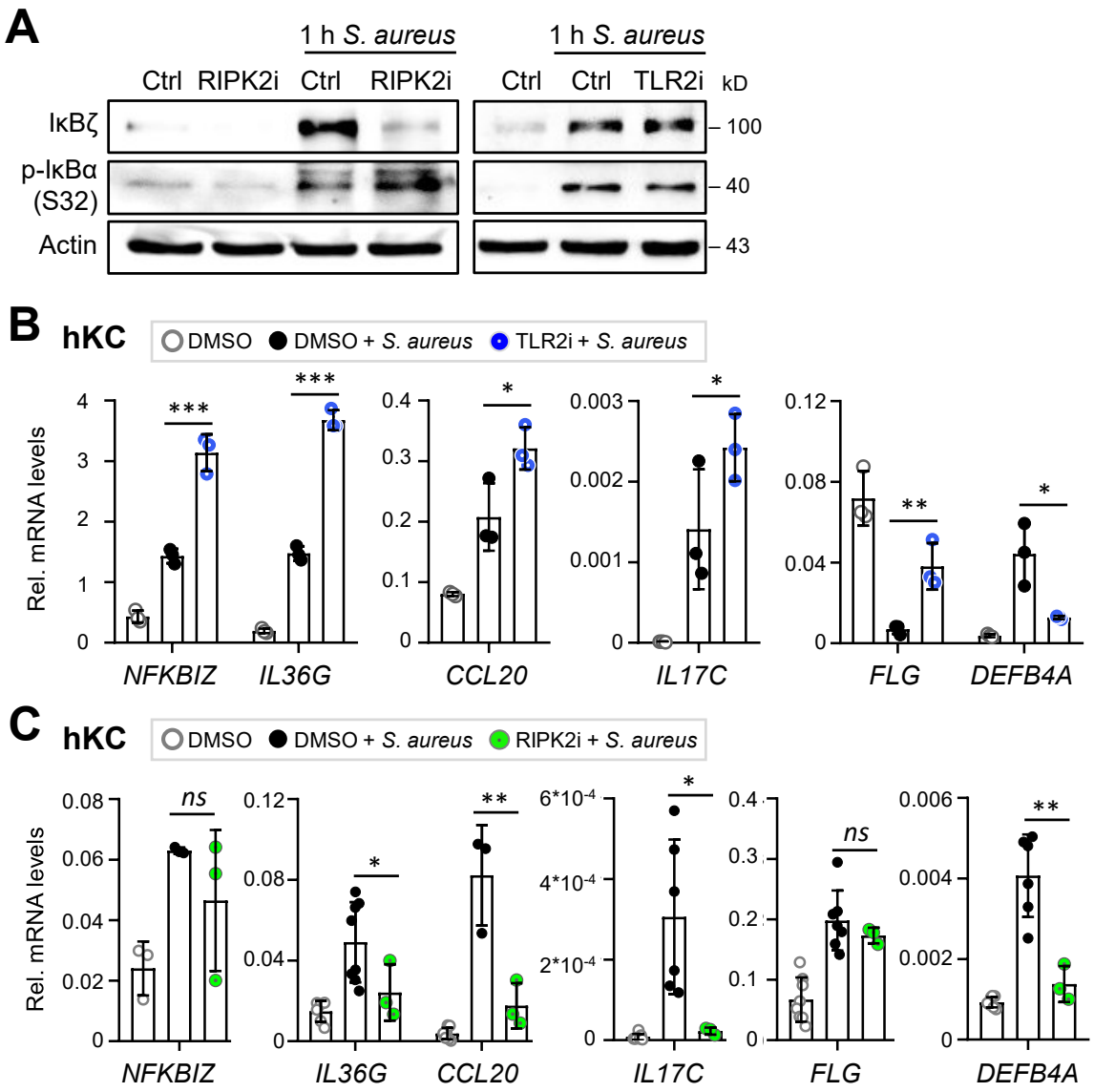

Figure 4.9: S. aureus-induced expression of IκBζ and target genes is exclusively quenched with absent NOD2 receptor activation but not during TLR2 inhibition in primary keratinocytes.

A. *IκBζ protein levels of differentiated hKC after treatment for 1 h with S. aureus (MOI30) in presence or absence of 5 µM RIPK2 inhibitor GSK385 (RIPK2i) or 50 µM TLR2 inhibitor TL2-C29 (TLR2i). Control cells were treated with DMSO as a vehicle. Before infection, cells were pre-treated with inhibitors or DMSO for about 4 h. Detection of phospho-IκBα (S32) was applied to control infection efficacy, and ϐ-Actin served as a loading control.* ***B+C.*** *Gene expression analysis of differentiated hKC infected for 1 h with S. aureus as in (A), but with an additional incubation for 23 h in the presence or absence of inhibitors or DMSO vehicle. Cells were harvested 24 h after infection. All relative mRNA levels were calculated over the U6RNA reference gene.* ***B.*** *Gene expression of infected keratinocytes under TLR2 inhibition (TLR2i).* ***C.*** *Gene expression of infected keratinocytes under indirect blockage of the NOD2 activation via RIPK2 inhibition (RIPK2i). (B) and (C) show the mean values of 3 biological replicates ± standard deviation (SD). Significance was calculated using a 2-tailed Student's t-test (*p < 0.05, **p < 0.01, ***p < 0.001, ns = not significant).*

4.10 IκBζ promotes the expression of key target genes involved in the host defense against *S. aureus* infection in keratinocytes

To investigate transcriptional changes in keratinocytes during *S. aureus* infections in greater detail and especially their dependency on IκBζ, we depleted the latter from hKC with a *NFKBIZ*-specific shRNA construct, similar to the aforementioned transcriptome analysis of MDP-stimulated cells.

Knockdown efficiency was validated by immunoblot analysis, immediately after 1 h *S. aureus* (MOI30) infection (see ***Figure 4.10***A). For transcriptome analysis, untreated or infected control and knockdown cells were further incubated for 23 h in the presence of antibiotics to kill external bacteria and harvested after 24 h in total (***Figure 4.10***B – D).

In total, we evaluated 919 genes being significantly regulated upon *S. aureus* infection (cut-off: p-values ≤ 0.05, fold change absolute >2, difference absolute >3), of which we identified approx. 22% as IκBζ target genes (***Figure 4.10***B). Most of the latter became significantly downregulated in the knockdown, which validates IκBζ as an important transcriptional co-activator in the *S. aureus*-induced gene expression in differentiated primary hKC.

Gene set enrichment analysis (GSEA) disclosed, that the *S. aureus*-induced IκBζ target genes mirrored the MDP-stimulated responses (seen in ***Figure 4.4***) and mainly comprised antimicrobial peptides, such as defensins (*DEFB4A, DEFB1*), peptidoglycan recognition proteins (*PGLYRP4*) or S100 proteins (*S100A8, S100A9*), and pro-inflammatory cytokines (*IL17C, IL36G*) and chemokines (*CCL20, CXCL1, CXCL10*) of the IL-17/IL-36-signaling pathways. Moreover, the absence of IκBζ during infection disturbed both genes being involved in the maintenance of the skin barrier and proper cell differentiation processes (***Figure 4.10***C), which require the expression of filaggrins (*FLG, FLG2*), and involucrin *(IVL*) besides late cornified envelope proteins (*LCE2A to D*). For illustrative purposes, we depicted selected target genes for each pathway in the heatmap of ***Figure 4.10***D. Of note, pathways of genes being induced by *S. aureus* and further upregulated in *NFKBIZ*-depleted cells are enclosed in ***Supplementary Figure V***.

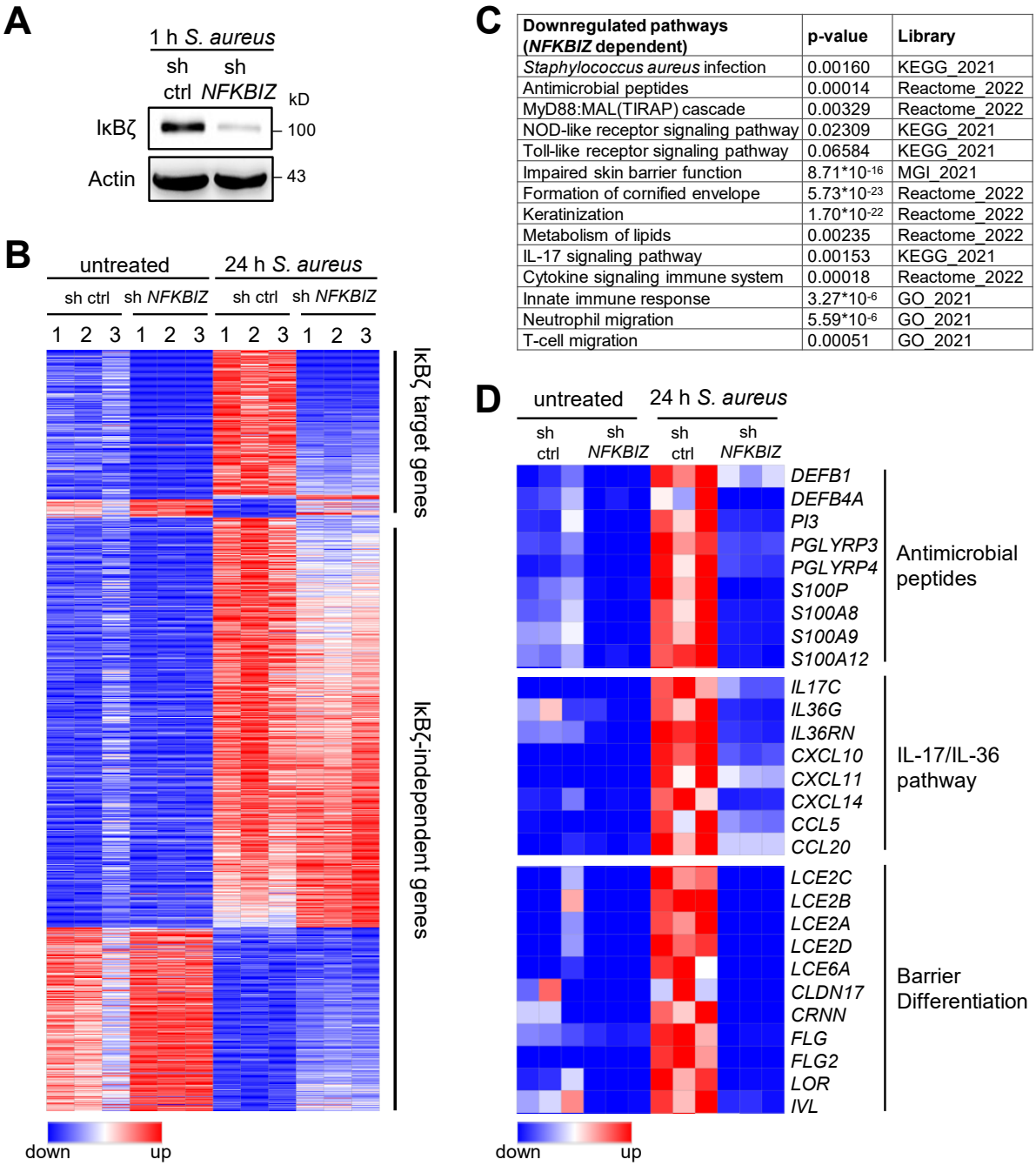

Downregulated pathways (*NFKBIZ* dependent)	p-value	Library
Staphylococcus aureus infection	0.00160	KEGG_2021
Antimicrobial peptides	0.00014	Reactome_2022
MyD88:MAL(TIRAP) cascade	0.00329	Reactome_2022
NOD-like receptor signaling pathway	0.02309	KEGG_2021
Toll-like receptor signaling pathway	0.06584	KEGG_2021
Impaired skin barrier function	$8.71*10^{-16}$	MGI_2021
Formation of cornified envelope	$5.73*10^{-23}$	Reactome_2022
Keratinization	$1.70*10^{-22}$	Reactome_2022
Metabolism of lipids	0.00235	Reactome_2022
IL-17 signaling pathway	0.00153	KEGG_2021
Cytokine signaling immune system	0.00018	Reactome_2022
Innate immune response	$3.27*10^{-6}$	GO_2021
Neutrophil migration	$5.59*10^{-6}$	GO_2021
T-cell migration	0.00051	GO_2021

Figure 4.10: Transcriptome analysis of S. aureus-stimulated keratinocytes reveals NFKBIZ-dependent regulation of genes encoding antimicrobial peptides, proteins responsible for the maintenance and formation of the epidermal layer and IL-17/IL-36 target genes.

A. *Immunoblot showing knockdown validation of differentiated control (sh ctrl) and knockdown (sh NFKBIZ) hKC, infected for 1 h with S. aureus (MOI30). ß-Actin served as a loading control.* ***B.*** *Heatmap of all S. aureus-dependent genes after infecting control and NFKBIZ-depleted differentiated hKC for 24 h with S. aureus (MOI30, 1 h). Cut-off: p-values ≤ 0.05, fold change absolute >2, difference absolute >3). Red color indicates up- and blue color down-regulated gene expression.* ***C.*** *Gene set enrichment analysis (GSEA) of downregulated, IκBζ-dependent target genes after 24 h S. aureus infection (from (B)). GSEA was performed using EnrichR. Shown are significantly enriched pathways, sorted by pathway and p-value.* ***D.*** *Heatmap of selected IκBζ target genes from (B), encoding antimicrobial peptides, genes involved in IL-17 and IL-36 signaling or protein-coding genes required to maintain a functional skin barrier.*

4.11 *S. aureus*-mediated induction of IκBζ regulates the expression of target genes upon its direct binding to their promoter regions *in vitro*

Besides transcriptome analysis, we additionally validated our results with qPCR and enclosed relative mRNA levels of the aforementioned genes from ***Figure 4.10***D in greater detail in ***Figure 4.11***A. All depicted genes were significantly induced upon *S. aureus* infection but, for illustrative reasons, only significance levels between treated control and treated *NFKBIZ*-depleted hKC are tagged. In line with these findings, similar gene expression changes were observed in *S. aureus*-infected murine control and *Nfkbiz* knockout keratinocytes (***Figure 4.11***B) isolated from tail tissue of *Nfkbiz*$^{\Delta K14\text{-}cre}$ mice.

The ability of IκBζ to shape immune responses in the context of cutaneous bacterial infections raised the question, whether IκBζ can bind to the chromatin and regulate the transcriptional activity of pro-inflammatory genes. First, we performed a chromatin fractionation of differentiated control and *NFKBIZ*-depleted hKC, being either non-treated or infected with *S. aureus* (MOI30) for 1 h (***Figure 4.11***C). Besides clearly validating the knockdown, IκBζ protein levels were exclusively detected in the chromatin-bound fraction of *S. aureus*-infected control hKC. Immunoblot staining for the cytoplasmic marker GAPDH testified equal amounts of sample input in the chromatin unbound fraction, while histone H3 protein levels are exclusively found in the nuclear cell compartment. Thereby, we validated the purity of both chromatin unbound and bound fractions and ensured the sample enrichment without spillovers, respectively.

With chromatin fractionation serving as our input control and proof, that IκBζ localizes to the nucleus upon its *S. aureus*-dependent induction, we continued to study the ability of IκBζ to bind promoter regions of putative target genes, such as depicted in ***Figure 4.11***A, to regulate their downstream transcription. This was achieved via chromatin immunoprecipitation (ChIP) assay of untreated control and *S. aureus*-infected (2 h, MOI30) control or *NFKBIZ*-depleted hKC (***Figure 4.11***D). For the evaluation of the IκBζ ChIP, the percentage of input was calculated and the human myoglobin (*MB*) locus served as an internal negative control. Apparently, we examined a direct IκBζ-dependent promoter activation of genes encoding antimicrobial peptides (*PI3*) or IL-17/IL-36 responsive genes (*IL17C, IL36G*) in infected keratinocytes, giving proof to our hypothesis that IκBζ directly influences the transcriptional activity of pro-inflammatory genes during *S. aureus* infections *in vitro*.

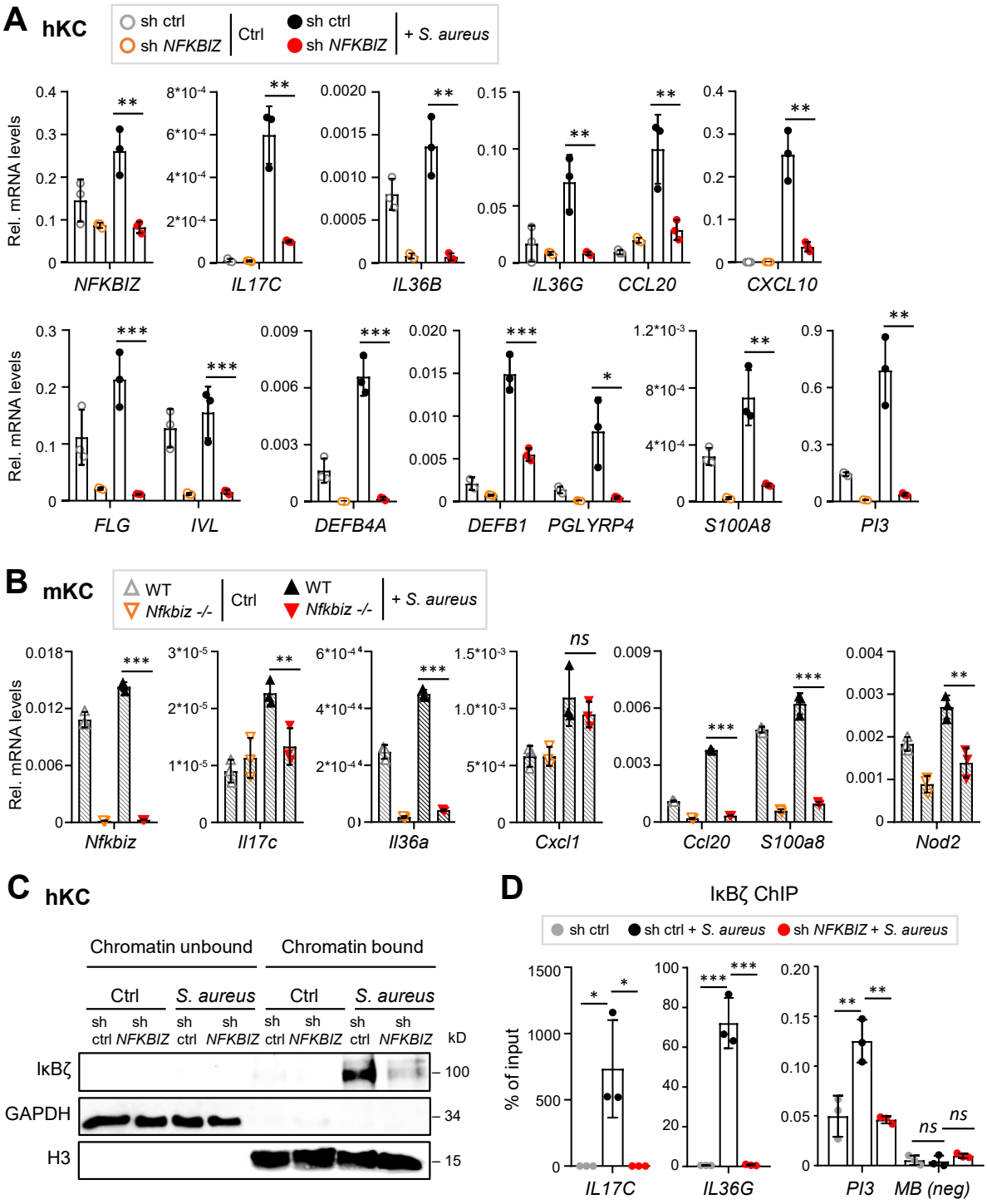

Figure 4.11: Validation of RNAseq shows IκBζ-dependent transcriptional regulation in keratinocytes upon S. aureus infection and reveals direct binding to promoter regions of target genes.

A. *Gene expression of IκBζ target genes in control (sh ctrl) and NFKBIZ-depleted (sh NFKBIZ) hKC 24 h after S. aureus infection (1 h, MOI30). Relative mRNA expression was normalized to the reference gene RPL37A.* ***B.*** *Gene expression of IκBζ target genes in mKC derived from WT or Nfkbiz-depleted (Nfkbiz$^{-/-}$) mice, pooled from 2 - 3 animals per group before treatment. Cells were treated as in (A). Relative mRNA levels were normalized over Actb.*

C. *Fractionation of untreated (Ctrl) and S. aureus-infected (1 h, MOI30) control (sh ctrl) or NFKBIZ-depleted (sh NFKBIZ) hKC into chromatin-unbound and chromatin-bound proteins. Cytoplasmic GAPDH marks chromatin unbound fraction, histone H3 levels serve as control for chromatin-bound proteins. (C) serves as input control for (D).*
D. *Chromatin immunoprecipitation (ChIP) of IκBζ or IgG control on promoters of putative IκBζ target genes in S. aureus-infected (2 h, MOI30) control (sh ctrl) and NFKBIZ-depleted (sh NFKBIZ) hKC, compared to untreated control cells. Shown is the percentage of input of the mean of 3 replicates ± standard deviation (SD). The MB locus served as an internal negative control. ChIP assay was performed by Antonia Kolb. (A), (B) and (D) show the mean of 3 biological replicates ± standard deviation (SD). Significance was calculated using a 2-tailed Student's t-test (*p < 0.05, **p < 0.01, and ***p < 0.001; ns = not significant).*

4.12 *S. aureus* infection triggers IκBζ expression in a Regnase-1-dependent manner in keratinocytes

So far, we have not addressed potential regulatory mechanisms upstream of *S. aureus*-induced IκBζ expression in keratinocytes, such as the activation of the caspase recruitment domain-containing protein 14 and the subsequent CARD14-BCL-10-MALT1 complex formation triggered by host cell-derived pattern recognition receptors [30, 34-36]. Hence, we wondered whether the *NFKBIZ* mRNA stability could be influenced enzymatically post transcription by RNases, such as the RNA-binding protein regulatory RNase 1 (short Regnase-1) to prevent pro-inflammatory signaling. Regnase-1 is encoded by the zinc finger protein *ZC3H12A* and is known to destabilize the mRNA of *NFKBIZ* among others via the integration of stem-loop structures into the 3'-untranslated region (3' UTR) [29].

To analyze the effects of a Regnase-1 knockout in *S. aureus*-infected mKC, we treated control cells derived from wild-type (WT) mice or OH-Tamoxifen inducible Regnase-1 knockout (*Zc3h12a*$^{-/-}$) animals [104] *in vitro* for 1 h with *S. aureus* (MOI30) (***Figure 4.12***). IκBζ expression was increased in the absence of Regnase-1 on both translational (***Figure 4.12***A) and transcriptional level (***Figure 4.12***B), as well as IκBζ target genes comprised significantly elevated mRNA levels. From these results we hypothesize, that *S. aureus* promotes the degradation of Regnase-1, followed by an accumulation of IκBζ protein and thus, its mRNA stabilization. However, no experimental proof for decomposed Regnase-1 components can be provided, as well as the contribution of other post-translational or transcriptional events cannot be excluded.

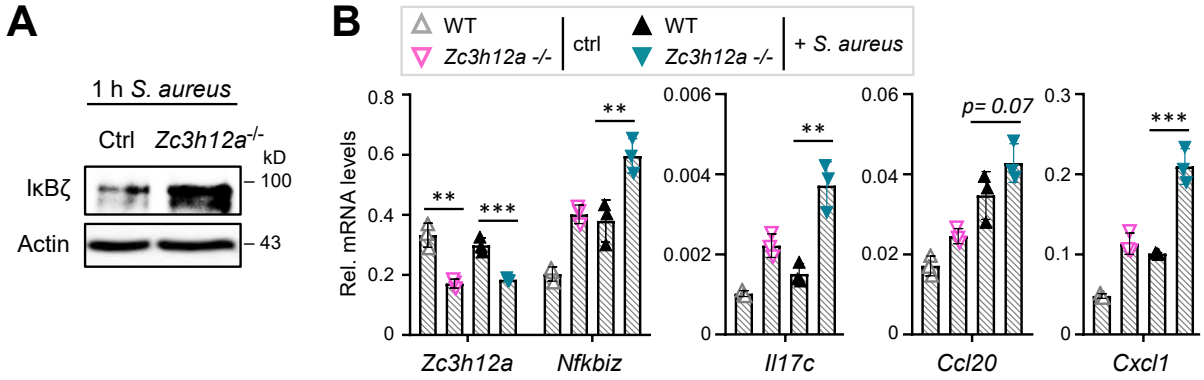

Figure 4.12: Keratinocyte-derived IκBζ is induced during S. aureus infections in a Regnase-1-dependent manner in vitro.

A. *Immunoblot analysis of mKC derived from wildtype (WT) mice and Regnase-1 knockout (Zc3h12a*$^{-/-}$*) animals under the control of a Tamoxifen-inducible promoter. mKC were pooled from 2 -3 animals per group before treatment. Knockout was induced in vitro for 4 days in the presence of 1 µM OH-Tamoxifen prior to infection with S. aureus (1 h, MOI30). ß-Actin served as a loading control. Immunoblot staining was performed by Antonia Kolb.* ***B.*** *Gene expression of NFKBIZ and IκBζ target genes in mKC derived from WT or Regnase-1-depleted (Zc3h12a*$^{-/-}$*) mice. Cells were treated as in (A). All relative mRNA levels were significantly induced in control mKC upon infection (not shown) and were normalized over Rpl37a. Shown is the mean of 3 biological replicates ± standard deviation (SD). Significance was calculated using a 2-tailed Student's t-test (*p < 0.05, **p < 0.01, and ***p < 0.001).*

4.13 IκBζ-dependent gene expression shows conserved pathways between *S. aureus*-infected and NOD2-stimulated keratinocytes

To this point, we successfully evaluated both human and murine keratinocyte-derived IκBζ as a key mediator promoting host cell immune responses, not only upon NOD2 receptor activation but also during *S. aureus* infections *in vitro*. Based on the aforementioned transcriptome analysis results of treated control versus *NFKBIZ*-depleted hKC, we aimed to investigate their stimuli-specific similarities and differences with greater detail (see ***Figure 4.13***).

First, we compared the afore-created lists of genes being significantly regulated (cut-off values: p-values≤ 0.05, fold change absolute >2, difference absolute >3) in stimulated versus untreated control cells, comprising 919 *S. aureus*-dependent and 379 MDP-dependent genes (as already depicted in ***Figure 4.4***B and ***Figure 4.10***B). Among these, IκBζ-dependent target genes were represented in one-third of all MDP-induced and in one-fifth of all *S. aureus*-induced genes. Creation of a Venn diagram, using the internet-based Venny 2.1.0 package, between both lists identified an overlap of 160 genes in total. Further analysis of the overlapping genes revealed 69 out of these 160 genes being IκBζ-dependently regulated under both *S. aureus* and MDP treatment for 24 h, of which 91% were downregulated in *NFKBIZ*-depleted cells. For illustrative purposes, see ***Figure 4.13***A.

In a final gene set enrichment analysis using EnrichR, we validated overlapping *S. aureus*- and NOD2-dependent pathways being downregulated in *NFKBIZ* knockdown cells (see ***Figure 4.13***B). Strikingly, we identified gene sets being very similar to the regulated pathways of the individual treatments, as already described in ***Figure 4.4***C and ***Figure 4.10***C, besides a significant absence of *NOD2* expression in *NFKBIZ*-depleted hKC independent of MDP or *S. aureus* treatment.

In summary, we found that the antimicrobial peptide expression and bacterial defense, genes involved in the maintenance of a functional skin barrier and differentiation markers, as well as innate immune responses such as IL-17/IL-36-signaling pathways, are indeed conserved among *S. aureus*-infected and NOD2-stimulated human keratinocytes.

Out of these, selected IκBζ target genes are further illustrated in ***Figure 4.13***C, an overview of all 69 IκBζ target genes is provided in ***Supplementary Figure VI***. Of note, the few mentioned target genes being *NFKBIZ*-dependently upregulated can be assigned cellular functions during cell adhesion, signal transduction or formation of the cytoskeleton and proliferation, which won't be discussed in greater detail.

A

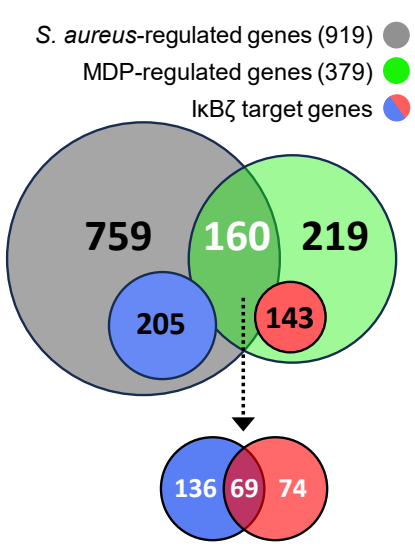

B

Overlapping *S. aureus*- and NOD2-dependent pathways (downregulated, *NFKBIZ* dependent)	p-value	Library
Antimicrobial peptides	0.00363	Reactome_2022
Defense response to bacterium	$1.84*10^{-10}$	GO_2021
Metal sequestration by antimicrobial proteins	0.00015	Reactome_2022
Staphylococcus aureus infection	0.00336	KEGG_2021
Toll-like receptor cascades	0.00016	Reactome_2022
TAK1-dependent IKK and NF-kappa-B activation	0.00038	Reactome_2022
Innate immune response	0.00034	GO_2021
Interleukin-1 family signaling	0.00135	Reactome_2022
IL-17 signaling pathway	0.03546	KEGG_2021
Neutrophil mediated immunity	0.00014	GO_2021
Formation of cornified envelope	0.00120	Reactome_2022
Impaired skin barrier function	$6.69*10^{-10}$	MGI_2021
Keratinization	$4.02*10^{-6}$	Reactome_2022
Epidermis development	$6.34*10^{-6}$	GO_2021

C

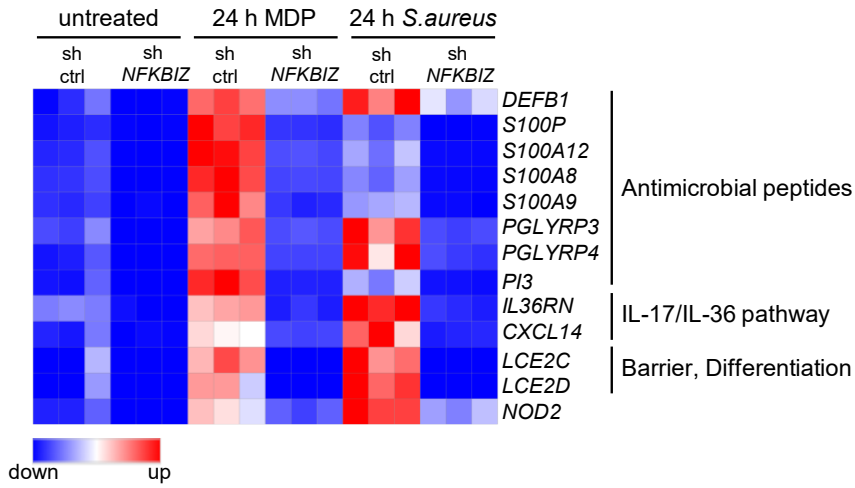

Figure 4.13: Comparative analysis of the IκBζ-dependent transcriptome in S. aureus-infected and NOD2-activated human keratinocytes.

A. *Schematic overview showing significantly up- and down-regulated genes (cut-off: p-values ≤ 0.05, fold change absolute >2, difference absolute >3) after 24 h upon S. aureus infection (grey, taken from* **Figure 4.4***B) or MDP treatment (green, taken from* **Figure 4.10***B), with an overlap of 160 genes. IκBζ-dependent target genes of each stimulus are indicated in smaller circles in blue or red, which are further represented in the Venn diagram below. In total, both stimuli overlap in 69 IκBζ target genes, of which 63 genes (91%) are negatively affected in NFKBIZ-depleted cells.* ***B.*** *Gene set enrichment analysis (GSEA) of overlapping IκBζ target genes identified in (A), being significantly downregulated in treated NFKBIZ-depleted cells after 24 h. GSEA was performed using EnrichR, shown are significantly enriched pathways sorted by pathway and p-value.* ***C.*** *Heatmap of selected IκBζ target genes of the overlap group shown in (A), that encode antimicrobial peptides (defensin DEFB1, S100 proteins and peptidoglycan recognition proteins (PGLYRP)), genes encoding proteins involved in skin barrier maintenance and differentiation (late cornified envelope proteins (LCE)), or downstream of IL-17 and IL-36 (chemokine CXCL14, IL-36 receptor antagonist IL36RN). Blue indicates downregulated gene expression; red indicates upregulated gene expression. The full heatmap is enclosed in* **Supplementary Figure VI**.

4.14 Suppressed NOD2 signaling in *S. aureus* infection quenches pro-inflammatory responses but can be rescued by IκBζ overexpression

To address our posed assumption, we investigated whether *S. aureus*-infected but NOD2-signaling-repressed keratinocytes can overcome suppression of pro-inflammatory gene responses by an exogenous IκBζ overexpression.

Therefore, we generated control- or IκBζ-overexpressing primary hKC using lentivirus and infected these for 1 h with *S. aureus* (MOI30) in the absence or presence of the previously validated RIPK2 inhibitor GSK583 or DMSO vehicle control, as already described prior in *chapter 4.9* (see ***Figure 4.9***). Successful overexpression was verified with immunoblot staining in ***Figure 4.14***A and equal infection efficiency was validated with phosphorylated levels of IκBα (p-IκBα (S32)) in both infected control and IκBζ-overexpressing cells. Development of the immunoblot with high exposure successfully detected endogenous IκBζ protein levels in the *S. aureus*-infected control cells, even though the effect was rather marginal, compared to the strong signal elicited by the exogenous IκBζ overexpression.

We further incubated the samples for 23 h post-infection in the presence or absence of RIPK2 inhibitor, respectively, to assess the *NFKBIZ* expression on transcriptional level. While *S. aureus*-infected control cells showed a significant increase in *NFKBIZ* mRNA level compared to untreated hKC, which was significantly abrogated upon addition of RIPK2 inhibitor (see ***Figure 4.14***B, green), this effect was completely revoked in IκBζ-overexpressing cells being treated with *S. aureus* and RIPK2 inhibitor in parallel (see ***Figure 4.14***B, purple).

As depicted in ***Figure 4.14***C, equal results in IκBζ target genes being involved in IL-17/IL-36-signaling responses (*IL17C, IL36B, IL36G, CCL20*) or in antimicrobial peptide expression such as defensins (*DEFB4A*) were obtained from treated and inhibited IκBζ-overexpressing hKC. These results further emphasize, that IκBζ indeed represents an important downstream mediator of NOD2 responses in *S. aureus*-infected keratinocytes.

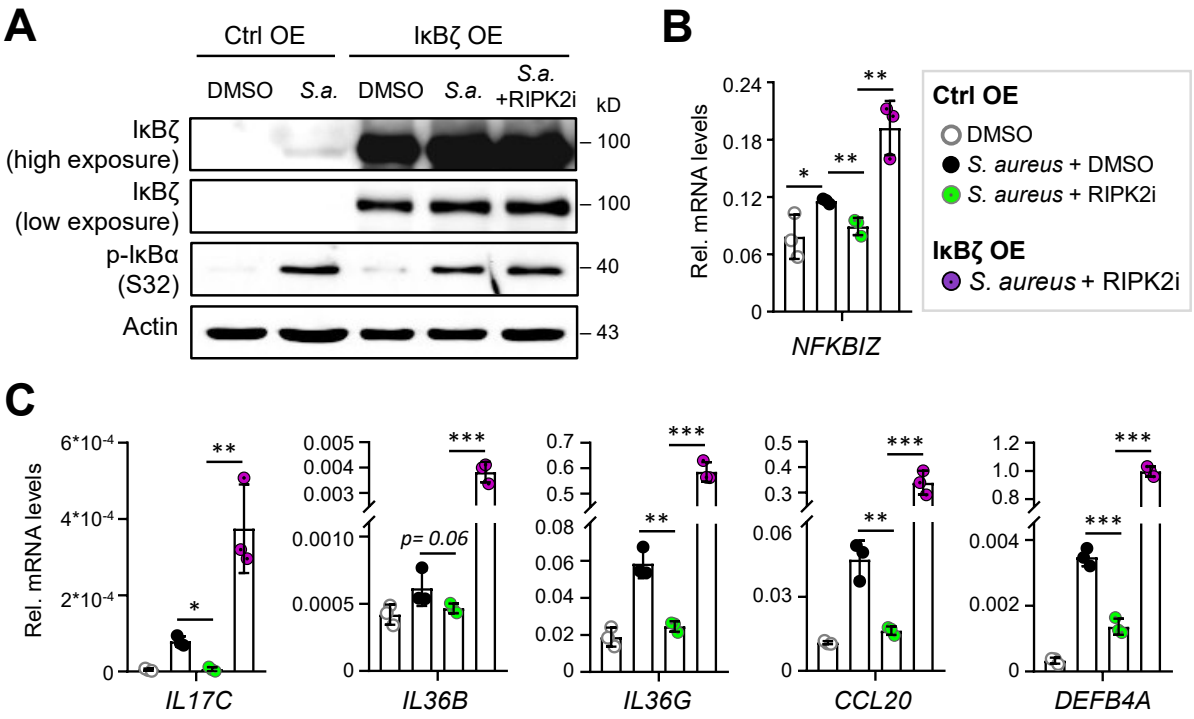

Figure 4.14: IκBζ overexpression rescues the inhibitory effect of RIPK2 inhibitor treatment during S. aureus infection in hKC.

A. *Immunoblot analysis of S. aureus-infected (1 h, MOI30) differentiated keratinocytes being lentivirally transfected with control and IκBζ-overexpression plasmids, in the presence or absence of 5 µM RIPK2 inhibitor GSK583 (RIPK2i) or DMSO vehicle control. At high exposure, endogenous levels of IκBζ in control cells being induced upon S. aureus infection are visualized. Equal phosphorylation levels of IκBα (p-IκBα(S32)) control efficient S. aureus infection in general. ß-actin served as a loading control.* ***B.*** *Relative NFKBIZ mRNA expression levels of control cells being infected with S. aureus or additionally treated with RIPK2 inhibitor compared to infected, RIPK2 inhibitor-treated IκBζ-overexpressing keratinocytes. Infection and stimulation were conducted for 24 h (MOI30, 1 h) in the presence or absence of 5 µM GSK583 or DMSO vehicle control.* ***C.*** *Gene expression analysis of control and IκBζ-overexpressing cells as in (B), showing relative mRNA levels of IκBζ target genes involved in IL-17/IL-36-responses (IL17C, IL36B, IL36G, CCL20) or in antimicrobial peptide expression (DEFB4A). For (B) and (C) values were normalized to the reference gene RPL37A. Shown is the mean of 3 biological replicates ± standard deviation (SD). Significance was calculated using a 2-tailed Student's t-test (*p < 0.05, **p < 0.01, and ***p < 0.001).*

4.15 IκBζ inhibits bacterial internalization into human keratinocytes showing a similar phenotype to NOD2 inhibition

Apart from *S. aureus*- and NOD2-mediated pro-inflammatory gene responses, we wanted to investigate how far the presence of keratinocyte-derived IκBζ influences the capacity of *S. aureus* to invade, survive and proliferate within primary keratinocytes. Albeit this characteristic feature represents a hallmark of virulent *S. aureus* strains, contributing to its pathogenicity and the development of persistent or chronic skin infections, the underlying molecular mechanism remains poorly understood [60-62]. Therefore, we infected differentiated hKC for 1 h with living *S. aureus* cultures (MOI30) and further incubated the cells for 23 h post-infection to perform the following internalization assays. First, we assessed NOD2-mediated effects by application of the RIPK2 inhibitor GSK583, which was present or absent throughout the entire incubation time and infection (***Figure 4.15***A). Interestingly, we recovered significantly higher numbers of colony-forming units (CFU) on TSB-agar from plated cell lysates of infected, NOD2-inhibited hKC compared to infected control cells. In agreement with that, we observed a similar phenotype in *NFKBIZ*-depleted hKC (***Figure 4.15***B) compared to infected control cells, showing an increased survival and overall internalization of the bacteria. Hence, these findings further underline a correlation between NOD2 and IκBζ, since the absent induction of keratinocyte-derived IκBζ seems to exacerbate *S. aureus* infections *in vitro*, which in turn impedes bacterial clearance.

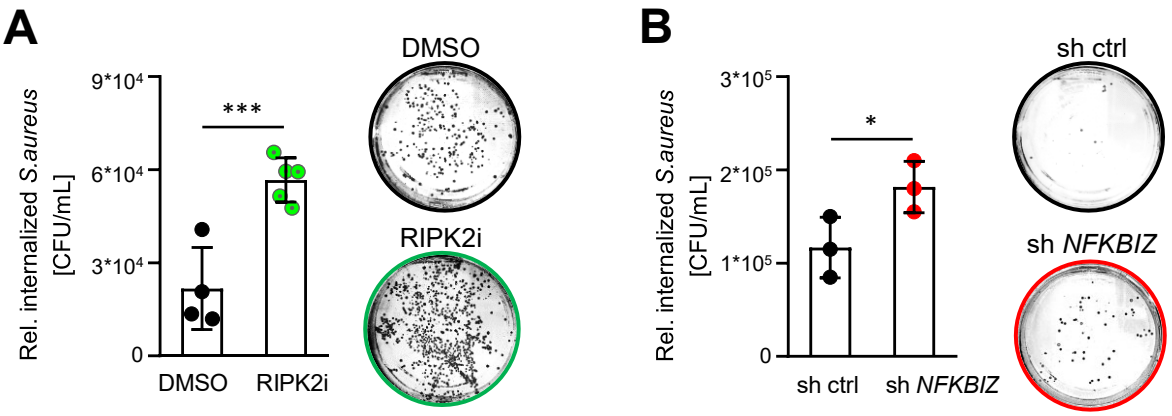

Figure 4.15: Loss of NOD2 receptor activation and NFKBIZ knockdown both exacerbate S. aureus internalization into human keratinocytes.

A. *Relative internalized S. aureus colony forming units (CFU) per mL in control (DMSO, black) or RIPK2 inhibitor-treated (RIPK2i, green) hKC. Cells were starved overnight in the absence or presence of RIPK2i, infected with S. aureus (MOI 30, 1 h), and further incubated for 23 h in the absence or presence of fresh RIPK2i and antibiotics to kill external bacteria. For internalization assay, the cells were trypsinized, washed and lysed in 0.1% Triton-X-100 for 1 h at RT before the suspension was plated in different dilutions on TSB agar plates. CFU were counted the next day after an overnight incubation at 37°C.* ***B.*** *Relative internalized S. aureus CFUs per mL in control (sh ctrl, black) or NFKBIZ-depleted (sh NFKBIZ, red) primary hKC. Knockdown and control cells were infected similar to (A) without RIPK2i addition. Internalization assay was performed as in (A). (A) and (B) show data of recovered CFUs from 2 individual experiments (bar diagram) and images of TSB-agar plates.*

4.16 Tape-stripping-induced skin barrier defect is a prerequisite for the establishment of an epicutaneous *S. aureus* infection in mice

Since we validated keratinocyte-derived IκBζ as a crucial mediator of host responses in the context of *S. aureus* infections *in vitro*, we were further interested in its potential to shape the immune responses against bacterial infections in the skin *in vivo.*

For this reason, we generated a mouse line with a tissue-specific *Nfkbiz* knockout using the Cre-loxP system by crossing floxed *Nfkbiz* mice (*Nfkbiz*$^{fl/fl}$) with a KRT14-cre recombinase expressing strain. This breeding strategy resulted in offspring bearing the site-specific deletion of *Nfkbiz* DNA in all KRT14-expressing keratinocytes (*Nfkbiz*$^{\Delta K14\text{-}cre}$), while floxed *Nfkbiz* mice served as controls.

First, it was excluded that the skin of *Nfkbiz*$^{\Delta K14\text{-}cre}$ KO mice was colonized by *S. aureus* or that persistent skin infections were acquired before the start of the infection model. Therefore, we analyzed both control (Ctrl) and knockout (KO) skin lysates at steady-state using immunoblot by staining with antiserum against *S. aureus.* An infected skin sample served as positive control (***Figure 4.16***A). Besides, at steady-state neither the fur of control, nor of knockout animals showed any visual signs of skin damage or spontaneous skin infections. The mice were kept under surveillance until adulthood and, as depicted on example photos in ***Figure 4.16***B, the back skin remained unscathed and healthy.

Next, we optimized our experimental set-up for the *S. aureus* infection *in vivo* independent of a genetic IκBζ-depletion*,* whilst comparing gene expression in skin samples of *Nfkbiz*$^{fl/fl}$ control animals treated with PBS or subjected to epicutaneous *S. aureus* application for 7 days (10^8 CFU/animal)*.* Hereby, we divided the mice into two groups, of which the back skin was either shaved or additionally subjected to depilation and tape-stripping prior infection, in order to create a mild barrier damage (see ***Figure 4.16***C). Interestingly, we found that *S. aureus*-infected skin samples without a precedent barrier defect showed no significant effects regarding elevated IκBζ target gene expression, while a tape-stripping-induced skin damage strongly increased pro-inflammatory gene expression in epicutaneously infected control mice *in vivo*. Hence, we decided to conduct all following *in vivo* studies using tape-stripping prior to the topical application of living *S. aureus* cultures to establish distinctly measurable differences between PBS-treated and infected skin samples.

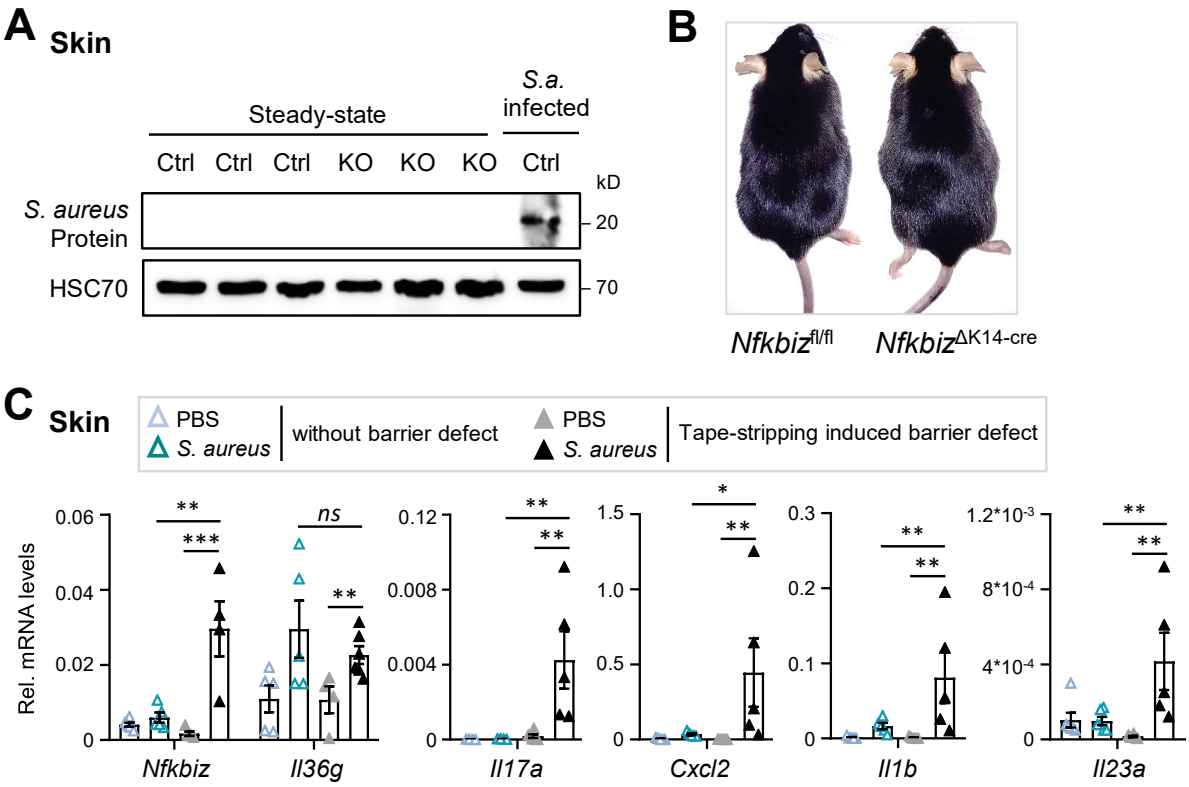

Figure 4.16: Analysis of Nfkbiz$^{\Delta K14\text{-}cre}$ KO mice at steady-state and optimization of the in vivo infection mouse model.

A. *Immunoblot of S. aureus protein A in PBS-treated Nfkbiz$^{fl/fl}$ control (Ctrl) and Nfkbiz$^{\Delta K14\text{-}cre}$ (KO) skin lysates at steady-state. Skin lysate of a S. aureus-infected control animal served as a positive control, HSC70 served as a loading control.* ***B.*** *Visual controls of the back skin of aged Nfkbiz$^{fl/fl}$ control mice and Nfkbiz$^{\Delta K14\text{-}cre}$ animals (both > 37 weeks).* ***C.*** *Gene expression analysis of skin derived from Nfkbiz$^{fl/fl}$ control animals being treated with PBS or subjected to epicutaneous S. aureus infection. Prior treatment, the back skin was either shaved (without barrier defect) or additionally depilated and tape-stripped to cause a mild barrier defect. Equal amounts of living bacteria (10^8 CFU) or PBS were applied on the back skin, covered for 7 days, and subsequently analyzed by qPCR. Relative mRNA levels were normalized to Actb. Shown is the mean ± SEM (n = 4 - 5 animals per group). Significance was calculated using a 2-tailed Student's t-test (*p < 0.05, **p < 0.01, and ***p < 0.001, ns = not significant).*

4.17 IκBζ decreases *S. aureus*-induced inflammation in epicutaneous infection *in vivo* and improves the overall health condition

To clarify which role the absence of keratinocyte-derived IκBζ plays in an epicutaneous *S. aureus* infection model *in vivo*, we shaved and depilated both the aforementioned control (*Nfkbiz*$^{fl/fl}$) and *Nfkbiz*-depleted (*Nfkbiz*$^{\Delta K14\text{-cre}}$) animals one day prior infection (day 0). The next day (day 1), a mild skin barrier defect was created via tape-stripping immediately before the topical application of small filter disks on the skin, which were either soaked with PBS only or 1*10^8 CFU of living *S. aureus* USA300 WT cultures. Subsequently, the back of the mice were covered with dressings and Fixomull to avoid bacterial contamination of the cages and other body parts, as well as unwanted side effects caused by oral uptake of bacteria. On day 7, all mice were sacrificed, and analysis was conducted. A treatment scheme is enclosed in ***Figure 4.17***A.

All *S. aureus*-infected mice developed strong skin inflammation in the treated area of the back skin, as visually documented in ***Figure 4.17***B, while the *Nfkbiz*-depleted animals seemed to be stronger affected. To assess the overall health condition and potential differences between control *Nfkbiz*$^{fl/fl}$ and *Nfkbiz*$^{\Delta K14\text{-cre}}$ animals, we evaluated the severeness of infection by grading the extent of inflammation, allocating the following score points: Starting from healthy appearing skin (0 points) and beginning dryness and scaling (0.5 to 1 point), over mildly increasing skin redness and swelling (1.5 points) in the infected area, we scored moderate inflammation in case of deteriorating wounds (2 to 2.5 points) until the development of severe skin infections with abscess and pus formation (3 points). While the PBS-treated control mice yielded low scores, potentially caused by a mild barrier defect due to tape-stripping, *S. aureus* infection strongly increased the inflammation scores. However, in the group of infected, IκBζ-depleted *Nfkbiz*$^{\Delta K14\text{-cre}}$ mice significantly more animals reached the maximal score points (***Figure 4.17***C). This effect was inversely proportional to the documented percentage of remaining weight on day 7, compared to day 1 of the *in vivo* model, showing only a marginal weight loss in infected *Nfkbiz*$^{fl/fl}$ mice, but a significant weight reduction and thus, a deteriorating overall health condition of infected *Nfkbiz*$^{\Delta K14\text{-cre}}$ animals (***Figure 4.17***D). Aside from that, immunohistology staining of skin samples obtained from the affected area confirmed massive local inflammation and infiltration of immune cells upon topical *S. aureus* application (see H&E in ***Figure 4.17***E, above) compared to PBS-treated skin, presented by the epidermal hyperproliferation in the upper layer of the skin section. Strikingly, the lack of keratinocyte-derived IκBζ not only revealed a disrupted or missing epidermal layer, but also a disturbed integrity of the whitish fat layer (black arrow in H&E in ***Figure 4.17***E). Thus, we hypothesized that epidermal cells in *S. aureus*-infected *Nfkbiz*$^{\Delta K14\text{-cre}}$ animals are more prone to become apoptotic compared to infected control animals. This was immunohistologically confirmed by staining for cleaved caspase-3 (see CC3 in ***Figure 4.17***E, below), a selective marker for apoptosis, showing a distinct coloration in the upper skin layer exclusively of infected IκBζ-depleted back skin samples.

All in all, these results indicate that keratinocyte-derived IκBζ indeed limits *S. aureus*-induced tissue damage *in vivo*.

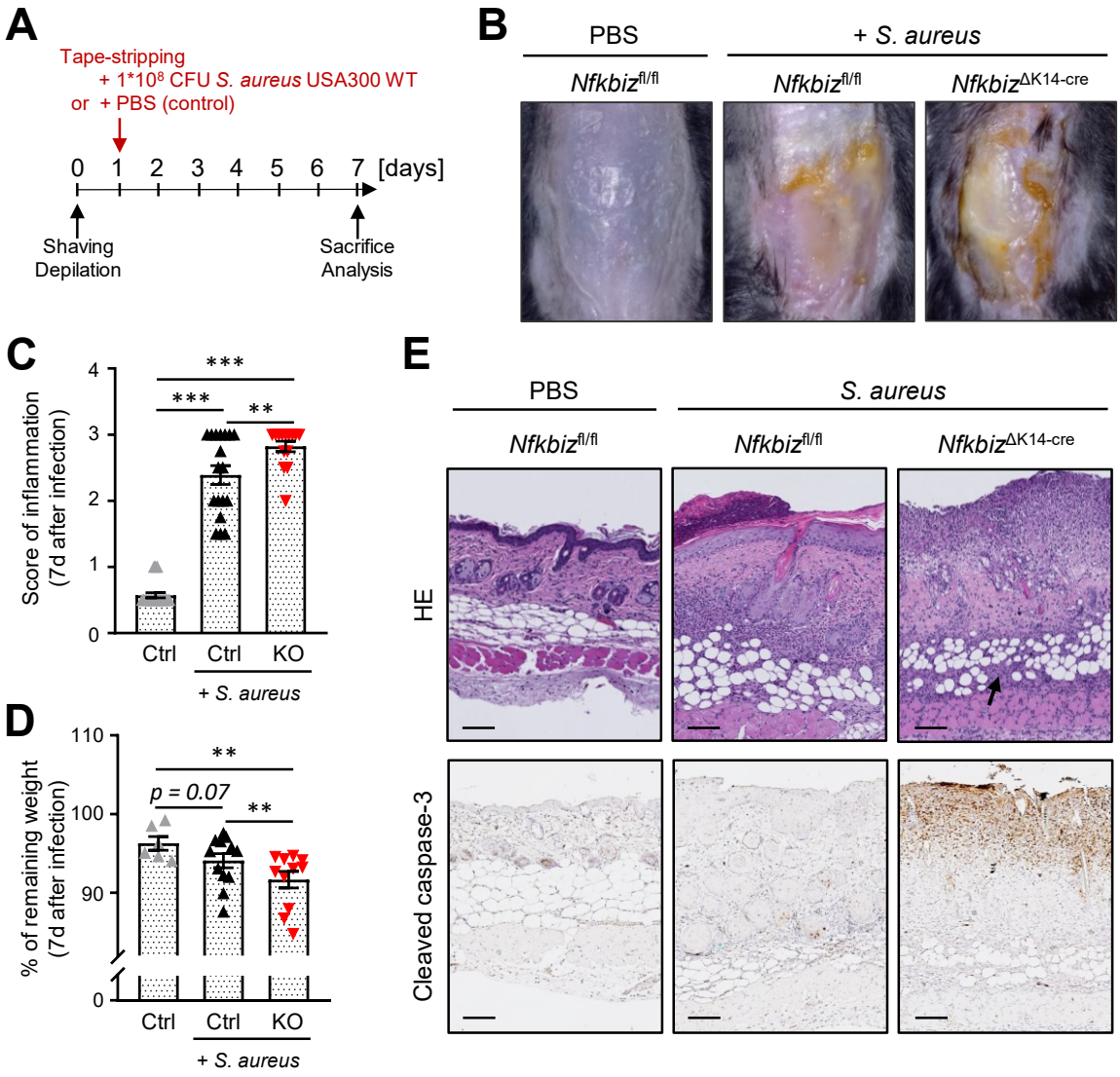

Figure 4.17: S. aureus-infected mouse skin lacking keratinocyte-derived IκBζ shows elevated inflammation and skin damage with an overall decreased health condition compared to infected control animals.

A. *Treatment scheme. At day 0 all mice (aged 9-11 weeks) were shaved and depilated. On day 1, back skin was disinfected with 70% isopropanol and tape-stripped immediately before application of either PBS or 1*10^8 CFU living S. aureus USA300 WT cultures. On day 7, mice were sacrificed and analyzed.* ***B – E.*** *Evaluation of Nfkbiz$^{fl/fl}$ control mice treated with PBS (Ctrl) and Nfkbiz$^{fl/fl}$ or IκBζ-depleted Nfkbiz$^{ΔK14\text{-}cre}$ mice (KO) after 7 days S. aureus infection.* ***B.*** *Pictures of back skin on day 7.* ***C.*** *Score of inflammation of the respective back skin on day 7, indicating the severity of infection (n = 14 - 21 animals per group).* ***D.*** *Relative weight loss of each mouse on day 7, compared to its weight at starting point on day 1. Score numbers were obtained from n = 6 -12 mice per group and indicate the following: from 0 = healthy appearing skin to 3 = strong skin inflammation. (C) and (D) show mean values ± SEM, significance was calculated using a 2-tailed Student's t-test (*p < 0.05, **p < 0.01, and ***p < 0.001).* ***E.*** *Immunohistology of formalin-fixed paraffin-embedded (FFPE) back skin material of PBS-treated or S. aureus-infected control and IκBζ-depleted animals, taken at the endpoint on day 7. Staining shows hematoxylin and eosin (H&E) to visualize cellular structures or cleaved caspase-3 staining, indicating apoptotic cells. Black arrow indicates disturbance of fat tissue. Scale bars: 100 µm. Histology stainings were performed by Claudia Braun and Dagmar Löck.*

4.18 IκBζ mediates pro-inflammatory gene expression and secretion of cytokines and chemokines against *S. aureus* infections *in vivo*

Based on our data obtained from immunohistology staining after an infection course of 7 days we hypothesized that at first the absence of IκBζ leads to an impaired host defense, such as an altered sensitivity of keratinocytes towards bacterial sensing or a decreased recruitment of immune cells, which in turn results in a decline of pro-inflammatory responses.

To address this matter, gene expression analyses from the back skin derived from *Nfkbiz*$^{fl/fl}$ control animals, infected for 7 days, were conducted and, as expected, confirmed a significant induction in our previously identified IκBζ target genes involved in IL-17/IL-36 signaling pathways (*Il17a, Il17c, Il36a, IL36g, Ccl20*) or antimicrobial peptides (*Defb4a, Defb1, S100a8*) compared to the PBS-treated control skin.

However, relative mRNA expression of these genes was significantly decreased in infected *Nfkbiz*$^{\Delta K14\text{-}cre}$ knockout skin (***Figure 4.18***A). Fitting to these data, we obtained similar results in a cytokine array, where we assessed the protein levels of pro-inflammatory cytokines and chemokines in duplicates by applying pooled skin lysates of n = 3 animals per group in a proteome profiler array. For illustrative reasons, we visualized *S. aureus*-induced protein levels with colored boxes on the array membranes (***Figure 4.18***B), as well as we calculated the relative pixel values of each individual spot (***Figure 4.18***C). For the latter, we normalized each value to the reference spots of *S. aureus*-infected *Nfkbiz*$^{fl/fl}$ control lysates, revealing significantly less IL-17 signaling pathway-related cytokines and chemokines being expressed in the *S. aureus*-infected *Nfkbiz*$^{\Delta K14\text{-}cre}$ KO skin.

All in all, we proved that once the epicutaneous *S. aureus* infection is established after the course of 7 days, a part of the pro-inflammatory host response in the skin is mediated by keratinocyte-derived IκBζ. Nevertheless, it needs to be clarified that these data do not provide information regarding the initial gene expression levels at earlier time points of infection *in vivo*.

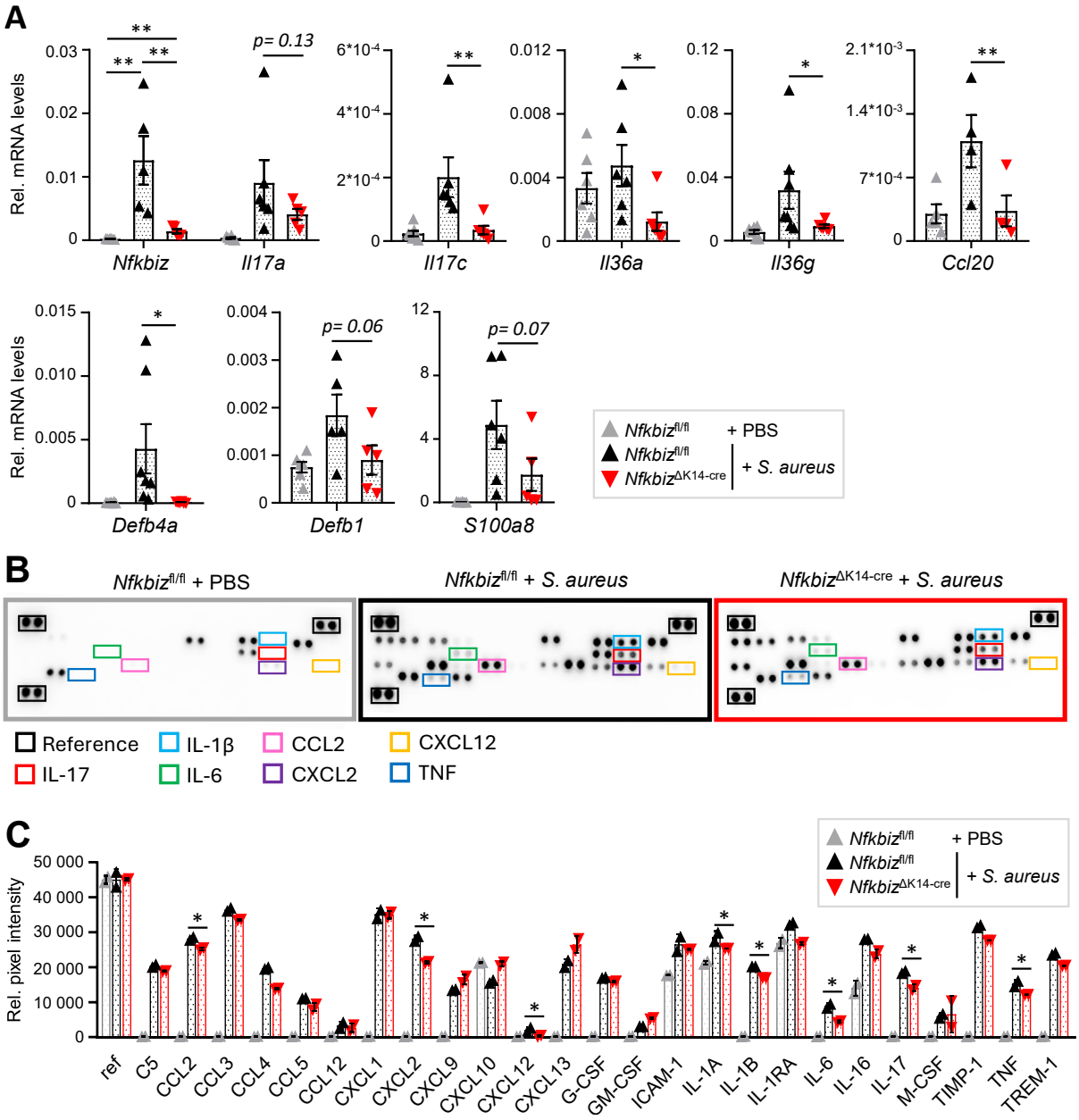

Figure 4.18: Keratinocyte-derived IκBζ mediates pro-inflammatory gene expression and secretion of cytokines and chemokines upon epicutaneous S. aureus infection in vivo.
A. *Gene expression analysis of PBS-treated Nfkbiz$^{fl/fl}$ control animals and S. aureus-infected Nfkbiz$^{fl/fl}$ or Nfkbiz$^{\Delta K14\text{-}cre}$ mice 7 days after infection. Shown are IκBζ target genes being regulated in IL-17/IL-36 signaling pathways (above) or antimicrobial peptides (below). Relative mRNA expression was normalized to Rpl37a and shows the mean ± SEM of n = 5 - 7 animals per group.* ***B + C.*** *Proteome profiler array of skin lysates (pooled from n= 3 animals per group) obtained from back skin of PBS-treated controls or S. aureus-infected Nfkbiz$^{fl/fl}$ controls and IκBζ-depleted Nfkbiz$^{\Delta K14\text{-}cre}$ mice after 7 days. Proteins are detected in duplicates.* ***B.*** *Blot images of cytokine array. Protein levels significantly differing between the S. aureus-infected samples are marked in boxes.* ***C.*** *Protein levels of detected cytokines and chemokines, extracted from blot images in (B) using the Dotblot analyzer of ImageJ software. Shown is the evaluation normalized to the reference spots of S. aureus-infected Nfkbiz$^{fl/fl}$ control samples, which is depicted as relative pixel values. Cytokine array was performed by Tanja Kübelbeck. Significance was calculated using a 2-tailed Student's t-test (* p < 0.05, ** p < 0.01, *** p< 0.001, ns = not significant).*

4.19 Keratinocyte-derived IκBζ mediates the local innate immune response against epicutaneous *S. aureus* infections *in vivo*

Next, we wanted to investigate how IκBζ shapes the local immune response in the skin regarding the recruitment of innate immune cell populations to the side of infection. Since H&E staining (see again ***Figure 4.17***E) revealed massive cell infiltrates in *S. aureus*-infected mouse skin after 7 days, we further stained FFPE skin sections immunohistologically for the myeloperoxidase MPO, which is mainly expressed in neutrophils and, to a lesser extent, also in monocytes (see ***Figure 4.19***A). Interestingly, MPO was strongly expressed upon epicutaneous *S. aureus* infection in the epidermis and lower dermis of *Nfkbiz*$^{fl/fl}$ animals, but to a lesser extent in infected *Nfkbiz*$^{\Delta K14\text{-}cre}$ knockout skin. Since we observed no visible differences in PBS-treated skin sections between *Nfkbiz*$^{fl/fl}$ control and *Nfkbiz*$^{\Delta K14\text{-}cre}$ knockout animals regarding the amount of MPO expression (see ***Supplementary Figure VII***A), we refrained from including the group PBS-treated *Nfkbiz*$^{\Delta K14\text{-}cre}$ from further flow cytometric analysis.

Based on previous *in vivo* results, indicating an aggravation of the overall health condition and higher bacterial burden in infected, IκBζ-depleted mouse skin after 7 days, we hypothesized that the dampened host response resulted from an attenuated activation of innate immune responses in these mice. In order to test this, we conducted flow cytometry analysis, with the respective gating strategy enclosed in ***Supplementary Figure VIII***.

At an earlier stage of infection, only marginal effects of neutrophil and monocyte recruitment to the infected area were detected after 2 days (see ***Figure 4.19***B), showing no significant differences between *S. aureus*-infected control or knockout animals but nevertheless, an already slightly increased number of infiltrating neutrophils compared to PBS-treated skin samples.

However, at a later stage of infection, FACS analysis revealed a significant increase in these populations upon infection, while showing a distinct reduction of recruited immune cells in *Nfkbiz*$^{\Delta K14\text{-}cre}$ knockout skin (***Figure 4.19***C and D, 7 days). Moreover, the total amount of cells producing reactive oxygen species (ROS) to support bacterial clearance, such as neutrophils, was strongly reduced in infected *Nfkbiz* knockout mice, suggesting an additional function of IκBζ in cellular stimulation and activation. The gating strategy for ROS staining is enclosed in ***Supplementary Figure IX***.

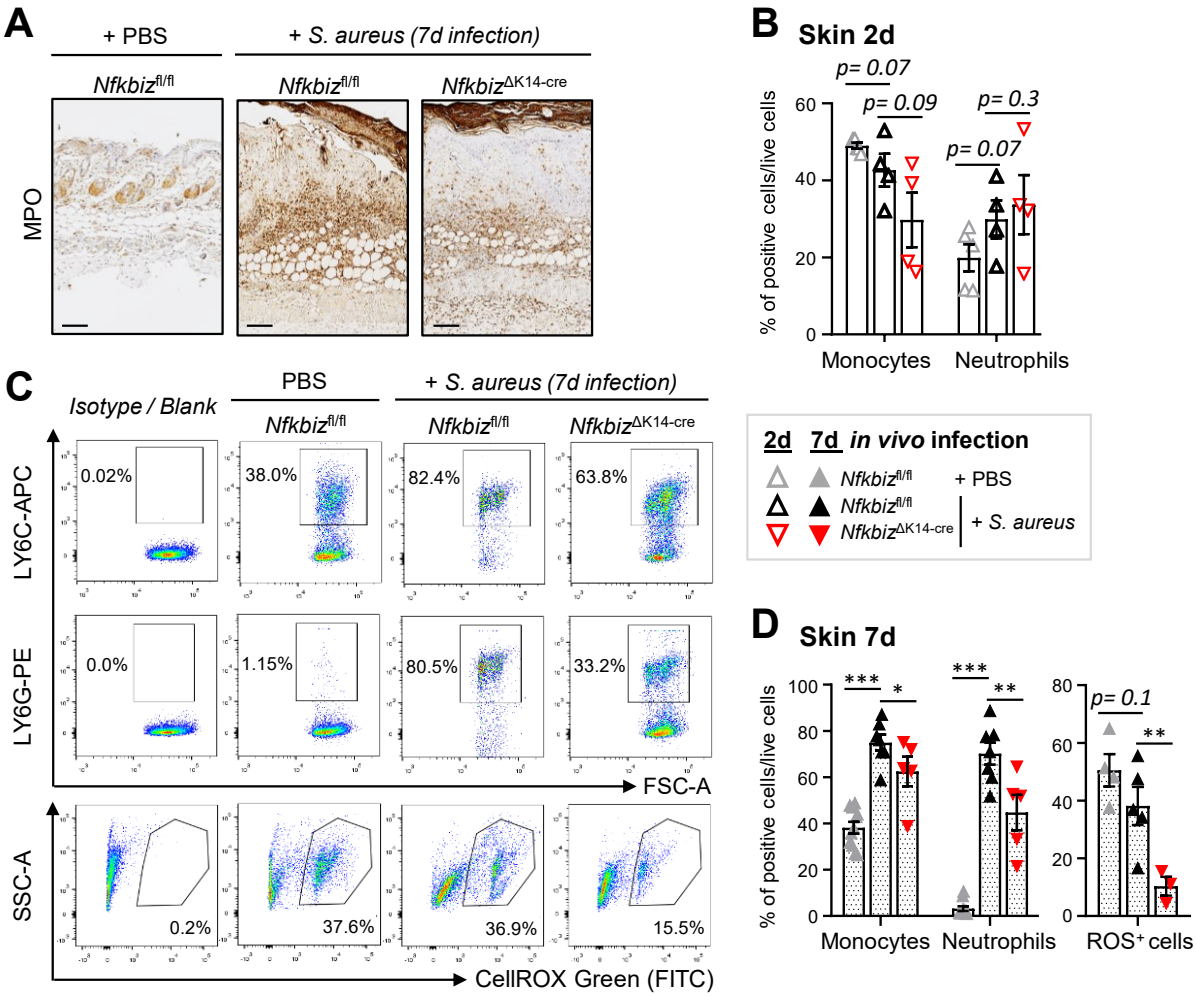

Figure 4.19: IκBζ shapes the local innate immune responses in epicutaneous S. aureus infections in the skin in vivo.

A. *Immunohistology of FFPE back skin material of PBS-treated or S. aureus-infected Nfkbiz$^{fl/fl}$ control and infected IκBζ-depleted Nfkbiz$^{ΔK14\text{-}cre}$ animals, taken at the endpoint on day 7. Skin sections were stained for myeloperoxidase MPO, a marker for neutrophils and, to lesser extent, monocytes. Scale bars: 100 µm. Histology stainings were performed by Dagmar Löck.* ***B. – D.*** *Flow cytometry analysis of innate immune cell populations in digested skin tissue obtained from PBS-treated Nfkbiz$^{fl/fl}$ control and S. aureus-infected Nfkbiz$^{fl/fl}$ control and Nfkbiz$^{ΔK14\text{-}cre}$ knockout animals.* ***B.*** *Evaluation of skin FACS from mice sacrificed after 2 days. Shown is the mean ± SEM (n = 4 - 5 animals per group) of the percentage of skin-infiltrating neutrophils (Ly6G+) or monocytes (Ly6C+) per live cells.* ***C + D.*** *Skin samples obtained from mice sacrificed at the endpoint on day 7.* ***C.*** *Examples of gated living cell populations, with monocytes being assigned Ly6G-positive and neutrophils as Ly6C-positive. ROS-producing cells were gated for CellROX positive signals in the FITC channel. FACS plots were evaluated using FlowJo (Tree Star Inc.) software.* ***D.*** *Evaluation of skin FACS from (C). Neutrophils show the mean ± SEM of n = 5 - 11 animals per group, ROS-positive cells the mean ± SEM of n = 3 - 5 animals per group. Significances were calculated using a 2-tailed Student's t-test (*p < 0.05, **p < 0.01, and ***p < 0.001, ns= not significant).*

4.20 Keratinocyte-derived IκBζ mediates the local adaptive immune response against epicutaneous *S. aureus* infections *in vivo*

Aside from the immunomodulatory effects of IκBζ on innate immune responses, we further investigated whether this applies to the recruitment of adaptive immune cell populations in a similar fashion. First, we analyzed the distribution of T-lymphocytes in the skin immunohistologically, after an *in vivo* model of 7 days via staining for the universal T-cell surface marker CD3. Strikingly, massive amounts of CD3-positive T-cells were detected in infected *Nfkbiz*$^{fl/fl}$ control animals (***Figure 4.20***A), while highly reduced numbers of skin-infiltrating T-cells were stained in skin sections of infected *Nfkbiz*$^{\Delta K14\text{-}cre}$ knockout mice. Likewise, T-cells were equally spread in the skin of PBS-treated animals independent of their genetic background, albeit in very low numbers (see ***Supplementary Figure VII***B).

To better distinguish single T-cell subsets, we further conducted FACS analysis. As the adaptive immune response is not activated at an early time point, expectedly no T-cell infiltration was observed after only 2 days of *S. aureus* infection (see ***Figure 4.20***B). However, after 7 days we discovered a strong *S. aureus*-induced recruitment of $CD4^+$ effector T-cells ($CD4^+$ $CD25^-$ T-cells) and cells expressing the γδ T-cell receptor ($γδ^+$ T-cells) to the side of infection in *Nfkbiz*$^{fl/fl}$ control animals (***Figure 4.20***C and D). On the contrary, the recruitment of these populations was significantly attenuated in *Nfkbiz*$^{\Delta K14\text{-}cre}$ knockouts.

All in all, we successfully demonstrated the important role of IκBζ in the recruitment and activation of both innate and adaptive immune cell populations in an experimentally induced *S. aureus* infection *in vivo,* making IκBζ an indispensable factor promoting both antibacterial and pro-inflammatory responses in the skin.

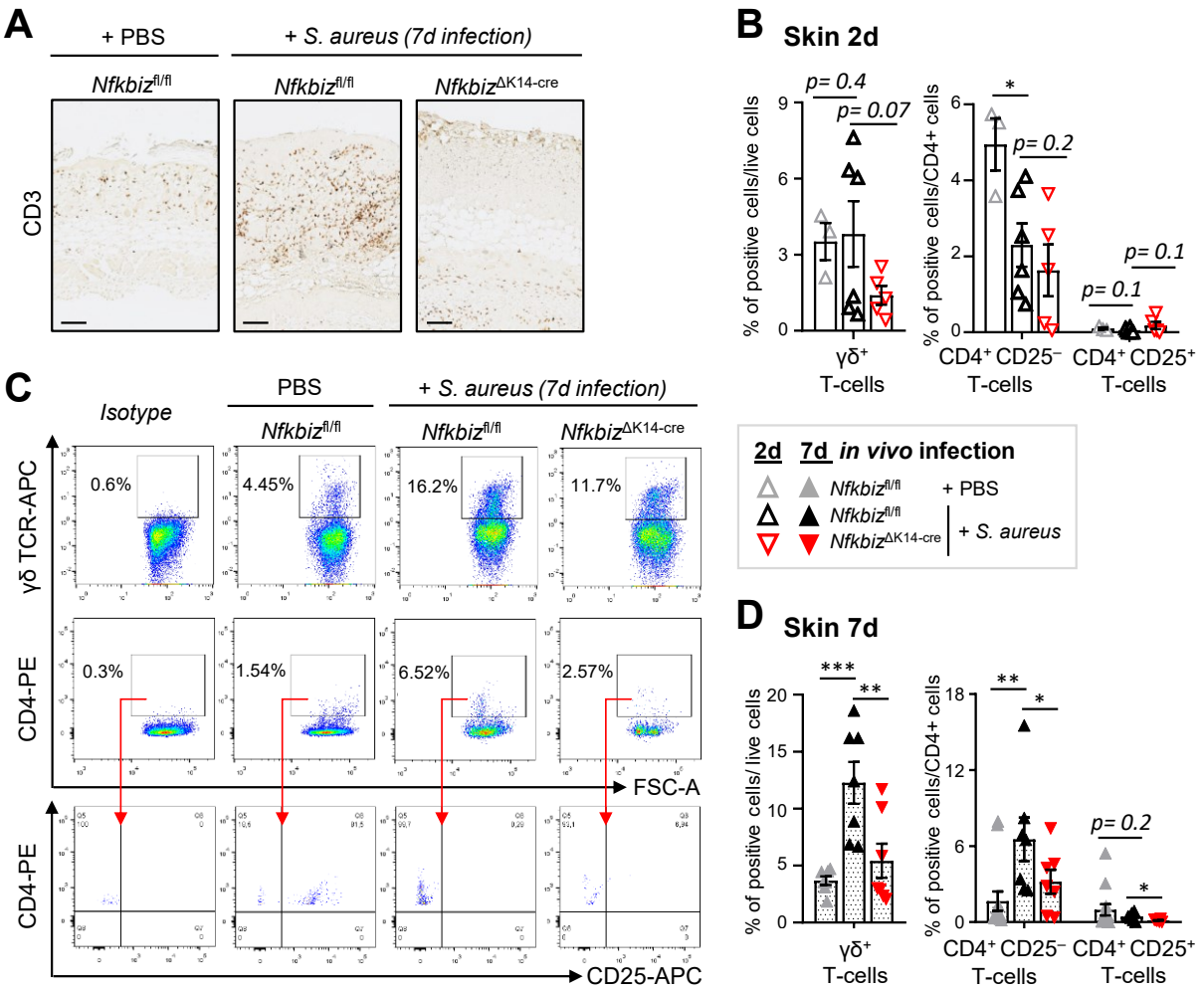

Figure 4.20: IκBζ shapes the local adaptive immune response in epicutaneous S. aureus infections in the skin.

A. *Immunohistology of FFPE back skin material of PBS-treated Nfkbiz$^{fl/fl}$ control and S. aureus-infected Nfkbiz$^{fl/fl}$ control or IκBζ-depleted Nfkbiz$^{\Delta K14\text{-}cre}$ animals, taken at the endpoint on day 7. Skin sections were stained for the universal T cell surface marker CD3. Scale bars: 100 µm. Histology stainings were performed by Dagmar Löck.* ***B – D.*** *Flow cytometry analysis of adaptive immune cell populations in digested skin tissue obtained from PBS-treated Nfkbiz$^{fl/fl}$ control and S. aureus-infected Nfkbiz$^{fl/fl}$ control and Nfkbiz$^{\Delta K14\text{-}cre}$ knockout animals.* ***B.*** *Evaluation of skin FACS from mice sacrificed after 2 days. Shown is the mean ± SEM (n = 3 - 6 animals per group) of the percentage of skin-infiltrating γδ-TCR positive T-cells, CD4-positive effector T cells (CD4+ CD25-) and CD4-positive regulatory T-cells (CD4+ CD25+) per live cells.* ***C + D.*** *Skin samples obtained from mice sacrificed at the endpoint on day 7.* ***C.*** *Examples of gated living cell populations showing γδ T-cells (γδTCR+). Besides, effector T cells (CD4+ CD25-) and regulatory T cells (CD4+ CD25+) were determined after pre-gating on viable CD4+ T-cells. FACS plots were evaluated using FlowJo (Tree Star Inc.) software.* ***D.*** *Evaluation of skin FACS from (C). Shown is the mean ± SEM (n = 7 - 13 animals per group). Significances were calculated using a 2-tailed Student's t-test (*p < 0.05, **p < 0.01, and ***p < 0.001, ns= not significant).*

4.21 IκBζ prevents deeper infiltration and dissemination of *S. aureus* in the course of infection over 7 days *in vivo*

Since the absence of IκBζ resulted in increased apoptosis and significantly stronger disruption of the epidermal skin layer after an infection course of 7 days *in vivo,* we were interested to study the effects related to IκBζ depletion regarding the progression of an epicutaneous *S. aureus* infection and the dissemination of bacteria over time. We addressed this question by conducting confocal immunofluorescence microscopy of formalin-fixed paraffin-embedded (FFPE) skin sections obtained after 2 days or 7 days from PBS-treated or *S. aureus*-infected animals (see ***Figure 4.21***). Localization of bacteria was assessed via staining for *S. aureus*-derived Protein A, while the DNA-staining Hoechst solution was used to outline the cellular compartments.

At an early time point of infection, the *S. aureus* remained exclusively superficial, regardless of the genetic background of the infected mouse skin, which is visualized by the red staining on top of the epidermal compartment (***Figure 4.21***A). Normalization of the fluorescence intensity of Protein A, present in each cell, further confirmed no significant differences between infected *Nfkbiz*$^{fl/fl}$ control and *Nfkbiz*$^{\Delta K14\text{-}cre}$ knockout skin sections after 2 days of infection (***Figure 4.21***B).

After 7 days, however, the bacterial burden was significantly enlarged exclusively in IκBζ-depleted mouse skin (***Figure 4.21***C and D). Also, deeper infiltrates and stronger dissemination of bacteria through the epidermis into the dermis were observed, while on the contrary the infection in *Nfkbiz*$^{fl/fl}$ control mice remained superficial, as seen after only 2 days of infection. These results imply that the presence of IκBζ per se does not prevent an epicutaneous infection, but it is essential to suppress deeper pathogen infiltration into the skin *in vivo*, counteracting apoptosis and damage of the skin barrier in the epidermal compartment. This finding also fits our obtained *in vitro* results from infected primary hKC, where we recovered higher amounts of internalized *S. aureus* from *NFKBIZ*-depleted cells (see again ***Figure 4.15***B).

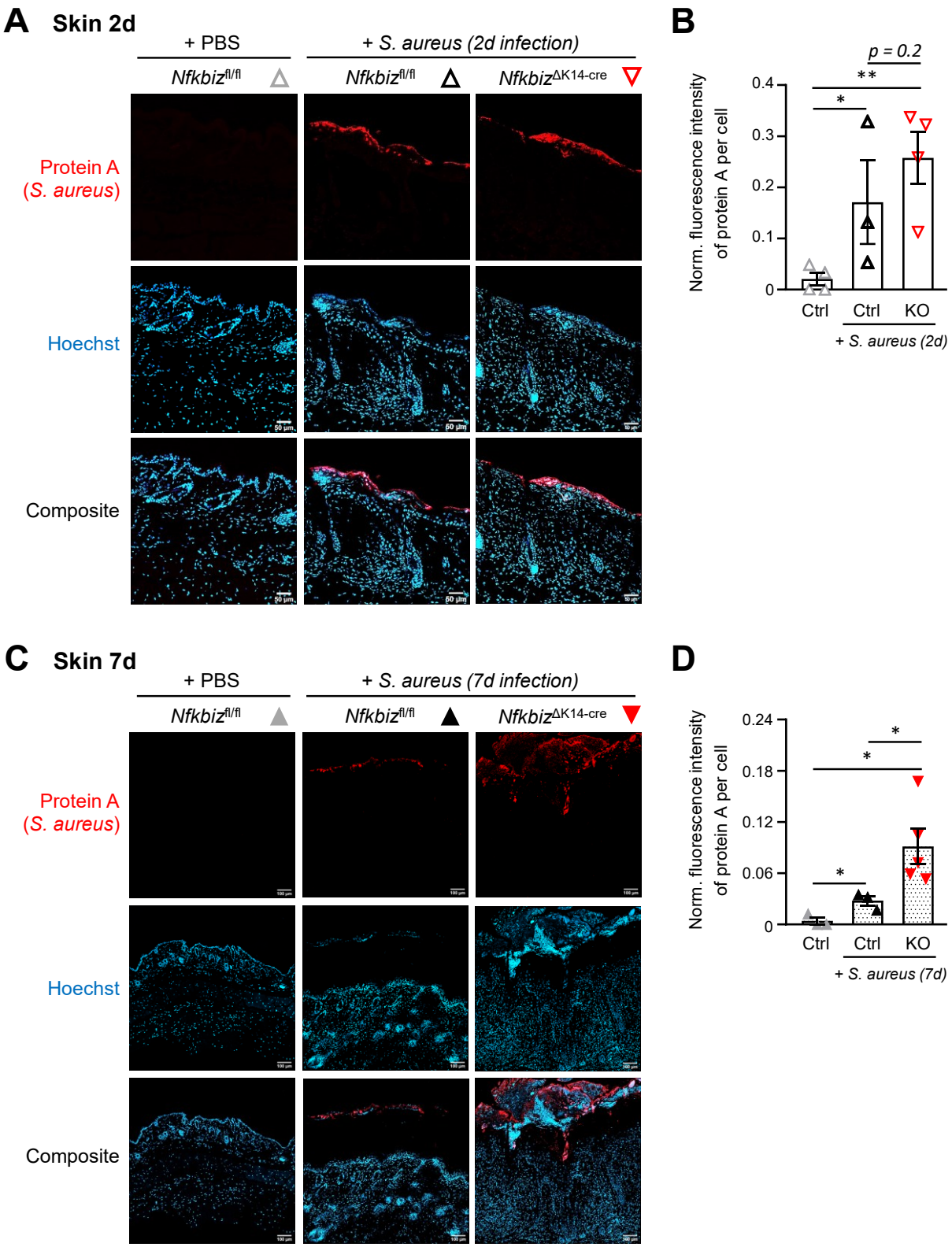

Figure 4.21: Keratinocyte-derived IκBζ prevents dissemination of living S. aureus into skin tissue in a time-independent manner, while its absence results in deeper infiltration at later time points.

A. *Immunofluorescence staining of FFPE skin material taken from PBS-treated control animals (Ctrl) and S. aureus-infected Nfkbiz$^{fl/fl}$ (Ctrl) or Nfkbiz$^{\Delta K14\text{-}cre}$ (KO) mice after 2 days of infection. Bacteria were detected by staining for S. aureus-derived Protein A (red), nuclei were stained with Hoechst dye (blue). Composite images were generated with ImageJ software. Scale bars: 50 µm.*

B. *Bar diagram showing fluorescence intensity from (A). Intensities of Hoechst staining from infected mice were equated to PBS control mice and normalized to the amount of Protein A per cell, respectively. Shown are data obtained from n = 3 - 4 animals per group.*
C. *Immunofluorescence staining of back skin after 7 days S. aureus infection, same as in (A). Scale bars: 100 µm.*
D. *Fluorescence intensity of immunofluorescence staining from (C), described as in (B). Shown are data obtained from n = 3 - 5 animals per group. Bar diagrams in (B) and (D) show the mean values ± SEM, significance was calculated using a 2-tailed Student's t-test (*p < 0.05, **p < 0.01, and ***p < 0.001). IF staining and microscopy was performed in collaboration with Francesca Bork (AG Weber, Eberhard Karls University of Tübingen).*

4.22 Bacterial internalization is a prerequisite to drive *S. aureus*-induced and NOD2-mediated expression of IκBζ and its target genes

Albeit we discovered several IκBζ-dependent effects during an epicutaneous *S. aureus* infection in mice, such as stronger dissemination of bacteria into deeper skin tissues, we did not experimentally address the involvement of pathogen recognition receptors *in vivo*. Since the oligomerization and final activation of the intracellular NOD2 receptor can be triggered in the cytoplasm upon encounter with bacterial components or living staphylococci, we were wondering whether the process of bacterial internalization constitutes a prerequisite for the induction of IκBζ and its subsequent regulation of host cell responses *in vitro* against pathogenic bacteria. To provide further insight into the hitherto unexplored IκBζ-NOD2 axis in skin cells, we infected differentiated primary hKC with *S. aureus,* while manipulating the invasion capability of the bacteria. In the first experiment, we conducted an infection (1 h, MOI30) either in absence or presence of the actin-remodeling agent cytochalasin D (CytoD), which directly inhibits phagocytosis and thus, the subsequent internalization of bacterial components [46, 127], resulting in the missing activation of cytoplasmic NOD2 receptors as a direct consequence.
Interestingly, IκBζ protein expression was abolished in infected cytochalasin D-treated cells without affecting NF-κB activation, represented by unaltered phosphorylated IκBα levels (see ***Figure 4.22***A). As an inhibitor control, we conducted an internalization assay in parallel (***Figure 4.22***B). Besides, gene expression analysis 24 h post-infection revealed suppressed mRNA levels of both *NFKBIZ* and *NOD2* in the presence of cytochalasin D, which in turn resulted in a partial repression of IκBζ target genes, such as cytokine-encoding genes related to IL-17/IL-36 responses (***Figure 4.22***C). However, the expression of genes encoding antimicrobial peptides (*S100A8, DEFB4*) was even more elevated when internalization was blocked, providing substantial evidence that *S. aureus* can still be sensed by other non-cytoplasmic receptors, such as extracellular TLR2.
Moreover, we aimed to test the dependency of pro-inflammatory responses on the ability of *S. aureus* to internalize in another set-up, where we infected differentiated hKC for 1 h (MOI30) side by side with either living bacteria or heat-inactivated *S. aureus* cultures (*HiSa*, 1 h boiled at 90°C in advance).

While *HiSa* infection failed to induce IκBζ protein (***Figure 4.22***D) and subsequently, IκBζ target gene expression 24 h post-infection (***Figure 4.22***E, left), the expression of IκBζ-independent NF-κB target genes, such as *NFKBIA* or *ICAM1*, remained intact whether the bacteria were inactivated or alive (see ***Figure 4.22***E, right).

Taken together, these results imply that the induction of keratinocyte-derived IκBζ and subsequently, its pro-inflammatory target gene expression, strongly depends on the internalization capacity of *S. aureus* strains, attributing the NOD2 receptor activation upstream of IκBζ a substantial part in the epidermal host defense.

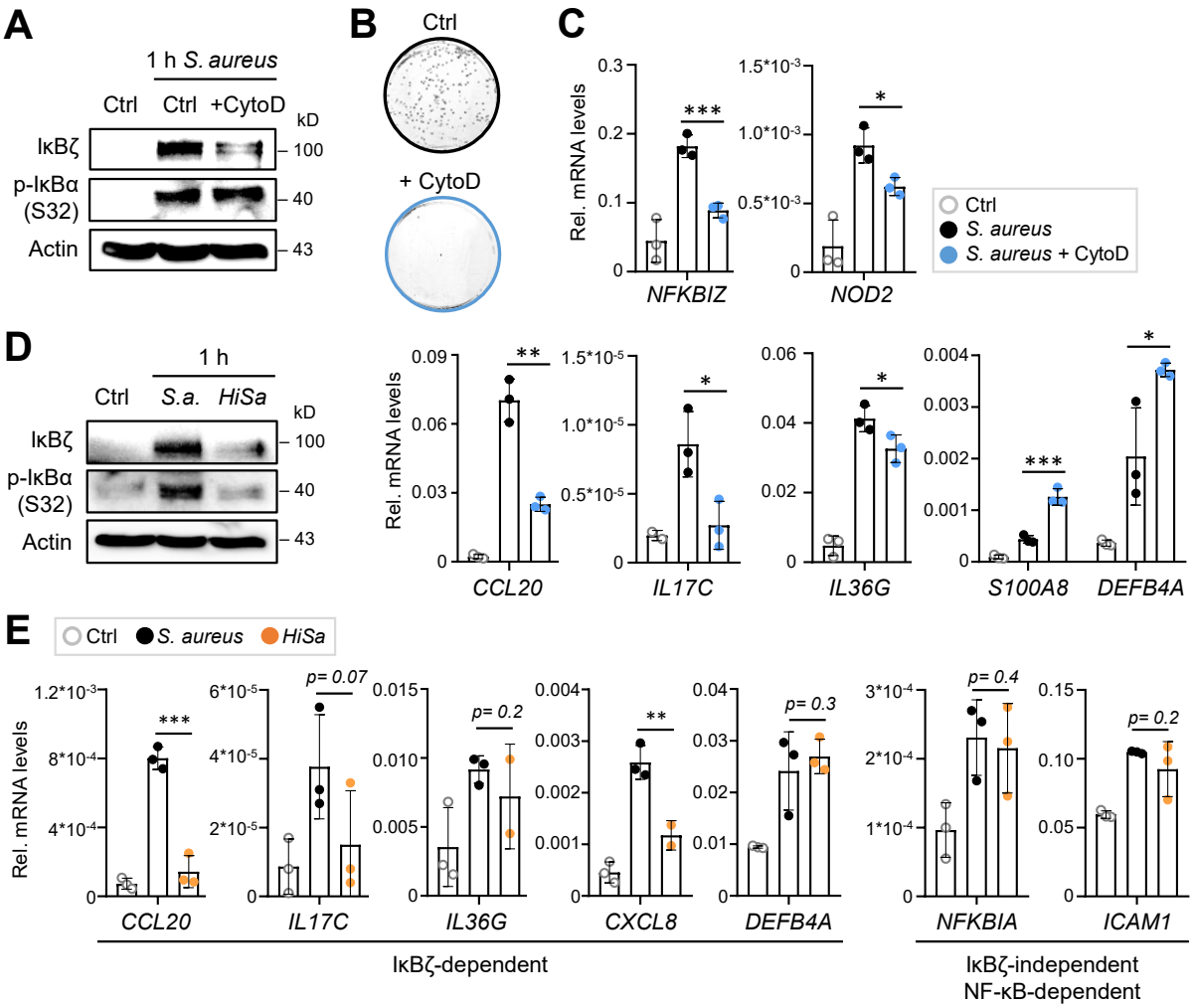

Figure 4.22: Expression of IκBζ and its target genes is highly dependent on the ability of S. aureus to internalize into keratinocytes.

A. *IκBζ protein levels in control treated or S. aureus infected (1h, MOI30) differentiated primary hKC, in presence or absence of the actin remodelling agent cytochalasin D (CytoD, 0.5µM) to block internalization. DMSO served as vehicle control. Phosphorylated IκBα levels (p-IκBα (S32)) indicate treatment and activation of the cells, ß-actin served as loading control.* ***B.*** *Internalization assay showing S. aureus colony forming units (CFU) recovered from differentiated hKC on TSB agar plates after treating and infecting cells for 24 h (MOI30, 1 h) in presence or absence of CytoD (0.5µM, blue) or DMSO.* ***C.*** *Gene expression analysis of primary hKC treated as in (B). S. aureus-dependent genes are either repressed (IL-17/IL-36 signaling) or upregulated (antimicrobial peptides e.g. S100A8, DEFB4A) by CytoD.*

D. *IκBζ protein levels in differentiated primary hKC infected with living (S.a.) or heat-inactivated S. aureus cultures (HiSa) for 1 h (MOI30). Phosphorylated IκBα levels indicate activation of the cells due to bacteria, β-actin served as loading control. Immunoblot was stained by Antonia Kolb.*
E. *Gene expression analysis of S. aureus- (MOI 30, black) or HiSa-infected (orange) primary hKC after 24 h. Shown are IκBζ-dependent target genes and IκBζ-independent NF-κB target genes being significantly induced upon infection. (C) and (E) show the mean of 3 biological replicates ± standard deviation (SD). Relative mRNA levels were normalized to the reference gene RPL37A. Significance was calculated using a 2-tailed Student's t-test (*p < 0.05, **p < 0.01, and ***p < 0.001, ns = not significant).*

5. Discussion

5.1 Activation of NOD-receptors induce IκBζ protein expression in differentiated primary keratinocytes at an early time point

In the past, several studies have implicated a link between the pro-inflammatory role of keratinocyte-derived IκBζ and the maintenance of both skin tissue and microbial homeostasis [37-39, 44]. However, they did not investigate the relevance of IκBζ expression in the context of cutaneous infection.

As a starting point, we aimed to investigate the potential of NOD1 and/or NOD2 agonists to activate intracellular pathogen recognition receptors of the NOD-like receptor family and subsequently, to induce the expression of IκBζ protein in primary keratinocytes. Interestingly, IκBζ levels were not only induced on translational and transcriptional levels but were slightly increased in treated differentiated hKC compared to undifferentiated cells at an early time point, when treated simultaneously with the NOD2 receptor agonist MDP.

This result could be explained by the fact that terminally differentiated keratinocytes located in the upper epidermal layers consistently encounter skin commensals, as well as pathogens and thus, require fast and reliable responses for bacteria recognition.

While the level of differentiation goes along with rising calcium gradients compared to undifferentiated skin cells [3], it is known that terminally differentiated hKC attempt to dampen their immune responses on purpose via a diminished expression of pro-inflammatory pathogen recognition receptors in the outermost layer of the epidermis [128, 129]. This helps our skin to discriminate between the needed antimicrobial responses when stimulated with commensal bacteria and the host responses triggered by skin injury, inflammation or infection with microbiota.

However, since the activation of intracellular NOD-like receptors requires the translocation of bacterial components into the cytoplasm of skin cells, keratinocytes have established an additional mechanism to transfer PGN fragments from the extracellular to intracellular space via peptide transporter proteins, such as PEPT1 and PEPT2 [130], apart from the phagocytosis of particles or pathogens, the endocytosis of PGN fragments or the engulfment of outer membrane vesicles being a specific feature of gram-negative bacteria [131]. Interestingly, the expression of these transporter proteins provably depends on the differentiation status of keratinocytes [130], fitting to our stronger responses obtained in MDP-treated, differentiated hKC. For instance, in the latter high levels of exclusively PEPT1 transporters are expressed, which can transfer both NOD2-agonist MDP and NOD1-agonist Tri-DAP (Tri-diaminopimelic acid) [132] into the cells. On the contrary, basal, undifferentiated keratinocytes are rather programmed to perform self-renewal and express PEPT2 transporter proteins responsible for the transition of only MDP [130, 133]. Hence, we hypothesized that keratinocytes require a regulatory protein downstream of NOD-like receptors, such as IκBζ, capable of fine-tuning pro-inflammation and microbial tolerance in the epidermis.

Interestingly, we proofed that, besides the activation of NOD2, also NOD1 receptor stimulation induces pro-inflammatory signaling cascades leading to the expression of IκBζ protein *in vitro,* when exposing hKC to NOD1-specific agonists. One reason might be, that both NOD receptors activate the obligate downstream receptor-interacting Serine/ Threonine kinase 2 (RIPK2), independently of the amount of N-terminal CARD molecules present in each NOD receptor [126].
However, while NOD1 receptors target the PGN fragment Tri-DAP, exclusively found in gram-negative strains, e.g. in *Pseudomonas aeruginosa* [126], NOD2 receptors mostly allow the detection of gram-positive bacteria, such as *S. aureus*, and few gram-negative specimen based on the abundance of the PGN component MDP [88, 126, 134].
NOD1 receptors exist in various cell types and tissues, however, in skin they are mainly expressed in skin-homing immune cells while NOD2 receptors are expressed in keratinocytes, in a variety of epithelial tissues, as well as different immune cell populations [126, 129].
Based on the fact, that NOD2 deficiencies in particular elevate the risk for the development of atopic dermatitis [129], which is often accompanied with *S. aureus* colonization of the skin [135], we exclusively focused our study on NOD2-mediated pro-inflammatory responses to investigate the regulatory effects of IκBζ during skin infections with pathogenic MRSA.

5.2 Loss of IκBζ deregulates genes responsible for the maintenance and functionality of the skin barrier during *S. aureus* infections

With the aid of transcriptome analysis obtained from *NFKBIZ*-depleted hKC, either infected with *S. aureus* or stimulated with MDP to activate NOD2 receptor signaling, we discovered an unacquainted function of IκBζ to sustain and strengthen the epidermal barrier. Hereby, loss of IκBζ downregulated several genes being involved in the regulation of keratinocyte differentiation and the maintenance of the epidermal layer, such as filaggrin, loricrin or involucrin (*FLG, LOR, IVL*) and many different late cornified envelope proteins (*LCE2C, LCE2D*). This hitherto unpublished finding is of great importance, since barrier disruption is associated with desiccation of the skin which represents a hallmark of many skin-related inflammatory diseases such as psoriasis, ichthyosis and atopic dermatitis [136, 137].
Comprising mainly terminally differentiated keratinocytes, the outer epidermal layer is formed under rising calcium concentrations. Consequently, damage of the skin barrier leads to an alteration of the calcium gradient [138]. In case of atopic dermatitis patients, several studies have implicated elevated levels of calcium in the skin accompanied by an aggravated risk in exhibiting a deficiency in the gene filaggrin (*FLG*), which correlates with an increased susceptibility for epicutaneous infections with *S. aureus* [15, 69, 139].

Since we observed an IκBζ-dependent regulation of *FLG*, we even presume that patients suffering from dryness-related skin diseases potentially possess lower levels of keratinocyte-derived IκBζ and consequently become more susceptible to bacterial infections in the long term.

Previously, the absence of IκBζ was reported to broaden colonization of the skin with different staphylococcal species, such as *Staphylococcus xylosus*, and thereby created a dysbiosis of skin-derived microbiota in *Nfkbiz*-deficient mice [38, 44]. Hence, the integrity of the epidermis is a critical factor in microbial skin homeostasis [140] and, since the skin constitutes a mechanical barrier, it plays a crucial part in the host defense against infections with pathogenic microbiota like *S. aureus* [141].

Since infected wild-type mice without a precedent damage to the epidermal layer exhibited only marginal effects on IκBζ-dependent pro-inflammatory gene expression levels, we extended our *in vivo* study and introduced a mild barrier defect with tape-stripping. Interestingly, we discovered that barrier disruption indeed exhibits a prerequisite for the establishment of an epicutaneous infection in general. Likewise, studies with animals exhibiting a loss-of-function mutation in the gene *Flg* revealed the development of cutaneous inflammation, similar to the phenotype observed in atopic dermatitis models, exclusively when barrier disruption prior infection had been conducted via tape-stripping [140]. Moreover, loss of filaggrin increased and facilitated the microbial entry into keratinocytes via the epidermal barrier [140].

This result prompted us to further investigate the effects of blocked or incomplete IκBζ signaling regarding dysregulated gene expression in barrier genes, caused by internalization with subsequent survival of living *S. aureus* cultures in keratinocytes, escaping bacterial clearance. At this point we speculated that in keratinocyte-specific *Nfkbiz* knockout mice damage of the outer epidermal layer is caused only upon stronger propagation and dissemination of bacteria into deeper skin tissues *in vivo*.

Fitting to our assumption, a recent study assigned calcium as a key regulator and super adhesive, which not only amplifies the interaction between microbiota and the host cell, but further contributes to an enhanced adhesion of *S. aureus* to the skin [138]. However, an attenuation of calcium levels could decrease staphylococcal adhesion and colonization and thus, might present a potential target when treating epicutaneous infections. Thus, it would be of great interest to study clinical isolates derived from atopic dermatitis patients in order to investigate whether a correlation between barrier loss and expression levels of keratinocyte-derived IκBζ influences the ability of a particular *S. aureus* strain to colonize and infect host cells.

5.3 Keratinocyte-derived IκBζ regulates expression of antimicrobial peptides as a first-line defense mechanism

In accordance with the increased responsiveness of differentiated keratinocytes compared to basal cells, we detected high levels of genes encoding for antimicrobial peptides (AMPs) under both MDP stimulation and *S. aureus* infection. However, in terms of sensing skin microbiota, loss of IκBζ resulted in a strong abrogation of peptidoglycan recognition proteins (*PGLYRP3, 4*) and defensins (*DEFB1, DEFB4A*), RNase-7 or several S100 proteins and therefore, the loss of an important first-line host defense mechanism. A similar phenotype is exhibited in the disease pathology of atopic dermatitis, linking a diminished expression of AMPs with increased *S. aureus* colonization due to dysbiosis of skin microbiota in affected patients [142].

While the antimicrobial ribonuclease RNase-7 is constantly expressed and secreted by keratinocytes under healthy conditions, its expression is increased upon activation of cytokines, such as IL-17 and IL-1 cytokine family signaling [143], growth factors and bacterial components [144]. Regarding the latter, our study revealed a significant, IκBζ-dependent induction of *RNASE7* during MDP stimulation, supporting control against colonization of pathogens at the skin surface [144].

Moreover, defensins can trigger the activation of several chemokine receptors in a variety of immune cells and keratinocytes. While their implications in the signaling pathway of pathogen recognition receptor NOD2 has been reported in previous studies [145, 146], we hereby confirmed their IκBζ-dependent induction in both MDP-stimulated and *S. aureus*-infected primary keratinocytes, which underlines the ability of defensins to shape local immune responses in the skin to support wound healing and to counteract epicutaneous infections *in vivo* [147].

Expectedly, we confirmed previous results revealing a strong upregulation of S100 proteins during activation of NOD2 receptor-mediated skin inflammation in IκBζ-expressing keratinocytes [148]. Since this group of antimicrobial peptides is abundant in many different cell types and held responsible for various cellular processes, such as differentiation, calcium homeostasis, apoptosis and proliferation, its primary function highly contributes to both pro-inflammatory and homeostatic signaling in the skin [149, 150]. Hence, in diseased skin tissue, such as in lesional atopic dermatitis, S100 proteins represent useful disease markers and might become a therapeutic target in the future fighting MRSA infections.

In general, expression of endogenous antimicrobial peptides in the epidermis does not primarily depend on the pathogenicity of the staphylococcal strain or whether living or heat-inactivated bacteria are used, indicating that the signaling pathways involved in their induction require complex regulation [52, 151]. The latter is also of great importance with respect to the permanent exposure of the skin to both commensal and pathogenic bacteria, as an overshooting immune response, triggered by antimicrobial responses, needs to be avoided to maintain a healthy skin homeostasis [52, 142].

Also, we assume that this effect relies on a compensatory mechanism that is supposed to mediate the pro-inflammatory gene induction in case NOD2 activation fails to prevent bacterial infestation [152].
Fitting to recent reports about late cornified envelope (LCE) proteins contributing to the antimicrobial activity of terminally differentiated cells [7, 8], we presume a secondary auxiliary mechanism regarding the rapid pathogen response in the skin, assuring that microbial sensing is established at the skin barrier, albeit the reduced expression of pathogen recognition receptors in the epidermis in general.

5.4 Internalization and dissemination of *S. aureus* is a pre-requisite for the NOD2-mediated induction of IκBζ *in vitro* and *in vivo*

Albeit IκBζ reportedly exhibits an immunomodulatory role in the skin, we and others showed that Krt14-specific *Nfkbiz*$^{\Delta K14\text{-cre}}$ knockout animals remained unscathed at steady-state until adulthood, without the development of spontaneous or the presence of persistent skin infections with staphylococci [37]. Likewise, global *Nod2*$^{-/-}$ receptor knockout mice were provably spared from impromptu *S. aureus* infections [91, 153].
However, this was not the case for keratinocyte-specific or global knockout animals bearing a deletion in the extracellular pathogen recognition receptor *Tlr2*$^{-/-}$ [87] or its subsequent adapter protein *Myd88* [89], making these mice susceptible to bacterial infections. For example, being activated downstream of IL-1- or TLR2-mediated signaling pathways, deletion of *Myd88* was reported to eventually cause skin lesions accompanied by spontaneous infections with different *Staphylococcus* strains [87, 89].
Hence, we suspected intracellular signaling rather than extracellular pathogen recognition receptor activation to drive IκBζ-dependent host responses and bacterial clearance, which is why we examined the effects of a Krt14-specific *Nfkbiz* deletion in an experimentally induced *S. aureus* infection model *in vivo*.
Immunofluorescence staining of epicutaneously infected mouse skin revealed a clear coherence between the expanding dissemination of *S. aureus* into deeper skin tissues and the absence of keratinocyte-derived IκBζ, as well as the augmented internalization and proliferation of bacteria in absence of either IκBζ itself or the NOD2-mediated IκBζ induction *in vitro*. This hitherto unpublished finding led us to the assumption that the internalization of bacteria into keratinocytes is indispensable to activate the intracellular NOD2 receptor
To confirm that bacterial internalization rather than the presence of bacterial fragments in the extracellular space constitutes a fundamental prerequisite for keratinocyte-derived IκBζ induction, we oriented our experiments towards established protocols from previous studies using *HiSa* or the internalization blocker cytochalasin D [46]. Hereby, we either exposed the bacteria to heat, leading to the destruction of their membrane integrity and a reduced stability of toxins [154], or we abrogated the actin-dependent phagocytic uptake [127] of living *S. aureus* cultures by challenging the hKC, respectively.

Interestingly, *S. aureus* internalization deficiency failed to induce IκBζ in both settings and we were able to rule out a NF-κB-dependent induction of IκBζ and its target genes. This novel discovery is of great importance, since *S. aureus* consistently attempts to circumvent, manipulate, and escape the host immune system, making IκBζ an attractive target for the treatment of epicutaneous MRSA infections.

5.5 Pathogenic *S. aureus* induces keratinocyte-derived IκBζ via intracellular NOD2 receptors rather than extracellular TLR2

Besides the intracellular NOD2 receptor activation, TLR1/2 receptor signaling has previously been described to mediate a protective host response against *S. aureus* [88, 155, 156]. However, it remained ambiguous, whether the IκBζ-mediated pro-inflammatory responses in an epicutaneous infection scenario with *S. aureus* are rather driven by the activation of NOD2 alone, than in combination or exclusively by TLR2. In the past, for instance, the co-stimulation of both receptors *in vitro* was reported in murine bone marrow-derived dendritic cells [157].

Addressing a potential synergy between different bacterial sensing receptors is quite complex, since their elicited pro-inflammatory responses might be highly host cell-type- and pathogen-specific, in order to develop and activate robust host defense mechanisms to clear bacterial infections whilst tolerating skin commensals [158]. Moreover, our immune system requires a constant adaptation to environmental stimuli, which should further include strategies to compensate loss or impairment of a particular pathogen recognition receptor [158].

Surprisingly, only the indirect inhibition of NOD2 receptor signaling using RIPK2 inhibitor, but not TLR2 inhibition, was able to abrogate the early protein expression of IκBζ in *S. aureus*-infected human primary keratinocytes, albeit the ability of TLR1/2 ligands to elicit the expression of IκBζ similar to NOD1 and NOD2 agonists. Hence, we speculated that TLR2-mediated effects fail to counteract *S. aureus* internalization into keratinocytes but rather keep the extracellular proliferation of pathogenic *S. aureus* strains in check, which is further supported by TLR2 activation established by the commensal strain *S. epidermidis* to protect the skin from excessive *S. aureus* colonization [152].

Loss of TLR2 activation further increased the expression levels of *NFKBIZ* and certain target genes in hKC 24 h post infection, which probably resulted from an unimpeded bacterial invasion that finally led to a full-blown activation of intracellular NOD2 receptors. Thus, we denote the TLR2 receptor activation as dispensable when addressing the evoked, IκBζ-dependent pro-inflammatory responses counteracting the internalization of *S. aureus* into keratinocytes *in vitro.* Besides, a dampened activation of external TLR2, as well as a TLR2-independent expression of IκBζ could represent a self-control mechanism in differentiated hKC to prevent an undesired removal of required skin commensals and thus, disturbance of the microbial homeostasis to an overshooting immune response [159].

On the contrary, *S. aureus*-induced IκBζ protein levels were abrogated with RIPK2 inhibitor, as well as the expression of IκBζ target genes after 24 h, despite the lack of significant downregulation in *NFKBIZ* mRNA levels. For the latter, however, different reasons could apply. First, one could argue that after 24 h the *S. aureus*-mediated induction of *NFKBIZ* mRNA levels already declined, as the induction of IκBζ protein levels oscillate at different time points [22]. Hence, the differences between infected RIPK2 inhibitor-treated and infected non-treated cells remain marginal. Secondly, we hypothesized that *NFKBIZ* mRNA is stabilized over time and thereby the amount of inhibitor becomes insufficient. However, by overexpressing IκBζ exogenously in hKC, inhibition of RIPK2 and thus, NOD2 receptor activation, was overwritten compared to keratinocytes with endogenous IκBζ expression.
All in all, we provide hitherto unbeknownst evidence, that during the infection of differentiated primary hKC with pathogenic *S. aureus* the intracellular NOD2 receptor, but not extracellular TLR2, acts as the main mediator inducing IκBζ-dependent, pro-inflammatory host responses.

5.6 NOD2 receptor activation triggers IκBζ-dependent IL-17/IL-36-signaling *in vitro* and *in vivo* while shaping local immune responses

The IL-17/IL-36-signaling pathway and its promoted anti-inflammatory immune responses has been reported in several studies addressing both autoinflammatory skin diseases, such as psoriasis [22, 37, 42], and host defense mechanisms when combating epicutaneous exposure to *S. aureus* [155, 160]. Interestingly, transcriptome analysis revealed a highly IκBζ-dependent induction of IL-17/IL-36-responsive genes in both MDP-treated and *S. aureus*-infected keratinocytes, which was further confirmed in our *in vivo* infection model, again using a virulent MRSA strain.
Regarding the *in vitro* infection with *S. aureus*, pathway enrichment analysis revealed that loss of keratinocyte-derived IκBζ reduced the expression of genes responsible for immune cell recruitment through chemotaxis *in vitro*, for instance *IL17C, IL36G, CCL20, CXCL8* and *CXCL10.* Equal results were obtained in back skin samples of *S. aureus*-infected control and *Nfkbiz* knockout animals, showing recruitment deficiencies of both adaptive and innate immune cell populations, as well as augmented apoptosis signals due to the lacking expression of IκBζ. However, significant differences appeared exclusively 7 days post-infection. Expectedly, loss of IκBζ diminished the *S. aureus*-induced infiltration of monocytes and neutrophils, as well as effector $CD4^+$ T-cells ($CD4^+$ $CD25^-$) and γδ T-cells at the side of infection due to the absence of host immune responses combating pathogenic bacteria. T-cell responses are established in recurrent infections over time [161], however in *Nfkbiz* knockout mice they significantly declined.
For instance, as IL-36 possesses a key function in both the recruitment and activation of T-cells and neutrophils [155], it promotes a functional host defense against bacterial infections [162], which is compromised in infected *Nfkbiz* knockout mice of this study.

In general, IL-36 cytokines, such as IL36-γ or IL-36 receptor antagonist (*IL36G, IL36RN*), strongly depend on keratinocyte-derived IκBζ *in vitro* and *in vivo*. [162]. Similar to IL-36-signaling, IL-17-signaling represents another important host defense mechanism that strongly applies to keratinocytes, which sense cellular stress of inflamed, neighboring skin cells and counteract with an elevated expression of *IL17C,* thereby promoting wound closure during infection [163]. Moreover, it directly affects the activation of certain subtypes of T-cells. For instance, it was reported that mice lacking keratinocyte-derived IL-17 receptor antagonist (*IL17RA*) exhibit higher numbers of IL-17A-producing γδ T-cells, which increases their susceptibility to epicutaneous *S. aureus* infection. Likewise, *IL-17A/IL-17F* knockout animals lacking the IL-17A- and IL-17F-secreting CD4+ T helper cells (Th17 cells), which represent an important cell type fighting extracellular pathogens, are also prone to develop spontaneous, superficial *S. aureus* infections [160].

In our study we show that activation of the pathogen recognition receptors further results in the IκBζ-dependent expression of chemokines by keratinocytes being relevant for the recruitment of dermal dendritic cells (*CCL20*) or neutrophils (*CXCL8, CXCL10*). Expectedly, infected *Nfkbiz*$^{\Delta K14\text{-cre}}$ knockout mice exhibited an impaired neutrophil activity, visualized in declining numbers of cells producing reactive oxygen species (ROS), which is responsible for the generation of oxidative stress and thus comprises an important first-line host defense mechanism against epicutaneous *S. aureus* infection [72, 73].

Above that, infected *Nfkbiz* knockout animals scored a higher inflammation score and showed stronger levels of apoptosis compared to infected control animals, assigning IκBζ a supportive role not only in the recruitment of immune cells to the side of infection, but also in maintaining the vitality of infected skin cells. These results affirmed our hypothesis that skin cells lacking IκBζ expression possess a diminished host defense, which might result directly from a low secretion of both antimicrobial peptides and IL-17/IL-36-related cytokines and chemokines, which subsequently lead to an impaired recruitment of immune cell populations. Moreover, we validated the IκBζ-dependent expression of these genes in an independent setup using murine keratinocytes extracted from wildtype and *Nfkbiz*-depleted mice, proofing this pathway being conserved among both species.

Hence, we provide evidence that keratinocyte-derived IκBζ indeed shapes the activation of local innate and adaptive immune responses upon epicutaneous *S. aureus* infections *in vivo*, confirming the acquired *in vitro* data.

5.7 *NFKBIZ* mRNA is stabilized in a Regnase-1-dependent manner during *S. aureus* infection *in vitro*

Many host cell immune responses modulate the expression of inflammatory proteins in a post-transcriptional manner, e.g. by stabilizing or de-stabilizing mRNA through regulatory RNases and thus, fine-tune the translation of proteins [164]. Interestingly, we found that during *S. aureus* infection IκBζ directly binds to promoter regions of its target genes while *NFKBIZ* mRNA gets stabilized in the cytosol in a Regnase-1-dependent manner. As expected, Regnase-1 degradation seems to promote IκBζ expression upon *S. aureus* infection and is regulated by MALT-1-mediated cleavage.

Regnase-1 signaling has already been implicated in restraining inflammatory responses upon infection [29]. Surprisingly and fitting to our project, *MALT1* deficiency was already clinically described in patients with higher susceptibility to *S. aureus* infections, assumably through an impaired immune response of Th17 cells, as seen in a deficient IL-17 signaling pathway [165]. Above that, dysregulation of *MALT1* has classically been observed in malignant cancer [30], but also serves as a potential biomarker in gut tissue to distinguish inflammatory bowel diseases, such as ulcerative colitis or Crohn's [166, 167]. The latter not only exhibits an upregulation of *MALT1* [166], but is also known for its high risk to develop in patients with NOD2-associated genetic mutations [168, 169].

However, NOD2-mediated IκBζ expression so far has not been investigated when it comes to the functionality of Regnase-1 in inflammatory bowel diseases and constitutes a very interesting topic for future research.

5.8 Implications of IκBζ in IL-36-responsive, NOD2 receptor-mediated and *S. aureus*-driven inflammation and related diseases

Albeit the disease-promoting role of IκBζ in the context of auto-inflammatory skin diseases has been treated in earlier studies, the underlying molecular mechanisms leading to its induction vary greatly in a stimulus-dependent manner, and IκBζ has never been investigated in infection experiments with a pathogenic MRSA strain before.

Previously, STAT3 and NF-kB have been revealed as the main transcription factors mediating IκBζ induction, as least in psoriasis [22]. Searching for a possible regulator upstream of IκBζ, we tested the influence of STAT1/STAT3 or IKKβ inhibitors on the NOD2 receptor-mediated induction of IκBζ in differentiated hKC, revealing that the transcription factor NF-κB, rather than STAT3, binds to the promoter region of *NFKBIZ* and regulates target gene expression upon *S. aureus* infection. However, we did not further investigate potential IκBζ-interacting transcription factors being accountable for the *S. aureus*-induced and NOD2-mediated gene repression or induction, which would be of great interest and requires follow-up experiments.

We further investigated whether a co-stimulation of differentiated hKC with the NOD2 receptor agonist MDP and psoriasis-related cytokines [22] influences the quantity of IκBζ protein expression. Although no synergistic effects were observed under combined treatment conditions on translational level at an early time point, we assumed that IκBζ, being a transcriptional co-factor, binds different transcription factors in order to regulate stimulus-dependent gene expression.

To summarize potential similarities of IκBζ-dependent pro-inflammatory responses, we compared transcriptome data obtained from *NFKBIZ*-depleted hKC stimulated with either IL-36α (1.5 h and 24 h, retrieved from a previously published data set [22]), NOD2 receptor agonist MDP and *S. aureus* (both 24 h). Selected genes being significantly induced in treated control, however, downregulated in *NFKBIZ*-depleted cells (absolute fold change >2) are covered by the Venn diagram in ***Figure 5.8***, the used gene lists are further enclosed in ***Supplementary Table IV***.

Astonishingly, genes overlapping among the stimuli can be categorized once again into antimicrobial peptides, IL-17-/IL-36-related signaling, and genes encoding proteins involved in the formation of the cornified envelope and thus, differentiation and functionality of the epidermal layer. However, the analysis revealed only a minority of overlapping IκBζ target genes being conserved in the treated keratinocytes, further emphasizing the high stimulus-dependency and variability when it comes to the induction of IκBζ and its target genes.

In a direct comparison of transcriptome data obtained in the MDP-stimulated and *S. aureus*-infected *NFKBIZ* knockdown keratinocytes, it stands out that, although equal pathways are affected under both stimuli, *S. aureus* infection regulates higher numbers of genes in total, while 1/3 of all detected MDP- and thus, NOD2-responsive genes are included in the overlap group. We speculate that these differences arise from the oscillating dynamics of IκBζ induction [22], since we exclusively evaluated control and *NFKBIZ*-depleted cells at one time point after 24 h, as well as the fact that *S. aureus* additionally triggers TLR2-mediated but IκBζ-independent responses in keratinocytes, compared to NOD2 receptor stimulation alone.

Although cutaneous infection with *S. aureus* occurs less frequently in IL-36α-mediated psoriasis compared to its high prevalence in atopic dermatitis patients [170], we are profoundly convinced that keratinocyte-derived IκBζ seems to be induced by upstream mediators, such as IL-36 and NOD2 receptor, promoting the binding of different transcription factors to the promoter region of *NFKBIZ*. For example, while psoriasis-mediated IκBζ expression occurs in a NF-κB-dependent manner [22], non-canonical NF-κB has been implicated in the disease manifestations of IBD [171] which is highly associated with NOD2 receptor deficiencies. Hence, the identification of interaction and transcription partners for IκBζ constitutes a highly interesting research field, since its deregulation has been implicated in various diseases affecting different tissues and cell types, making it a potential target for novel treatment approaches in the near future.

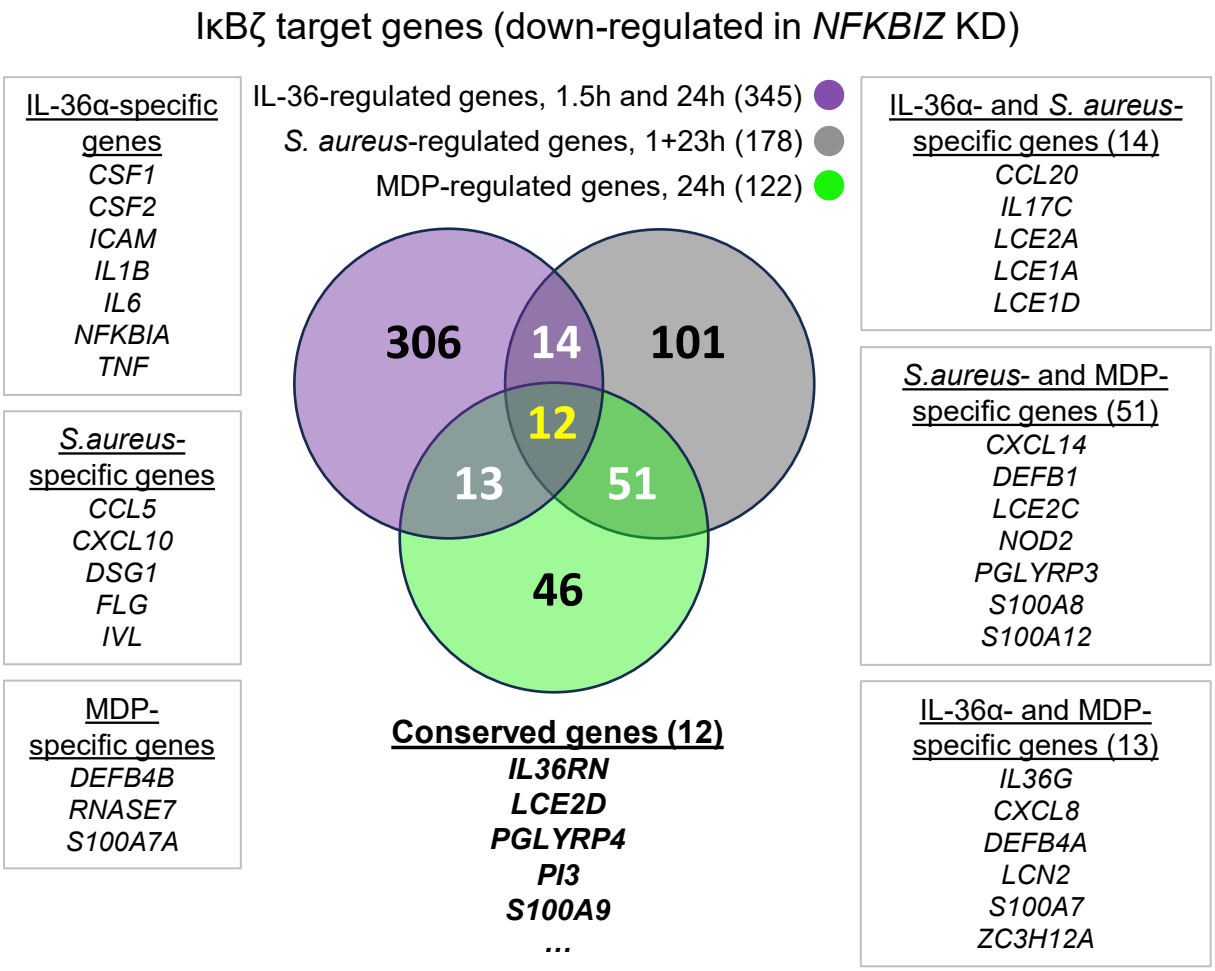

Figure 5.8: Intersection of IκBζ target genes downregulated in NFKBIZ-depleted hKC exhibiting IL-36-related, NOD2 receptor-mediated and S. aureus-driven pro-inflammatory gene expression.
Overlay of IκBζ target genes in primary keratinocytes incubated with different stimuli. Data were derived from the current study, examining gene expression after 24 h of either MDP-stimulation or S. aureus infection. These data were further compared to keratinocytes stimulated for 1.5 h and 24 h with recombinant human IL-36 (retrieved from data set published in [22]). Depicted genes were significantly induced upon stimulation and significantly downregulated in NFKBIZ-depleted cells compared to treated controls (fold change absolute >2). The gene list used for this comparison is provided in **Supplementary Table IV**.

5.9 Limitations of this study

The herein studied immune responses *in vivo* apply exclusively to epicutaneous *S. aureus* infection in skin tissue exhibiting a mild barrier defect. Hence, changes in the experimental set-up or the type of infection to e.g., subcutaneous or intravenous application of bacteria, as well as the duration of skin contact with living *S. aureus* cultures, might drastically change the expression of the discussed gene clusters.
The importance of IκBζ, concerning *S. aureus* colonization of the skin, remains still unaddressed and requires further investigation with the aid of *in vivo* infection models. Compared to *S. aureus*, the commensal *S. epidermidis* represents a coagulase-negative strain with weak internalisation capabilities [64] and a cell wall composed of different cell wall anchored surface proteins [172]. Besides, it is known for its TLR2-mediated expression of antimicrobial peptides [152] without inducing an overwhelming skin inflammation [46], fitting to our result that IκBζ expression in keratinocytes was considerably less induced upon colonization with the commensal *S. epidermidis*. Thus, we hypothesize that the keratinocytes established independent pathogen recognition mechanisms on purpose, to shield themselves from any bacteria slipping unnoticed through the skin barrier by the immune system, and to support both antimicrobial responses and bacterial clearance, as quickly as possible.
However, we did not include further studies addressing the IκBζ-dependent host response in internalisation-deficient strains, as well as no other than MRSA strain USA300 wild-type LAC was considered. Hence, we can only speculate that less pathogenic *Staphylococcus* strains elicit low levels of intracellular NOD2, whereupon the expression of IκBζ and its target genes would be diminished, as well.
Another limitation of this study is the lack of knowledge regarding the coverage of *S. aureus*-derived components triggering IκBζ expression, which might comprise bacterial RNA associated with neutrophil extracellular traps (NETs) [86] or toxins alongside of the herein investigated NOD2 receptor agonist MDP. Likewise, it remains completely unaddressed whether keratinocytes can differentiate between viable and dead bacteria, since it is not well studied which effects heat-inactivation of *S. aureus* cultures unleashes [46]. Moreover, heat-inactivated bacteria might be ineligible when studying *S. aureus*-derived proteins involved in the induction of pro-inflammatory host responses. So far, no reports have been published addressing the heat stability of the *S. aureus* specific type VII secretion system (T7SS) contributing to the strain-specific pathogenicity, respectively [173].
Moreover, the herein outlined Regnase-1-dependent regulation of *Nfkbiz* mRNA comprises a fine-tuning mechanism of gene regulation in skin infections. To completely exclude that a TLR2-mediated *Nfkbiz* induction remains unaffected by regulatory RNases, additional experiments using NOD2 agonists or TLR2 ligands instead of *S. aureus* need to be carried out.

However, a critical interpretation of murine *in vitro* data needs to be considered, since the obtained inflammatory responses in murine and human skin cells cannot be completely transferred. For instance, the chemokine encoding gene *CXCL8*, as well as the ribonuclease RNase-7, are completely absent in murine cells while their expression remains restricted to primates and humans, which in turn limits murine *in vivo* studies in the context of antimicrobial responses [174].
Also, *in vivo* data acquired in this project exclusively focus on IκBζ depletion but do not address direct effects of a *NOD2* deficiency e.g. addressable with *Nod2*$^{-/-}$*/Nfkbiz*$^{-/-}$ double knockout animals, which would give further insights into the coherence between the pathogenicity and NOD2 receptor activation during infection with gram-positive *Staphylococcus* strains. Regarding NOD1 receptor signaling, an *S. aureus*-mediated induction can be excluded due to the absence of a potential NOD1 agonist Tri-DAP.
With regard to the downstream regulation of IκBζ, the general molecular mechanism of how IκBζ binds promoter regions of target genes to elicit antimicrobial responses is quite difficult to address in our experimental set-up. On the one hand, primary keratinocytes cannot be cultivated until high passage numbers due to their short lifespan when reaching their terminal differentiation, hence such an experimental approach would consume a variety of materials and primary skin material. On the other hand, immunoprecipitation of chromatin represents the method of choice to determine protein-DNA interactions, however in *S. aureus*-treated hKC the highly abundant staphylococcal protein A interferes with the binding affinity of the respective antibodies. Thus, to prevent falsification, protein A needs to be removed in an additional pre-clearing step in order to enhance specific antibody binding of proteins or transcription factors bound to the chromatin [175]. Nevertheless, further investigations need to be carried out in the future to investigate potential transcription factors interacting with IκBζ in the context of epicutaneous infections.

5.10 Outlook and concluding remarks

Within this project we discovered a hitherto unknown coherence between internalization of bacteria and the subsequent *S. aureus*-mediated induction of IκBζ and its target genes, downstream of NOD2 receptor signaling pathways. Nevertheless, the exact molecular mechanisms triggering the switch from *S. aureus* skin colonization, as investigated for example in Krt5-cre specific *Nfkbiz* knockouts by *Terui et al.* [44] among others, to a keratinocyte-internalizing and thereby NOD2 receptor-activating pathogenic MRSA strain, require follow-up investigations. For instance, future studies should elaborate TLR2/NOD2 receptor signaling in different cell types present in the epidermis, in order to investigate to what extent TLR2 receptor signaling contributes to IκBζ-mediated antibacterial host responses upon contact with *S. aureus.*

These findings in turn could support further classification of different *Staphylococcus* strains or *S. aureus* mutants regarding their pathogenicity, distinguishing opportunistic skin commensals from dangerous specimens, which might also give insight into potential transcription factors, so far unknown, being involved in the upstream regulation of IκBζ.
Therefore, it would be of great interest to study clinical isolates with staphylococcal infestation in the future, in order to discover IκBζ-dependent effects correlating with the severity of disease pathology displaying skin barrier damage, as well as the differing capacity among the isolates to induce IκBζ in keratinocytes. This in turn would further contribute to improve the understanding of *S. aureus*-mediated diseases elevating hospitalization rates, such as life-threatening bacteremia or multi-organ failure due to septic shock [51], where living bacteria are distributed via the blood stream into the entire organism.
Since dysregulated IκBζ expression in epithelia is highly involved in the disease pathology of psoriasis [37, 39, 42] and, to a lesser extent in atopic dermatitis [176], our data indicate a high possibility for its involvement in intestinal inflammation, such as Crohn`s or granulomatous disease [92, 177, 178]. Interestingly, patients with genetic variations in *NOD2*, for instance *NOD2* mutations or polymorphisms, bear a high risk in developing inflammatory bowel diseases due to the induction of abnormal signaling of Th2 cells in the skin [81, 82, 135, 179], which links the disease pathologies of atopic dermatitis and Crohn's.
Likewise, special emphasis needs to be put on adverse treatment effects when using antibodies targeting the classical IL-17A-driven skin inflammation in psoriasis vulgaris. Due to its systemic application, several case studies reported the development of new-onset Crohn's disease in treated psoriasis patients, since inhibiting the dysregulated IL-17A-producing Th17 cells the skin also affected their functionality in the gut, where Th17 cells possess an important function in fighting infections while maintaining the homeostasis in gut mucosa [180, 181]. Hence, further investigations tackling the novel function of NOD2-dependent IκBζ expression in the maintenance of the intestinal mucosa would be of great interest for inflammatory bowel diseases, as well as their coherent implications for auto-inflammatory skin diseases.
As a concluding remark, to preserve an intact and wholesome homeostasis of the skin, counterbalancing the expression of keratinocyte-derived IκBζ represents a critical mechanism, since its deregulation has been associated with autoinflammation, for instance in psoriasis, where it strongly promotes overshooting immune responses [22].
All in all, this project validated epidermal IκBζ as a crucial mediator downstream of NOD2 receptor signaling, shaping the host immune response in both human and murine skin cells, *in vivo* and *in vitro*, to combat epicutaneous *S. aureus* infection with antimicrobial and pro-inflammatory host responses and finally, to mediate bacterial clearance of infected host cells.

A graphical summary of the key events and discovered findings in this study, leading to keratinocyte-derived IκBζ expression upon *S. aureus* infection, is enclosed in ***Figure 5.10:***. Hence, our study discovered IκBζ as the key player in a newly identified course of NOD2-IκBζ signaling pathway, which provides substantial support in protecting keratinocytes against pathogenic *S. aureus* skin infections.

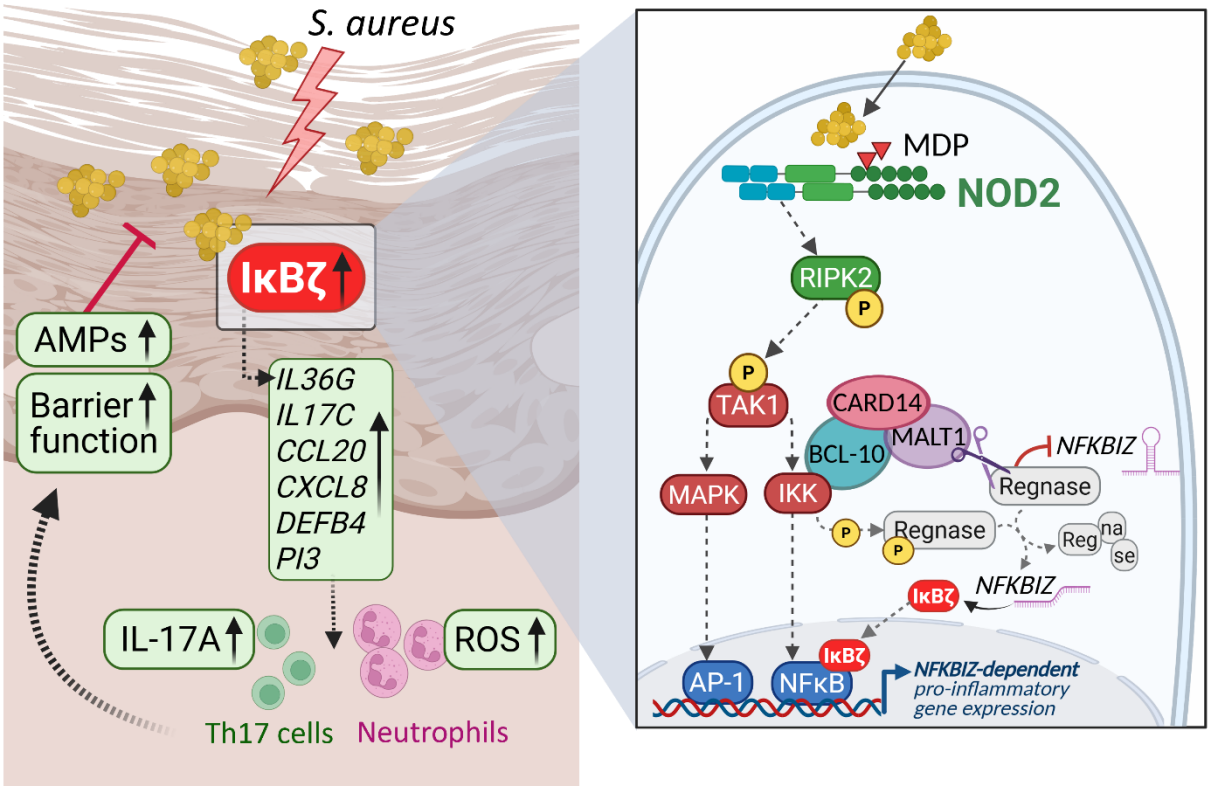

Figure 5.10: Graphical summary of this study showing the NOD2-mediated induction and Regnase-1-dependent stabilization of IκBζ during epicutaneous S. aureus infections, resulting in local pro-inflammatory and antimicrobial host responses while supporting skin barrier functions.

S. aureus mediates the activation of NOD2 and TLR2 receptors, leading to the auto-phosphorylation of TAK1 (TGFβ-associated kinase 1) and consequently, activation of MAPK (mitogen-activated protein kinase) and IκB kinase (IKK) signaling cascades. These in turn result in NF-κB-dependent immune responses: TLR2 signaling leads to the expression of genes encoding antimicrobial peptides (AMPs), however, during in vitro infection independent of IκBζ. NOD2 receptor mediates NF-κB activation, resulting not only in direct induction of IκBζ and its target genes, but cytoplasmic NFKBIZ mRNA is stabilized in a Regnase-1-dependent manner upon activation of the CARD14-BCL-10-MALT1 complex. Translated IκBζ protein translocates to the nucleus, acting as a transcriptional co-factor for previously recruited transcription factors, e.g. NF-κB and activator protein-1 (AP-1) family members, leading to the induction of IκBζ-dependent pro-inflammatory gene expressions [30, 34-36]. These in turn result in the secretion of cytokines and chemokines required to recruit and activate innate and adaptive immune cells to establish local immune responses mediated by ROS-producing neutrophils and T-cell subsets. Created with BioRender (for reference see chapter 6.1)

6. References

6.1 Reference and publication license of created images

The following images were created in BioRender:

Figure 1.1.1 Fischer, B. (**2025**) https://BioRender.com/2pog5jk

Figure 1.2.2 Fischer, B. (**2025**) https://BioRender.com/h32cc7r

Figure 1.5.1 Fischer, B. (**2025**) https://BioRender.com/b25ynhn

Figure 5.10 Fischer, B. (**2025**) https://BioRender.com/76u3u12

6.2 General references

[1] Nestle FO, Di Meglio P, Qin JZ, Nickoloff BJ. *Skin immune sentinels in health and disease*. Nat Rev Immunol. **2009**;9(10):679-91.

[2] Jiang Y, Tsoi LC, Billi AC, Ward NL, Harms PW, Zeng C, et al. *Cytokinocytes: the diverse contribution of keratinocytes to immune responses in skin*. JCI Insight. **2020**;5(20).

[3] Bikle DD, Xie Z, Tu CL. *Calcium regulation of keratinocyte differentiation*. Expert Rev Endocrinol Metab. **2012**;7(4):461-72.

[4] Lesniak W. *Epigenetic Regulation of Epidermal Differentiation*. Epigenomes. **2021**;5(1).

[5] Rajkumar J, Chandan N, Lio P, Shi V. *The Skin Barrier and Moisturization: Function, Disruption, and Mechanisms of Repair*. Skin Pharmacol Physiol. **2023**;36(4):174-85.

[6] Dull K, Lenart K, Dajnoki Z, Poliska S, Uchiyama E, Hendrik Z, et al. *Barrier function-related genes and proteins have an altered expression in acne-involved skin*. J Eur Acad Dermatol Venereol. **2023**;37(7):1415-25.

[7] Marshall D, Hardman MJ, Nield KM, Byrne C. *Differentially expressed late constituents of the epidermal cornified envelope*. Proc Natl Acad Sci U S A. **2001**;98(23):13031-6.

[8] Niehues H, van der Krieken DA, Ederveen THA, Jansen PAM, van Niftrik L, Mesman R, et al. *Antimicrobial Late Cornified Envelope Proteins: The Psoriasis Risk Factor Deletion of LCE3B/C Genes Affects Microbiota Composition*. J Invest Dermatol. **2022**;142(7):1947-55 e6.

[9] Bitschar K, Wolz C, Krismer B, Peschel A, Schittek B. *Keratinocytes as sensors and central players in the immune defense against Staphylococcus aureus in the skin*. J Dermatol Sci. **2017**;87(3):215-20.

[10] Bonecchi R, Galliera E, Borroni EM, Corsi MM, Locati M, Mantovani A. *Chemokines and chemokine receptors: an overview*. Front Biosci (Landmark Ed). **2009**;14(2):540-51.

[11] Simmons J, Gallo RL. *The Central Roles of Keratinocytes in Coordinating Skin Immunity*. J Invest Dermatol. **2024**;144(11):2377-98.

[12] Moran MC, Chinchilli E, Kenney HM, Pope EM, Scott G, Brewer MG, et al. *Stage of Keratinocyte Differentiation Is a Key Determinant of Viral Susceptibility in Human Skin*. J Invest Dermatol. **2023**;143(9):1838-41 e7.

[13] Pasparakis M, Haase I, Nestle FO. *Mechanisms regulating skin immunity and inflammation*. Nat Rev Immunol. **2014**;14(5):289-301.

[14] Schuler CFt, Tsoi LC, Billi AC, Harms PW, Weidinger S, Gudjonsson JE. *Genetic and Immunological Pathogenesis of Atopic Dermatitis*. J Invest Dermatol. **2024**;144(5):954-68.

[15] Kim J, Kim BE, Ahn K, Leung DYM. *Interactions Between Atopic Dermatitis and Staphylococcus aureus Infection: Clinical Implications*. Allergy Asthma Immunol Res. **2019**;11(5):593-603.
[16] Hayden MS, Ghosh S. *NF-kappaB, the first quarter-century: remarkable progress and outstanding questions*. Genes Dev. **2012**;26(3):203-34.
[17] Alpsoy A, Wu XS, Pal S, Klingbeil O, Kumar P, El Demerdash O, et al. *IkappaBzeta is a dual-use coactivator of NF-kappaB and POU transcription factors*. Mol Cell. **2024**;84(6):1149-57 e7.
[18] Concetti J, Wilson CL. *NFKB1 and Cancer: Friend or Foe?* Cells. **2018**;7(9).
[19] Yamazaki S. *The Nuclear NF-kappaB Regulator IkappaBzeta: Updates on Its Molecular Functions and Pathophysiological Roles*. Cells. **2024**;13(17).
[20] Feng Y, Chen Z, Xu Y, Han Y, Jia X, Wang Z, et al. *The central inflammatory regulator IkappaBzeta: induction, regulation and physiological functions*. Front Immunol. **2023**;14:1188253.
[21] Smale ST. *Selective transcription in response to an inflammatory stimulus*. Cell. **2010**;140(6):833-44.
[22] Müller A, Hennig A, Lorscheid S, Grondona P, Schulze-Osthoff K, Hailfinger S, et al. *IkappaBzeta is a key transcriptional regulator of IL-36-driven psoriasis-related gene expression in keratinocytes*. Proc Natl Acad Sci U S A. **2018**;115(40):10088-93.
[23] MaruYama T, Kobayashi S, Ogasawara K, Yoshimura A, Chen W, Muta T. *Control of IFN-gamma production and regulatory function by the inducible nuclear protein IkappaB-zeta in T cells*. J Leukoc Biol. **2015**;98(3):385-93.
[24] Karakaslar EO, Katiyar N, Hasham M, Youn A, Sharma S, Chung CH, et al. *Transcriptional activation of Jun and Fos members of the AP-1 complex is a conserved signature of immune aging that contributes to inflammaging*. Aging Cell. **2023**;22(4):e13792.
[25] Martincuks A, Andryka K, Kuster A, Schmitz-Van de Leur H, Komorowski M, Muller-Newen G. *Nuclear translocation of STAT3 and NF-kappaB are independent of each other but NF-kappaB supports expression and activation of STAT3*. Cell Signal. **2017**;32:36-47.
[26] Tartey S, Matsushita K, Vandenbon A, Ori D, Imamura T, Mino T, et al. *Akirin2 is critical for inducing inflammatory genes by bridging I kappa B-zeta and the SWI/SNF complex*. Embo Journal. **2014**;33(20):2332-48.
[27] Li M, Hada A, Sen P, Olufemi L, Hall MA, Smith BY, et al. *Dynamic regulation of transcription factors by nucleosome remodeling*. Elife. **2015**;4.
[28] Sun SC. *The non-canonical NF-kappaB pathway in immunity and inflammation*. Nat Rev Immunol. **2017**;17(9):545-58.
[29] Behrens G, Winzen R, Rehage N, Dorrie A, Barsch M, Hoffmann A, et al. *A translational silencing function of MCPIP1/Regnase-1 specified by the target site context*. Nucleic Acids Res. **2018**;46(8):4256-70.
[30] Gomez Solsona B, Schmitt A, Schulze-Osthoff K, Hailfinger S. *The Paracaspase MALT1 in Cancer*. Biomedicines. **2022**;10(2).
[31] Yamazaki S, Muta T, Matsuo S, Takeshige K. *Stimulus-specific induction of a novel nuclear factor-kappaB regulator, IkappaB-zeta, via Toll/Interleukin-1 receptor is mediated by mRNA stabilization*. J Biol Chem. **2005**;280(2):1678-87.
[32] Bataclan M, Leoni C, Moro SG, Pecoraro M, Wong EH, Heissmeyer V, et al. *Crosstalk between Regnase-1 and -3 shapes mast cell survival and cytokine expression*. Life Sci Alliance. **2024**;7(8).
[33] Liu B, Huang J, Ashraf A, Rahaman O, Lou J, Wang L, et al. *The RNase MCPIP3 promotes skin inflammation by orchestrating myeloid cytokine response*. Nat Commun. **2021**;12(1):4105.
[34] Schmitt A, Grondona P, Maier T, Brandle M, Schonfeld C, Jager G, et al. *MALT1 Protease Activity Controls the Expression of Inflammatory Genes in Keratinocytes upon Zymosan Stimulation*. J Invest Dermatol. **2016**;136(4):788-97.
[35] Juilland M, Thome M. *Holding All the CARDs: How MALT1 Controls CARMA/CARD-Dependent Signaling*. Front Immunol. **2018**;9:1927.

[36] Ruland J, Hartjes L. *CARD-BCL-10-MALT1 signalling in protective and pathological immunity*. Nat Rev Immunol. **2019**;19(2):118-34.
[37] Lorscheid S, Muller A, Loffler J, Resch C, Bucher P, Kurschus FC, et al. *Keratinocyte-derived IkappaBzeta drives psoriasis and associated systemic inflammation*. JCI Insight. **2019**;4(22).
[38] Kim Y, Lee YS, Yang JY, Lee SH, Park YY, Kweon MN. *The resident pathobiont Staphylococcus xylosus in Nfkbiz-deficient skin accelerates spontaneous skin inflammation*. Sci Rep. **2017**;7(1):6348.
[39] Johansen C, Mose M, Ommen P, Bertelsen T, Vinter H, Hailfinger S, et al. *I kappa B zeta is a key driver in the development of psoriasis*. Proceedings of the National Academy of Sciences of the United States of America. **2015**;112(43):E5825-E33.
[40] Annemann M, Plaza-Sirvent C, Schuster M, Katsoulis-Dimitriou K, Kliche S, Schraven B, et al. *Atypical IkappaB proteins in immune cell differentiation and function*. Immunol Lett. **2016**;171:26-35.
[41] Gautam P, Maenner S, Cailotto F, Reboul P, Labialle S, Jouzeau JY, et al. *Emerging role of IkappaBzeta in inflammation: Emphasis on psoriasis*. Clin Transl Med. **2022**;12(10):e1032.
[42] Fischer B, Kubelbeck T, Kolb A, Ringen J, Waisman A, Wittmann M, et al. *IL-17A-driven psoriasis is critically dependent on IL-36 signaling*. Front Immunol. **2023**;14:1256133.
[43] Johansen C, Mose M, Bertelsen T, Vinter H, Lorscheid S, Schulze-Osthoff K, et al. *The I kappa B zeta protein is a downstream target of interleukin-17A and a key driver in the development of psoriasis*. British Journal of Dermatology. **2014**;171(6):E107-E.
[44] Terui H, Yamasaki K, Wada-Irimada M, Onodera-Amagai M, Hatchome N, Mizuashi M, et al. *Staphylococcus aureus skin colonization promotes SLE-like autoimmune inflammation via neutrophil activation and the IL-23/IL-17 axis*. Sci Immunol. **2022**;7(76):eabm9811.
[45] Wertheim HF, Melles DC, Vos MC, van Leeuwen W, van Belkum A, Verbrugh HA, et al. *The role of nasal carriage in Staphylococcus aureus infections*. Lancet Infect Dis. **2005**;5(12):751-62.
[46] Ngo QV, Faass L, Sahr A, Hildebrand D, Eigenbrod T, Heeg K, et al. *Inflammatory Response Against Staphylococcus aureus via Intracellular Sensing of Nucleic Acids in Keratinocytes*. Front Immunol. **2022**;13:828626.
[47] Nouwen JL, Ott A, Kluytmans-Vandenbergh MF, Boelens HA, Hofman A, van Belkum A, et al. *Predicting the Staphylococcus aureus nasal carrier state: derivation and validation of a "culture rule"*. Clin Infect Dis. **2004**;39(6):806-11.
[48] Simanski M, Dressel S, Glaser R, Harder J. *RNase 7 protects healthy skin from Staphylococcus aureus colonization*. J Invest Dermatol. **2010**;130(12):2836-8.
[49] Zanger P, Holzer J, Schleucher R, Steffen H, Schittek B, Gabrysch S. *Constitutive expression of the antimicrobial peptide RNase 7 is associated with Staphylococcus aureus infection of the skin*. J Infect Dis. **2009**;200(12):1907-15.
[50] Burian M, Bitschar K, Dylus B, Peschel A, Schittek B. *The Protective Effect of Microbiota on S. aureus Skin Colonization Depends on the Integrity of the Epithelial Barrier*. J Invest Dermatol. **2017**;137(4):976-9.
[51] Del Giudice P. *Skin Infections Caused by Staphylococcus aureus*. Acta Derm Venereol. **2020**;100(9):adv00110.
[52] Wanke I, Steffen H, Christ C, Krismer B, Gotz F, Peschel A, et al. *Skin commensals amplify the innate immune response to pathogens by activation of distinct signaling pathways*. J Invest Dermatol. **2011**;131(2):382-90.
[53] Krishna S, Miller LS. *Innate and adaptive immune responses against Staphylococcus aureus skin infections*. Semin Immunopathol. **2012**;34(2):261-80.
[54] Antimicrobial Resistance C. *Global burden of bacterial antimicrobial resistance in 2019: a systematic analysis*. Lancet. **2022**;399(10325):629-55.
[55] Thurlow LR, Joshi GS, Richardson AR. *Virulence strategies of the dominant USA300 lineage of community-associated methicillin-resistant Staphylococcus aureus (CA-MRSA)*. FEMS Immunol Med Microbiol. **2012**;65(1):5-22.

[56] Miller LG, Perdreau-Remington F, Rieg G, Mehdi S, Perlroth J, Bayer AS, et al. *Necrotizing fasciitis caused by community-associated methicillin-resistant Staphylococcus aureus in Los Angeles*. N Engl J Med. **2005**;352(14):1445-53.
[57] Centers for Disease C, Prevention. *Outbreaks of community-associated methicillin-resistant Staphylococcus aureus skin infections--Los Angeles County, California, 2002-2003*. MMWR Morb Mortal Wkly Rep. **2003**;52(5):88.
[58] Nikolic P, Mudgil P. *The Cell Wall, Cell Membrane and Virulence Factors of Staphylococcus aureus and Their Role in Antibiotic Resistance*. Microorganisms. **2023**;11(2).
[59] Matias VR, Beveridge TJ. *Native cell wall organization shown by cryo-electron microscopy confirms the existence of a periplasmic space in Staphylococcus aureus*. J Bacteriol. **2006**;188(3):1011-21.
[60] Al Kindi A, Alkahtani AM, Nalubega M, El-Chami C, O'Neill C, Arkwright PD, et al. *Staphylococcus aureus Internalized by Skin Keratinocytes Evade Antibiotic Killing*. Front Microbiol. **2019**;10:2242.
[61] Shoaib M, Aqib AI, Muzammil I, Majeed N, Bhutta ZA, Kulyar MF, et al. *MRSA compendium of epidemiology, transmission, pathophysiology, treatment, and prevention within one health framework*. Front Microbiol. **2022**;13:1067284.
[62] Chen H, Zhang J, He Y, Lv Z, Liang Z, Chen J, et al. *Exploring the Role of Staphylococcus aureus in Inflammatory Diseases*. Toxins (Basel). **2022**;14(7).
[63] Kubica M, Guzik K, Koziel J, Zarebski M, Richter W, Gajkowska B, et al. *A potential new pathway for Staphylococcus aureus dissemination: the silent survival of S. aureus phagocytosed by human monocyte-derived macrophages*. PLoS One. **2008**;3(1):e1409.
[64] Josse J, Laurent F, Diot A. *Staphylococcal Adhesion and Host Cell Invasion: Fibronectin-Binding and Other Mechanisms*. Front Microbiol. **2017**;8:2433.
[65] Cruz AR, Bentlage AEH, Blonk R, de Haas CJC, Aerts PC, Scheepmaker LM, et al. *Toward Understanding How Staphylococcal Protein A Inhibits IgG-Mediated Phagocytosis*. J Immunol. **2022**;209(6):1146-55.
[66] Fox PG, Schiavetti F, Rappuoli R, McLoughlin RM, Bagnoli F. *Staphylococcal Protein A Induces Leukocyte Necrosis by Complexing with Human Immunoglobulins*. mBio. **2021**;12(3):e0089921.
[67] McCormick JK, Yarwood JM, Schlievert PM. *Toxic shock syndrome and bacterial superantigens: an update*. Annu Rev Microbiol. **2001**;55:77-104.
[68] Howden BP, Giulieri SG, Wong Fok Lung T, Baines SL, Sharkey LK, Lee JYH, et al. *Staphylococcus aureus host interactions and adaptation*. Nat Rev Microbiol. **2023**;21(6):380-95.
[69] Miyake R, Iwamoto K, Sakai N, Matsunae K, Aziz F, Sugai M, et al. *Uptake of Staphylococcus aureus by keratinocytes is reduced by interferon-fibronectin pathway and filaggrin expression*. J Dermatol. **2022**;49(11):1148-57.
[70] Pidwill GR, Gibson JF, Cole J, Renshaw SA, Foster SJ. *The Role of Macrophages in Staphylococcus aureus Infection*. Front Immunol. **2020**;11:620339.
[71] Karauzum H, Datta SK. *Adaptive Immunity Against Staphylococcus aureus*. Curr Top Microbiol Immunol. **2017**;409:419-39.
[72] Painter KL, Strange E, Parkhill J, Bamford KB, Armstrong-James D, Edwards AM. *Staphylococcus aureus adapts to oxidative stress by producing H2O2-resistant small-colony variants via the SOS response*. Infect Immun. **2015**;83(5):1830-44.
[73] Focken J, Scheurer J, Jager A, Schurch CM, Kamereit S, Riel S, et al. *Neutrophil extracellular traps enhance S. aureus skin colonization by oxidative stress induction and downregulation of epidermal barrier genes*. Cell Rep. **2023**;42(10):113148.
[74] Brinkmann V, Reichard U, Goosmann C, Fauler B, Uhlemann Y, Weiss DS, et al. *Neutrophil extracellular traps kill bacteria*. Science. **2004**;303(5663):1532-5.
[75] Bröker BM, Mrochen D, Peton V. *The T Cell Response to Staphylococcus aureus*. Pathogens. **2016**;5(1).
[76] Duan T, Du Y, Xing C, Wang HY, Wang RF. *Toll-Like Receptor Signaling and Its Role in Cell-Mediated Immunity*. Front Immunol. **2022**;13:812774.

[77] Askarian F, Wagner T, Johannessen M, Nizet V. *Staphylococcus aureus modulation of innate immune responses through Toll-like (TLR), (NOD)-like (NLR) and C-type lectin (CLR) receptors*. FEMS Microbiol Rev. **2018**;42(5):656-71.
[78] Caruso R, Warner N, Inohara N, Nunez G. *NOD1 and NOD2: signaling, host defense, and inflammatory disease*. Immunity. **2014**;41(6):898-908.
[79] Keestra-Gounder AM, Tsolis RM. *NOD1 and NOD2: Beyond Peptidoglycan Sensing*. Trends Immunol. **2017**;38(10):758-67.
[80] Lorenz E, Mira JP, Cornish KL, Arbour NC, Schwartz DA. *A novel polymorphism in the toll-like receptor 2 gene and its potential association with staphylococcal infection*. Infect Immun. **2000**;68(11):6398-401.
[81] Macaluso F, Nothnagel M, Parwez Q, Petrasch-Parwez E, Bechara FG, Epplen JT, et al. *Polymorphisms in NACHT-LRR (NLR) genes in atopic dermatitis*. Exp Dermatol. **2007**;16(8):692-8.
[82] Kabesch M, Peters W, Carr D, Leupold W, Weiland SK, von Mutius E. *Association between polymorphisms in caspase recruitment domain containing protein 15 and allergy in two German populations*. J Allergy Clin Immunol. **2003**;111(4):813-7.
[83] McClure R, Massari P. *TLR-Dependent Human Mucosal Epithelial Cell Responses to Microbial Pathogens*. Front Immunol. **2014**;5:386.
[84] Goncharov T, Hedayati S, Mulvihill MM, Izrael-Tomasevic A, Zobel K, Jeet S, et al. *Disruption of XIAP-RIP2 Association Blocks NOD2-Mediated Inflammatory Signaling*. Mol Cell. **2018**;69(4):551-65 e7.
[85] Kishimoto K, Matsumoto, K., Ninomiya-Tsuji, J.,. *TAK1 Mitogen-activated Protein Kinase Kinase Kinase Is Activated by Autophosphorylation within Its Activation Loop*. Journal of Biological Chemistry. **2000**;275:7359–64.
[86] Bork F, Greve CL, Youn C, Chen S, V NCL, Wang Y, et al. *naRNA-LL37 composite DAMPs define sterile NETs as self-propagating drivers of inflammation*. EMBO Rep. **2024**;25(7):2914-49.
[87] Takeuchi O, Hoshino K, Akira S. *Cutting edge: TLR2-deficient and MyD88-deficient mice are highly susceptible to Staphylococcus aureus infection*. J Immunol. **2000**;165(10):5392-6.
[88] Roth SA, Simanski M, Rademacher F, Schroder L, Harder J. *The pattern recognition receptor NOD2 mediates Staphylococcus aureus-induced IL-17C expression in keratinocytes*. J Invest Dermatol. **2014**;134(2):374-80.
[89] Miller LS, O'Connell RM, Gutierrez MA, Pietras EM, Shahangian A, Gross CE, et al. *MyD88 mediates neutrophil recruitment initiated by IL-1R but not TLR2 activation in immunity against Staphylococcus aureus*. Immunity. **2006**;24(1):79-91.
[90] Hruz P, Zinkernagel AS, Jenikova G, Botwin GJ, Hugot JP, Karin M, et al. *NOD2 contributes to cutaneous defense against Staphylococcus aureus through alpha-toxin-dependent innate immune activation*. Proc Natl Acad Sci U S A. **2009**;106(31):12873-8.
[91] Stroo I, Butter LM, Claessen N, Teske GJ, Rubino SJ, Girardin SE, et al. *Phenotyping of Nod1/2 double deficient mice and characterization of Nod1/2 in systemic inflammation and associated renal disease*. Biol Open. **2012**;1(12):1239-47.
[92] Ogura Y, Bonen DK, Inohara N, Nicolae DL, Chen FF, Ramos R, et al. *A frameshift mutation in NOD2 associated with susceptibility to Crohn's disease*. Nature. **2001**;411(6837):603-6.
[93] Inohara N, Ogura Y, Fontalba A, Gutierrez O, Pons F, Crespo J, et al. *Host recognition of bacterial muramyl dipeptide mediated through NOD2. Implications for Crohn's disease*. J Biol Chem. **2003**;278(8):5509-12.
[94] Hugot JP, Chamaillard M, Zouali H, Lesage S, Cezard JP, Belaiche J, et al. *Association of NOD2 leucine-rich repeat variants with susceptibility to Crohn's disease*. Nature. **2001**;411(6837):599-603.
[95] Kanazawa N, Okafuji I, Kambe N, Nishikomori R, Nakata-Hizume M, Nagai S, et al. *Early-onset sarcoidosis and CARD15 mutations with constitutive nuclear factor-kappaB activation: common genetic etiology with Blau syndrome*. Blood. **2005**;105(3):1195-7.

[96] Miceli-Richard C, Lesage S, Rybojad M, Prieur AM, Manouvrier-Hanu S, Hafner R, et al. *CARD15 mutations in Blau syndrome*. Nat Genet. **2001**;29(1):19-20.
[97] Chamaillard M, Philpott D, Girardin SE, Zouali H, Lesage S, Chareyre F, et al. *Gene-environment interaction modulated by allelic heterogeneity in inflammatory diseases*. Proc Natl Acad Sci U S A. **2003**;100(6):3455-60.
[98] Stevens C, Henderson P, Nimmo ER, Soares DC, Dogan B, Simpson KW, et al. *The intermediate filament protein, vimentin, is a regulator of NOD2 activity*. Gut. **2013**;62(5):695-707.
[99] Sabbah A, Chang TH, Harnack R, Frohlich V, Tominaga K, Dube PH, et al. *Activation of innate immune antiviral responses by Nod2*. Nat Immunol. **2009**;10(10):1073-80.
[100] Roberson EC, Tully JE, Guala AS, Reiss JN, Godburn KE, Pociask DA, et al. *Influenza induces endoplasmic reticulum stress, caspase-12-dependent apoptosis, and c-Jun N-terminal kinase-mediated transforming growth factor-beta release in lung epithelial cells*. Am J Respir Cell Mol Biol. **2012**;46(5):573-81.
[101] Celli J, Tsolis RM. *Bacteria, the endoplasmic reticulum and the unfolded protein response: friends or foes?* Nat Rev Microbiol. **2015**;13(2):71-82.
[102] Okuma A, Hoshino K, Ohba T, Fukushi S, Aiba S, Akira S, et al. *Enhanced apoptosis by disruption of the STAT3-IkappaB-zeta signaling pathway in epithelial cells induces Sjogren's syndrome-like autoimmune disease*. Immunity. **2013**;38(3):450-60.
[103] Dassule HR, Lewis P, Bei M, Maas R, McMahon AP. *Sonic hedgehog regulates growth and morphogenesis of the tooth*. Development. **2000**;127(22):4775-85.
[104] Behrens G, Edelmann SL, Raj T, Kronbeck N, Monecke T, Davydova E, et al. *Disrupting Roquin-1 interaction with Regnase-1 induces autoimmunity and enhances antitumor responses*. Nat Immunol. **2021**;22(12):1563-76.
[105] Li Y, Huang X, Huang S, He H, Lei T, Saaoud F, et al. *Central role of myeloid MCPIP1 in protecting against LPS-induced inflammation and lung injury*. Signal Transduct Target Ther. **2017**;2:17066.
[106] Boukamp P, Petrussevska RT, Breitkreutz D, Hornung J, Markham A, Fusenig NE. *Normal keratinization in a spontaneously immortalized aneuploid human keratinocyte cell line*. J Cell Biol. **1988**;106(3):761-71.
[107] Voss E, Wehkamp J, Wehkamp K, Stange EF, Schroder JM, Harder J. *NOD2/CARD15 mediates induction of the antimicrobial peptide human beta-defensin-2*. J Biol Chem. **2006**;281(4):2005-11.
[108] Guo L, Wang L, Yang R, Feng R, Li Z, Zhou X, et al. *Optimizing conditions for calcium phosphate mediated transient transfection*. Saudi J Biol Sci. **2017**;24(3):622-9.
[109] Evangelista JE, Xie Z, Marino GB, Nguyen N, Clarke DJB, Ma'ayan A. *Enrichr-KG: bridging enrichment analysis across multiple libraries*. Nucleic Acids Res. **2023**;51(W1):W168-W79.
[110] Untergasser A, Cutcutache I, Koressaar T, Ye J, Faircloth BC, Remm M, et al. *Primer3--new capabilities and interfaces*. Nucleic Acids Res. **2012**;40(15):e115.
[111] Koressaar T, Lepamets M, Kaplinski L, Raime K, Andreson R, Remm M. *Primer3_masker: integrating masking of template sequence with primer design software*. Bioinformatics. **2018**;34(11):1937-8.
[112] Koressaar T, Remm M. *Enhancements and modifications of primer design program Primer3*. Bioinformatics. **2007**;23(10):1289-91.
[113] Ye J, Coulouris G, Zaretskaya I, Cutcutache I, Rozen S, Madden TL. *Primer-BLAST: a tool to design target-specific primers for polymerase chain reaction*. BMC Bioinformatics. **2012**;13:134.
[114] Bankhead P, Loughrey MB, Fernandez JA, Dombrowski Y, McArt DG, Dunne PD, et al. *QuPath: Open source software for digital pathology image analysis*. Sci Rep. **2017**;7(1):16878.
[115] Perez G, Barber GP, Benet-Pages A, Casper J, Clawson H, Diekhans M, et al. *The UCSC Genome Browser database: 2025 update*. Nucleic Acids Res. **2025**;53(D1):D1243-D9.
[116] Karolchik D, Hinrichs AS, Kent WJ. *The UCSC Genome Browser*. Curr Protoc Bioinformatics. **2009**;Chapter 1:Unit1 4.

[117] Mendez J, Stillman B. *Chromatin association of human origin recognition complex, cdc6, and minichromosome maintenance proteins during the cell cycle: assembly of prereplication complexes in late mitosis*. Mol Cell Biol. **2000**;20(22):8602-12.
[118] Kim H, Kim M, Im SK, Fang S. *Mouse Cre-LoxP system: general principles to determine tissue-specific roles of target genes*. Lab Anim Res. **2018**;34(4):147-59.
[119] Fischer AH, Jacobson KA, Rose J, Zeller R. *Hematoxylin and eosin staining of tissue and cell sections*. CSH Protoc. **2008**;2008:pdb prot4986.
[120] Pina R, Santos-Diaz AI, Orta-Salazar E, Aguilar-Vazquez AR, Mantellero CA, Acosta-Galeana I, et al. *Ten Approaches That Improve Immunostaining: A Review of the Latest Advances for the Optimization of Immunofluorescence*. Int J Mol Sci. **2022**;23(3).
[121] Shehata WA, Shoeib M, Shoeib MM, Shokhba H, Shams A. *Nucleotide binding and oligomerization domain 2 in psoriasis: a clinical and immunohistochemical study*. J Immunoassay Immunochem. **2022**;43(1):43-53.
[122] Ramos YAL, Pietrobon AJ, Teixeira FME, Aoki V, Sato MN, Orfali RL. *Inflammasome pathways in atopic dermatitis: insights into inflammatory mechanisms and therapeutic targets*. An Bras Dermatol. **2025**;100(4):501136.
[123] Liu Z, Zhang Y, Jin T, Yi C, Ocansey DKW, Mao F. *The role of NOD2 in intestinal immune response and microbiota modulation: A therapeutic target in inflammatory bowel disease*. Int Immunopharmacol. **2022**;113(Pt B):109466.
[124] Jeon DI, Park SR, Ahn MY, Ahn SG, Park JH, Yoon JH. *NOD1 and NOD2 stimulation triggers innate immune responses of human periodontal ligament cells*. Int J Mol Med. **2012**;29(4):699-703.
[125] Chen YJ, Chan YJ, Chen WJ, Li YM, Zhang CY. *Muramyl dipeptide promotes Abeta1-42 oligomer production via the NOD2/p-p38 MAPK/BACE1 signaling pathway in the SH-SY5Y cells*. J Integr Neurosci. **2020**;19(3):421-8.
[126] Moreira LO, Zamboni DS. *NOD1 and NOD2 Signaling in Infection and Inflammation*. Front Immunol. **2012**;3:328.
[127] Haglund CM, Welch MD. *Pathogens and polymers: microbe-host interactions illuminate the cytoskeleton*. J Cell Biol. **2011**;195(1):7-17.
[128] Liu Y, Chen Y, Batzorig U, Li J, Fernandez-Mendez C, Mahapatra S, et al. *The transcription regulators ZNF750 and LSD1/KDM1A dampen inflammation on the skin's surface by silencing pattern recognition receptors*. Immunity. **2024**;57(10):2296-309 e5.
[129] Danis J, Mellett M. *Nod-Like Receptors in Host Defence and Disease at the Epidermal Barrier*. Int J Mol Sci. **2021**;22(9).
[130] Kudo M, Kobayashi-Nakamura K, Kitajima N, Tsuji-Naito K. *Alternate expression of PEPT1 and PEPT2 in epidermal differentiation is required for NOD2 immune responses by bacteria-derived muramyl dipeptide*. Biochem Biophys Res Commun. **2020**;522(1):151-6.
[131] Trindade BC, Chen GY. *NOD1 and NOD2 in inflammatory and infectious diseases*. Immunol Rev. **2020**;297(1):139-61.
[132] Laroui H, Yan Y, Narui Y, Ingersoll SA, Ayyadurai S, Charania MA, et al. *L-Ala-gamma-D-Glu-meso-diaminopimelic acid (DAP) interacts directly with leucine-rich region domain of nucleotide-binding oligomerization domain 1, increasing phosphorylation activity of receptor-interacting serine/threonine-protein kinase 2 and its interaction with nucleotide-binding oligomerization domain 1*. J Biol Chem. **2011**;286(35):31003-13.
[133] Swaan PW, Bensman T, Bahadduri PM, Hall MW, Sarkar A, Bao S, et al. *Bacterial peptide recognition and immune activation facilitated by human peptide transporter PEPT2*. Am J Respir Cell Mol Biol. **2008**;39(5):536-42.
[134] Franchi L, Warner N, Viani K, Nunez G. *Function of Nod-like receptors in microbial recognition and host defense*. Immunol Rev. **2009**;227(1):106-28.

[135] Gimenez-Rivera VA, Patel H, Dupuy FP, Allakhverdi Z, Bouchard C, Madrenas J, et al. *NOD2 Agonism Counter-Regulates Human Type 2 T Cell Functions in Peripheral Blood Mononuclear Cell Cultures: Implications for Atopic Dermatitis*. Biomolecules. **2023**;13(2).
[136] Hoffjan S, Stemmler S. *On the role of the epidermal differentiation complex in ichthyosis vulgaris, atopic dermatitis and psoriasis*. Br J Dermatol. **2007**;157(3):441-9.
[137] Che-Wen Y, Lin FL, Chen KH, Cheng YP, Cheng YC, Guo JW. *Transcriptional dysregulation of skin barrier genes in atopic dermatitis and psoriasis: Mechanistic insights and emerging therapeutic strategies*. Biomed Pharmacother. **2025**;191:118508.
[138] Chantraine C, Gomes P, Mathelie-Guinlet M, Gomes DEB, Zheng Z, Clowry J, et al. *Ultrastrong Staphylococcus aureus adhesion to human skin: Calcium as a key regulator of noncovalent interactions*. Sci Adv. **2025**;11(36):eadu7457.
[139] Ogonowska P, Gilaberte Y, Baranska-Rybak W, Nakonieczna J. *Colonization With Staphylococcus aureus in Atopic Dermatitis Patients: Attempts to Reveal the Unknown*. Front Microbiol. **2020**;11:567090.
[140] Nakatsuji T, Chen TH, Two AM, Chun KA, Narala S, Geha RS, et al. *Staphylococcus aureus Exploits Epidermal Barrier Defects in Atopic Dermatitis to Trigger Cytokine Expression*. J Invest Dermatol. **2016**;136(11):2192-200.
[141] Miller LS, Cho JS. *Immunity against Staphylococcus aureus cutaneous infections*. Nat Rev Immunol. **2011**;11(8):505-18.
[142] Joshi AA, Vocanson M, Nicolas JF, Wolf P, Patra V. *Microbial derived antimicrobial peptides as potential therapeutics in atopic dermatitis*. Front Immunol. **2023**;14:1125635.
[143] Harder J, Schroder JM. *RNase 7, a novel innate immune defense antimicrobial protein of healthy human skin*. J Biol Chem. **2002**;277(48):46779-84.
[144] Rademacher F, Dreyer S, Kopfnagel V, Glaser R, Werfel T, Harder J. *The Antimicrobial and Immunomodulatory Function of RNase 7 in Skin*. Front Immunol. **2019**;10:2553.
[145] Balaji SK, Balasundarasekar B, Khuwaja WM, Dolan KM, Dong X. *Antimicrobial Peptide Signaling in Skin Diseases*. JID Innov. **2025**;5(3):100354.
[146] Kim J, Yang YL, Jang YS. *Human beta-defensin 2 is involved in CCR2-mediated Nod2 signal transduction, leading to activation of the innate immune response in macrophages*. Immunobiology. **2019**;224(4):502-10.
[147] Williams H, Campbell L, Crompton RA, Singh G, McHugh BJ, Davidson DJ, et al. *Microbial Host Interactions and Impaired Wound Healing in Mice and Humans: Defining a Role for BD14 and NOD2*. J Invest Dermatol. **2018**;138(10):2264-74.
[148] Yamamoto-Tanaka M, Miyai M, Sawane M, Yamanishi H, Sakaguchi M, Tsuboi R, et al. *Mechanism of S100A9 induction in the skin with atopic dermatitis - Involvement of NOD2 inflammasome activation*. Journal of Dermatological Science. **2016**;84(1):e99.
[149] Abdi W, Romasco A, Alkurdi D, Santacruz E, Okinedo I, Zhang Y, et al. *An overview of S100 proteins and their functions in skin homeostasis, interface dermatitis conditions and other skin pathologies*. Exp Dermatol. **2024**;33(8):e15158.
[150] Xia P, Ji X, Yan L, Lian S, Chen Z, Luo Y. *Roles of S100A8, S100A9 and S100A12 in infection, inflammation and immunity*. Immunology. **2024**;171(3):365-76.
[151] Menzies BE, Kenoyer A. *Staphylococcus aureus infection of epidermal keratinocytes promotes expression of innate antimicrobial peptides*. Infect Immun. **2005**;73(8):5241-4.
[152] Lai Y, Cogen AL, Radek KA, Park HJ, Macleod DT, Leichtle A, et al. *Activation of TLR2 by a small molecule produced by Staphylococcus epidermidis increases antimicrobial defense against bacterial skin infections*. J Invest Dermatol. **2010**;130(9):2211-21.
[153] Williams H, Crompton RA, Thomason HA, Campbell L, Singh G, McBain AJ, et al. *Cutaneous Nod2 Expression Regulates the Skin Microbiome and Wound Healing in a Murine Model*. J Invest Dermatol. **2017**;137(11):2427-36.

[154] Necidova L, Bursova S, Harustiakova D, Bogdanovicova K, Lacanin I. *Effect of heat treatment on activity of staphylococcal enterotoxins of type A, B, and C in milk*. J Dairy Sci. **2019**;102(5):3924-32.
[155] Liu H, Archer NK, Dillen CA, Wang Y, Ashbaugh AG, Ortines RV, et al. *Staphylococcus aureus Epicutaneous Exposure Drives Skin Inflammation via IL-36-Mediated T Cell Responses*. Cell Host Microbe. **2017**;22(5):653-66 e5.
[156] Luo CH, Lai AC, Tsai CC, Chen WY, Chang YS, Chung EJ, et al. *Staphylococcus aureus exacerbates dermal IL-33/ILC2 axis activation through evoking RIPK3/MLKL-mediated necroptosis of dry skin*. JCI Insight. **2024**;9(6).
[157] Schaffler H, Demircioglu DD, Kuhner D, Menz S, Bender A, Autenrieth IB, et al. *NOD2 stimulation by Staphylococcus aureus-derived peptidoglycan is boosted by Toll-like receptor 2 costimulation with lipoproteins in dendritic cells*. Infect Immun. **2014**;82(11):4681-8.
[158] Li Z, Shang D. *NOD1 and NOD2: Essential Monitoring Partners in the Innate Immune System*. Curr Issues Mol Biol. **2024**;46(9):9463-79.
[159] Gan Y, Zhang J, Qi F, Hu Z, Sweren E, Reddy SK, et al. *Commensal microbe regulation of skin cells in disease*. Cell Host Microbe. **2024**;32(8):1264-79.
[160] Moos S, Regen T, Wanke F, Tian Y, Arendholz LT, Hauptmann J, et al. *IL-17 Signaling in Keratinocytes Orchestrates the Defense against Staphylococcus aureus Skin Infection*. J Invest Dermatol. **2023**;143(7):1257-67 e10.
[161] Lee B, Olaniyi R, Kwiecinski JM, Wardenburg JB. *Staphylococcus aureus toxin suppresses antigen-specific T cell responses*. J Clin Invest. **2020**;130(3):1122-7.
[162] Macleod T, Ainscough JS, Hesse C, Konzok S, Braun A, Buhl AL, et al. *The Proinflammatory Cytokine IL-36gamma Is a Global Discriminator of Harmless Microbes and Invasive Pathogens within Epithelial Tissues*. Cell Rep. **2020**;33(11):108515.
[163] Patzold L, Stark A, Ritzmann F, Meier C, Tschernig T, Reichrath J, et al. *IL-17C and IL-17RE Promote Wound Closure in a Staphylococcus aureus-Based Murine Wound Infection Model*. Microorganisms. **2021**;9(9).
[164] Guillemin A, Kumar A, Wencker M, Ricci EP. *Shaping the Innate Immune Response Through Post-Transcriptional Regulation of Gene Expression Mediated by RNA-Binding Proteins*. Front Immunol. **2021**;12:796012.
[165] Lu HY, Turvey SE. *Human MALT1 deficiency and predisposition to infections*. Curr Opin Immunol. **2021**;72:1-12.
[166] Wang Q, Wang Y, Liu Q, Chu Y, Mi R, Jiang F, et al. *MALT1 regulates Th2 and Th17 differentiation via NF-kappaB and JNK pathways, as well as correlates with disease activity and treatment outcome in rheumatoid arthritis*. Front Immunol. **2022**;13:913830.
[167] Wu Z, Bi Y. *Potential role of MALT1 as a candidate biomarker of disease surveillance and treatment response prediction in inflammatory bowel disease patients*. J Clin Lab Anal. **2022**;36(2):e24130.
[168] Kayali S, Fantasia S, Gaiani F, Cavallaro LG, de'Angelis GL, Laghi L. *NOD2 and Crohn's Disease Clinical Practice: From Epidemiology to Diagnosis and Therapy, Rewired*. Inflamm Bowel Dis. **2025**;31(2):552-62.
[169] Ashton JJ, Seaby EG, Beattie RM, Ennis S. *NOD2 in Crohn's Disease-Unfinished Business*. J Crohns Colitis. **2023**;17(3):450-8.
[170] Moran MC, Beck LA, Richardson CT. *A Spectrum of Skin Disease: How Staphylococcus aureus Colonization, Barrier Dysfunction, and Cytokines Shape the Skin*. J Invest Dermatol. **2020**;140(5):941-4.
[171] McDaniel DK, Eden K, Ringel VM, Allen IC. *Emerging Roles for Noncanonical NF-kappaB Signaling in the Modulation of Inflammatory Bowel Disease Pathobiology*. Inflamm Bowel Dis. **2016**;22(9):2265-79.
[172] Foster TJ. *Surface Proteins of Staphylococcus epidermidis*. Front Microbiol. **2020**;11:1829.

[173] Yang Y, Scott AA, Kneuper H, Alcock F, Palmer T. *High-throughput functional analysis provides novel insight into type VII secretion in Staphylococcus aureus*. Open Biol. **2024**;14(8):240060.
[174] Becknell B, Eichler TE, Beceiro S, Li B, Easterling RS, Carpenter AR, et al. *Ribonucleases 6 and 7 have antimicrobial function in the human and murine urinary tract*. Kidney Int. **2015**;87(1):151-61.
[175] Gade P, Kalvakolanu DV. *Chromatin immunoprecipitation assay as a tool for analyzing transcription factor activity*. Methods Mol Biol. **2012**;809:85-104.
[176] Ishiguro-Oonuma T, Ochiai K, Hashizume K, Iwanaga T, Morimatsu M. *Nfkbiz regulates the proliferation and differentiation of keratinocytes*. Jpn J Vet Res. **2015**;63(3):107-14.
[177] Sidiq T, Yoshihama S, Downs I, Kobayashi KS. *Nod2: A Critical Regulator of Ileal Microbiota and Crohn's Disease*. Front Immunol. **2016**;7:367.
[178] Negroni A, Pierdomenico M, Cucchiara S, Stronati L. *NOD2 and inflammation: current insights*. J Inflamm Res. **2018**;11:49-60.
[179] Jiao D, Wong CK, Qiu HN, Dong J, Cai Z, Chu M, et al. *NOD2 and TLR2 ligands trigger the activation of basophils and eosinophils by interacting with dermal fibroblasts in atopic dermatitis-like skin inflammation*. Cell Mol Immunol. **2016**;13(4):535-50.
[180] Dai H, Xu C, Wang Y, Wu K, Zhang Y, Ge H, et al. *Secukinumab-induced Crohn's disease in a psoriasis patient: a case report highlighting paradoxical reactions to IL-17 inhibition*. Front Immunol. **2025**;16:1628461.
[181] Chen L, Ruan G, Cheng Y, Yi A, Chen D, Wei Y. *The role of Th17 cells in inflammatory bowel disease and the research progress*. Front Immunol. **2022**;13:1055914.
[182] Fischer B, Kolb A, Focaccia E, Kübelbeck T, Klein M, Löck D, et al. *NOD2-Induced IκBζ Mediates a Protective Host Response against Epicutaneous Staphylococcus aureus Infection*. J Invest Dermatol. **2025**.

Appendix

List of Figures

List of Tables

Supplementary Appendix

Supplementary Figures

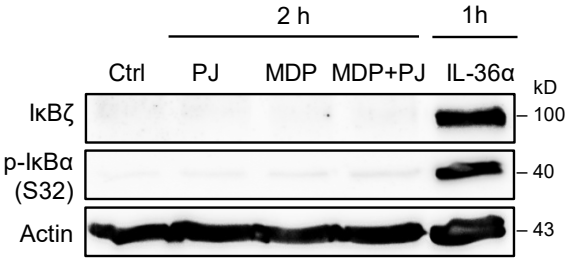

Supplementary Figure I: HaCaT cells do not respond to MDP stimulation.
Immunoblot analysis of IκBζ staining in immortalized HaCaT cells after stimulation for either 2 h with 20 µg/ml MDP (NOD2 agonist) and 2.5 µL per 6-well of the transfection reagent ProteoJuice or for 1 h with 100 µg/mL recombinant human IL-36α. Before treatment, HaCaT cells were starved overnight in DMEM basic medium without FCS, the same medium was used for stimulation. Phosphorylated levels of IκBα (p-IκBα (S32)) indicate activation of the cells, ß-Actin served as a loading control. Stimulation with IL-36 served as a positive control.

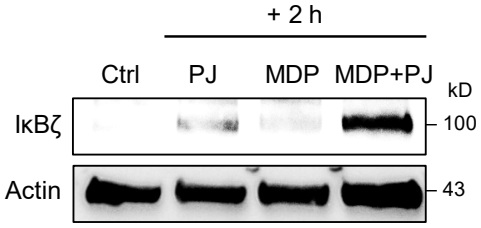

Supplementary Figure II: IκBζ protein expression is not induced by a single application of ProteoJuice transfection reagent compared to its combination with MDP.
Immunoblot analysis of IκBζ staining in undifferentiated hKC after stimulation for 2 h with either 20 µg/ml MDP (NOD2 agonist), transfection reagent ProteoJuice or a combination of both. ß-Actin served as a loading control.

Upregulated pathways in MDP-stimulated hKC (*NFKBIZ* dependent)	**p-value**	**Library**
Abnormal vascular smooth muscle morphology	0.00088	MGI_2021
Cell junction assembly	0.00508	GO_2021
Decreased angiogenesis	0.00229	MGI_2021
Extracellular matrix organization	0.03690	Reactome_2022
Fibronectin matrix formation	0.00628	Reactome_2022
Platelet aggregation (plug formation)	0.03720	Reactome_2022
Peptide cross-linking	0.00048	GO_2021
Post-translational protein phosphorylation	0.00547	Reactome_2022
Regulation of intracellular protein transport	0.00051	GO_2021
Decreased susceptibility to injury	0.00243	MGI_2021
Regulation of T-cell receptor signaling pathway	0.00061	GO_2021

Supplementary Figure III: GSEA results show pathways being significantly upregulated by MDP stimulation in human keratinocytes and even strongly induced in an IκBζ-dependent manner.
Differentiated control (sh ctrl) and knockdown (sh NFKBIZ) human keratinocytes were transfected and treated with 20 µg/mL MDP and ProteoJuice for 24 h. The table shows pathways of identified upregulated IκBζ target genes which were significantly induced after 24 h MDP stimulation (applied cut-off: p-values ≤ 0.05, fold change absolute >2, difference absolute >3). Gene set enrichment analysis (GSEA) was performed using EnrichR. Shown are significantly enriched pathways, sorted by pathway and p-value.

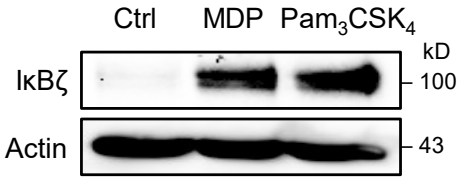

Supplementary Figure IV: IκBζ expression can be induced with both NOD2 and TLR2 agonists in keratinocytes.
Immunoblot analysis showing IκBζ protein levels in differentiated hKC stimulated for 1 h either with 20 µg/mL MDP and ProteoJuice (NOD2 agonist) or 10 µg/mL Pam_3CSK_4 (TLR1/2 ligand). ß-Actin served as a loading control.

Upregulated pathways in *S. aureus*-infected hKC (*NFKBIZ* dependent)	**p-value**	**Library**
Extrinsic apoptotic signaling pathway via death domain receptors	0.00748	GO_2021
Negative regulation of axon extension	0.00499	GO_2021
Neural crest cell migration	0.00922	GO_2021
Plasma membrane tubulation	0.00325	GO_2021
TRAIL-activated apoptotic signaling pathway	0.00175	GO_2021
Viral protein interaction with cytokine and receptors	0.02475	KEGG_2021

Supplementary Figure V: GSEA results showing pathways being significantly upregulated by S. aureus infection in human keratinocytes and even stronger induced in an IκBζ-dependent manner.
Differentiated control (sh ctrl) and knockdown (sh NFKBIZ) human keratinocytes were infected with S. aureus (1 h, MOI30), washed with PBS, and further incubated for 23 h. Table shows pathways of identified upregulated IκBζ target genes which were significantly induced after 24 h infection (applied cut-off: p-values ≤ 0.05, fold change absolute >2, difference absolute >3). Gene set enrichment analysis (GSEA) was performed using EnrichR. Shown are significantly enriched pathways, sorted by pathway and p-value.

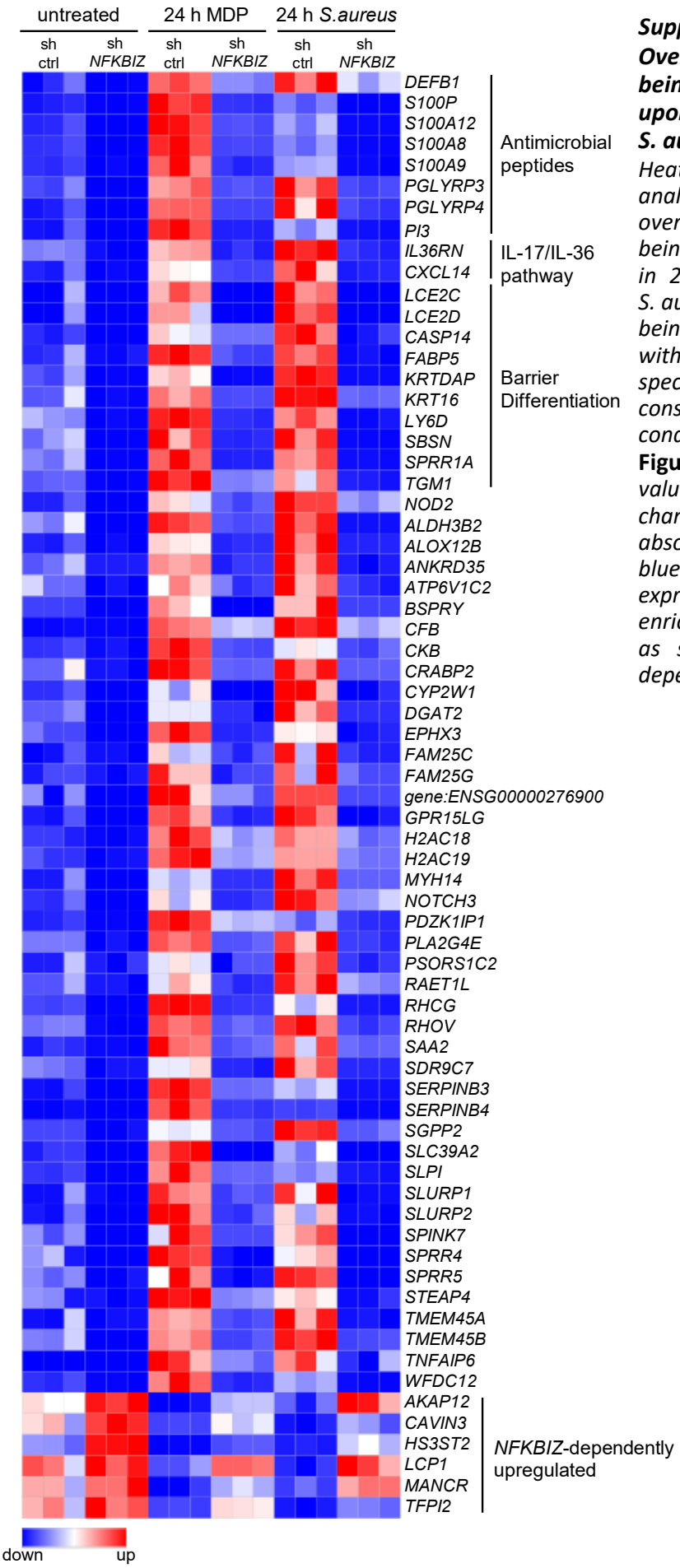

Supplementary Figure VI: Overlapping IκBζ target genes being significantly regulated upon 24 h MDP stimulation or S. aureus infection in hKC.

Heatmap shows transcriptome analysis with a total of 69 overlapping IκBζ target genes being significantly regulated in 24 h MDP stimulation and S. aureus infection in diff. hKC being lenti-virally transfected with control (sh ctrl) or NFKBIZ-specific shRNA (sh NFKBIZ) constructs. Stimulations were conducted as described in **Figure 4.13**. *Applied cut-off values: p-values ≤ 0.05, fold change absolute >2, difference absolute >3). Red indicates up-, blue indicates downregulated expression values. Genes of enriched pathways are marked as such, as well as NFKBIZ-dependent upregulated genes.*

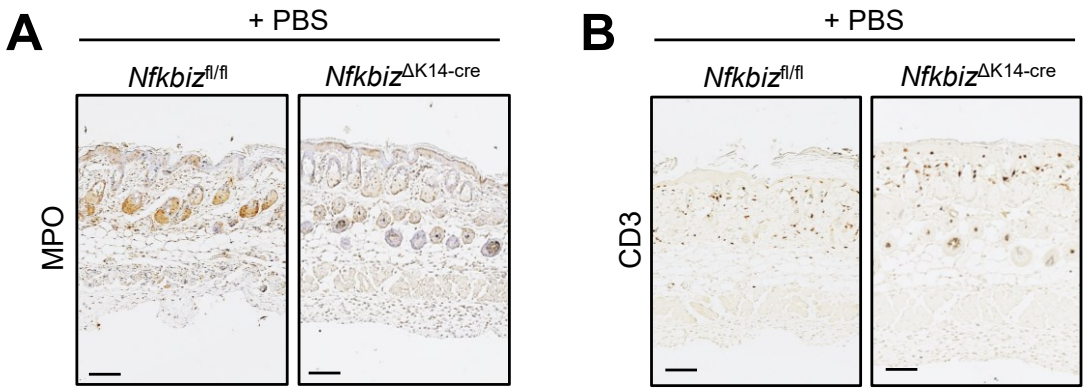

Supplementary Figure VII: PBS-treated skin sections of Nfkbiz$^{fl/fl}$ control and Nfkbiz$^{\Delta K14\text{-}cre}$ knockout animals do not differ in numbers of cells expressing MPO or CD3.
A + B. *Immunohistology of FFPE back skin material of PBS-treated Nfkbiz$^{fl/fl}$ control and IκBζ-depleted Nfkbiz$^{\Delta K14\text{-}cre}$ animals, taken at the endpoint on day 7. Scale bars: 100 µm. Histology stainings were performed by Dagmar Löck.* ***A.*** *Skin sections were stained for myeloperoxidase MPO, a marker for neutrophils and, to lesser extent, monocytes.* ***B.*** *Skin sections were stained for the universal T-cell surface marker CD3.*

Skin FACS gating strategy: immune cell populations

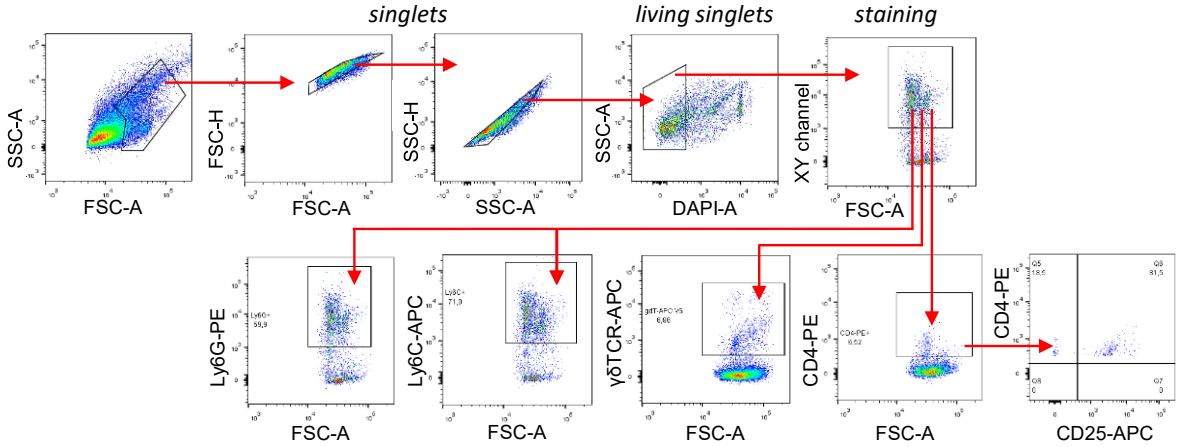

Supplementary Figure VIII: FACS gating strategy of innate and adaptive immune cell populations present in digested skin samples.
FACS plots of innate and adaptive immune cell populations in digested skin tissue obtained from PBS-treated and S. aureus-infected Nfkbiz$^{fl/fl}$ control or Nfkbiz$^{\Delta K14\text{-}cre}$ knockout animals, which were killed after 2 days or 7 days. Skin-infiltrating immune cells were gated on living single cells using DAPI viability dye, showing the relative percentage of the following populations: neutrophils (Ly6G-PE), monocytes (Ly6C-APC), γδ T-cells (γδTCR-APC) and CD4-positive T-cells. Effector T-cells (CD4+ CD25-) and regulatory T-cells (CD4+ CD25+) were determined after pre-gating on viable CD4+ T-cells. FACS plots were evaluated using FlowJo (Tree Star Inc.) software.

Skin FACS gating strategy: ROS-producing cells

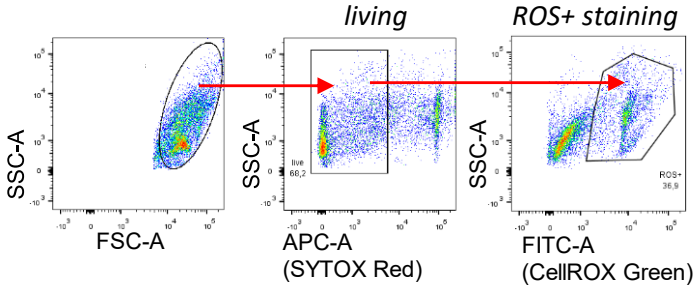

Supplementary Figure IX: FACS gating strategy of ROS-producing cells present in digested skin samples.
FACS plots of ROS-producing cells in digested skin tissue obtained from PBS-treated and S. aureus-infected Nfkbiz$^{fl/fl}$ control or Nfkbiz$^{\Delta K14\text{-}cre}$ knockout animals at the endpoint on day 7. Skin-infiltrating immune cells were gated on living single cells using sytox red viability dye. ROS-producing cells were further gated for CellROX positive signals in the FITC channel, showing their relative percentage. FACS plots were evaluated using FlowJo (Tree Star Inc.) software.

Supplementary Tables

Supplementary Table I: Expression values of selected MDP-induced genes being NFKBIZ-dependently downregulated in differentiated hKC after 24 h treatment

Gene	Expression values											
	sh Ctrl untreated			*sh NFKBIZ* untreated			*sh Ctrl* 24 h MDP			*sh NFKBIZ* 24 h MDP		
	1	2	3	1	2	3	1	2	3	1	2	3
DEFB1	6.4	16.7	34.1	5.9	5.7	6.0	106.3	116.2	104.5	41.0	40.5	34.0
DEFB4A	2.2	3.7	7.0	0.0	1.1	0.0	140.7	189.3	128.6	3.1	4.4	3.3
LCN2	202.4	177.3	124.6	29.4	26.6	31.3	421.8	480.6	390.4	30.9	28.9	34.5
PGLYRP3	7.2	6.3	12.5	2.0	1.6	1.6	29.3	31.6	35.6	7.3	8.0	7.8
PGLYRP4	2.6	3.4	9.2	0.2	0.4	0.6	42.2	43.3	43.7	7.3	7.7	7.4
PI3	167.2	132.3	800.2	20.0	18.0	19.9	3749	4071	3468	266.9	283.5	275.7
RNASE7	68.4	62.1	44.0	20.9	20.1	19.0	146.2	179.2	170.5	52.1	55.9	51.5
S100A7A	1.1	0.8	0.9	0.0	0.0	0.0	38.5	36.1	37.0	1.5	1.3	1.1
S100A7	189.6	94.3	76.9	4.9	3.3	5.7	1023	1635	926.6	39.3	34.3	56.2
S100A8	633.6	710.1	1307	110.3	95.0	95.0	7769	7590	6779	1249	1336	1154
S100A9	2722	2847	4113	302.7	282.5	327.7	24116	26112	22346	3715	3936	3793
S100A12	6.1	5.9	8.3	0.0	1.1	0.0	52.8	64.6	47.5	7.7	4.6	6.0
S100P	17.3	27.4	37.2	5.1	3.0	5.2	406.6	355.0	375.0	45.0	43.2	38.5
IL36G	39.3	71.3	16.7	16.1	5.3	4.2	86.3	104.2	88.0	11.8	12.7	11.4
IL36RN	11.3	12.9	12.0	3.2	2.3	2.7	25.2	27.6	29.0	4.5	6.2	4.7
CXCL6	8.1	7.4	0.7	0.8	0.4	0.8	15.2	16.8	21.8	3.0	3.0	2.9
CXCL8	8.1	12.9	1.4	3.6	0.7	2.4	54.2	66.1	63.7	18.4	21.5	22.0
CXCL14	8.0	5.6	28.9	0.7	2.3	1.6	68.3	61.6	59.5	17.2	15.3	17.0
LCE2C	0.6	0.6	5.3	0.0	0.0	0.0	10.0	12.1	10.7	0.4	0.4	0.7
LCE2D	0.6	0.6	3.5	0.0	0.0	0.0	7.1	7.9	4.1	0.0	0.4	0.0
NOD2	1.4	1.8	3.3	0.8	0.6	0.3	10.3	9.5	7.9	3.2	2.8	3.5

Supplementary Table II: Expression values of selected S. aureus-induced genes being NFKBIZ-dependently downregulated in differentiated hKC after 24 h infection

Gene	Expression values											
	***sh Ctrl* untreated**			***sh NFKBIZ* untreated**			***sh Ctrl* 24 h *S. aureus***			***sh NFKBIZ* 24 h *S. aureus***		
	1	**2**	**3**	**1**	**2**	**3**	**1**	**2**	**3**	**1**	**2**	**3**
DEFB1	6.4	16.7	34.1	5.9	5.7	6.0	125.3	100.8	132.5	62.9	42.2	59.3
DEFB4A	2.2	3.7	7.0	0.0	1.1	0.0	10.4	6.6	19.1	0.5	0.0	0.0
PI3	167.2	132.3	800.2	20.0	18.0	19.9	1414	972.8	1650	152.2	134.4	100.4
PGLYRP3	7.2	6.3	12.5	2.0	1.6	1.6	42.6	30.4	38.1	7.1	6.2	7.5
PGLYRP4	2.6	3.4	9.2	0.2	0.4	0.6	52.5	29.4	53.7	9.0	6.7	5.7
S100P	17.3	27.4	37.2	5.1	3.0	5.2	105.9	67.8	105.5	3.8	3.3	6.0
S100A8	633.6	710.1	1307	110.3	95.0	95.0	2593	1757	3048	232.8	214.7	202.6
S100A9	2722	2847	4113	302.7	282.5	327.7	7049	5269	8312	701.4	608.0	539.8
S100A12	6.1	5.9	8.3	0.0	1.1	0.0	19.5	21.7	23.7	1.8	1.8	0.4
IL17C	0.0	0.3	0.0	0.0	0.0	0.1	5.3	6.8	4.5	2.2	1.7	1.6
IL36G	39.3	71.3	16.7	16.1	5.3	4.2	96.3	70.4	113.9	13.4	10.3	8.7
IL36RN	11.3	12.9	12.0	3.2	2.3	2.7	40.0	36.2	39.8	6.7	5.9	4.6
CXCL10	0.6	1.4	0.0	0.3	0.6	0.1	535.7	457.2	557.4	100.4	69.0	92.3
CXCL11	0.8	1.1	0.2	0.4	0.2	0.3	121.2	66.6	127.5	59.4	46.5	43.1
CXCL14	8.0	5.6	28.9	0.7	2.3	1.6	95.6	118.3	68.5	6.9	8.3	9.7
CCL5	1.7	1.0	0.4	0.0	0.0	0.0	42.7	21.3	47.5	14.1	11.6	10.6
CCL20	0.6	0.8	2.4	1.0	0.2	1.7	25.1	16.9	25.2	10.3	10.9	10.6
LCE2C	0.6	0.6	5.3	0.0	0.0	0.0	14.8	10.4	11.1	0.0	0.0	0.3
LCE2B	0.3	0.6	6.6	0.0	0.0	0.0	8.4	9.6	9.5	0.3	0.0	0.0
LCE2A	0.0	0.0	2.1	0.0	0.0	0.0	6.4	5.3	7.7	0.3	0.0	0.0
LCE2D	0.6	0.6	3.5	0.0	0.0	0.0	10.2	8.1	9.7	0.9	0.0	0.0
LCE6A	0.3	0.0	2.0	0.0	0.3	0.3	9.9	10.4	5.3	0.3	0.5	0.6
CLDN17	1.3	4.5	0.4	0.9	0.6	0.1	3.0	5.5	2.3	0.1	0.0	0.0
CRNN	2.0	2.1	1.0	0.1	0.1	0.0	5.0	3.4	5.2	0.2	0.5	0.2
FLG	14.8	13.7	9.6	6.2	4.6	5.9	46.0	48.2	32.6	2.7	3.2	3.1
FLG2	0.6	0.7	0.9	0.0	0.1	0.1	9.9	10.1	7.8	0.2	0.2	0.3
LOR	4.2	6.0	27.8	0.6	0.0	0.1	64.1	42.4	58.9	0.4	1.7	1.5
IVL	107.1	137.0	227.3	17.7	14.3	18.2	275.6	197.2	305.4	36.3	41.5	22.2

Supplementary Table III: Expression values of 69 overlapping IκBζ target genes significantly regulated in hKC after 24 h treatment with MDP/S. aureus

Gene	Expression values																	
	***sh Ctrl* untreated**			***sh NFKBIZ* untreated**			***sh Ctrl* 24 h MDP**			***sh NFKBIZ* 24 h MDP**			***sh Ctrl* 24 h *S. aureus***			***sh NFKBIZ* 24 h *S. aureus***		
	1	**2**	**3**	**1**	**2**	**3**	**1**	**2**	**3**	**1**	**2**	**3**	**1**	**2**	**3**	**1**	**2**	**3**
DEFB1	6.4	16.7	34.1	5.9	5.7	6.0	106.3	116.2	104.5	41.0	40.5	34.0	125.3	100.8	132.5	62.9	42.2	59.3
S100P	17.3	27.4	37.2	5.1	3.0	5.2	406.6	355.0	375.0	45.0	43.2	38.5	105.9	67.8	105.5	3.8	3.3	6.0
S100A8	633.6	710.1	1306.6	110.3	95.0	95.0	7769.2	7589.6	6778.8	1249.0	1336.3	1153.9	2592.5	1757.1	3047.5	232.8	214.7	202.6
S100A9	2722.1	2847.3	4113.2	302.7	282.5	327.7	24116	26112	22346	3715.4	3936.0	3792.9	7049.1	5269.3	8311.7	701.4	608.0	539.8
S100A12	6.1	5.9	8.3	0.0	1.1	0.0	52.8	64.6	47.5	7.7	4.6	6.0	19.5	21.7	23.7	1.8	1.8	0.4
PGLYRP3	7.2	6.3	12.5	2.0	1.6	1.6	29.3	31.6	35.6	7.3	8.0	7.8	42.6	30.4	38.1	7.1	6.2	7.5
PGLYRP4	2.6	3.4	9.2	0.2	0.4	0.6	42.2	43.3	43.7	7.3	7.7	7.4	52.5	29.4	53.7	9.0	6.7	5.7
PI3	167.2	132.3	800.2	20.0	18.0	19.9	3749.2	4070.6	3468.1	266.9	283.5	275.7	1414.2	972.8	1649.8	152.2	134.4	100.4
IL36RN	11.3	12.9	12.0	3.2	2.3	2.7	25.2	27.6	29.0	4.5	6.2	4.7	40.0	36.2	39.8	6.7	5.9	4.6
CXCL14	8.0	5.6	28.9	0.7	2.3	1.6	68.3	61.6	59.5	17.2	15.3	17.0	95.6	118.3	68.5	6.9	8.3	9.7
LCE2C	0.6	0.6	5.3	0.0	0.0	0.0	10.0	12.1	10.7	0.4	0.4	0.7	14.8	10.4	11.1	0.0	0.0	0.3
LCE2D	0.6	0.6	3.5	0.0	0.0	0.0	7.1	7.9	4.1	0.0	0.4	0.0	10.2	8.1	9.7	0.9	0.0	0.0
CASP14	2.1	1.1	3.1	0.2	0.8	0.5	14.5	11.8	10.6	5.2	5.2	5.1	21.8	23.4	17.3	0.9	1.9	3.0
FABP5	141.2	149.0	235.2	123.4	120.8	135.0	426.5	452.9	415.5	177.6	158.9	156.5	408.4	370.5	412.4	122.0	128.9	116.8
KRTDAP	99.5	72.6	182.1	4.2	8.8	7.6	334.2	366.8	291.3	10.0	14.1	15.2	520.7	566.2	527.0	15.1	17.2	14.7
KRT16	1527.0	1573.6	3131.1	599.8	704.4	641.9	4914.9	4260.6	4943.7	1393.4	1439.0	1409.8	6118.2	5990.4	6170.5	1761.5	1654.8	1752.1
LY6D	336.1	279.2	251.3	38.6	52.3	46.2	804.7	856.3	792.9	115.2	112.1	98.4	628.0	763.0	619.0	49.4	49.1	75.4
SBSN	201.1	290.3	372.0	45.7	47.4	48.4	842.2	551.6	744.7	105.3	100.9	114.2	839.1	611.6	792.0	57.6	54.5	51.1
SPRR1A	1570.6	1306.8	2114.4	226.7	253.1	248.5	4358.8	5328.1	4352.4	527.6	563.7	577.0	4044.9	3752.5	4657.0	348.4	355.4	315.4
TGM1	109.5	123.8	124.4	26.6	22.0	24.5	544.3	491.4	548.2	152.8	149.2	170.7	390.3	248.6	428.1	54.8	50.5	39.4
NOD2	1.4	1.8	3.3	0.8	0.6	0.3	10.3	9.5	7.9	3.2	2.8	3.5	16.6	14.5	14.6	5.7	5.0	6.5
ALDH3B2	24.6	20.0	36.0	3.5	3.5	3.5	71.0	65.2	60.4	15.6	13.6	14.7	73.9	59.4	70.3	5.5	5.5	5.2
ALOX12B	3.4	3.0	8.5	0.5	1.1	0.6	26.8	24.9	23.4	3.7	4.7	4.6	44.2	32.2	44.3	3.4	3.4	3.5

Gene	Expression values																	
	***sh Ctrl* untreated**			***sh NFKBIZ* untreated**			***sh Ctrl* 24 h MDP**			***sh NFKBIZ* 24 h MDP**			***sh Ctrl* 24 h *S. aureus***			***sh NFKBIZ* 24 h *S. aureus***		
	1	**2**	**3**	**1**	**2**	**3**	**1**	**2**	**3**	**1**	**2**	**3**	**1**	**2**	**3**	**1**	**2**	**3**
ANKRD35	3.5	4.5	7.5	1.1	1.0	1.1	13.6	12.8	13.5	1.8	2.8	2.5	18.6	12.3	17.3	1.3	0.6	1.5
ATP6V1C2	11.7	6.2	6.1	1.3	2.9	1.7	13.4	19.5	15.6	7.7	3.3	4.9	25.6	16.3	20.7	4.1	3.5	2.2
BSPRY	1.0	1.3	1.7	0.3	0.2	0.0	6.2	5.8	4.4	0.7	0.8	0.9	5.6	5.7	8.3	1.4	1.3	1.4
CFB	1.3	1.6	2.0	1.4	1.1	0.9	74.4	68.1	64.6	31.7	36.4	34.0	88.4	81.9	87.6	33.5	26.6	36.0
CKB	23.9	24.5	29.2	14.6	17.0	12.7	117.4	131.9	115.5	32.3	29.5	28.3	65.9	77.8	68.2	29.6	26.3	38.4
CRABP2	127.8	128.4	256.4	66.0	67.6	52.2	438.8	434.6	379.3	127.6	122.1	127.8	431.1	333.2	426.5	122.0	123.7	123.9
CYP2W1	1.5	1.8	2.9	0.1	0.4	0.6	5.4	3.9	6.0	0.7	0.8	0.7	11.3	11.7	7.2	0.7	0.6	1.3
DGAT2	2.2	2.1	3.0	0.3	0.4	0.4	6.0	5.5	5.9	1.1	1.2	0.9	11.8	7.4	9.0	1.9	1.7	2.0
EPHX3	11.5	7.3	7.7	1.5	1.6	1.2	36.8	44.5	38.7	4.1	4.8	5.7	24.4	23.5	25.7	1.7	3.4	4.0
FAM25C	0.0	1.5	6.2	1.6	1.0	1.0	20.2	12.9	14.4	5.3	2.1	7.0	33.2	12.1	34.1	4.6	2.9	2.7
FAM25G	1.2	3.8	3.9	1.2	0.4	1.1	20.7	14.0	13.2	1.7	3.1	3.8	17.4	7.7	21.1	5.3	3.3	3.6
gene:ENSG 00000276900	2.4	0.8	2.0	0.4	0.9	0.9	7.0	7.2	4.7	2.0	2.7	1.1	6.8	6.9	6.4	1.7	1.6	1.5
GPR15LG	2.2	1.7	6.9	0.2	0.2	0.0	30.5	32.9	24.3	4.5	2.1	3.8	36.3	33.8	27.7	0.7	0.6	2.0
H2AC18	23.9	23.5	18.8	14.9	13.6	15.7	77.7	99.5	87.4	47.7	37.7	43.2	81.2	71.3	71.4	41.3	29.7	33.0
H2AC19	27.3	21.1	21.2	13.8	15.3	16.9	78.8	91.9	95.0	40.2	38.6	42.3	70.7	69.7	69.6	35.5	31.9	31.5
MYH14	1.6	1.8	6.7	0.5	0.6	0.6	9.7	7.5	9.9	2.3	2.3	2.7	21.1	16.9	20.9	4.3	4.1	4.4
NOTCH3	7.3	6.3	13.8	2.1	2.4	2.5	31.8	19.9	29.8	6.9	6.6	8.3	53.6	51.4	41.9	16.4	17.6	23.2
PDZK1IP1	23.5	26.7	40.3	7.9	8.7	5.7	275.9	300.2	267.8	125.7	109.6	116.1	96.2	54.6	107.9	39.1	30.0	29.1
PLA2G4E	6.8	6.0	6.7	0.8	1.1	0.8	22.0	19.4	21.5	4.3	4.6	5.2	22.7	15.2	25.0	3.2	3.3	2.2
PSORS1C2	1.9	1.2	7.1	1.1	0.8	2.8	8.2	10.4	8.8	0.9	3.1	3.6	18.4	13.7	16.7	2.7	2.0	2.8
RAET1L	10.7	10.5	18.0	5.6	5.5	3.2	22.8	32.7	26.2	9.8	6.9	7.1	44.1	34.1	46.5	19.0	15.2	13.6
RHCG	139.5	126.7	147.5	14.3	16.3	14.5	883.3	918.7	888.9	103.0	112.9	115.9	488.6	314.3	507.0	59.7	59.7	47.8
RHOV	13.1	15.6	15.3	2.7	1.4	1.6	49.5	44.3	47.2	10.1	13.1	11.3	53.0	57.3	43.6	9.9	7.0	10.0
SAA2	4.0	8.5	6.5	2.6	2.2	1.9	62.9	49.8	47.4	10.0	12.5	14.3	49.4	26.6	55.0	14.2	12.2	13.2

Gene	Expression values																	
	***sh Ctrl* untreated**			***sh NFKBIZ* untreated**			***sh Ctrl* 24 h MDP**			***sh NFKBIZ* 24 h MDP**			***sh Ctrl* 24 h *S. aureus***			***sh NFKBIZ* 24 h *S. aureus***		
	1	**2**	**3**	**1**	**2**	**3**	**1**	**2**	**3**	**1**	**2**	**3**	**1**	**2**	**3**	**1**	**2**	**3**
SDR9C7	7.3	6.8	5.4	0.8	1.5	1.6	12.2	12.8	15.2	2.4	2.1	1.5	26.0	17.9	22.3	2.2	2.4	2.8
SERPINB3	30.5	19.2	104.0	7.7	5.4	7.2	669.4	740.7	657.7	159.0	155.1	167.9	292.0	236.8	322.0	29.1	30.1	28.7
SERPINB4	2.6	1.9	8.1	0.5	0.0	0.5	247.0	296.3	244.2	32.3	34.5	29.4	39.7	35.1	44.7	3.6	4.3	3.4
SGPP2	5.1	5.9	6.0	1.8	1.6	2.2	15.0	14.6	15.5	6.5	6.3	5.9	30.3	27.6	28.1	6.9	6.0	8.3
SLC39A2	1.9	2.5	2.2	0.1	0.3	0.0	14.6	17.7	18.3	0.5	0.9	0.9	6.9	4.9	9.8	0.2	0.2	0.7
SLPI	450.2	403.8	533.5	128.5	126.9	118.7	2395.0	3268.7	2535.7	720.4	756.6	730.2	1035.1	860.7	1153.7	277.8	251.8	204.5
SLURP1	1.8	1.4	14.9	1.0	0.3	0.0	41.4	33.3	31.1	5.0	8.8	7.6	40.1	21.5	44.3	0.7	1.6	1.4
SLURP2	5.4	2.8	24.1	0.0	0.6	0.3	102.4	102.6	75.2	11.8	9.7	21.9	59.8	32.6	64.1	2.1	3.2	0.0
SPINK7	2.6	1.3	3.0	0.0	0.2	0.8	3.6	7.3	6.9	1.7	1.1	1.3	4.8	5.6	6.3	0.9	0.7	0.5
SPRR4	6.9	8.1	1.5	0.2	0.9	0.0	21.9	19.1	18.7	1.1	1.0	0.3	10.9	12.4	14.2	0.0	0.5	0.2
SPRR5	6.1	4.5	6.7	0.2	0.7	1.6	12.0	22.3	16.0	1.4	0.3	1.5	21.5	20.4	18.9	0.7	0.5	0.7
STEAP4	18.3	17.9	6.8	6.2	4.2	5.1	52.9	50.4	52.8	16.6	17.7	19.4	30.1	35.0	29.2	5.8	5.6	9.8
TMEM45A	10.9	9.6	34.2	8.1	10.5	10.2	53.0	49.3	52.1	18.1	16.7	18.9	71.7	49.6	69.0	10.4	11.1	8.9
TMEM45B	17.4	16.1	26.2	3.9	3.3	3.9	44.6	41.9	46.1	10.1	10.9	13.5	57.0	52.3	59.6	10.6	11.8	13.0
TNFAIP6	0.0	0.3	0.0	0.1	0.0	0.2	11.7	10.1	7.0	3.2	3.7	2.6	8.2	10.8	5.8	1.5	0.8	4.0
WFDC12	9.3	7.9	14.4	1.4	1.1	0.4	71.8	96.4	77.4	9.6	6.3	8.7	34.2	27.4	33.8	2.8	1.3	1.4
AKAP12	19.4	17.4	17.3	29.4	28.0	30.4	4.9	4.3	5.9	13.2	14.1	15.0	9.6	5.3	10.1	30.9	29.8	21.9
CAVIN3	330.3	368.2	204.6	471.0	528.4	491.7	128.3	133.8	128.1	308.3	242.4	281.5	86.1	70.8	103.7	231.3	205.5	140.3
HS3ST2	42.4	41.1	30.8	121.1	122.7	125.4	7.5	8.9	8.9	25.0	28.7	28.5	13.9	15.2	12.6	55.9	66.8	48.9
LCP1	27.8	25.4	16.4	31.3	26.7	30.6	9.3	10.0	13.8	26.1	26.1	25.6	7.3	5.6	8.5	31.1	29.0	22.9
MANCR	6.6	6.6	3.3	7.6	7.9	9.2	0.8	0.6	1.5	3.8	5.0	3.1	1.8	2.6	1.8	6.1	7.2	7.0
TFPI2	112.4	129.8	68.2	166.6	128.1	142.4	31.7	33.3	29.6	101.0	98.5	94.1	18.1	11.7	19.1	51.8	49.2	41.9

Supplementary Table IV: List of genes with significant induction upon treatment (1.5h and 24 h IL-36α, 24 h S. aureus or 24 h MDP) in primary control hKC, which were significantly downregulated in NFKBIZ-depleted hKC.

Raw data was obtained from RNA-seq data sets (cut-off: absolute fold change > 2, p-value of ≤ 0.05). For reference see *chapter 3.9 Data Availability*.

Individual treatments			**Evaluation**						
IL-36α 1.5 h, 24 h	***S. aureus* 24 h**	**MDP 24 h**	**Exclusively IL-36α 1.5 h, 24 h**	**Exclusively *S. aureus* 24 h**	**Exclusively MDP 24 h**	***S. aureus* + MDP**	***S. aureus* + IL-36α**	**IL-36α + MDP**	***S. aureus* + IL-36α + MDP**
345 genes	**178 genes**	**122 genes**	**306 genes**	**101 genes**	**46 genes**	**51 genes**	**14 genes**	**13 genes**	**12 genes**
AC004231.2	ACER1	ADAP2	AC004231.2	ACER1	ADAP2	ALDH3B2	CCL20	CSF3	CFB
AC005022.1	ALDH3B2	AKR1B10	AC005022.1	ANKRD22	AKR1B10	ALOX12B	EVPLL	CXCL6	IL36RN
AC005029.1	ALOX12B	ALDH3B2	AC005029.1	AQP3	ANXA9	ANKRD35	GBP2	CXCL8	LCE2D
AC006262.10	ANKRD22	ALOX12B	AC006262.10	ASPRV1	AQP9	ATP6V1C2	GBP4	DEFB4A	PDZK1IP1
AC008074.3	ANKRD35	ANKRD35	AC008074.3	ATP10B	BPGM	BSPRY	IL17C	IL23A	PGLYRP4
AC013444.1	AQP3	ANXA9	AC013444.1	AZGP1	C11orf96	CASP14	LCE1A	IL36G	PI3
AC022816.2	ASPRV1	AQP9	AC022816.2	BBOX1	C15orf48	CKB	LCE1D	LCN2	RAET1L
AC023115.2	ATP10B	ATP6V1C2	AC023115.2	BNIPL	C6orf15	CRABP2	LCE1F	PLA2G3	S100A9
AC062017.1	ATP6V1C2	BPGM	AC062017.1	CARD18	CHI3L2	CXCL14	LCE2A	RARRES1	SERPINB4
AC104777.2	AZGP1	BSPRY	AC104777.2	CCL5	CLIC3	CYP2W1	LCE6A	S100A7	SGPP2
AC107399.2	BBOX1	C11orf96	AC107399.2	CDHR1	CNFN	DEFB1	SLC28A3	SPRR2B	STEAP4
ACRC	BNIPL	C15orf48	ACRC	CWH43	CPM	DGAT2	SOD2	SPRR2G	TNFAIP6
ADAMTS4	BSPRY	C6orf15	ADAMTS4	CXCL10	CSTA	EPHX3	WNT4	ZC3H12A	
ADORA2BP	CARD18	CASP14	ADORA2BP	CXCL11	CSTB	FABP5	ZBTB16		
AF064858.8	CASP14	CFB	AF064858.8	CYP4B1	DEFB103A	FAM25C			
AL021068.1	CCL20	CHI3L2	AL021068.1	CYP4F22	DEFB4B	FAM25G			
ALOX15B	CCL5	CKB	ALOX15B	DLX2	GDPD3	gene:ENSG 00000276900			
ANGPT4	CDHR1	CLIC3	ANGPT4	DSC1	gene:ENSG 00000231412	GPR15LG			
ANKRD33B	CFB	CNFN	ANKRD33B	DSG1	GPC1-AS1	H2AC18			
AOAH	CKB	CPM	AOAH	DUSP1	H2BC8	H2AC19			
AP000322.53	CRABP2	CRABP2	AP000322.53	EPHB6	HES4	KRT16			
AP000640.2	CWH43	CSF3	AP000640.2	FAM43A	KLK14	KRTDAP			
AP001607.1	CXCL10	CSTA	AP001607.1	FLG	KRT42P	LCE2C			
AP003733.1	CXCL11	CSTB	AP003733.1	FLG2	KRT78	LY6D			
APOBEC3A	CXCL14	CXCL14	APOBEC3A	GDA	LEMD1	MYH14			

Individual treatments			**Evaluation**						
IL-36α 1.5 h, 24 h	***S. aureus* 24 h**	**MDP 24 h**	**Exclusively IL-36α 1.5 h, 24 h**	**Exclusively *S. aureus* 24 h**	**Exclusively MDP 24 h**	***S. aureus* + MDP**	***S. aureus* + IL-36α**	**IL-36α + MDP**	***S. aureus* + IL-36α + MDP**
APOBEC3G	CYP2W1	CXCL6	APOBEC3G	gene:ENSG 00000205236	LINC00520	NOD2			
ASB2	CYP4B1	CXCL8	ASB2	gene:ENSG 00000224260	LYPD2	NOTCH3			
ATF3	CYP4F22	CYP2W1	ATF3	gene:ENSG 00000256514	LYPD2	PGLYRP3			
BAMBI	DEFB1	DEFB1	BAMBI	gene:ENSG 00000284976	NDRG2	PLA2G4E			
BBC3	DGAT2	DEFB103A	BBC3	gene:ENSG 00000289007	PDE2A-AS2	PSORS1C2			
BCL2A1	DLX2	DEFB4A	BCL2A1	GLTP	PLBD1	RHCG			
BCL6B	DSC1	DEFB4B	BCL6B	GMPR	PRSS22	RHOV			
BHLHE40-AS1	DSG1	DGAT2	BHLHE40-AS1	GPNMB	PSCA	S100A12			
BHLHE41	DUSP1	EPHX3	BHLHE41	GPRIN2	PSG5	S100A8			
BIRC3	EPHB6	FABP5	BIRC3	H19	RNASE7	S100P			
BMP2	EPHX3	FAM25C	BMP2	H2AC25	S100A7A	SAA2			
BTG1	EVPLL	FAM25G	BTG1	H2AC6	SAA2-SAA4	SBSN			
BTG2	FABP5	GDPD3	BTG2	H2BC21	SAT1	SDR9C7			
BTG4	FAM25C	gene:ENSG 00000231412	BTG4	HCAR3	SLC6A14	SERPINB3			
BX255923.3	FAM25G	gene:ENSG 00000276900	BX255923.3	HS3ST6	SPINK6	SLC39A2			
C10orf99	FAM43A	GPC1-AS1	C10orf99	IFIT2	SPRR1B	SLPI			
C16orf86	FLG	GPR15LG	C16orf86	IFIT3	SPRR2E	SLURP1			
C1QTNF1	FLG2	H2AC18	C1QTNF1	IGFL2	SPRR2F	SLURP2			
C1QTNF1-AS1	GBP2	H2AC19	C1QTNF1-AS1	KCNK7	SPRR3	SPINK7			
C1R	GBP4	H2BC8	C1R	KLHDC7B	TMPRSS11D	SPRR1A			
C20orf197	GDA	HES4	C20orf197	KLK11	UPK2	SPRR4			
C2CD4A	gene:ENSG 00000205236	IL23A	C2CD4A	KLK12	WFDC5	SPRR5			
C2CD4B	gene:ENSG 00000224260	IL36G	C2CD4B	KRT1		TGM1			
C3	gene:ENSG 00000256514	IL36RN	C3	KRT10		TMEM45A			
CAMK1G	gene:ENSG 00000276900	KLK14	CAMK1G	KRT2		TMEM45B			

Individual treatments			**Evaluation**						
IL-36α 1.5 h, 24 h	***S. aureus* 24 h**	**MDP 24 h**	**Exclusively IL-36α 1.5 h, 24 h**	**Exclusively *S. aureus* 24 h**	**Exclusively MDP 24 h**	***S. aureus* + MDP**	***S. aureus* + IL-36α**	**IL-36α + MDP**	***S. aureus* + IL-36α + MDP**
CCDC147-AS1	gene:ENSG 00000284976	KRT16	CCDC147-AS1	KRT6C		WFDC12			
CCL2	gene:ENSG 00000289007	KRT42P	CCL2	KRT77					
CCL20	GLTP	KRT78	CCRN4L	KRT79					
CCRN4L	GMPR	KRTDAP	CD200	LCE2B					
CD200	GPNMB	LCE2C	CD83	LCE3E					
CD83	GPR15LG	LCE2D	CES1	LGALS7					
CES1	GPRIN2	LCN2	CES1P1	LGALS7B					
CES1P1	H19	LEMD1	CHST1	LGALS9B					
CFB	H2AC18	LINC00520	CLDN16	LIPM					
CHST1	H2AC19	LY6D	CLEC2D	LORICRIN					
CLDN16	H2AC25	LYPD2	CPAMD8	LY6G6C					
CLEC2D	H2AC6	MYH14	CSF1	LYNX1					
CPAMD8	H2BC21	NDRG2	CSF2	MAFB					
CSF1	HCAR3	NOD2	CTA-293F17.1	MTSS1					
CSF2	HS3ST6	NOTCH3	CTD-2020K17.1	MUC15					
CSF3	IFIT2	PDE2A-AS2	CTD-2369P2.5	MX2					
CTA-293F17.1	IFIT3	PDZK1IP1	CTD-2532N20.1	NIPAL4					
CTD-2020K17.1	IGFL2	PGLYRP3	CTSS	NKPD1					
CTD-2369P2.5	IL17C	PGLYRP4	CXCL1	ODF3B					
CTD-2532N20.1	IL36RN	PI3	CXCL2	OTUD1					
CTSS	KCNK7	PLA2G3	CXCL3	PADI1					
CXCL1	KLHDC7B	PLA2G4E	CXCL5	PDZD2					
CXCL2	KLK11	PLBD1	DDIT4	PLA2G4B					
CXCL3	KLK12	PRSS22	DEC1	PLA2G4D					
CXCL5	KRT1	PSCA	DENND3	PLAAT2					
CXCL6	KRT10	PSG5	DMBT1	PLXDC2					
CXCL8	KRT16	PSORS1C2	DNAJB5	PRODH					
DDIT4	KRT2	RAET1L	EDN1	PRRX2					
DEC1	KRT6C	RARRES1	EFNA1	RAPGEFL1					
DEFB4A	KRT77	RHCG	ELF3	RDH12					

Individual treatments			**Evaluation**						
IL-36α 1.5 h, 24 h	***S. aureus* 24 h**	**MDP 24 h**	**Exclusively IL-36α 1.5 h, 24 h**	**Exclusively *S. aureus* 24 h**	**Exclusively MDP 24 h**	***S. aureus* + MDP**	***S. aureus* + IL-36α**	**IL-36α + MDP**	***S. aureus* + IL-36α + MDP**
DENND3	KRT79	RHOV	EPHA6	RORA					
DMBT1	KRTDAP	RNASE7	EPOR	RRAD					
DNAJB5	LCE1A	S100A12	FAM65C	RSAD2					
EDN1	LCE1D	S100A7	FGF5	RTN4RL1					
EFNA1	LCE1F	S100A7A	FGFR3	SCN4B					
ELF3	LCE2A	S100A8	FIBIN	SPINK5					
EPHA6	LCE2B	S100A9	FZD2	SPTSSB					
EPOR	LCE2C	S100P	FZD8	TMEM184A					
EVPLL	LCE2D	SAA2	GATA6	TMEM229B					
FAM65C	LCE3E	SAA2-SAA4	GATA6-AS1	TMPRSS4					
FGF5	LCE6A	SAT1	GDF15	TNFAIP8L3					
FGFR3	LGALS7	SBSN	GJB7	TNFSF10					
FIBIN	LGALS7B	SDR9C7	GPR156	TREX2					
FZD2	LGALS9B	SERPINB3	GPR37L1	TSHZ2					
FZD8	LIPM	SERPINB4	GUCY2D	TTLL11					
GATA6	LORICRIN	SGPP2	H1FX-AS1	UGT1A7					
GATA6-AS1	LY6D	SLC39A2	HAND1	UPK3BL1					
GBP2	LY6G6C	SLC6A14	HEPHL1	UPK3BL2					
GBP4	LYNX1	SLPI	HES7	VSIG10L					
GDF15	MAFB	SLURP1	HEY1	VSIG8					
GJB7	MTSS1	SLURP2	HIST1H2BD	ZNF467					
GPR156	MUC15	SPINK6	HNF1B						
GPR37L1	MX2	SPINK7	HS3ST3B1						
GUCY2D	MYH14	SPRR1A	HSD17B2						
H1FX-AS1	NIPAL4	SPRR1B	HSD3BP5						
HAND1	NKPD1	SPRR2B	ICAM1						
HEPHL1	NOD2	SPRR2E	ID4						
HES7	NOTCH3	SPRR2F	IFNAR2						
HEY1	ODF3B	SPRR2G	IGFBP3						
HIST1H2BD	OTUD1	SPRR3	IGFL1						
HNF1B	PADI1	SPRR4	IL16						

Individual treatments			**Evaluation**						
IL-36α 1.5 h, 24 h	***S. aureus* 24 h**	**MDP 24 h**	**Exclusively IL-36α 1.5 h, 24 h**	**Exclusively *S. aureus* 24 h**	**Exclusively MDP 24 h**	***S. aureus* + MDP**	***S. aureus* + IL-36α**	**IL-36α + MDP**	***S. aureus* + IL-36α + MDP**
HS3ST3B1	PDZD2	SPRR5	IL1B						
HSD17B2	PDZK1IP1	STEAP4	IL1RN						
HSD3BP5	PGLYRP3	TGM1	IL20						
ICAM1	PGLYRP4	TMEM45A	IL32						
ID4	PI3	TMEM45B	IL33						
IFNAR2	PLA2G4B	TMPRSS11D	IL6						
IGFBP3	PLA2G4D	TNFAIP6	IL7R						
IGFL1	PLA2G4E	UPK2	IRAK2						
IL16	PLAAT2	WFDC12	IRF1						
IL17C	PLXDC2	WFDC5	ITPKC						
IL1B	PRODH	ZC3H12A	JAK3						
IL1RN	PRRX2		KBTBD7						
IL20	PSORS1C2		KCNJ2						
IL23A	RAET1L		KCNJ5						
IL32	RAPGEFL1		KDM6B						
IL33	RDH12		KIAA1045						
IL36G	RHCG		KIAA1683						
IL36RN	RHOV		KIF21B						
IL6	RORA		KLHL35						
IL7R	RRAD		KMO						
IRAK2	RSAD2		KPNA7						
IRF1	RTN4RL1		KREMEN2						
ITPKC	S100A12		KRT16P5						
JAK3	S100A8		KRT34						
KBTBD7	S100A9		LA16c-380H5.3						
KCNJ2	S100P		LA16c-380H5.4						
KCNJ5	SAA2		LCE1B						
KDM6B	SBSN		LCE1C						
KIAA1045	SCN4B		LCE3A						
KIAA1683	SDR9C7		LCE3C						
KIF21B	SERPINB3		LGALSL						

Individual treatments			**Evaluation**						
IL-36α 1.5 h, 24 h	***S. aureus* 24 h**	**MDP 24 h**	**Exclusively IL-36α 1.5 h, 24 h**	**Exclusively *S. aureus* 24 h**	**Exclusively MDP 24 h**	***S. aureus* + MDP**	***S. aureus* + IL-36α**	**IL-36α + MDP**	***S. aureus* + IL-36α + MDP**
KLHL35	SERPINB4		LIF						
KMO	SGPP2		LINC00086						
KPNA7	SLC28A3		LINC00162						
KREMEN2	SLC39A2		LINC00173						
KRT16P5	SLPI		LINC00370						
KRT34	SLURP1		LINC00514						
LA16c-380H5.3	SLURP2		LINC00578						
LA16c-380H5.4	SOD2		LINC00882						
LCE1A	SPINK5		LINC01137						
LCE1B	SPINK7		LRP1B						
LCE1C	SPRR1A		MAP3K8						
LCE1D	SPRR4		MARCKSL1						
LCE1F	SPRR5		MARCO						
LCE2A	SPTSSB		MCHR1						
LCE2D	STEAP4		MDGA1						
LCE3A	TGM1		METTL7A						
LCE3C	TMEM184A		MGAM						
LCE6A	TMEM229B		MIR146A						
LCN2	TMEM45A		MIR155HG						
LGALSL	TMEM45B		MIR200A						
LIF	TMPRSS4		MIR200B						
LINC00086	TNFAIP6		MIR429						
LINC00162	TNFAIP8L3		MRGPRX3						
LINC00173	TNFSF10		MRVI1						
LINC00370	TREX2		MYO16						
LINC00514	TSHZ2		MYOZ3						
LINC00578	TTLL11		NALCN						
LINC00882	UGT1A7		NANOS3						
LINC01137	UPK3BL1		NBPF18P						
LRP1B	UPK3BL2		NCOA7						
MAP3K8	VSIG10L		NEGR1						

Individual treatments			**Evaluation**						
IL-36α 1.5 h, 24 h	***S. aureus* 24 h**	**MDP 24 h**	**Exclusively IL-36α 1.5 h, 24 h**	**Exclusively *S. aureus* 24 h**	**Exclusively MDP 24 h**	***S. aureus* + MDP**	***S. aureus* + IL-36α**	**IL-36α + MDP**	***S. aureus* + IL-36α + MDP**
MARCKSL1	VSIG8		NEURL3						
MARCO	WFDC12		NFATC1						
MCHR1	WNT4		NFATC4						
MDGA1	ZBTB16		NFKB1						
METTL7A	ZNF467		NFKB2						
MGAM			NFKBIA						
MIR146A			NFKBID						
MIR155HG			NFKBIZ						
MIR200A			NGFR						
MIR200B			NINJ1						
MIR429			NMNAT2						
MRGPRX3			NOTCH4						
MRVI1			NOXO1						
MYO16			NPR1						
MYOZ3			NR4A3						
NALCN			NRARP						
NANOS3			NTSR1						
NBPF18P			OLR1						
NCOA7			PCP4L1						
NEGR1			PDE2A						
NEURL3			PDE4B						
NFATC1			PDGFB						
NFATC4			PGLYRP2						
NFKB1			PKD1L2						
NFKB2			PKLR						
NFKBIA			PLAT						
NFKBID			PLAUR						
NFKBIZ			PNRC1						
NGFR			POU2F2						
NINJ1			PPP1R3C						
NMNAT2			PRDM1						

Individual treatments			**Evaluation**						
IL-36α 1.5 h, 24 h	***S. aureus* 24 h**	**MDP 24 h**	**Exclusively IL-36α 1.5 h, 24 h**	**Exclusively *S. aureus* 24 h**	**Exclusively MDP 24 h**	***S. aureus* + MDP**	***S. aureus* + IL-36α**	**IL-36α + MDP**	***S. aureus* + IL-36α + MDP**
NOTCH4			PYY						
NOXO1			RCAN1						
NPR1			RGPD2						
NR4A3			RIPK2						
NRARP			RND1						
NTSR1			RND3						
OLR1			RORC						
PCP4L1			RP11-108K14.8						
PDE2A			RP11-1096G20.5						
PDE4B			RP11-184A2.3						
PDGFB			RP11-193H5.1						
PDZK1IP1			RP11-20B7.1						
PGLYRP2			RP11-215G15.5						
PGLYRP4			RP11-221N13.4						
PI3			RP11-327F22.2						
PKD1L2			RP11-356I2.1						
PKLR			RP11-356I2.4						
PLA2G3			RP11-367G18.1						
PLAT			RP11-37B2.1						
PLAUR			RP11-3L8.3						
PNRC1			RP11-403A21.1						
POU2F2			RP11-408H1.3						
PPP1R3C			RP11-42I10.1						
PRDM1			RP11-439L18.2						
PYY			RP11-439L18.3						
RAET1L			RP11-465B22.8						
RARRES1			RP1-151F17.2						
RCAN1			RP11-529G21.2						
RGPD2			RP11-54F2.1						
RIPK2			RP11-551L14.1						
RND1			RP11-568N6.1						

Individual treatments			**Evaluation**						
IL-36α 1.5 h, 24 h	***S. aureus* 24 h**	**MDP 24 h**	**Exclusively IL-36α 1.5 h, 24 h**	**Exclusively *S. aureus* 24 h**	**Exclusively MDP 24 h**	***S. aureus* + MDP**	***S. aureus* + IL-36α**	**IL-36α + MDP**	***S. aureus* + IL-36α + MDP**
RND3			RP11-588G21.2						
RORC			RP11-60A8.1						
RP11-108K14.8			RP11-64D24.2						
RP11-1096G20.5			RP11-654A16.3						
RP11-184A2.3			RP11-654D12.2						
RP11-193H5.1			RP11-666A8.8						
RP11-20B7.1			RP11-680H20.2						
RP11-215G15.5			RP11-779O18.3						
RP11-221N13.4			RP11-796E2.4						
RP11-327F22.2			RP11-79H23.3						
RP11-356I2.1			RP11-861A13.4						
RP11-356I2.4			RP11-88H9.2						
RP11-367G18.1			RP11-893F2.9						
RP11-37B2.1			RP11-91K9.1						
RP11-3L8.3			RP11-95M15.2						
RP11-403A21.1			RP1-209A6.1						
RP11-408H1.3			RP1-261G23.5						
RP11-42I10.1			RP1-28O10.1						
RP11-439L18.2			RP4-607I7.1						
RP11-439L18.3			RPL3L						
RP11-465B22.8			RPLP0P2						
RP1-151F17.2			S100A11						
RP11-529G21.2			SAA1						
RP11-54F2.1			SCNN1D						
RP11-551L14.1			SDC4						
RP11-568N6.1			SERPINA1						
RP11-588G21.2			SERPINA10						
RP11-60A8.1			SERPINA6						
RP11-64D24.2			SERPINF2						
RP11-654A16.3			SH2D3C						
RP11-654D12.2			SLC25A29						

Individual treatments			**Evaluation**						
IL-36α 1.5 h, 24 h	***S. aureus* 24 h**	**MDP 24 h**	**Exclusively IL-36α 1.5 h, 24 h**	**Exclusively *S. aureus* 24 h**	**Exclusively MDP 24 h**	***S. aureus* + MDP**	***S. aureus* + IL-36α**	**IL-36α + MDP**	***S. aureus* + IL-36α + MDP**
RP11-666A8.8			SLC44A4						
RP11-680H20.2			SNCAIP						
RP11-779O18.3			SNORD3B-2						
RP11-796E2.4			SOCS3						
RP11-79H23.3			SOX4						
RP11-861A13.4			SPRED3						
RP11-88H9.2			SPRR2A						
RP11-893F2.9			SPRR2D						
RP11-91K9.1			SSPN						
RP11-95M15.2			SSUH2						
RP1-209A6.1			ST7-AS1						
RP1-261G23.5			STAT5A						
RP1-28O10.1			STX11						
RP4-607I7.1			TEX14						
RPL3L			TGM3						
RPLP0P2			TGM4						
S100A11			TMCC3						
S100A7			TMEM217						
S100A9			TMEM52B						
SAA1			TMEM88						
SCNN1D			TMEM92						
SDC4			TNF						
SERPINA1			TNFAIP2						
SERPINA10			TNFAIP3						
SERPINA6			TNFAIP8						
SERPINB4			TNFRSF9						
SERPINF2			TNFSF15						
SGPP2			TNIP3						
SH2D3C			TRAF1						
SLC25A29			TREM2						
SLC28A3			TSLP						

Individual treatments			**Evaluation**						
IL-36α 1.5 h, 24 h	***S. aureus* 24 h**	**MDP 24 h**	**Exclusively IL-36α 1.5 h, 24 h**	**Exclusively *S. aureus* 24 h**	**Exclusively MDP 24 h**	***S. aureus* + MDP**	***S. aureus* + IL-36α**	**IL-36α + MDP**	***S. aureus* + IL-36α + MDP**
SLC44A4			TTLL10						
SNCAIP			USH1G						
SNORD3B-2			USP43						
SOCS3			VNN1						
SOD2			VNN3						
SOX4			ZBTB10						
SPRED3			ZG16B						
SPRR2A			ZMYND15						
SPRR2B			ZNF812						
SPRR2D									
SPRR2G									
SSPN									
SSUH2									
ST7-AS1									
STAT5A									
STEAP4									
STX11									
TEX14									
TGM3									
TGM4									
TMCC3									
TMEM217									
TMEM52B									
TMEM88									
TMEM92									
TNF									
TNFAIP2									
TNFAIP3									
TNFAIP6									
TNFAIP8									
TNFRSF9									

Individual treatments			**Evaluation**						
IL-36α 1.5 h, 24 h	***S. aureus* 24 h**	**MDP 24 h**	**Exclusively IL-36α 1.5 h, 24 h**	**Exclusively *S. aureus* 24 h**	**Exclusively MDP 24 h**	***S. aureus* + MDP**	***S. aureus* + IL-36α**	**IL-36α + MDP**	***S. aureus* + IL-36α + MDP**
TNFSF15									
TNIP3									
TRAF1									
TREM2									
TSLP									
TTLL10									
USH1G									
USP43									
VNN1									
VNN3									
WNT4									
ZBTB10									
ZBTB16									
ZC3H12A									
ZG16B									
ZMYND15									
ZNF812									

Publications

Raw data of research findings acquired within the frame of published manuscripts, other than *Fischer et al. 2025*, are not included in this dissertation.

First-author publications

Fischer et al., 2025 [182]

“NOD2-induced IκBζ mediates a protective host response against epicutaneous *Staphylococcus aureus* infection”
Published in Journal Invest Dermatol. (JID), 2025 May 22:S0022-202X(25)00494-4.
DOI: 10.1016/j.jid.2025.04.036 / PMID: 40412468

Fischer et al., 2023 [42]

“IL-17A-driven psoriasis is critically dependent on IL-36 signaling”
Published in Frontiers in Immunology, 2023 Dec 11;14:1256133.
DOI: 10.3389/fimmu.2023.1256133 / PMID: 38162658

Co-author publications (until submission date of this dissertation)

Bork et al., 2024 [86]

“naRNA-LL37 composite DAMPs define sterile NETs as self-propagating drivers of inflammation “
Published in EMBO Reports, 2024 Jul;25(7):2914-2949.
DOI: 10.1038/s44319-024-00150-5 / PMID: 38783164

Kommoss et al., 2024

“A simple tool for evaluation of inflammation in psoriasis: Neutrophil-to-lymphocyte and platelet-to-lymphocyte ratio as markers in patients and murine psoriasis models”
Published in Journal Mol. Med., 2024 Feb;102(2):247-255.
DOI: 10.1007/s00109-023-02406-4 / PMID: 38127137

Schaller and Ringen et al., 2023

“Reactive oxygen species produced by myeloid cells in psoriasis as a potential biofactor contributing to the development of vascular inflammation”
Published in Biofactors, 2023 Jul-Aug;49(4):861-874.
DOI: 10.1002/biof.1949 / PMID: 37139784

Acknowledgment of contributors

Personal acknowledgment